



Master's Thesis

# Rock Mass Characterisation and Reinforcement Strategies for Tunnels in Iceland

---

## Fáskrúðsfjörður Tunnel

Gunnar Arnar Gunnarsson

October, 2008

In corporation with:





## Preface

This Master Thesis is written at the Department of Civil Engineering, DTU-Byg, at the Technical University of Denmark in the field of geotechnical and rock mechanics. The thesis was worked out in a cooperation with the University of Iceland, Faculty of Civil and Environmental Engineering (UoB-HÍ), and GeoTek Ltd.. The thesis has the size of 30 ECTS credit points and the work has been carried out over seven months period from April to October 2008.

The supervisors on the project were Niels Foged, Sigurður Erlingsson and Oddur Sigurðsson. The project was funded by the Icelandic Road Administration (Vegagerðin).



## Acknowledgement

I would like to express my gratitude to those who gave help during my work on this thesis. I will give special thanks to:

Niels Foged – For his guidance and great interest in the project, which would not have been the same without his interest in Icelandic geology. Also for a very interesting study tour around Iceland in mid August.

Sigurður Erlingsson – For his guidance and inspiration during the project work, also providing literatures and useful comments on structure of the thesis.

Oddur Sigurðsson – For his guidance in the Héðinsfjörður tunnel during my stay in the north of Iceland and for giving me the opportunity to use *Phase2* for modelling. Also providing vital literatures about the Fáskrúðsfjörður tunnel and for always being available when needed.

Hallgrímur Örn Arngrímsson – For his participation in the final part of the thesis and great help in rock cores classification.

Katrine Alling Andreason – For her guidance during the triaxial tests in MTS 815 Rock Triaxial System and useful comments.

Ole Hededal – For good and useful comments during modeling phase of the thesis.

Birgir Jónsson – For providing literatures during my stay in Iceland.

Ágúst Guðmundsson – For providing important literatures about the Fáskrúðsfjörður tunnel.

Vilhjálmur Ívar Sigurjónsson – For preparation of the rock cores for transport and sending to Denmark.

Vita Larsen – For a friendly help in the DTU laboratory.

GEO – For allowance to use their equipments, diamond disc saw and compression machine. I would also like to give special thanks to Kaj West for instructions on the diamond disc saw and Frederik Ditlevsen for guidance on the compression machine.

Vegagerðin – For their interest in the thesis and support of allowance. Special thanks to employees of Vegagerðin at Reyðarfjörður for helping with selection of rock cores.

Elvar Jóhannesson and Guðjón Magnússon – For invaluable proofreading of the thesis and good comments.

## Abstract

The thesis starts with a short description of Icelandic geology and the most common rock types, with a brief description of their material and engineering properties.

Tunnelling in Iceland's rock mass can deliver quite special and challenging conditions, some of them varying from those known from other countries in the world. A chapter about Icelandic conditions for tunnelling, deals with some of the most important factors during tunnelling in Iceland, e.g. mixed face tunnel, groundwater, rock stresses, faults etc., how these factors affect the tunnel excavation and how it is possible to avoid problems are related to these factors.

A brief description of the most common rock classification systems is available in the report as well as a portrayal of their advantages and disadvantages. Their purposes are to classify and store knowledge from previous projects for the use to select tunnelling methods and to estimate need of reinforcement. The NGI tunnel quality index (Q-system) is the most used rock classification system in Iceland and has been adjusted to Icelandic conditions during the last three decades.

Chapter 4.2 defines rock support systems used in Icelandic rock mass, consisting mainly of various types of rock bolts and shotcrete. These different support types are discussed and evaluated, and their theoretical background is also introduced. The usage of rock bolts and shotcrete from previous constructed road tunnels in Iceland is presented too.

The main aim of the project is to investigate by means of numerical analyses the reliability and the quality of the reinforcement used in the Fáskrúðsfjörður tunnel in the eastern part of Iceland. The tunnel is the only road tunnel in Iceland where stress measurement has been carried out during the excavation. The results from the stress measurements will be used in the numerical analysis part of the thesis. Three various models were analysed, a model with typical Icelandic mixed face and

two models cross sections based on geological and geotechnical conditions from the Fáskrúðsfjörður tunnel. The numerical analysis was carried out in the finite element program *Phase2*.

Brazil tests, unconfined compression tests and triaxial tests were performed at DTU and GEO on rock cores from borehole FF-04, drilled inside the Fáskrúðsfjörður tunnel. To obtain the mechanical properties for the rock mass surrounding the tunnel, a laboratory tests dataset from the headrace tunnel in Kárahnjúkar hydroelectric project was analysed and later compared with the presented laboratory results.

From the comparison of laboratory test results from Kárahnjúkar and the Fáskrúðsfjörður tunnel the difference is obvious. Strength and stiffness parameters for different rock types from the Fáskrúðsfjörður tunnel are much lower, particularly for the various basalts where unconfined compression strength is more than six times larger from Kárahnjúkar than Fáskrúðsfjörður. The possible reasons for this gap between the two sites, is a selection of porous rock cores from the Fáskrúðsfjörður tunnel and older rock mass in Fáskrúðsfjörður which has reduced its strength cause of weathering and high stress conditions.

Practical support used in the Fáskrúðsfjörður tunnel for both stations 6530 and 7615 is well optimised, despite of the maximum displacements exceeding 10 mm, which was chosen as a maximum acceptable displacement according to Icelandic geotechnical tunnel engineers. Some rock bolts presented yielding but at both sites the shotcrete liner carried the rest of the load and secured sufficient stability. The supplementary support models for both stations did not decrease the maximum displacements as expected. The cost for the additional support is more than two times higher than in the practical supported models. The use of additional bolts gives no significant reduction in convergence.

In general, it is the conclusion of the modelling work that *Phase2* works well. It is recommended for future works to emphasise more rock stress measurements and more rock mechanical testing to provide better data for the convergence modelling work. Especially, the used GSI evaluation and definition of residual values calls for concurrent calibration of actual tunnelling sites with face logging and support strategy applied.



## Útdráttur

Í byrjun ritgerðar er fjallað um íslenska jarðfræði og helstu berggerðir landsins, þar sem efnis- og eðlisfræðilegum eiginleikum er gerð skil.

Jarðgangagerð í íslensku bergi orsakar oft mjög sérstakar og erfiðar aðstæður, aðstæður sem eru síður fundnar annars staðar í heiminum. Sérstakur kafli tekur á þessum þáttum, þar sem helst mætti nefna, misleit bergi í stafni, grunnvatn, bergspennur, misgengi ofl.. Einnig er komið inn á hvaða áhrif þessir þættir hafa á gangnagröft og hvernig mögulega er hægt að komast hjá vandamálum þeim tengd.

Í ritgerðinni er stutt ágríp af helstu berggæðamatskerfum og kostum þeirra og göllum lýst. Fjallað er um mikilvægi þeirra við geymslu á reynslu af eldri verkefnum og útvíkkun á þeim við mat á nauðsynlegum styrkingum. Mest hefur verið stuðst við Q-kerfið (NGI tunnel quality index) á Íslandi og hefur aðlögun að íslenskum aðstæðum staðið yfir í þrjú áratugi.

Fjallað er um helstu bergstyrkingaraðferðir sem notaðar eru á Íslandi, en þær samanstanda af mismunandi tegundum bergbolta og sprautusteypu. Þessum bergstyrkingaraðferðum eru gerð skil, en einnig er fjallað um þeirra fræðilegu skilyrði. Þá er notkun á bergboltum og sprautusteypu frá fyrri framkvæmum á Íslandi lýst.

Tilgangur verkefnisins er að rannsaka með tölulegum aðferðum áreiðanleika og gæði bergstyrkingar sem notuð var við gerð Fáskrúðsfjardarganga á austanverðu Íslandi. Göngin eru einu veggöngin á Íslandi þar sem spennumælingar hafa verið framkvæmdar samhliða gangnagreftri. Niðurstöður úr mælingunum verða að hluta til notaðar við lausn á verkefninu. Þrjú líkön voru gerð, dæmigerður íslenskur misleitur gangastafn og tvö gangnaþversnið þar sem jarðfræði- og jarðtæknilegum aðstæðum frá Fáskrúðsfjardargöngum var fylgt. Við lausn á verkefninu var stuðst við einingaraðferðar forritið *Phase2*.

Brazil próf, einása þrýstipróf og þríása þrýstipróf voru framkvæmd við DTU og GEO á bergkjörnum frá borholu FF-04, sem var boruð í miðjum Fáskrúðsfjarðargöngum. Til að öðlast styrktareiginleika þeirra berggerða sem umlykja Fáskrúðsfjarðargöng, var greining gerð á tilraunasafni frá aðaljarðgöngum við Kárahnjúka og hún notuð til samanburðar við niðurstöður tilrauna.

Mismunurinn er augljós á samanburði á niðurstöðum tilrauna frá Kárahnjúkum og Fáskrúðsfirði. Kennistærðir á styrk og stífni fyrir bergtegundir frá Fáskrúðsfirði eru miklu lægri, þá sérstaklega fyrir mismunandi tegundir basalts þar sem einása þrýstistyrkur er sex sinnum hærra fyrir sýni frá Kárahnjúkum. Hugsanlegar ástæður fyrir þessum mikla mun er val á blöðróttum sýnum frá Fáskrúðsfjarðargöngum, en þar er einnig eldri bergmassi sem hefur misst hluta styrk síns vegna veðrunar og hárna spennuáðstæðna.

Þær bergstyrkingar sem notaðar voru í Fáskrúðsfjarðargöngum á stöðvum 6530 og 7515 eru vel útfærðar þrátt fyrir að stærstu færslur fari yfir 10 mm, sem var valin stærsta leyfilega færsla samkvæmt íslenskum jarðgangnaverkfræðingum. Nokkrir bergboltar sýndu merki um formbreytingar en á báðum stöðvum bar sprautusteypu klæðningin bergrúmið uppi og tryggði öruggan stöðugleika. Viðbótastyrkingarlíkön fyrir báðar stöðvar náðu ekki að minnka færslurnar eins og til var ætlast. Áætla má að kostnaður við viðbótastyrkingarnar sé tvisvar sinnum meiri en við þær sem notaðar voru við gerð gangnanna og myndu þær skila litlum sem engum árangri.

Sem niðurstöðu má segja að *Phase2* virki í takt við fræðin. Í nánustu framtíð skal vera lögð áhersla á spennumælingar og frekari tilraunir til að öðlast betri og nákvæmari gögn fyrir líkanagerð. Þá sérstaklega fyrir mat á GSI gildum og “residual” kennistærðum sem nota mætti í líkanagerð á framkvæmdastað, þar sem greining á bergi og styrkingum væri fylgt eftir samfara líkanagerðinni.

## Table of Contents

Preface .....	i
Acknowledgement .....	ii
Abstract .....	iv
Útdráttur .....	vi
Table of Contents .....	viii
List of Figures.....	x
List of Tables.....	xiv
1 Introduction.....	1
2 The Geology of Iceland.....	2
2.1 The Volcanic Activity in Iceland.....	2
2.2 Icelandic Bedrock .....	3
2.2.1 Basalt.....	5
2.2.2 Acidic and Intermediate Rocks.....	8
2.2.3 Sedimentary Interbeds.....	9
2.2.4 Other Rock Types .....	10
3 Icelandic Conditions for Tunnelling.....	13
3.1 Mixed Face .....	13
3.2 Groundwater.....	15
3.3 Rock Stresses.....	16
3.4 Faults .....	22
3.5 Dikes.....	25
3.6 Seismic Activity.....	25
4 Reinforcement Strategies .....	29
4.1 Rock Classification Systems .....	29
4.1.1 Rock Quality Designation index, RQD.....	29
4.1.2 Rock Structure Rating, RSR .....	30
4.1.3 Rock Mass Rating, RMR.....	32
4.1.4 NGI Tunnelling Quality Index, Q .....	34
4.1.5 The Geological Strength Index, GSI.....	39
4.2 Rock Support Systems.....	41
4.2.1 Rock Bolt.....	42
4.2.2 Theoretical Concept of a Rock Bolt .....	44
4.2.3 Shotcrete.....	47
4.2.4 Theoretical Concept of Shotcrete .....	48
4.2.5 Combination of Rock Bolts and Shotcrete .....	49
4.2.6 Use of Rock Bolts and Shotcrete in Iceland .....	50

4.3	Stresses Around Underground Openings .....	52
5	The Fáskrúðsfjörður Tunnel .....	56
5.1	The Project.....	56
5.2	Geology at Fáskrúðsfjörður and Reyðarfjörður .....	58
5.3	Rock Support Systems in Fáskrúðsfjörður Tunnel .....	63
5.4	Stress Measurements in Fáskrúðsfjörður Tunnel.....	64
6	Laboratory Tests .....	67
6.1	Preparation for Laboratory Testing .....	68
6.2	Brazil Test.....	71
6.3	Unconfined Compression Test .....	72
6.4	Triaxial Test.....	73
6.5	Comparison to Dataset from Kárahnjúkar .....	74
7	Numerical Analysis .....	76
7.1	Introduction.....	76
7.2	Typical Icelandic Mixed Face Tunnel .....	76
7.2.1	Calculation Based on Elastic Model .....	78
7.2.2	Calculation Based on Elastic-Plastic Model .....	83
7.2.1	Supported Elastic-Plastic GSI=75 Model .....	88
7.2.2	Supported Elastic-Plastic GSI=50 Model.....	94
7.3	The Fáskrúðsfjörður Tunnel – Station 6530.....	99
7.3.1	Practical Support at Station 6530 in Fáskrúðsfjörður Tunnel.....	101
7.3.2	Supplementary Support for Station 6530 .....	105
7.4	The Fáskrúðsfjörður Tunnel – Station 7615.....	109
7.4.1	Practical Support at Station 7615 in Fáskrúðsfjörður Tunnel.....	110
7.4.2	Supplementary Support for Station 7615 .....	114
7.5	Discussion .....	118
8	Conclusion .....	120
9	Future work.....	122
10	References.....	123

Appendix 1

Appendix 2

Appendix 3

Appendix 4

Appendix 5

Appendix 6

## List of Figures

Figure 2-1: Active volcanic systems in Iceland. 1) Individual volcanic systems and 2) active volcanic zones [4].	3
Figure 2-2: Schematic structure of a single basalt lava [1].	5
Figure 2-3: Typical Icelandic basalt rock mass, above Blanda tailrace canal.	5
Figure 2-4: The Icelandic geological formation [7].	12
Figure 3-1: Typical mixed face for Icelandic conditions [1].	13
Figure 3-2: Mixed face from Fáskrúðsfjörður tunnel. At the top there is sediment underlain by a thin basalt layer, then another sediment layer and finally scoria from the middle to the bottom [46].	13
Figure 3-3: To left, excavation opposite to dip direction. To right, excavation in the same direction as dip [9].	15
Figure 3-4: Two different types of inflow into tunnels. To left, a permeable fault zone where $K$ is the permeability. To right, impermeable fault zone where $P$ is the pore water pressure [11].	16
Figure 3-5: Stresses in the rock mass at depth $z$ , where $\sigma_0 = \sigma_v$ [12].	17
Figure 3-6: Six different deformation measurements at Blanda powerhouse cavern, time dependent convergence after approximately half year diminishes to $< 10$ mm [13].	18
Figure 3-7: Stress ratio $K_0$ as function of depth and horizontal Young's modulus $E_h$ . Measurements in Iceland are normally within the dotted area [13].	19
Figure 3-8: Deformation measurements from Kárahnjúkar cavern at station 47 [13].	20
Figure 3-9: Rock stress measurements with hydraulic fracturing from hydropower stations sites in Iceland [11].	21
Figure 3-10: Horizontal movements in Iceland during the time period 1993 to 2004 based on repeated GPS measurements, the blue triangles are measurement stations. The brown and red zones are discussed in Figure 2-4 [15].	22
Figure 3-11: Different types of faults [16].	23
Figure 3-12: Dikes cutting the stratified formation [4].	25
Figure 3-13: A dike in Fáskrúðsfjörður tunnel [46].	25
Figure 3-14: The bedrock response due to the various types of seismic waves [17].	26
Figure 3-15: The black circles presents the most critical points in a typical Icelandic tunnel cross section during earthquake.	27
Figure 3-16: Horizontal bedrock acceleration map for Iceland [18].	28
Figure 4-1: RSR support estimation for 6 m diameter circular tunnel [21].	31
Figure 4-2: RMR in relation to roof span and stand up time for tunnels [23].	33
Figure 4-3: The relation between rock load and roof span for different RMR values [21].	34
Figure 4-4: Reinforcement design of excavations based on the Q system [14].	37
Figure 4-5: Determination of the GSI for jointed rocks [19].	40
Figure 4-6: Pressure relief of the rock mass after excavation, the most optimal support is the trajectory a-d. Referring to NATM (New Austrian Tunnel Method) [30].	42
Figure 4-7: Components of a grouted end anchored rock bolt [19].	43
Figure 4-8: Installation of rock bolts in Fáskrúðsfjörður tunnel [46].	44
Figure 4-9: Rock bolts installed in tunnel roof [14].	45
Figure 4-10: Rock bolts installed in a sliding rock wedge in a tunnel wall [31].	46
Figure 4-11: Shotcrete applied on a wall in Fáskrúðsfjörður tunnel [46].	48

Figure 4-12: Amount of rock bolts used per length meter in different road tunnels in Iceland [46].	50
Figure 4-13: Amount of shotcrete used per length meter in different road tunnels in Iceland [46].	51
Figure 4-14: Average amount of rock bolts used against cross section area for different road tunnels in Iceland [46].	51
Figure 4-15: Average amount of shotcrete used against cross section area for different road tunnels in Iceland [46].	52
Figure 4-16: A section from a finite element model for a circular tunnel, the figure presents the displacement vectors as well as the shape of the deformed tunnel profile [19].	53
Figure 4-17: The deformation in the rock mass surrounding an advancing tunnel [19].	53
Figure 4-18: Radial, tangential and shear stresses given at any point with polar coordinates [34].	54
Figure 4-19: Tangential stresses for an elliptical opening [34].	55
Figure 5-1: Project area for the Fáskrúðsfjörður tunnel [36].	56
Figure 5-2: Cross section of the mountain ridge, the tunnel route is marked as a violet line [36]. Scale 1:50.000.	57
Figure 5-3: A map over Fáskrúðsfjörður tunnel closest area [36]. Scale 1:200.000	59
Figure 5-4: A Rose diagram for the construction area, J-J' presents the tunnel route [36].	61
Figure 5-5: Typical properties of a basaltic lava section [36].	62
Figure 5-6: Amount of rock bolts used in the Fáskrúðsfjörður tunnel [35].	63
Figure 5-7: Amount of shotcrete used in the Fáskrúðsfjörður tunnel [35].	64
Figure 6-1: Location of the borehole FF-04. Appendix 3 displays a larger figure [36].	67
Figure 6-2: Core samples measured	68
Figure 6-3: Core sample cut in pieces.	68
Figure 6-4: Sample polished.	69
Figure 6-5: Sample compare with a setsquare	69
Figure 6-6: Samples marked	69
Figure 6-7: Siltstone waste away during cut off	70
Figure 6-8: Workshop at GEO	70
Figure 6-9: Samples water saturated	70
Figure 6-10: Test setup for Brazil test, includes a loading frame, a data logger, a load cell, a vertical strain gauge and a computer.	71
Figure 6-11: Scoria sample placed in between the two jaws, ready for testing.	71
Figure 6-12: The test setup is same as for Brazil test except for the disc shape jaws.	72
Figure 6-13: The MTS compression machine used for the triaxial testing.	73
Figure 6-14: Sandstone sample installed in the cell, ready for testing. Extensometers positioned at each side of the sample to measure radial and axial strains.	73
Figure 7-1: Cross section of the basic model, the dimensions are in meters.	77
Figure 7-2: Strength factor for GSI=75.	80
Figure 7-3: Strength factor for GSI=50.	80
Figure 7-4: Strength factor for GSI=25.	80
Figure 7-5: Total displacements for GSI=75, largest displacement is 7,1 mm.	81
Figure 7-6: Total displacements for GSI =50, largest displacement is 19 mm.	81
Figure 7-7: Total displacements for GSI =25, largest displacement is 97 mm.	81
Figure 7-8: Deformed boundaries and deformation vectors for GSI=75 (scale: x50).	82
Figure 7-9: Deformed boundaries and deformation vectors for GSI=50 (scale: x50).	82
Figure 7-10: Deformed boundaries and deformation vectors for GSI=25 (scale: x10).	82
Figure 7-11: Yielded elements for GSI=75, total number of yielded elements=244.	85

Figure 7-12: Yielded elements for GSI=50, total number of yielded elements=536. ....	85
Figure 7-13: Yielded elements for GSI=25, total number of yielded elements=961. ....	85
Figure 7-14: Total displacements for GSI=75, largest displacement is 16 mm. ....	86
Figure 7-15: Total displacements for GSI=50, largest displacement is 88 mm. ....	86
Figure 7-16: Total displacements for GSI=25, largest displacement is 933 mm. ....	86
Figure 7-17: Deformed boundaries and deformation vectors for GSI=75 (scale: x20). ....	87
Figure 7-18: Deformed boundaries and deformation vectors for GSI=50 (scale: x5). ....	87
Figure 7-19: Deformed boundaries and deformation vectors for GSI=25 (scale: x1). ....	87
Figure 7-20: Rock bolt pattern and shotcrete application. ....	89
Figure 7-21: Yielded elements for unsupported tunnel. Model GSI=75. ....	90
Figure 7-22: Yielded elements for bolt supported tunnel. Model GSI=75. ....	90
Figure 7-23: Yielded elements for bolt and shotcrete supported tunnel. Model GSI=75. ....	90
Figure 7-24: Total displacements for unsupported tunnel. Model GSI=75. ....	91
Figure 7-25: Total displacements for bolt supported tunnel. Model GSI=75. ....	91
Figure 7-26: Total displacements for bolt and shotcrete supported tunnel. Model GSI=75. ....	91
Figure 7-27: Deformed geometry for unsupported tunnel. Model GSI=75 (scale: x20). ....	92
Figure 7-28: Deformed geometry for bolt supported tunnel. Model GSI=75 (scale: x20). ....	92
Figure 7-29: Deformed geometry for bolt and shotcrete supported tunnel. GSI=75 (scale: x20). ....	92
Figure 7-30: Yielded elements for unsupported tunnel, GSI=50. ....	95
Figure 7-31: Yielded elements for bolt supported tunnel, GSI=50. ....	95
Figure 7-32: Yielded elements for bolt and shotcrete supported tunnel, GSI=50. ....	95
Figure 7-33: Total displacements for unsupported tunnel, GSI=50. ....	96
Figure 7-34: Total displacements for bolt supported tunnel, GSI=50. ....	96
Figure 7-35: Total displacements for bolt and shotcrete supported tunnel, GSI=50. ....	96
Figure 7-36: Deformed geometry for unsupported tunnel, GSI=50 (scale: x5). ....	97
Figure 7-37: Deformed geometry for bolt supported tunnel, GSI=50 (scale: x5). ....	97
Figure 7-38: Deformed geometry for bolt and shotcrete supported tunnel, GSI=50 (scale: x5). ....	97
Figure 7-39: Cross section part of the Fáskrúðsfjörður tunnel from Reyðarfjörður side, station 6530 is located on the right side of the figure [36]. ....	99
Figure 7-40: Tunnel cross section of station 6530, the dimensions are in meters. ....	100
Figure 7-41: Support setup for station 6530, based on rock bolts and shotcrete reports. ....	101
Figure 7-42: Yielded elements for unsupported model from station 6530. ....	102
Figure 7-43: Yielded elements for 80% stress relief model from station 6530. ....	102
Figure 7-44: Yielded elements for full supported and full stress relieved model from station 6530. ....	102
Figure 7-45: Total displacements for unsupported model from station 6530. ....	103
Figure 7-46: Total displacements for 80% stress relief model from station 6530. ....	103
Figure 7-47: Total displacements for full supported and full stress relieved model from station 6530. .....	103
Figure 7-48: Deformed geometry for unsupported model from station 6530 (scale: x30). ....	104
Figure 7-49: Deformed geometry for 80% stress relief model from station 6530 (scale: x30). ....	104
Figure 7-50: Deformed geometry for full supported and full stress relieved model from station 6530 (scale: x30). ....	104
Figure 7-51: Rock bolts from the practical support (1-10) and additional rock bolts (11-18). ....	106
Figure 7-52: Axial force in rock bolts in the tunnel walls in supplementary support model 1. ....	106
Figure 7-53: Rock bolt setup, additional rock bolts (19-22). ....	107
Figure 7-54: Axial force in rock bolts in the tunnel walls in supplementary support model 2. ....	107

Figure 7-55: Cross section part of the Fáskrúðsfjörður tunnel from Fáskrúðsfjörður side, station 7615 is located on the left side of the figure [36]. .....	109
Figure 7-56: Tunnel cross section of station 7615, the dimensions are in meters. ....	110
Figure 7-57: Support setup for station 7616, based on rock bolts and shotcrete reports.....	110
Figure 7-58: Yielded elements for unsupported model from station 7615.....	111
Figure 7-59: Yielded elements for 80% stress relief model from station 7615. ....	111
Figure 7-60: Yielded elements for full supported and full stress relieved model from station 7615. ....	111
Figure 7-61: Total displacements for unsupported model from station 7615.....	112
Figure 7-62: Total displacements for 80% stress relief model from station 7615. ....	112
Figure 7-63: Total displacements for full supported and full stress relieved model from station 7615. ....	112
Figure 7-64: Deformed geometry for unsupported model from station 7615 (scale: x40). ....	113
Figure 7-65: Deformed geometry for 80% stress relief model from station 7615 (scale: x40). ....	113
Figure 7-66: Deformed geometry for full supported and full stress relieved model from station 7615 (scale: x40).....	113
Figure 7-67: Rock bolts from the practical support (1-9) and additional rock bolts (10-15).....	115
Figure 7-68: Axial force in rock bolts in the tunnel roof corners in supplementary support model 1. ....	115
Figure 7-69: Rock bolt setup, additional rock bolts (16-19). ....	117
Figure 7-70: Axial force in rock bolts in the roof corners for supplementary support model 2. ....	117



## List of Tables

Table 2-1: Classification of igneous rock [4].	4
Table 2-2: Icelandic basalt classified according to rock engineering properties [6].	7
Table 2-3: Comparison of typical characteristic of Tholeiite and Olivine basalt [5].	8
Table 2-4: Sediment classification by grain size [4].	10
Table 3-1: Some geotechnical properties of Icelandic rocks [8].	14
Table 4-1 [20].	30
Table 4-2: Classification of RMR values [22].	32
Table 4-3: Recommended value for ESR [24].	36
Table 4-4: Most common values and ranges of Q indexes for different rock types from Hvalfjarðar tunnel [27].	38
Table 4-5: Advantages and disadvantages for dry mix and wet mix methods [33].	47
Table 5-1: Results from stress measurements in the Fáskrúðsfjörður tunnel [38].	65
Table 5-2: Theoretical stress values [38].	65
Table 6-1: Strength parameters from rock cores tested from the Fáskrúðsfjörður tunnel	75
Table 6-2: Strength parameters from Kárahnjúkar project analysis [5].	75
Table 7-1: Additional parameters in <i>RocLab</i> .	78
Table 7-2: Input parameters for elastic part modelled in <i>Phase2</i> .	78
Table 7-3: Input parameters for elastic-plastic part modelled in <i>Phase2</i> .	84
Table 7-4: Yielded elements and total displacements for various GSI values.	88
Table 7-5: Material properties for the grouted rebar rock bolt.	89
Table 7-6: Material properties for the shotcrete.	89
Table 7-7: Yielded elements and total displacements for various support types for GSI=75.	93
Table 7-8: Yielded elements and total displacements for various support types for GSI=50.	98
Table 7-9: Input parameters for station 6530 in <i>Phase2</i> .	100
Table 7-10: Yielded elements and total displacements for various models from station 6530.	105
Table 7-11: Maximum total displacements in red sediment layer in left and right wall.	108
Table 7-12: Yielded elements and total displacements for various models from station 7615.	114
Table 7-13: Maximum total displacements in scoria layer in left and right roof corner.	118



## 1 Introduction

Icelandic rock mass stratum consists in general of relatively thin layers. Tunnel faces are therefore frequently mixed faces with different mechanical properties. During tunnel excavations the surrounding rock mass expands due to the stress release. Stress concentrations can therefore take place at layers interfaces as their mechanical properties differ. This is highly dependent on the local geometry such as layer thickness, inclinations etc. as well as the in situ stress situation. As this affects the development of stresses around openings due to excavation this affects the support measures of the surrounding rock mass.

The aim of the project is to investigate by means of numerical analyses the reliability and the quality of the reinforcement used in the Fáskrúðsfjörður tunnel in Eastern Iceland. The Fáskrúðsfjörður tunnel is 5,7 km long horse shoe shape drilled and blast road tunnel. It is the only road tunnel in Iceland where stress measurements have been carried out during the excavation. In the modelling phase of this thesis three different models are analysed, a typical Icelandic mixed face model and two models with cross sections from the Fáskrúðsfjörður tunnel where stress measurements were performed. The finite element program *Phase2* is used in the modelling, parallel to *RocLab*.

To gather information about the rock mechanical properties for the rock from the Fáskrúðsfjörður tunnel, a laboratory dataset from headrace tunnel in Kárahnjúkar was analysed. Also some rock cores from borehole FF-04, drilled inside the Fáskrúðsfjörður tunnel, were transported from the Icelandic Road Administration at Reyðarfjörður to the Technical University of Denmark, where Brazil tests, Unconfined Compression tests and Triaxial tests were performed on various rock types and compared with the analysis from headrace tunnel in Kárahnjúkar.

## 2 The Geology of Iceland

Iceland is situated on the Mid Atlantic ridge on the rifting plate boundary between the Eurasian and North American plates. When the plates drift apart, the gap between them is constantly filled with extrusive and intrusive igneous rock. The active zone of rifting and volcanism crosses the country from the southwest Reykjanes peninsula to the northeast where it connects with the Iceland-Jan Mayen ridge, see Figure 2-1. Iceland is geologically very young and all of its rocks were formed within the past 25 million years. This makes the geology in Iceland very different from other countries in Scandinavia. The stratigraphical succession of Iceland spans over two geological periods, the Tertiary and the Quaternary periods. The oldest rock at the surface in Iceland are from late Tertiary time, about 15 million years old, and are found in the northwest and eastern coast of the island. The closer to the rifting plate boundary, the younger the rock [1].

The surface of Iceland has changed radically during its existence. The forces of nature that constantly mould and shape the face of the Earth operate faster in Iceland than in most other places. The rocks are shattered by the frequent change between frost and thaw, and the wind, seas and glaciers laboriously grind down the land. Erosion removes about one million cubic meters of land from Iceland each year, but volcanic activity and sedimentation more then counterbalances this loss [2].

### 2.1 The Volcanic Activity in Iceland

The volcanic activity in Iceland is attributed to the combination of Mid Atlantic Ridge activity and hot spot activity. Iceland is one of the most active volcanic regions on Earth. It is estimated that one third of lava erupted during the last 500 year was produced in Iceland. There are 35 volcanoes that have erupted in Iceland in the last 10.000 years. Lava produced during this time covers about 10.000 km<sup>2</sup>, which is approximately 10% of the area of Iceland, and altogether around 400 km<sup>3</sup> of volcanic products, have been produced. On average, a volcano erupts about once every 5 years [3],[4].

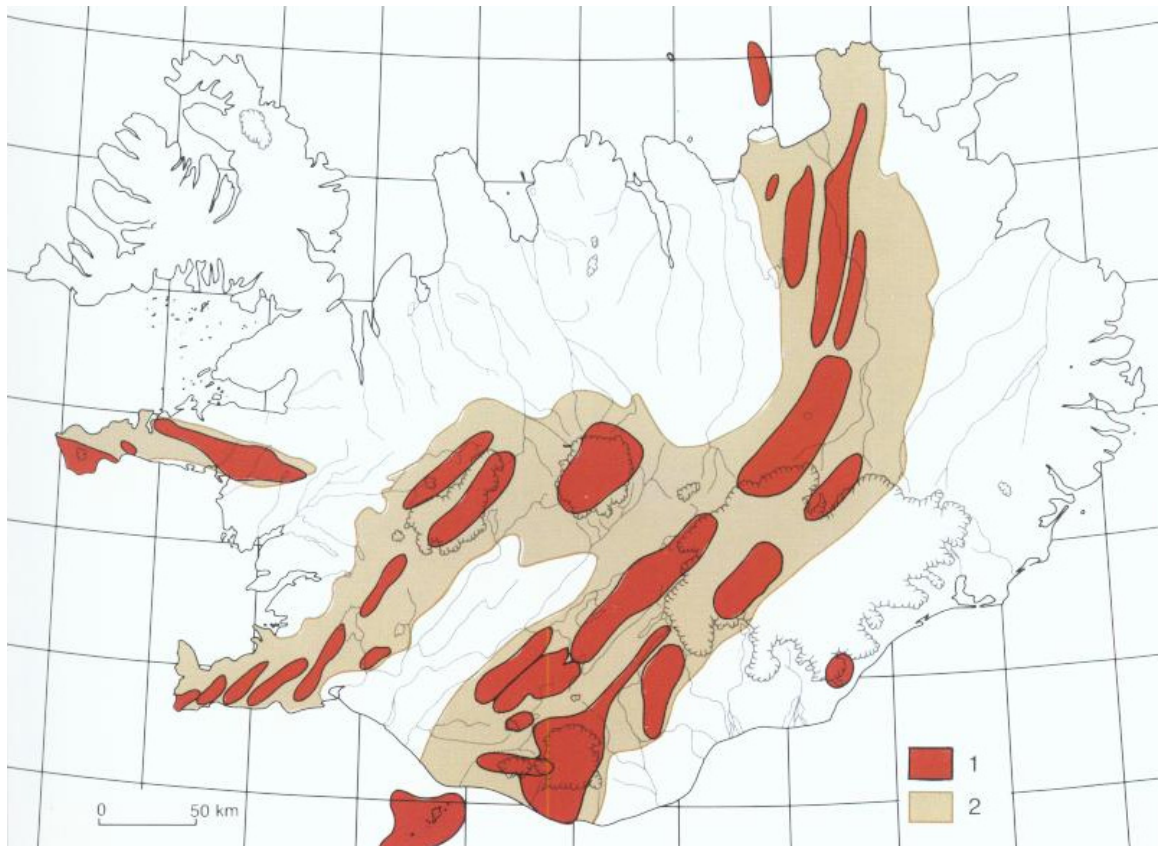


**Figure 2-1: Active volcanic systems in Iceland. 1) Individual volcanic systems and 2) active volcanic zones [4].**

## 2.2 Icelandic Bedrock

Rocks vary greatly in appearance either due to their internal structure, grain size and crystal size, or to their external structure such as bedding, flow banding or columnar size. Rocks are divided into three main groups according to its origin.

- Igneous rocks which are formed by solidification of magma, either at depth forming plutonic rock, at shallow depth forming dike rocks, or at the surface forming volcanic rocks.
- Sedimentary rocks are formed by accumulation of rock debris, sediments or clastic rocks (e.g. sandstone).

- Metamorphic rocks which are formed by recrystallisation of igneous or sedimentary rock deep within the Earth's crust, especially during fold mountain movements. Metamorphic rock can not be found in the Icelandic bedrock.

The greater part of the Earth's crust is made of igneous rock. It is primary rock of which other rocks are formed through weathering, erosion or recrystallisation. In the classification of igneous rock two factors are dominating, the silica content ( $\text{SiO}_2$ ) and the solidification [4], see Table 2-1.

**Table 2-1: Classification of igneous rock [4].**

----- $\text{SiO}_2$ - silica content----->				
		Basic <52% $\text{SiO}_2$	Intermediate 52-65% $\text{SiO}_2$	Acid > 65% $\text{SiO}_2$
Solidification	Volcanic rock	Basalt	Andesite	Rhyolite
	Dike rock			
	Plutonic rock	Gabbro	Diorite	Granophyre/ Granite
Rock forming minerals		Plagioclase, pyroxene, olivine, magnetite		Quartz, orthoclase, plagioclase, mica

From the silica content, igneous rock are classified as basic when they have less than 52% silica content, intermediate with 52% - 65% silica content and acid with more than 65% silica content.

The Icelandic bedrock consist of primary numerous, extensive but relatively thin basaltic lava flows, lying on top of each other, interbedded with subordinate acidic rock and relatively thin sedimentary beds. The bedrock's overall composition is as follows [5]

- 80-85 % basalt lava flows.
- 10 % acidic and intermediate rocks.
- 5-10 % sedimentary interbeds resulting from erosion and transport of volcanic rocks. Mainly consolidated tuff and eolian soil and to some extent sandstones and conglomerates.

### 2.2.1 Basalt

Each lava flow may be divided into three parts as follows

- The top scoria, often 10-25 % of the lava flow thickness.
- The dense crystalline middle part, often 60-85 % of the lava flow thickness.
- The bottom scoria, often 5-10 % of the lava flow thickness.

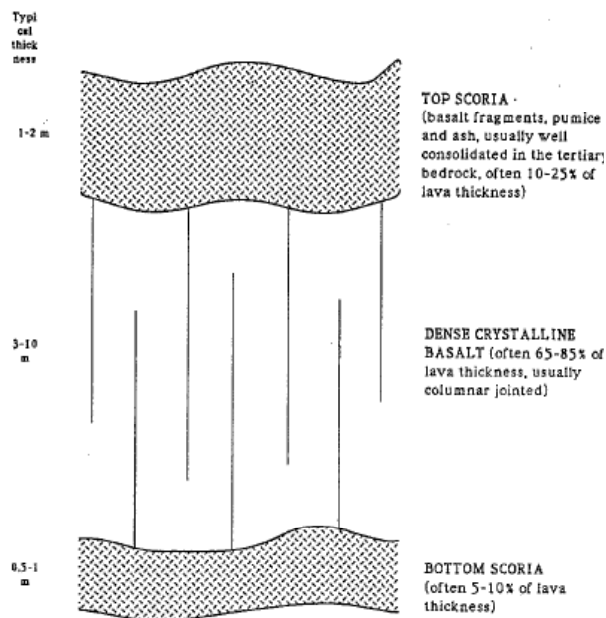


**Figure 2-2: Schematic structure of a single basalt lava [1].**



**Figure 2-3: Typical Icelandic basalt rock mass, above Blanda tailrace canal.**

The top scoria is to the uppermost portion of the lava flow, characterized by rapid cooling and brutal expansion of gas. The matrix of scoria is highly vesicular and glassy, almost uncrystallised. The structure is chaotic, with large voids of various sizes, some up to several meters. When the subsequent deposition of sediment occurred, these voids were infiltrated and filled with sand and silt. Palagonitisation later cemented the sediment into a sandstone and gives the rock mass a relatively compact aspect. In cores the top scoria often has the aspect of a matrix supported breccia with scoria fragments. The vesicles in the scoriaceous

fragment are also often filled with secondary zeolites or calcite. The scoria can easily be recognized due to its particular structure and due to reddish, orange and greenish colour, which is in contrast with the grey colour of the basalt [1],[5].

The crystalline middle part consists of hard, dense basalt and its colour varies from light to dark grey. The rock is usually affected by sub vertical columnar jointing, resulting from the cooling of the lava. The joint frequency is low for large columnar jointed basalts where spacing of columnar joints can be 1-2 m. For small columnar jointed basalts, the frequency is high or 0,1- 0,3 m and then its called sugar cube structure. The joint surfaces are usually smooth to slightly rough [1],[5].

The bottom scoria is most often relatively thin, well consolidated, sometimes containing sandstone fillings, mixed up from underlying sediments [1],[5].

The basalt was classified by to G. L. P. Walker in 1959 and has since then been referred to as the Walker's classification system [6]. The basalt is classified based on petrology and texture of the rock and is divided into three different petrographic types

- Tholeiite basalt.
- Olivine basalt.
- Porphyritic basalt.

The Walker's classification system does not focus on the structure of the basaltic layer, e.g. thickness, columnar width, thickness of top and bottom scoria, etc. which are more important for engineering purpose. In 1992 the idea came along of dividing the three main types into six basalt types [6]. By classifying the bedrock from the start into these six types instead of three types, and using them already from the first draft of the geological bedrock map in the draft profiles and cross sections, a much better geotechnical information is provided for geotechnical engineers. In Table 2-2 the six basalt types are listed.



**Table 2-2: Icelandic basalt classified according to rock engineering properties [6].**

Traditional field mapping of Icelandic basalts*	Proposed Legend on map	Proposed 'geotechnical' field mapping of basalt in Iceland	Structural / Mechanical properties		
			Scoria content [%]	Common thickness of lava unit [m]	Common uniaxial compressive strength [MPa]**
Tholeiite basalt	Thl	Tholeiite, thin layered, (associated with central volcanoes)	25 - 35	3 - 8	>200 (150-300)
	Tht	Tholeiite, thick layered (regional)	15 - 20	10 - 20	>200 (150-300)
Porphyritic basalt	Pom	Porphyritic basalt esp. Massive (phenocrysts > 10% by volume)	1 - 5	10 - 20	200 (100-300)
	Pob	Porphyritic basalt (phenocrysts < 10% by volume)	5 - 15	10 - 20	200 (100-300)
Olivine tholeiite (Olivine basalt)	Olt	Olivine basalt (Olivine tholeiite)	5 - 15	10 - 20	200 (100-300)
	Olc	Compound lavas (from lava shield volcanoes)	0 - 5	20 - 80	100 (80-140)

\* According to G.P.L. Walker (1959)

\*\* Fresh basalt

According to Table 2-2 the tholeiite basalt is divided in thin layered tholeiite, which is usually associated central with volcanoes, and thick or regional tholeiite. The difference between these two types is that the columnar part of the thin layered tholeiite is much more jointed than of the thick tholeiite, forming much smaller blocks. Also the percentage of cemented scoria at the top and bottom of each lava flow is higher in thin tholeiite than in the thick tholeiite. The cemented scoria contains very few joints even though tholeiite is the most jointed basalt type. Therefore, a rock core of tholeiite basalt lava flows therefore consists frequently of 60 % - 85 % of very jointed, hard and brittle, columnar tholeiite and 15 % - 40 % of sparsely jointed, clastic scoria, well cemented and also showing lower Young's modulus than the intact material of the columnar tholeiite [6].

There is great difference between the massive and porphyritic basalt, also known as porphyry, and the less porphyritic basalt which is very similar to olivine tholeiite in structure. The porphyry can contain large phenocrysts often over 10 %

of the total rock volume. The porphyry is much more massive in structure and is often used as armour stones for breakwaters.

The last type, olivine basalt, is divided in olivine basalt and compound lavas. These two subtype are very different in structure and therefore with very different qualities to engineering work. But according to petrologically and geochemically parts, they belong to the same basalt type [6].

**Table 2-3: Comparison of typical characteristic of Tholeiite and Olivine basalt [5].**

<b>Tholeiite</b>	<b>Olivine basalt</b>
Very fine grained	Coarse grained
Free olivine crystals are absent	Free olivine crystals visible
Total silica content: 48-50%	Total silica content: 46-48%
Weathered crust, pale brown	Weathered crust, dark brown to deep grey
Spheroidal weathering uncommon	Spheroidal weathering common
Amygdales rather without zeolites	Amygdales bear zeolites
Well developed flow structures	Less developed structures within flows
Microspores often arranged along sub horizontal surface with spacing < 1 cm resulting in faint cleavage	Microspores randomly scattered throughout the mass
Scoriaceous part of tholeiite basalt flows: usually 20-30% of the flow thickness	Scoriaceous part of olivine basalt flows: usually 5-15% of the flow thickness
Forms usually single lava flows	Forms both compound and single lava flows
Average thickness of lava flows:11 m	Average thickness of lava flows:10 m
Average width of columns: 2 m	Average width of columns: 1,5-2 m
Hardness of the dense matrix: I to II*	Hardness of the dense matrix: II*

**\*Hardness scale ISRM (1975)**

### 2.2.2 Acidic and Intermediate Rocks

As seen in Table 2-1 the most common acidic rocks are rhyolite and granophyre/granite. Rhyolite is usually grey, yellow or pinkish in colour which appears as light patches on mountains. Rhyolite is always microcrystalline or glassy, vesicular and flow banded, the bands often being in various colours. Granite appears always coarsely crystalline, while granophyre is finely crystalline. Granite is usually light grey reddish coloured with dark patches [4]. Rhyolite is divided into three groups based on engineering propose [6]

- “Sound” rhyolite, which is a competent rock in spite of being extremely jointed and flow banded.

- Altered and decomposed rhyolite, up to what geotechnical engineers call squeezing rock.
- Rhyolite ash, can make up formations reaching tens of meters in thickness, but generally poorly cemented and therefore very bad as tunnelling rock. However, well cemented tuff can be very compact and strong.

The altered and decomposed rhyolite and rhyolite ash can alter into clay materials, often resulting in swelling clay. During tunnelling the clay will expand when pressure is released and water is available. This type of rock should be avoided in tunnelling if possible [6].

Andesite and diorite are the intermediate rocks which can be found in Iceland. Diorite is rare in Iceland, but can be found in some places at Snæfellsnes peninsula. Andesite is a middle stage between rhyolite and basalt. Andesite is always flow banded, microcrystalline and very dark or black in colour, some confounded it with dark microcrystalline basalt [4]. For engineering propose in field it often looks very much like thick, densely flow banded tholeiite (Tht), see Table 2-2. Consequently, their engineering properties are similar. However, they should be distinguished if possible [6].

### **2.2.3 Sedimentary Interbeds**

Sediment is classified according to weathering mechanism, transport and how it accumulates into three main groups. Chemical sediment is formed by the precipitation of dissolved materials in the sea, lakes or soil. In Iceland there is little formation of chemical sediment apart from bog ore and calcareous travertine at warm mineral springs. Organic sediment is formed from plant and animal remains. When the organisms die their remains survive, often accumulating as thick beds, especially in the sea and in lakes where conditions are more favourable for their preservation than on dry land. Clastic sediments refer to rock composed of rock fragments. The classification is in various ways, firstly they are classified by grain size, the diameter of the grains of which they are composed. They are also classified according to means of transport and according to the mineral content. In Table 2-4 the classification for sediments by grain size is presented [4].

**Table 2-4: Sediment classification by grain size [4].**

<b>Grain diameter [mm]</b>	<b>Sediment</b>	<b>Sedimentary rock</b>
> 256	Boulders	Conglomerate
64 – 256	Stones	Stony breccia
2 – 64	Gravel	Breccia
0,063 – 2	Sand	Sandstone
0,004 – 0,063	Silt	Siltstone
< 0,004	Clay	Mudstone

Approximately 5-10 % of the Icelandic bedrock consists of sedimentary interbeds, they are presented as interbeds between the basalt layers. The most common types of sedimentary rocks in Iceland are made of silt (siltstone) and sand (sandstone and conglomerate). The thickness of the sediments can vary from few millimetres up to few meters. The sandy sediment are usually a good tunnelling rock, similar to weak concrete in strength and especially showing much greater tensile strength than the silty sediments. The fine grained interbeds are often reddish in colour or, in the case of rhyolitic ash layers, often yellow and greenish. The silty interbeds can show extremely low vertical tensile strength, so even 5 cm thick siltstone layers in between the basalts can cause serious stability problems in tunnels when they are located just above the tunnel roof. This can result in instability of a large block or wedges in the tunnel roof under the siltstone layer. One of the main reasons for the weakness of the siltstone layers is that some of the materials and glasses in the layers have altered into swelling clay materials that greatly reduce the tensile strength of the rock, especially the vertical tensile strength [6].

### 2.2.4 Other Rock Types

Móberg (Hyaloclastite) is the Icelandic term given to volcanic rocks that is formed in a water or glacial environment. Such type of volcanic eruption under high pressure causes formation of bodies with complex structure and composition. This type of formation has extremely irregular layering, the material is piled up over the eruptive event and a móberg formation from the same eruption usually displays many different rock faces, some with properties of clastic rock and others close to lava or minor intrusives. The five main groups of móberg are following [5]

- Pillow lava is made from volcanic eruption in water under relatively high water pressure. The magma flows as stream surrounded by a rapidly cooling crust. The structure of pillow lava forms a pile of elliptical or irregularly shaped pillows, of 0,3

- 1 m in diameter. A pillow consists of porous basalt cubes with dimensions ranging between 0,05 – 0,2 m. The space between pillows is filled with palagonitic tuff or fine grained agglomerate with fragment of glassy palagonite. Pillow lava bodies are normally highly pervious. When the ratio tuff/agglomerate is less than 20 % then is it defined as pillow lava. Tuff and agglomerates have a low bulk density.

- Pillow breccia consists of pillows and a matrix of tuff or agglomerate. This forms 20 – 70 % of the rock mass. In the higher range, the breccia is often matrix supported. With increasing proportion of the matrix the permeability of pillow breccia decreases.

- Cube jointed basalt occur as intrusion in the cooling pillow lava. Cube jointed basalt are systematically porous to vesicular basalt, with typical three sets of highly discontinuous joints dividing the rock mass into cubes with 0,1 – 0,5 m side length. Because of their high degree of jointing, cube jointed basalts are pervious.

- Tuff breccia consists of a palagonitic, tuffaceous matrix with up to 30 % fragments of crystalline basalt. The tuff breccia is formed under low water pressure, and has a relatively low bulk density and a low permeability.

- Móberg tuff is a glassy palagonite sediment, almost entirely of volcanic origin. Usually transported over a short distance that can build up thick stratified formations [5].

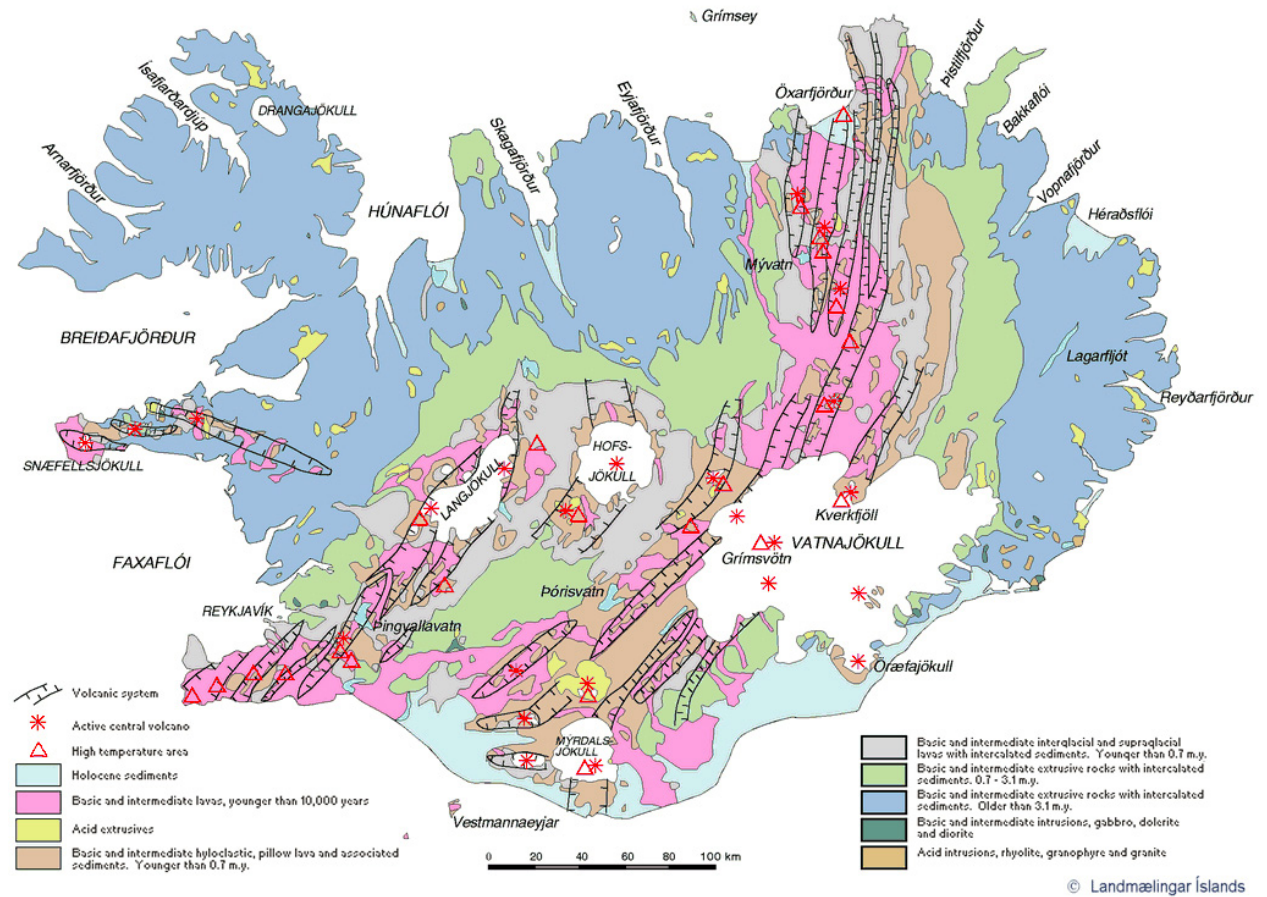


Figure 2-4: The Icelandic geological formation [7].

### 3 Icelandic Conditions for Tunnelling

In the following subchapters the main geological features and geotechnical problems related to tunnelling in Icelandic bedrock will be discussed.

#### 3.1 Mixed Face

As mentioned earlier, the Icelandic rock mass stratum consists in general of relatively thin layers. Due to that condition and the gentle dip of layers, often  $3^\circ$  -  $8^\circ$ , the tunnel faces consist frequently of mixed faces with different mechanical properties. A tunnel face can simultaneously be made out of two to four different rock types. Figure 3-1 and Figure 3-2 presents a typical mixed tunnel face [1].

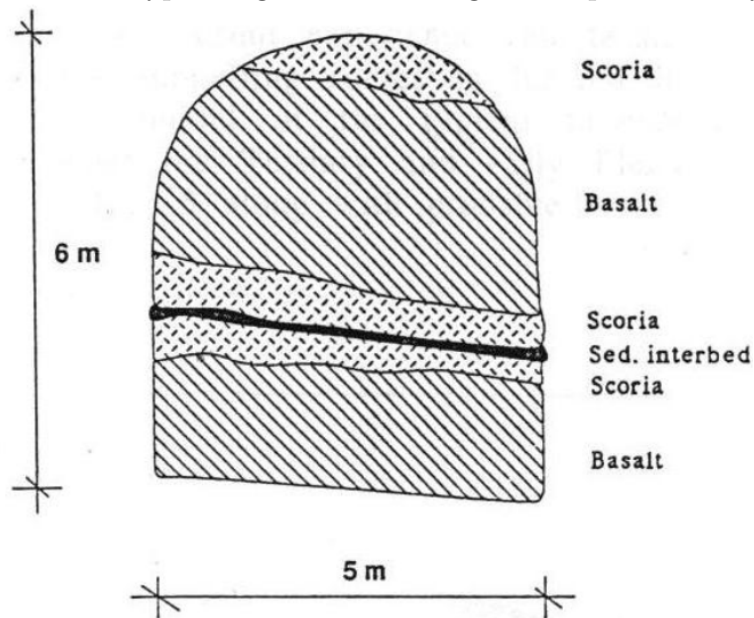


Figure 3-1: Typical mixed face for Icelandic conditions [1].



Figure 3-2: Mixed face from Fáskrúðsfjörður tunnel. At the top there is sediment underlain by a thin basalt layer, then another sediment layer and finally scoria from the middle to the bottom [46].

The rock types displayed in Figure 3-1 and Figure 3-2 have different geotechnical properties, in Table 3-1 some of the main properties are presented.

**Table 3-1: Some geotechnical properties of Icelandic rocks [8].**

<b>Properties</b>	<b>Basalt</b>	<b>Scoria</b>	<b>Sed. Rock Fine grained</b>	<b>Sed. Rock Coarse grained</b>	<b>Fault Breccias</b>
UCS [MPa]	100-300	10-50	5-30	5-80	1-20
Q-value [NGI]	5-15	3-10	0,1-3	0,5-4	0,01
Drillability [DRI]	Very low – med.	High	High	Med.	High
Abrasiveness [BWI]	Low-med.	Low	Low	Low	Low
Young's modulus, E [GPa]	20-60	2-20	2-10	2-15	-
Typical strata thickness [m]	4-15	0,5-4	0,2-5	1-10	0,1-2

In Table 3-1 UCS is uniaxial compression strength and the Q value is based on the Q system developed by the Norwegian Geotechnical Institute, DRI stands for drilling rate index and BWI is bit wear index. See further in chapter 4.

It is obvious from the table above that the properties differ between rock types. The basalt has high strength and stiffness but the scoria and the sediments much lower. The fault breccias gives in general the worst result. So it is very important to have a good understanding of the characteristics of the rock mass when designing a tunnel.

When excavation is carried out in a thin layered bedrock, which dips around 3°-8°, the direction of the excavation matters. The thin sedimentary interbeds usually have very low tensile strength, close to zero. It is very hazardous to have these weak layers located near the tunnel roof, which increases the possibility of wedges and blocks to move forward and fall from the roof, Figure 3-3. When excavating in the opposite direction to the dip, i.e. up dip, interbeds can be seen on the face and walls before excavating under them and supports can be installed. On the other hand, if the excavation is in the same direction as the dip, i.e. down dip, the interbeds can not be seen prior to the excavation and the risk of fall out is greater [9].



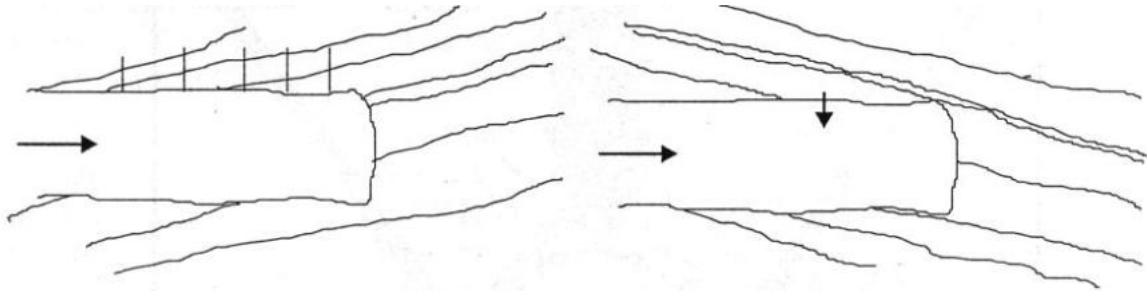


**Figure 3-3: To left, excavation opposite to dip direction. To right, excavation in the same direction as dip [9].**

## 3.2 Groundwater

A groundwater flow into a tunnel during the excavation can have serious consequences, whether it affects the stability during construction or after. A great groundwater flow into a tunnel can also cause a long delay in the construction, while draining of the tunnel is performed. Recognition and understanding of the geology of the tunnelling bedrock is essential for the prediction approach and evaluation of the groundwater condition that are encountered during the tunnelling work. It is necessary to map the most water bearing sites in the bedrock during the preliminary studies. The typical Icelandic basaltic rock mass is relatively pervious. The groundwater runs along the lava contacts, cooling joints and tectonic discontinuities (intrusive dykes and faults), see Figure 3-4. The tectonic discontinuities function as the main natural drains because of their continuity through the lava pile. The sedimentary interbeds on the other hand act as impervious – semi pervious barriers between the jointed lava joints [1].

Flow of groundwater into tunnels is often divided into regional inflow or seepage along the tunnel line mainly controlled by the stratigraphy of layers and joints, and inflows from water bearing discontinuities. Regional inflows are relatively small and decrease slowly with time, whereas inflow from water bearing discontinuities can be catastrophic but decreases normally rapidly with time, depending on fracture and extent [10].

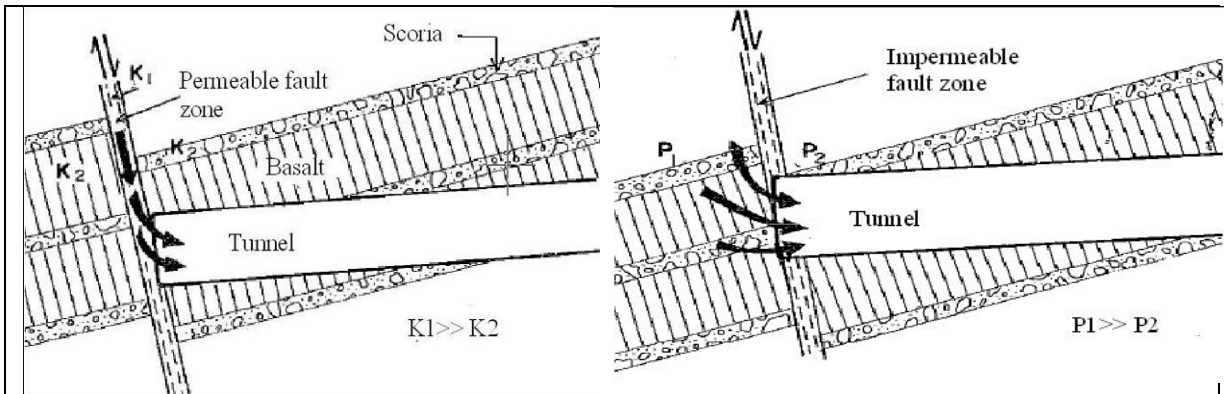


**Figure 3-4: Two different types of inflow into tunnels. To left, a permeable fault zone where  $K$  is the permeability. To right, impermeable fault zone where  $P$  is the pore water pressure [11].**

As previous mentioned, faults can cause serious water problem during tunnelling. Faults are classified in four different types based on their permeability [10].

- Aquicludes, yielding no water when excavation is made through the fault.
- Aquicludes/aquifers, yielding water when excavation is made past the discontinuity. Fault breccia is usually a water barrier and high water pressure is maintained behind the breccia until excavation is made through it.
- Aquifers not connected to potential source of water. Discharge is high when excavation is made into the discontinuity but is gradually dried.
- Aquifers which are connected to potential source of water supply. Discharge is maintained for unlimited period of time.

It is common that two or more of these types appear during construction of a tunnel. Therefore, understanding of the geology of the tunnelling bedrock is essential for the prediction approach and evaluation of the groundwater conditions that are encountered during tunnelling.

### 3.3 Rock Stresses

The vertical stresses result from the weight of the overburden rock mass, see Figure 3-5. The vertical stresses can be estimated from

$$\sigma_v = \gamma \cdot z = 0,027 \cdot z \quad (3.1)$$

where  $\gamma$  is the unit weight of the rock mass which is usually about  $0,027 \text{ MN/m}^3$  and  $z$  is the depth from the surface in meters. The effective vertical stress is defined

$$\sigma'_v = \sigma_v - u \quad (3.2)$$

where  $u$  is the pore pressure at depth  $z$ . The effective horizontal stresses acting on rock mass element are much more difficult to estimate rather than the vertical stresses. The effective horizontal stress can be calculated from the product of the effective vertical stress and the rock stress coefficient, see equation (3.3).

$$\sigma'_h = K_0 \cdot \sigma'_v \quad (3.3)$$

where  $K_0$  is the rock stress coefficient at rest [12].

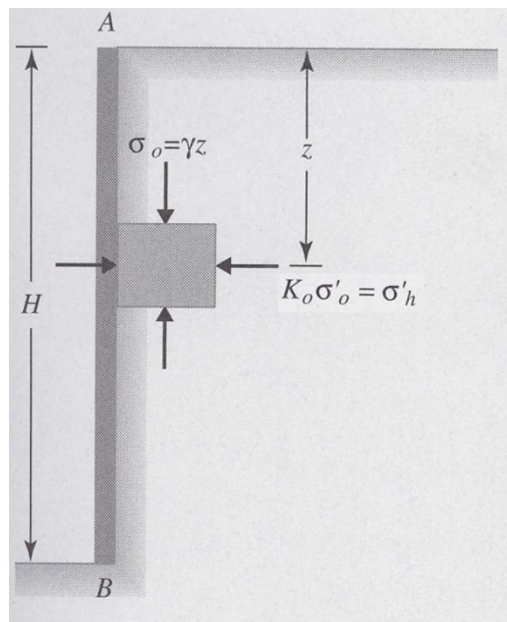


**Figure 3-5: Stresses in the rock mass at depth  $z$ , where  $\sigma_o = \sigma_v$  [12].**

The stress behaviour in the upper lithosphere of Iceland is to great extent explained by topographic relief and does not reflect the state of stress resulting of continental plate drifting mechanism. Factors like volcanism, pile up of basaltic

lavas and ice cover have built up stresses in the rock mass whereas tectonics, continental drift, erosion and isostasy have released the stresses.

Stresses increases while younger jointed basaltic rock layers piles up on the older layers. The rock mass drifts away from the active zone towards east and west, where magma intrusions are frequently penetrated, locally building up higher horizontal stresses than induced by gravity. The erosion carves the surface, the weight of the overlying rock mass is relieved but the horizontal stress relaxation is restricted by the intrusions and fillings within the rock mass [13].

Deformation measurements during 1987-2003 in the underground powerhouse at Blanda show that the relaxation of the Icelandic rock mass can continue for several years after construction of a large opening, see Figure 3-6. Impounding of the tunnel and minor vibrations from the engines can truly increase these deformations. Greatly fractured rock mass with clay filled joint and faults, together with soft scoria and sediments layers in between the basalt layers is most likely to be the cause of this long time creeping of the rock mass [13]. The deformation measurements were recorded at around 220 meters depth.

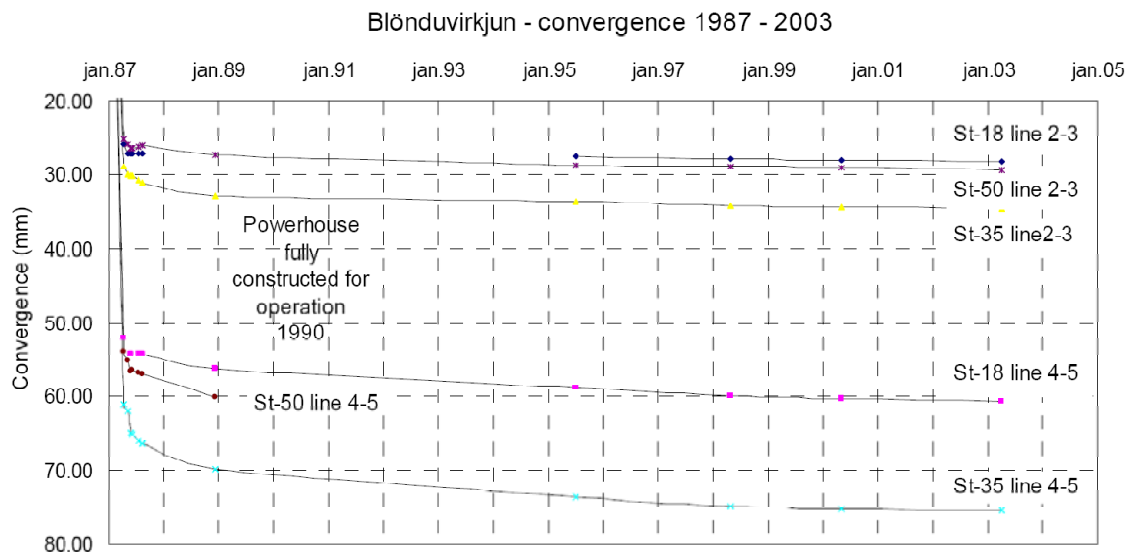


**Figure 3-6: Six different deformation measurements at Blanda powerhouse cavern, time dependent convergence after approximately half year diminishes to < 10 mm [13].**

Stress measurements in Iceland corresponds to values for a relatively low Young's modulus, Figure 3-7. This is in agreement with derived values from dynamic measurements and estimations based on degree of fracturing and rock mass classification for the highly jointed rock mass. Because of the high degree of

fracturing and intermediate layers of soft sedimentary rock and scoria, the Young's modulus for the rock mass is normally lower in Iceland than in the Scandinavian countries. This is the reason for greater deformations in underground openings for similar size openings under otherwise similar stress conditions.

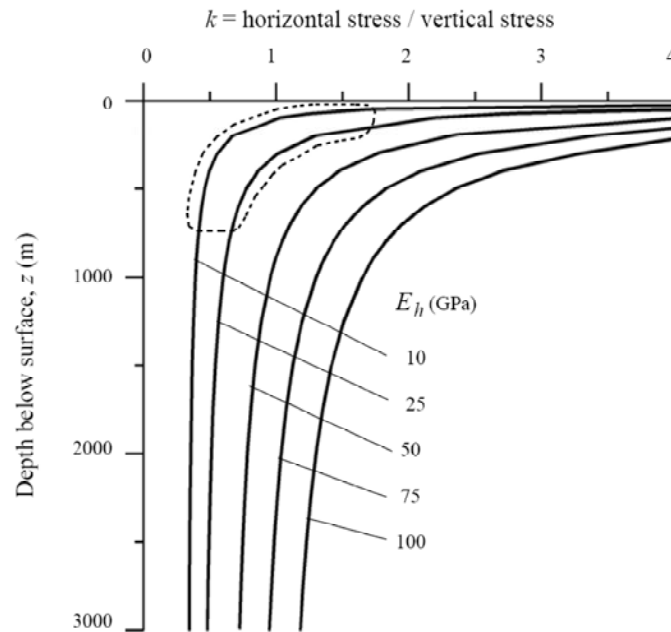


**Figure 3-7: Stress ratio  $K_0$  as function of depth and horizontal Young's modulus  $E_h$ . Measurements in Iceland are normally within the dotted area [13].**

The rock wall deformations and rock load surrounding the power station cavern for the Kárahnjúkar 690 MW hydroelectric power plant were monitored during and after the excavation phase. Extensometers and convergence points were installed in four sections and load anchors were installed in one section in the power station. The geology of the cavern area is typical for the Tertiary rock mass in Iceland and consist of hard basaltic rock layers with scoria and sedimentary rock interbeds. In addition, vertical or sub-vertical tectonic fractures, faults and dikes cut through the rock mass.

The largest deformation recorded was 170 mm during one and a half year close to the middle of the cavern at station 47, at level 25 m a.s.l. After installation of the measurement devices the greatest rate of deformation was 4-6 mm/day but after a year the average rate was 0,01 mm/day. Figure 3-8 illustrates these measurements which were recorded during one and a half year at around 500 m depth [13]. The cavern's height is 35 meters and it is 120 meters long with width of 14 meters.

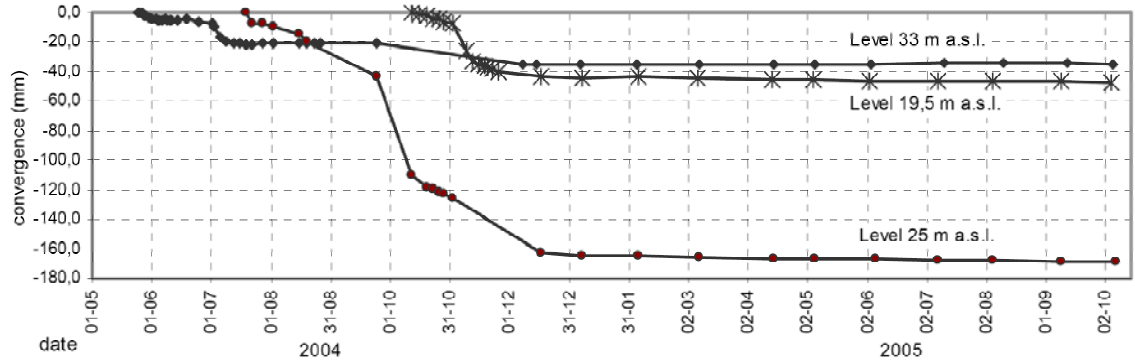


**Figure 3-8: Deformation measurements from Kárahnjúkar cavern at station 47 [13].**

Deformation measurements showed that the deformations are not only controlled by the geometry of the tunnel complex, but also to a great extent, controlled by the complexity in the geology. The weaker layers of scoria were pressed together with the load partly being transferred to the sub-vertical dikes.

Based on rock density measurements on core samples the average vertical in situ stress gradient is 0,027 MPa/m which gives a vertical stress of 13,5 MPa at 500 m where the Kárahnjúkar powerhouse is located. Hydrofracturing tests from 1998 and 1981 indicate that the horizontal stresses were between 5 and 6 MPa at that depth. After using typical input in a finite element program the results for vertical stresses were 15 MPa and 5-7 MPa for horizontal stresses. During construction of the cavern, in situ rock stress measurements were carried out to get better understanding of the behaviour of the Icelandic bedrock. The overcoring method was applied. The outcome from the measurements indicated that the vertical stresses were 9,4 MPa and the horizontal stresses were tensile -5,8 MPa for minimum value and -0,8 MPa for maximum value. This is lower than from the other measurements, and it is hard to believe that the horizontal stresses can be negative (tension). Possible cause of this error is that the basaltic layers are heavily jointed of varying intensity and contain some clay fillings, also the basalt contains small gas pores which, if in contact with a strain gauge, may influence the results. This confirms that it is necessary to apply more than one type of measurement in order to get as accurate outcome as possible [13].

Around 1980, some rock stress measurements from three different hydro power stations in Iceland were made, the results are displayed in Figure 3-9. From surface to 180 m depth the vertical and horizontal stresses are almost equal, but at greater depth the vertical stress becomes much greater than the horizontal stress. At the depth 500 m the vertical stress is 13 MPa and the horizontal one is only 5 MPa, giving the earth pressure coefficient  $K$  as 0,39. This is a low value compared to other parts of the world [11].

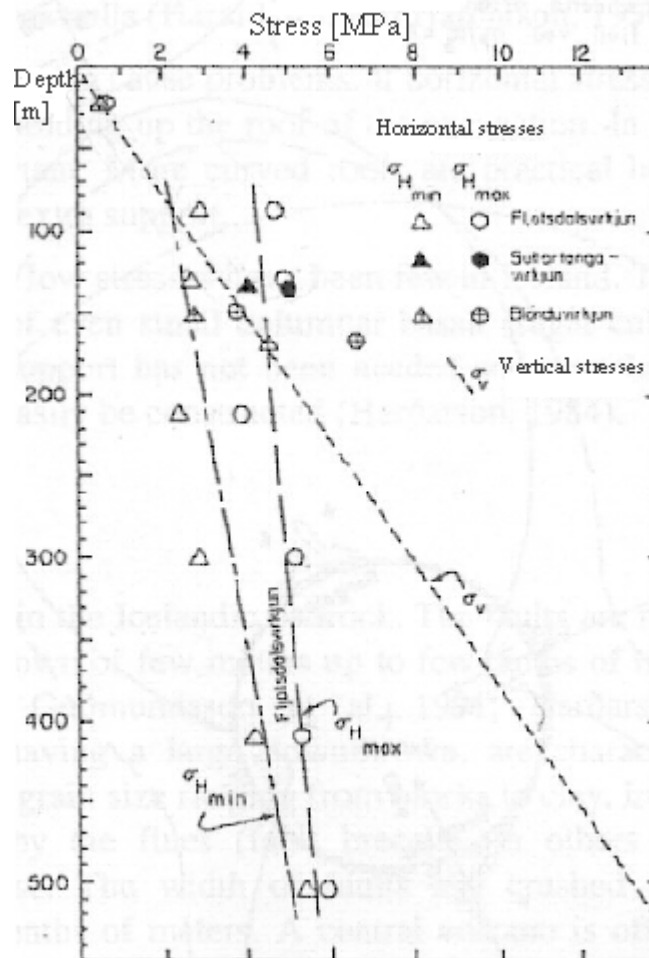


**Figure 3-9: Rock stress measurements with hydraulic fracturing from hydropower stations sites in Iceland [11].**

So far carried out the measurements of horizontal stresses in Iceland indicate that the horizontal stresses are much lower than in most other places in the world. Figure 3-10 illustrates the horizontal movements based on repeated GPS measurements from 1993 to 2004 by the National Land Survey of Iceland [14].

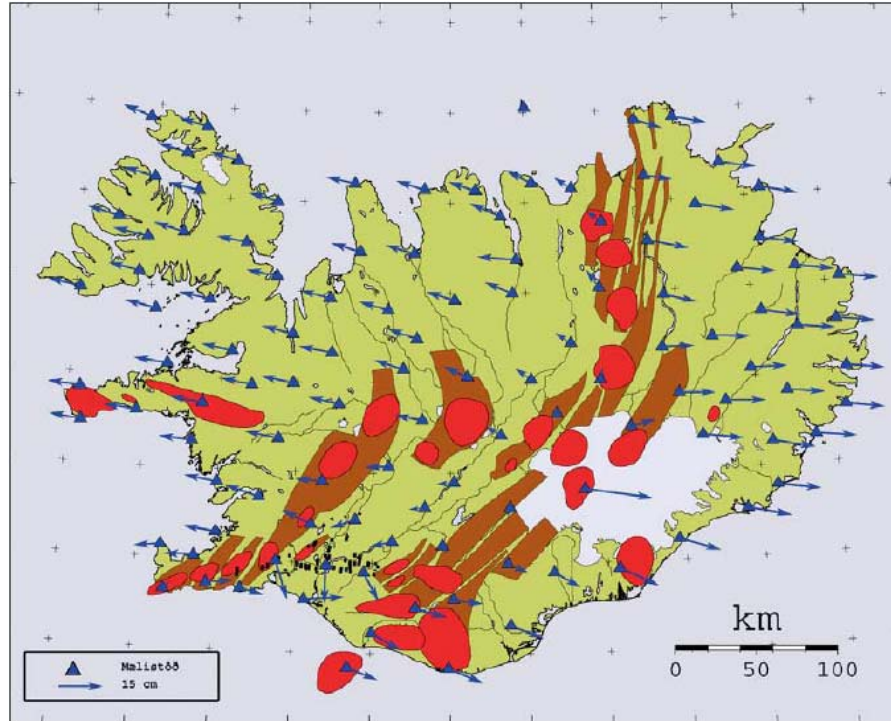


**Figure 3-10: Horizontal movements in Iceland during the time period 1993 to 2004 based on repeated GPS measurements, the blue triangles are measurement stations. The brown and red zones are discussed in Figure 2-4 [15].**

### 3.4 Faults

Faults are common in the Icelandic bedrock. They are characterized by sheared, crushed rock, with grain size distribution ranging from blocks down to clay. In some faults, the coarse grained crushed material is well cemented by fines (fault breccia), in others the crushed material is weathered and loose. The width of fault varies between 0,5 m up to tenths of meters. The faults are mostly sub vertical normal faults with downthrown of few meters up to few tenths of meters. Around central volcanoes, dykes and faults swarms are common. These systems have often tendency to follow one orientation, in south Iceland the fault swarms follow SW-NE but those on the north part of the country follows S-N trend, see Figure 2-4 and Figure 3-10.

Faults can generally act as main drains across the rock mass, due to their persistence and their aperture. The excavation process in faults can be very



difficult and risky. The excavation rate slows down and the support strategies changes from place to place.

Faults can be divided into several different types depending on the direction of the relative displacement, see Figure 3-11.

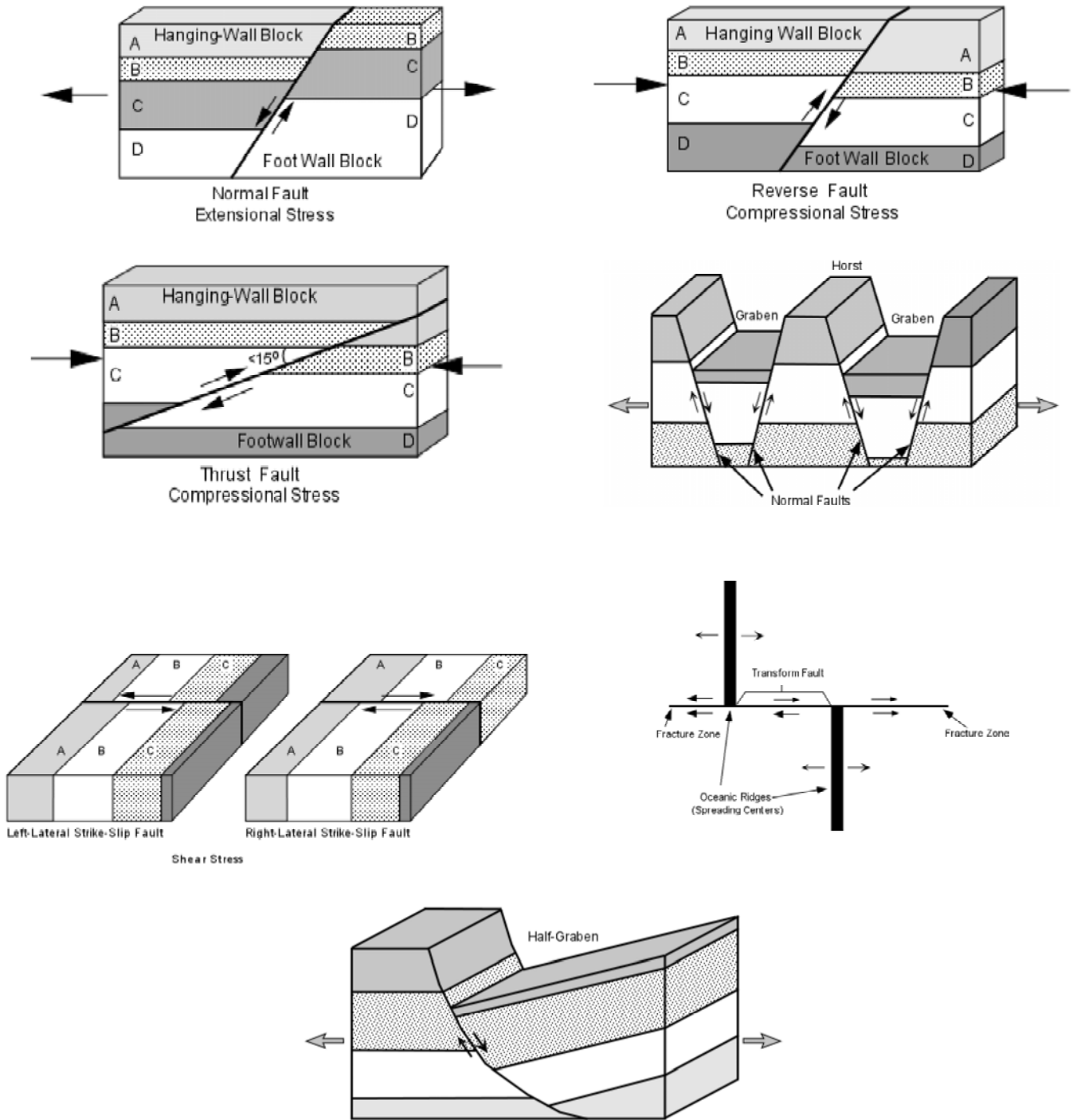


Figure 3-11: Different types of faults [16].

Normal faults result from horizontal tension stresses in brittle rocks and where the hanging wall block has moved down relative to the footwall block, e.g. Almannagjá at Þingvellir. Horst and grabens appear due to the tensional stress responsible for normal faults, they often occur in a series, with adjacent faults dipping in opposite directions. In such a case the down dropped blocks form blocks and the uplifted blocks form horsts, e.g. Almannagjá and Hrafnagjá at Þingvellir are examples of suchlike faults. A normal fault that has such a curved fault plane with the dip decreasing with depth, can cause the down dropped block to rotate. In such a case a half graben is produced, named because it is bounded by only one fault instead of the two that form a normal graben.

Reverse faults are resulted from horizontal compression stresses in brittle rocks, where the hanging wall block has moved up relative the footwall to block. A thrust fault is a special case of reverse fault where the dip of the fault is less than  $15^\circ$ , which can have considerable displacement, measuring hundreds of kilometres, and can result in older strata overlying younger strata. Reverse and thrust faults are rare in Iceland.

Strike slip faults are faults where the relative motion on the fault has taken place along a horizontal direction. Such faults results from shear stresses acting in the crust. Strike slip faults can be of two varieties, depending on the sense of displacement, left lateral strike slip and right lateral strike slip. These types of faults are rather rare in Iceland but appear e.g. in Þjórsárdalur.

Transform faults are a special class of strike slip faults. These are plate boundaries along which two plates slide past one another in a horizontal manner. The most common type of transform faults occur where oceanic ridges are offset. Note that the transform fault only occurs between the two segments of the ridge. Outside of this area there is no relative movement because blocks are moving in the same direction. These area are called fracture zones [4], [16].

### 3.5 Dikes

Dikes are very common in Iceland mainly in the Tertiary basalt areas. They are thin rock layers which have solidified in fractures. Dikes are normal located at right angles to the surrounding bedding, Figure 3-12. Dikes are usually thin, 1-2 m, the greatest 30-40 m, and are often in swarms. The length can be up to tens of kilometres which is hardly not surprising since eruption fissures are often of this length [4].

Normally there are no serious stability problems related to the dikes, but the border of the dikes can be fractured which can cause high permeability. That is the reason for their great water capacity, seen in tunnelling of Héðinsfjörður tunnel in Iceland.

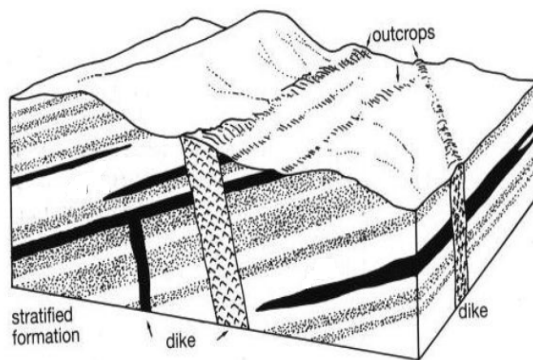


**Figure 3-12: Dikes cutting the stratified formation [4].**



**Figure 3-13: A dike in Fáskrúðsfjörður tunnel [46].**

### 3.6 Seismic Activity

As stated before, Iceland straddles the Mid Atlantic ridge where the Eurasian and North American tectonic plates move away from each other, causing volcanic and seismic activities. In this subchapter the main components related to seismic design of tunnels are mentioned.

Earthquake effects on underground tunnel structures can be categorised in two groups, ground shaking and ground failure.

Ground shaking refers to the vibration of ground produced by seismic waves propagating through the Earth's crust. Ground shaking motions are made of two different types of seismic waves, body waves and surface waves, each with two subtypes. Body waves propagate within the bedrock and can be divided into longitudinal P waves and transverse shear S waves, they can propagate in any directions. Surface waves propagate along the Earth's surface, classified in Rayleigh or Love waves, see Figure 3-14 [17]. It is obvious that a tunnel will be deformed as its surrounding bedrock during an earthquake. The damage caused by waves distortion of the surrounding rock mass nearest to the tunnel is generally related to slip at joints or fractures, with consequent displacement or even dislodgement of joint defined material blocks, and to local cracking and spalling of the rock surface [8].

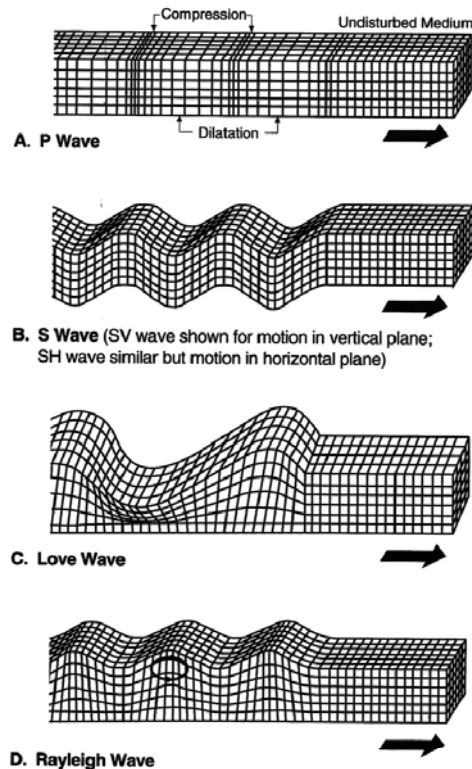
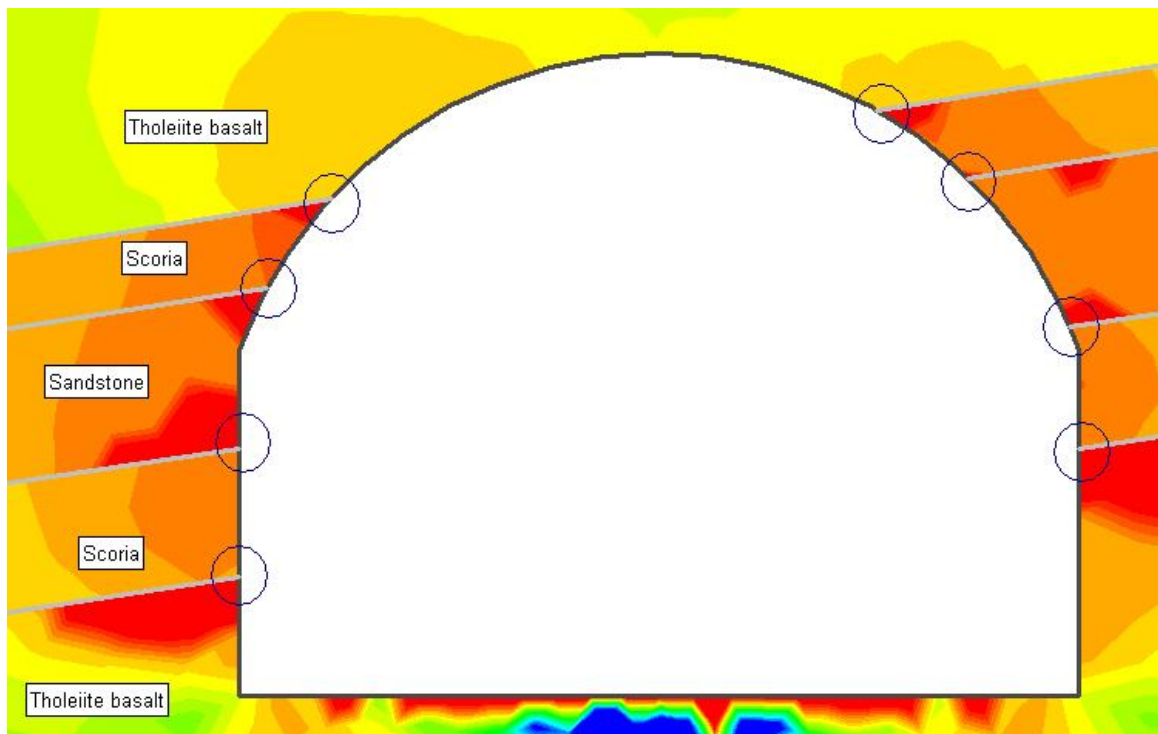


Figure 3-14: The bedrock response due to the various types of seismic waves [17].

Ground failure includes various types of ground instability problems such as faulting, landslides, liquefaction, tectonic uplift and subsidence. Crossing a tunnel through a active fault zone should be avoided, otherwise rupture displacement must be accepted and high risk of rock fall from walls and roof. Landslides, liquefaction, and related phenomena can cause serious problems at portals and other surface constructions related to tunnels [8],[17].

In a typical Icelandic tunnel face the most critical points are often between different rock layers, see Figure 3-15 from the finite element program *Phase2*. During support installation in earthquake prone areas, these points should always be kept in mind, because block units have potential to fall from walls and roof due to dynamic forces during a seismic event.



**Figure 3-15: The black circles presents the most critical points in a typical Icelandic tunnel cross section during earthquake.**

Underground constructions suffer much less damage during earthquake than surface construction. The reason for this difference is that the surface- and body are reduced with increased depth, seismic support design is however very important in earthquake prone zones [8]. In Figure 3-16 a horizontal bedrock acceleration map for Iceland is displayed. At the marked area a special precaution should be taken in to consideration because of risk of earthquakes. Many of the

tunnels, both road and hydro tunnels, build in Iceland, are excavated in the coloured regions. A special reinforcement analysis should have been considered during the design of the tunnels in these regions.

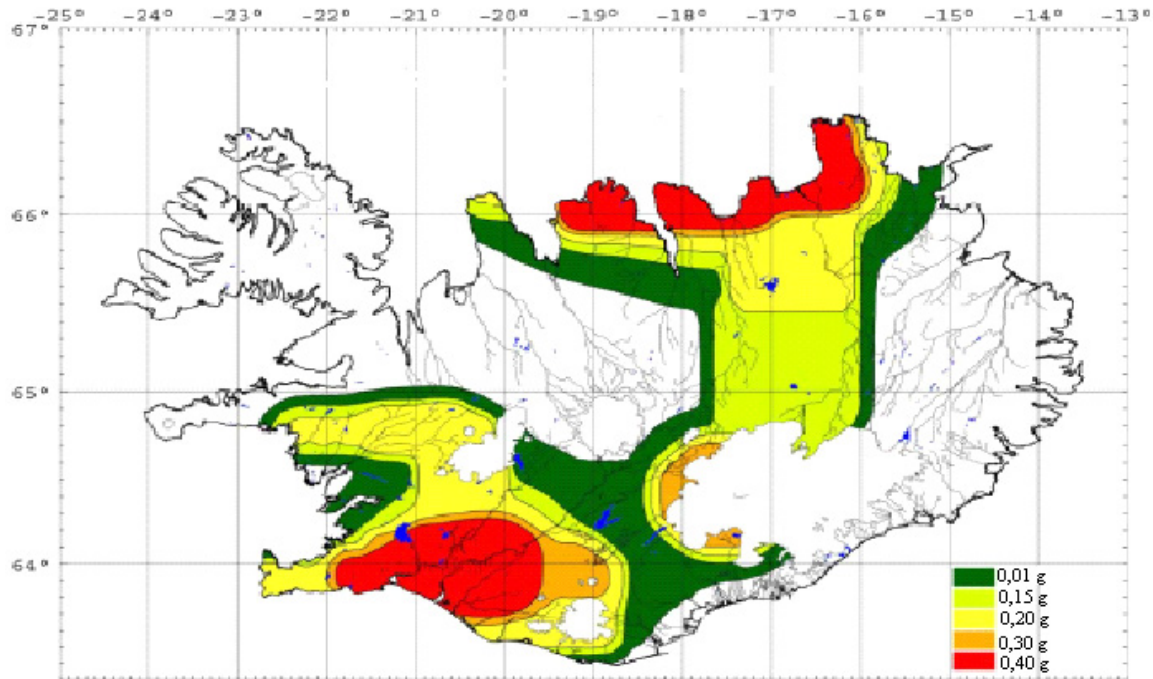


**Figure 3-16: Horizontal bedrock acceleration map for Iceland [18].**

McClure cited by Sigurður Erlingsson [8] report that, to minimize the potential of earthquake damage to an underground structure involving heavy economic risk this has to be taken in to consideration

- The facility should be located in rock having a shear wave velocity greater than 900 m/s.
- The overlaying cover should be at least 90 m.
- The facility should not be located in the immediate vicinity of active or potentially active faults.

McClure also states that by following these criteria in designing underground facilities, all risk of damage can be ignored.

## 4 Reinforcement Strategies

### 4.1 Rock Classification Systems

Rock classification systems have been in use for more than 50 years. Some of the developed systems are directed to characterize the rock mass in general or to give an input to the definition rock mass properties. Most of the systems are based on experience from older projects, and still today improvements are being made to get better reliability in the systems. Classification like this stores the knowledge from previous constructions which then can be used later on. It does also act as a refinement for the flow of information between designers, supervisors and contractors, which can make a huge difference in building a new underground construction. From some of the classification systems, reinforcement systems have been developed.

The following paragraphs describe some of the most important rock classification systems used today. The most used rock classification system in Iceland is the NGI tunnel quality index which is developed by the Norwegian Geotechnical Institute. During the last three decades geotechnical engineers have been trying to adjust the system to the Icelandic conditions.

#### 4.1.1 Rock Quality Designation index, RQD

The rock quality designation index, RQD, was developed by Deere et al. to provide a quantitative estimate of rock mass quality from drill core logs. The RQD value is defined as the percentage of intact core pieces longer than 100 mm of the total length of core. The core should be at least 54,7 mm in diameter and should be drilled with a double tube core barrel. Intact length of cores are only considered, core broken by joints and other naturally occurring discontinuities, so drill breaks must be ignored. Otherwise the resulting RQD will underestimate the rock mass quality [19].

$$RQD(\%) = \frac{\text{Length of the core in pieces } \geq 10 \text{ cm length}}{\text{Total length of core run}} \cdot 100 \quad (4.1)$$

The correlation between RQD values and rock quality is illustrated in Table 4-1.

**Table 4-1 [20].**

RQD (%)	Rock quality
<25	Very poor
25-49	Poor
50-74	Fair
75-89	Good
90-100	Very good

The RQD value is also used as a parameter in more advanced classification systems as RMR and NGI tunnelling quality index. Both systems will be described later on.

#### 4.1.2 Rock Structure Rating, RSR

The rock structure rating, RSR, was presented in 1972 by Wickham, Tiedmann and Skinner to describe the quality of a rock mass and for selecting appropriate support for tunnels. The system is often used for small tunnels supported by means of steel sets. The RSR value is summation of the parameters A, B and C [19].

- *Parameter A*, Geology: General appraisal of geological structure on the basis of:
  - A. Rock type origin (igneous, metamorphic, sedimentary)
  - B. Rock hardness (hard, medium, soft, decomposed)
  - C. Geological structure (massive, slightly faulted/folded, moderately faulted/ folded, intensely faulted/folded)
- *Parameter B*, Geometry: Effect of discontinuity pattern with respect to the direction of the tunnel drive on the basis of:
  - A. Joint spacing
  - B. Joint orientation (strike and dip)
  - C. Direction of tunnel drive
- *Parameter C*: Effect of groundwater inflow and joint condition on the basis of:



- A. Overall rock mass quality on the basis of A and B combined
- B. Joint condition (good, fair, poor)
- C. Amount of water inflow (in gallons per minute per 1000 feet of tunnel)

Tables which are used to evaluate the rating of each of the parameters are presented in Appendix 1.

Three equations related to the RSR system are used to estimate the tunnel support. An empirical relation between spacing of bolts and the rock loading is presented as following

$$\text{Spacing of bolts} = \frac{3,3}{\sqrt{W_r}} \quad (4.2)$$

where  $W_r$  is the rock load in tons/m<sup>2</sup> and spacing in meters. The equation (4.2) is for 25 mm diameter bolts with 10,9 tons working load. Equation (4.3) is related to the tunnel diameter and thickness  $t$  of the shotcrete in millimetres.

$$t = \frac{D \cdot (65 - RSR)}{1,8} \quad (4.3)$$

As an example, Figure 4-1 presents support estimation for circular 6 m diameter tunnel [19],[21].

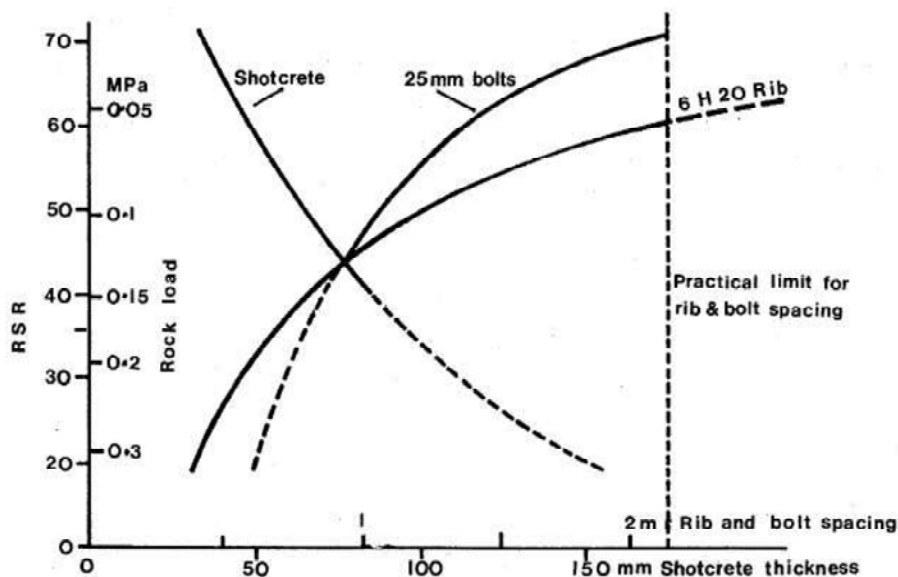


Figure 4-1: RSR support estimation for 6 m diameter circular tunnel [21].

### 4.1.3 Rock Mass Rating, RMR

Bieniawski (1976) published a classification system called the Geomechanics Classification or the Rock Mass Rating system. This system has thereafter been successively refined as more case records have been examined. The following six parameters are used to classify a rock mass using the RMR system

- Uniaxial compressive strength of rock material, UCS.
- Rock quality designation (RQD).
- Spacing of discontinuities.
- Condition of discontinuities.
- Groundwater conditions.
- Orientation of discontinuities.

Applying this classification system, the rock mass is divided into a number of structural regions and each region is classified separately. The parameters above are rated according to table in Appendix 1. The summation of these parameters gives the RMR value between 0 and 100, where 100 is high quality intact rock and 0 is very poor rock. The RMR values are classified in five different classes in Table 4-2 [22].

**Table 4-2: Classification of RMR values [22].**

<b>Class number</b>	<b>RMR</b>	<b>Rock quality</b>
I	81-100	Very good
II	61-80	Good
III	41-60	Fair
IV	21-40	Poor
V	<20	Very poor

Figure 4-2 presents the relation between the RMR value and the roof span and stand up time for tunnels.

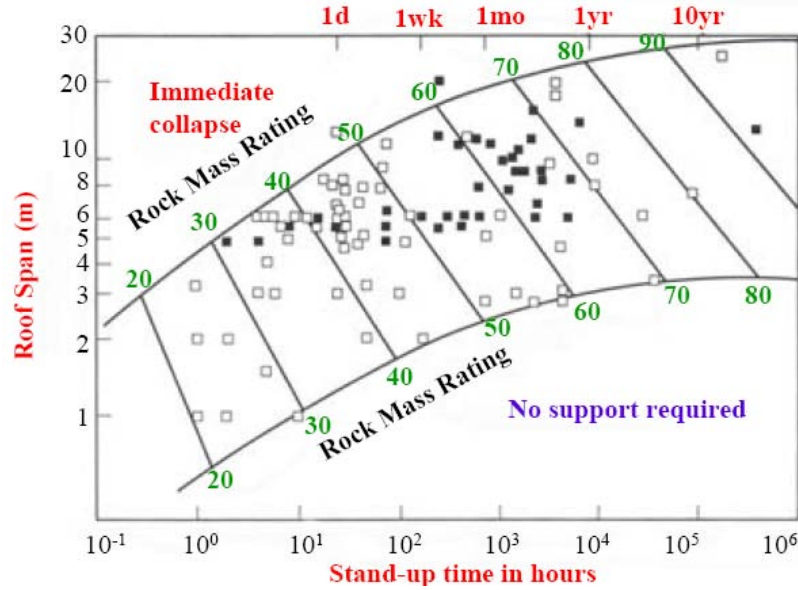


Figure 4-2: RMR in relation to roof span and stand up time for tunnels [23].

The RMR system is based on a set of case histories of relatively large tunnels excavated using drill and blast technique, where reinforcement like rock bolts, shotcrete, wire mesh and steel sets are used. The system is not suited for TBM(Tunnel Boring Machine) driven tunnel, where rock damage is less and immediate shotcrete application may not be feasible.

A relationship between rock load and roof span for different value of RMR is illustrated in Figure 4-3. The rock load height  $h_t$ , defined as the high of the rock mass over the tunnel to be stabilised, is given in meters

$$h_t = \frac{(100 - RMR)}{100} \cdot B \quad (4.4)$$

where  $B$  is the tunnel width in meters. The support rock load is given by following equation

$$P = \frac{(100 - RMR)}{100} \cdot B \cdot \gamma = h_t \cdot \gamma \quad (4.5)$$

where  $\gamma$  is the rock unit weight  $\text{kN/m}^3$  [19], [21], [24].

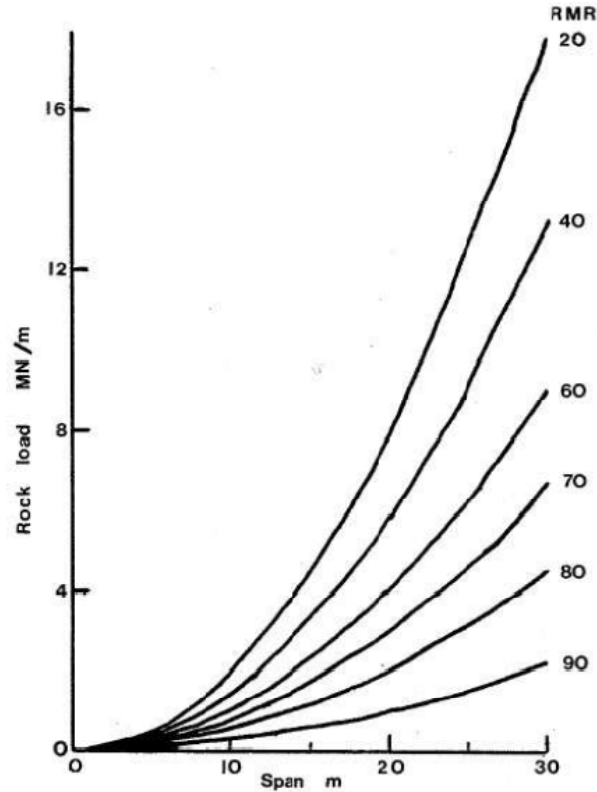


Figure 4-3: The relation between rock load and roof span for different RMR values [21].

#### 4.1.4 NGI Tunnelling Quality Index, Q

The NGI tunnel quality index also known as the Q method is a numerical description of the rock mass quality with respect to tunnel stability. On the basis of an evaluation of large number of case histories of underground excavations Barton, Lien and Lunde developed the Q method. The Q value is defined by a function consisting of six parameters which may be estimated either from geological mapping or from in situ measurements. The Q method is used internationally for general description of the rock mass quality and as a guide for estimating tunnel support requirement [25].

The Q value is a numerical description of the rock mass quality with regards to tunnel stability. The value varies on a logarithmic scale from 0,001 to a maximum of 1000. The Q value is expressed as following

$$Q = \frac{RQD}{J_n} \cdot \frac{J_r}{J_a} \cdot \frac{J_w}{SRF} \quad (4.6)$$

where the parameters are

$RQD$  is rock quality designation as described in chapter 4.1.1.  $RQD$  has values from zero to 100. The  $Q$  function specifies that the value 10 is the lowest  $RQD$  value used.

$J_n$  is the joint set number. The joint set number takes values from 0,5 for massive rocks with no or few joints, to 20 for crushed rocks.

$J_r$  is the joint roughness number. The joint roughness number varies from 0,5 for slickenside, planar joints to 4 for discontinuous joints. Usually the value for the weakest significant joint is used in the  $Q$  function.

$J_a$  express the joint alteration number. The alteration number varies from 0,75 for unaltered joint walls to 20 for rock with thick, continuous zones of swelling clay. In the  $Q$  function the weakest or most unfavourable joint set is generally used.

$J_w$  stands for the joint water reduction factor. The joint water reduction factor takes the values from 1 for dry excavations to 0,05 for excavations with exceptionally high inflow.

$SRF$  is the stress reduction factor. The stress reduction factor has values from 1 for medium rock pressure to 20 for heavy rock pressure. The values are taken relative to the rock strength.

The  $Q$  function may be considered as the product of the three quotients. The first quotient,  $RQD/J_n$ , is a measure for the relative block size. The second quotient,  $J_r/J_a$ , is a fair approximation to the actual interblock shear strength. The third quotient,  $J_w/SRF$ , describes the active stress. It is generally agreed that these three quotients represent three major parameters affecting the tunnel stability [25]. In Appendix 1 the rating of the parameters is clarified.

The main advantage to the  $Q$  classification system is that it is relatively sensitive to minor variation in rock properties. The most disadvantage of the  $Q$  system is that it is relatively difficult for inexperienced users to apply. The parameter  $J_n$  can cause problems, the inexperienced users have difficulties to estimate the parameter, counting to many joint sets which results in a low estimate of  $Q$ .

To relate the  $Q$  value to rock mass support requirements, an equivalent dimension ( $D_e$ ) defined as the width of the underground opening divided by the excavation support ratio (ESR), is given with

$$D_e = \frac{\text{Span, Diameter or Height (m)}}{ESR} \quad (4.7)$$

The value of ESR depends on the ultimate use of the underground opening and the time of exposure. Following recommended values of  $ESR$  are given in Table 4-3.

**Table 4-3: Recommended value for ESR [24].**

<b>Excavation category</b>	<b>Type of excavation</b>	<b>ESR</b>
A	Temporary mine openings	3-5
B	Vertical shafts (highest for circular cross sections)	2-2,5
C	Permanent mine openings, water tunnels for hydropower (excluding high pressure penstocks), pilot tunnels, drifts and heading for large openings	1,6
D	Storage caverns, water treatment plants, minor road and railway tunnels, access tunnel	1,3
E	Power stations, major road and railway stations, civil defence chambers, portals, intersections	1
F	Underground nuclear power stations, railway stations, sports and public facilities, factories, major gas pipeline tunnels	0,8

After the estimation for the  $Q$  value and the equivalent dimension the fulfilled support design can be estimated from Figure 4-4. Icelandic rocks are usually ranked between 0,4 and 15, but in a very fractured rock, like fault breccias, a value as 0,01 can be seen.

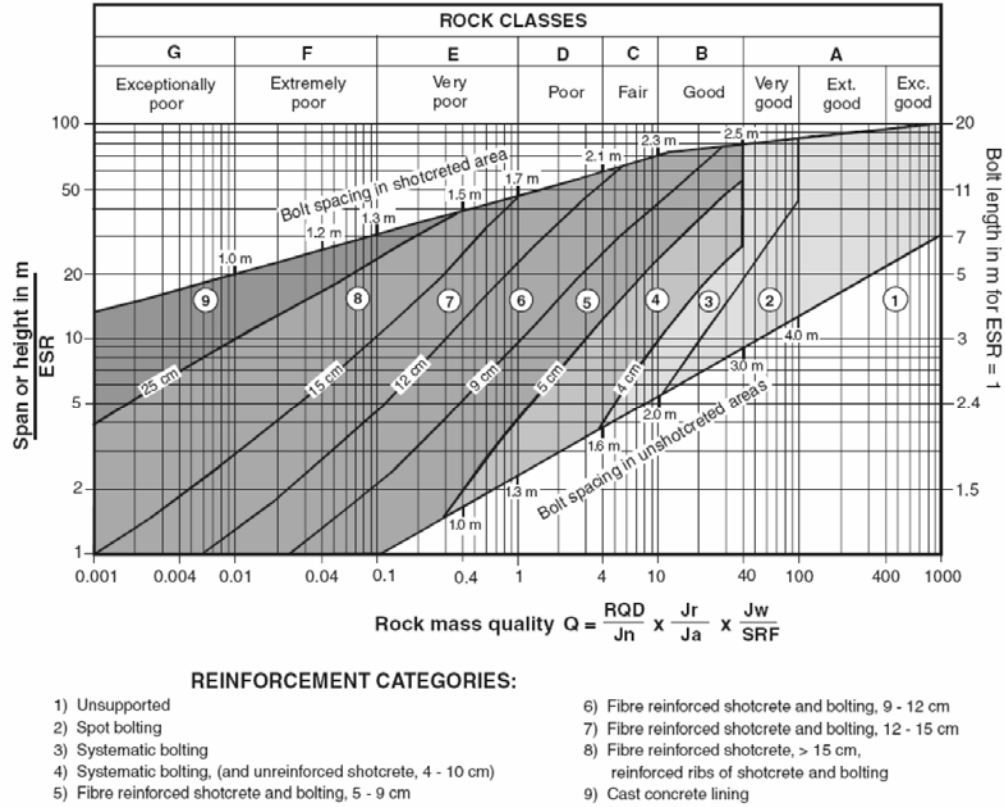


**Figure 4-4: Reinforcement design of excavations based on the Q system [14].**

Barton et al. provided additional information on rock bolt length, maximum unsupported spans and roof support pressure [19]. The length  $L$  for rock bolts can be estimated from the excavation width  $B$  and excavation support ratio  $ESR$  by the following equation

$$L = \frac{2 + 0,15 \cdot B}{ESR} \tag{4.8}$$

And the maximum unsupported span can be found using the following equation

$$Maximum\ span = 2 \cdot ESR \cdot Q^{0,4} \tag{4.9}$$

The relationship between the value of  $Q$  and the permanent roof support pressure  $P_{roof}$  is estimated from

$$P_{roof} = \frac{2 \cdot \sqrt{J_n} \cdot Q^{\frac{1}{3}}}{3 \cdot J_r} \tag{4.10}$$

During the last decades some attempts have been made to adjust the Q system to Icelandic environment, as Icelandic geology is quite different compared to most other countries in the world. During the construction of the Hvalfjörður tunnel in the southwest of Iceland the most common values and ranges of Q indexes were estimated for different rock types, see Table 4-4. Using the Q system to evaluate Icelandic rock mass, does not give a reliable results for all rock types, especially for small columnar jointed basalt. Since the parameter  $J_n$  clearly underestimates the rock type, the need for support becomes too high. The rating for  $J_r$  and  $J_a$  were also changed a bit [26].

**Table 4-4: Most common values and ranges of Q indexes for different rock types from Hvalfjarðar tunnel [27].**

Rock type	<i>RQD</i>	$J_n$	$J_r$	$J_a$	$J_w^*$	<i>SRF**</i>
Hard, large and medium columnar basalt	70-100	9-10	2-4	2-3	1	1
Hard, small columnar jointed (<15 cm) basalt	40-70	10-12	2-4	2-3	1	1
Scoriaceous basalt, competent	50-100	9-10	2-4	2-3	1	1
Highly altered basalt	50-100	9-10	2-4	2-4	1	1
Heavily jointed basalt	<40	12-14	2-4	2-3	1	1
Scoria, well consolidated	50-100	9-10	2-4	2-3	1	1
Scoria, poorly consolidated (loose) with soft sedimentary fillings	<50	9-20	1-4	2-4	1	1/2,5/5,0
Sedimentary rock, competent sandstone and siltstone	50-100	9	1-2	3-4	1	1
Sedimentary rock, incompetent sandstone and siltstone (soft)	<50	9	1-2	3-4	1	1/2,5/5,0
Fault breccia	<50	15-20	1	3-8	1	2,5/5,0

\* Preliminary procedures to use fixed value for  $J_w$ .

\*\* SRF 2,5 if overburden is < 2H or <1,5B (competent rock).

While using the Q system the lowest value of Q for the whole cross section is used to estimate the need of reinforcement. In the Icelandic rock mass the variability of the rock quality can be great, which means that one Q value for the whole cross section is far too pessimistic evaluation. For instance the difference between tunnel walls in the same cross section can be large, one rated much higher Q value than the another one, so using the same reinforcement strategy for both walls is witless and unpractical [27].



The Q system can be modified while designing a tunnel in a earthquake prone region, then the parameter  $SRF$  is decreased, which leads to lower Q value, resulting in a closer rock bolts spacing and mesh reinforcement of the shotcrete [8].

#### **4.1.5 The Geological Strength Index, GSI**

The geological strength index system described by Hoek et al (1998) provides a system for estimating a value for rock mass strength from descriptions based on field observations. The geological strength index, GSI, is used to minimize the strength of a rock mass according to geological conditions. The rock mass description considers the rock structure in terms of blockiness and the surface condition of the discontinuities, as indicated by joint roughness and alteration [28]. The range of the values within the GSI is between 0 and 100.

In the beginning the value of GSI was estimated directly from RMR. That correlation was proved to be unreliable, especially for poor quality rock masses and for rocks with lithological peculiarities which cannot be adjusted to the RMR classification system. Instead, the GSI value can be estimated by means of charts. Figure 4-5, which is for jointed rocks, in Appendix 1 is a chart for estimation of heterogeneous rock mass such as flysch.

**GEOLOGICAL STRENGTH INDEX FOR JOINTED ROCKS (Hoek and Marinos, 2000)**  
 From the lithology, structure and surface conditions of the discontinuities, estimate the average value of GSI. Do not try to be too precise. Quoting a range from 33 to 37 is more realistic than stating that GSI = 35. Note that the table does not apply to structurally controlled failures. Where weak planar structural planes are present in an unfavourable orientation with respect to the excavation face, these will dominate the rock mass behaviour. The shear strength of surfaces in rocks that are prone to deterioration as a result of changes in moisture content will be reduced if water is present. When working with rocks in the fair to very poor categories, a shift to the right may be made for wet conditions. Water pressure is dealt with by effective stress analysis.

STRUCTURE	DECREASING SURFACE QUALITY →	VERY GOOD Very rough, fresh unweathered surfaces	GOOD Rough, slightly weathered, iron stained surfaces	FAIR Smooth, moderately weathered and altered surfaces	POOR Slack-sided, highly weathered surfaces with compact coatings or fillings or angular fragments	VERY POOR Slack-sided, highly weathered surfaces with soft clay coatings or fillings
INTACT OR MASSIVE - intact rock specimens or massive in situ rock with few widely spaced discontinuities	90				N/A	N/A
BLOCKY - well interlocked undisturbed rock mass consisting of cubical blocks formed by three intersecting discontinuity sets	80					
VERY BLOCKY - interlocked, partially disturbed mass with multi-faceted angular blocks formed by 4 or more joint sets	70					
BLOCKY/DISTURBED/SEAMY - folded with angular blocks formed by many intersecting discontinuity sets. Persistence of bedding planes or schistosity	60					
DISINTEGRATED - poorly interlocked, heavily broken rock mass with mixture of angular and rounded rock pieces	50					
LAMINATED/SHEARED - Lack of blockiness due to close spacing of weak schistosity or shear planes	40					
	30					
	20					
	10					
	N/A	N/A				

Figure 4-5: Determination of the GSI for jointed rocks [19].

The Hoek-Brown failure criterion for rock mass is widely accepted and has been applied in a large number of projects around the world. The generalised Hoek-Brown can be expressed as following

$$\sigma_1' = \sigma_3' + \sigma_{ci}' \left( m_b \cdot \frac{\sigma_3'}{\sigma_{ci}'} + s \right)^a \tag{4.11}$$

where  $m_b$  is a reduced value of the material constant,  $m_i$ , and is given by

$$m_b = m_i \cdot \exp\left(\frac{GSI - 100}{28 - 14 \cdot D}\right) \tag{4.12}$$

and  $s$  and  $a$  are constants for the rock mass given by the following relationships

$$s = \exp\left(\frac{GSI - 100}{9 - 3 \cdot D}\right) \quad (4.13)$$

$$a = \frac{1}{2} + \frac{1}{6} \cdot \left( e^{\frac{GSI}{15}} - e^{\frac{20}{3}} \right) \quad (4.14)$$

parameter  $D$  is used to estimate the disturbance of the rock mass subjected by blast damage and stress relaxation. The range is from 0 for undisturbed rock mass to 1 for very disturbed rock mass [29].

For the estimation of the GSI and use of Hoek-Brown failure criterion the user friendly computer program, *RocLab*, has been design by Rocscience Inc. [19]. The program provides simple and intuitive implementation of the Hoek-Brown failure criterion, allowing users to easily obtain reliable estimates of rock mass properties. Also to visualize the effects of changing rock mass parameters. The program will be used in estimation of rock mass parameters in this thesis. In Appendix 1, a screenshot from the program is displayed.

Practical application of the GSI system and the Hoek-Brown failure criterion in number of engineering projects around the world have shown that the system gives reasonable estimation of the strength of a wide variety of rock masses [19].

## 4.2 Rock Support Systems

The stability of an underground opening depends on the behaviour of the rock mass surrounding it. It depends on time when the support is installed to the rock mass, because the support system must have enough strength and stiffness to carry the rock mass movements. After the excavation the rock mass expands, releasing stresses in the rock mass, causing the rock mass nearest to the wall surface to carry more load. The main idea is to put as much weight on the rock mass as possible, then the support system just has to carry the rest of the weight to prevent downfall [14].

Installation of rock support systems is often divided in two separated phases, primary and secondary. In the primary phase the tunnel surface is reinforced during excavation or just after excavation, just to ensure safe working conditions and prevent downfall from walls and roof. In the secondary phase the additional rock support is applied after blasting has been finalized, to secure stability through the construction's lifetime [27].

Some attempts have been made to estimate when support systems shall be installed, to get the best solution. Figure 4-6 describes a pressure relief of a rock mass after excavation and different timing of support installation. The trajectory a-b gives too stiff support, still on the elastic part, risk of overloading. On the other hand the support can also be too soft, trajectory a-f can cause collapse of the underground construction. A support with a right stiffness but not enough bearing capacity, see trajectory a-c-e. The most optimal support is the trajectory a-d, where the support trajectory crosses the pressure trajectory in middle of the rock mass plastic part [30].

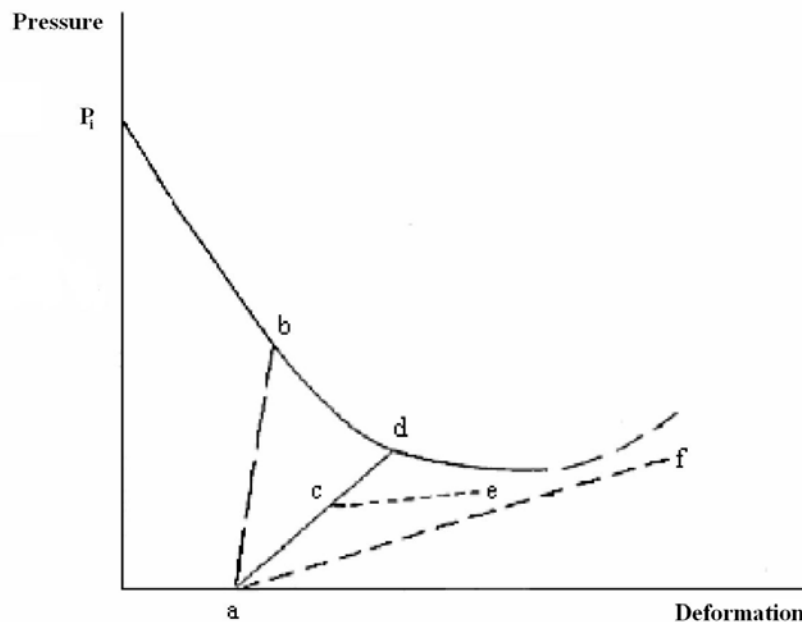


**Figure 4-6: Pressure relief of the rock mass after excavation, the most optimal support is the trajectory a-d. Referring to NATM (New Austrian Tunnel Method) [30].**

The most common rock support systems used in Iceland are rock bolts and shotcrete, with or without steel fibres. But where circumstances are very poor a wire mesh, chain links and steel beams are also used. In the next subchapters these systems will be described.

### 4.2.1 Rock Bolt

Rock bolts are used to stabilize rock excavations. Rock bolts role is to stabilize rock wedges and prevent movements of the rock mass nearest to the tunnel. A common length of rock bolt is from two to four meters, and depends on circumstances at each time. It is very important that the length of the bolts is sufficient to extend into a stable rock beyond the secondary, weak rock. The rock

bolts have to be capable to bear both tensile and shear forces. The most used rock bolts in Icelandic rocks are grouted rebar rock bolt (cast iron rod) and CT-bolts (grouted end anchored rock bolt). The difference between these types is that, the CT-bolt can be active just after installation but the grouted rebar rock bolt does not become active until the concrete surrounding it has hardened and some movements in the rock mass has occur [27].

A rock bolt generally consist of plane steel rod with a mechanical or chemical anchor at one end and a face plate and a nut at the other. A rock bolt is installed as following: The entire assembly from Figure 4-7 is inserted into a drilled hole. The length of the hole should be at least 100 mm longer than the bolt otherwise the bail will be dislodged by being forced against the end of the hole. After installation a sharp pull will seat the anchor. Then the bolt is tightened to force the cone into the wedge thereby increasing the anchor force, see Figure 4-8. For permanent use, the space between the bolt and the rock can be filled with cement or resin grout, but for a short term use the bolts are usually left ungrouted. The fill material also prevents the rock bolt against rust or corrosion because of groundwater which is the most common cause of failure [19].

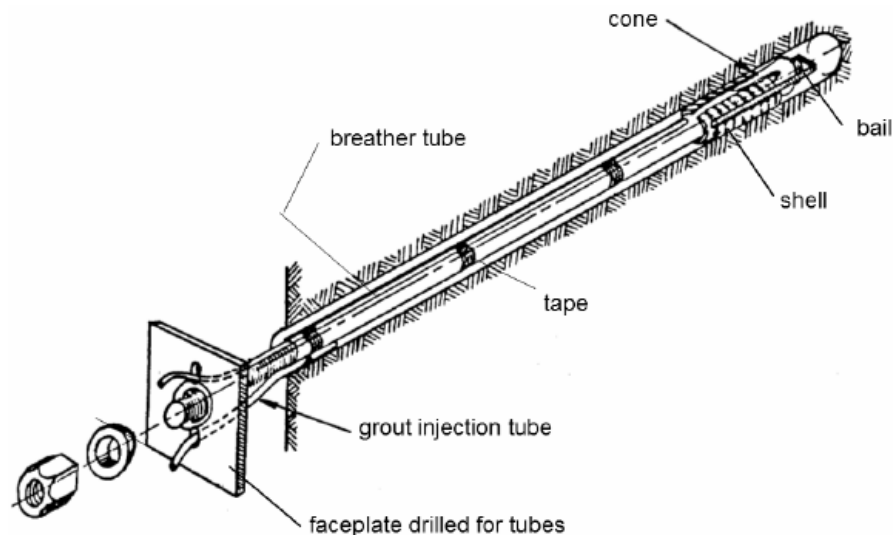


**Figure 4-7: Components of a grouted end anchored rock bolt [19].**

It is necessary to use tension the bolts to secure that all of the components are in contact and positive force is applied to the rock. It is enough to use conventional wrench to tighten the nut. Where the bolts are required to carry a huge load, then 70 % tension capacity of a bolt is applied after installation. This provides a known

load with a reserve in case of additional load being induced by displacements in the rock mass [19].

In the case of sidewall wedges the bolts have to be placed in such a way that the shear strength of sliding surfaces is increased, the bolts have to cross the sliding planes rather than cross the separation plane. The inclination should be between 15° and 30° which induces the highest shear resistance along the sliding surface.

The total force which will be applied by the reinforcement for roof wedges, should be sufficient to support the full dead weight of the wedge. The safety factor should be of 1,3 for temporary mine access opening, such as drilling drive, and 1,5 for more permanent access opening such as highway tunnel [19].



**Figure 4-8: Installation of rock bolts in Fáskrúðsfjörður tunnel [46].**

### 4.2.2 Theoretical Concept of a Rock Bolt

The stiffness parameter for anchored rock bolts depends on the distance between rock bolts,  $s_c$  and  $s_l$ , and the cross section of the rock bolt, see Figure 4-9. For a rock bolt with a circular cross section the stiffness  $k_b$  is given as following

$$k_b = \frac{\pi \cdot d^2}{4} \cdot \frac{E_b}{l} \cdot \frac{1}{s_c \cdot s_l} \cdot \frac{1}{\lambda} \quad (4.15)$$

where  $E_b$  is the Young's modulus for the rock bolt and  $l$  is the length of the rock bolt, i.e. the distance from wall surface to the anchor. The term  $\lambda$  is an empirical correction factor which will balance the unforeseen displacement around the anchor and the faceplate. The term  $\lambda$  can be estimated by performing tensile tests on rock bolts. A common value for  $\lambda$  is between two and four [14]. The ultimate tensile strength for an anchored rock bolt is given as

$$p_{b_{\max}} = \frac{P_{b_{\max}}}{s_c \cdot s_l} \quad (4.16)$$

which can never be greater than the ultimate tensile strength for the rock bolt without the anchor, which is expressed as

$$p_{b_{\max}} = \frac{\sigma_s \cdot \pi \cdot d^2}{4 \cdot s_c \cdot s_l} \quad (4.17)$$

where the  $\sigma_s$  is the yield strength for the rock bolt [14].

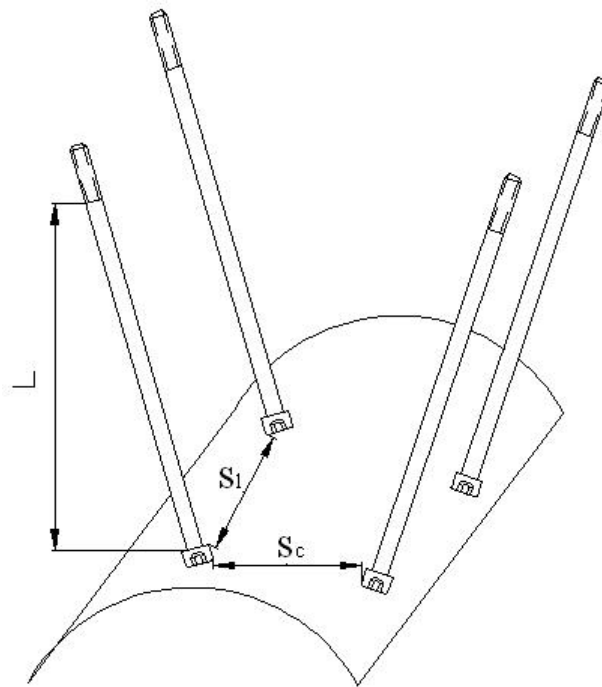


**Figure 4-9: Rock bolts installed in tunnel roof [14].**

To estimate the required amount of rock bolts to stabilize a rock sliding wedge the following must be taken in consideration. It is necessary to calculate the weight of the wedge,  $W$ , and then draw a force polygon with  $W$  given, see Figure 4-10. The direction of the resultant,  $R$ , of the shear force,  $S$ , along the separation plane and the normal force,  $N$ , to the separation plane is known, applying a relevant friction angle  $\phi$ . Then the polygon is completed and gives the total tensile force  $D$  [31].

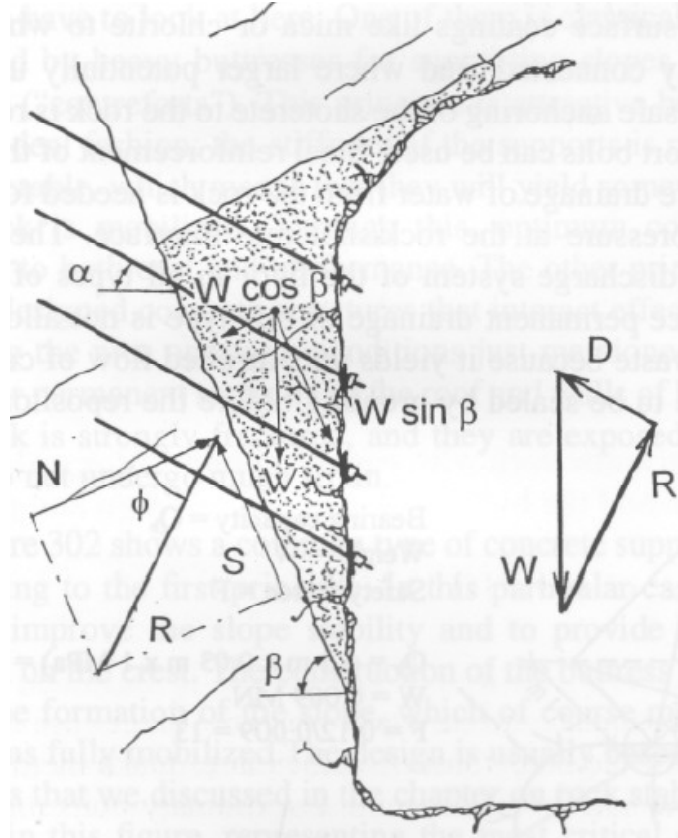


**Figure 4-10: Rock bolts installed in a sliding rock wedge in a tunnel wall [31].**

The required number of bolts  $N_b$  can be estimated from equation

$$N_b = \frac{W \cdot F}{B} = \frac{D}{B} \quad (4.18)$$

where  $W$  is the weight of the wedge,  $F$  is the safety factor and  $B$  is the product of the cross section area and the yield strength of the bolt [31].



### 4.2.3 Shotcrete

Shotcrete is the common name for cement, sand and fine aggregate concrete which is applied pneumatically and compacted dynamically under high velocity. There are two types of shotcrete, dry mix and wet mix shotcrete. The latter one is most used in Iceland and the Scandinavian countries. In Table 4-5 the advantage and disadvantage for these methods are listed up.

In the dry mix method the dry components are placed in a hopper with continuous agitation, where it is compressed with air to the delivery nozzle, water is then added to the mixture at the nozzle. The operator adjust the amount of water [32].

In the wet mix method the same ideology is used, where a compressed air is used to force the wet mix through a hose and out of a nozzle. But in the wet mix method the water has already been added to the dry components in a concrete plant and transported to the delivery place by trucks [32].

**Table 4-5: Advantages and disadvantages for dry mix and wet mix methods [33].**

Type	Advantages	Disadvantages
<b>Dry mix</b>	<ul style="list-style-type: none"> <li>• Quite simple method</li> <li>• The w/s ratio can be low</li> <li>• A good compaction, cause of high speed</li> <li>• Possibility to use coarse material</li> </ul>	<ul style="list-style-type: none"> <li>• Material drop out is much</li> <li>• Difficulties to get a equal damp distributions</li> <li>• The operator decides the quality of the shotcrete</li> <li>• Less output than wet mix method</li> </ul>
<b>Wet mix</b>	<ul style="list-style-type: none"> <li>• Little material drop out</li> <li>• The mixture is made in concrete plant, uniform quality</li> <li>• Little dust pollution</li> <li>• More output than dry mix</li> </ul>	<ul style="list-style-type: none"> <li>• Difficulties to use coarse fill materials</li> <li>• Much use of cement</li> <li>• Use of accelerator, to get quicker coagulation</li> </ul>

The final shotcrete product depends mainly on following the factors: Surface preparation, nuzzling technique, lightning, ventilation, communications and crew training. The worst surface conditions are dry, dusty and frozen rock surface. The surface area should be sprayed with an air-water jet to removed loose rocks and dust. The damp rock will create a good surface to bond the initials layer of the shotcrete. The shooting distance is ideally about one to one and a half meters, see Figure 4-11 [19]. The most effective way to apply shotcrete on a wall is to begin at the lowest point and move to the sides towards the roof [27].

To increase shotcrete tensile strength steel fibres are often mixed in. The advantage using steel fibre mixed shotcrete instead of traditional wire is much

shorter time in application, but also less expensive, especially when dealing with irregular surface.

Some experience values of amount of shotcrete used in the primary phase for various rock types are available. Often for sound basalt no support is needed, but for moderately broken basalts 3-4 cm thick shotcrete is needed. Approximately 3-10 cm thick shotcrete is used for scoria and sedimentary interbeds. Were circumstances are very poor e.g. fault zone, 10-15 cm of shotcrete is required [1].



Figure 4-11: Shotcrete applied on a wall in Fáskrúðsfjörður tunnel [46].

#### 4.2.4 Theoretical Concept of Shotcrete

For a circular cross section tunnel with prefabricated concrete lining or full covered with shotcrete, with a thickness  $t_c$  and a radius  $r_i$ , the stiffness factor  $k_c$  can be expressed as

$$k_c = \frac{E_c [r_i^2 - (r_i - t_c)^2]}{(1 + \nu_c) [(1 - 2 \cdot \nu_c) \cdot r_i^2 + (r_i - t_c)^2]} \quad (4.19)$$

where the  $E_c$  is the Young's modulus and  $\nu_c$  is the Poisson's ratio for the concrete. If the concrete thickness is small compared to the tunnel radius then the stiffness can be written as the approximation

$$k_c \cong \frac{E_c \cdot t_c}{r_i^2} \quad (4.20)$$

The ultimate strength for the concrete can be found from a hollow cylinder, which is effected with pressure stresses, the relation is expressed with equation

$$p_{c_{\max}} = \frac{1}{2} \cdot \sigma_c \cdot \left[ 1 - \frac{(r_i - t_c)^2}{r_i^2} \right] \quad (4.21)$$

where the  $\sigma_c$  is the unconfined compression strength of the concrete [14].

#### 4.2.5 Combination of Rock Bolts and Shotcrete

When reinforcing underground structures, a combination of rock bolts and shotcrete is very common. But it can be problematic to estimate the combined stiffness for rock bolts and shotcrete, especially if the rock bolts are grouted. That grouted rock bolts acting with the rock mass, making it difficult to separate the displacements between these two phenomena. For solving such a problem, a numerical analysis is needed, to take into account concurrent effects from the grouted rock bolt and the rock mass [14].

But when using two different reinforcement system e.g. shotcrete and anchored rock bolts the stiffness can be estimated as

$$k_{total} = k_b + k_c \quad (4.22)$$

where  $k_b$  is the stiffness for the anchored rock bolt and  $k_c$  is the stiffness for the shotcrete.

### 4.2.6 Use of Rock Bolts and Shotcrete in Iceland

A summation from GeoTek on use of rock bolts and shotcrete in constructed road tunnels in Iceland.

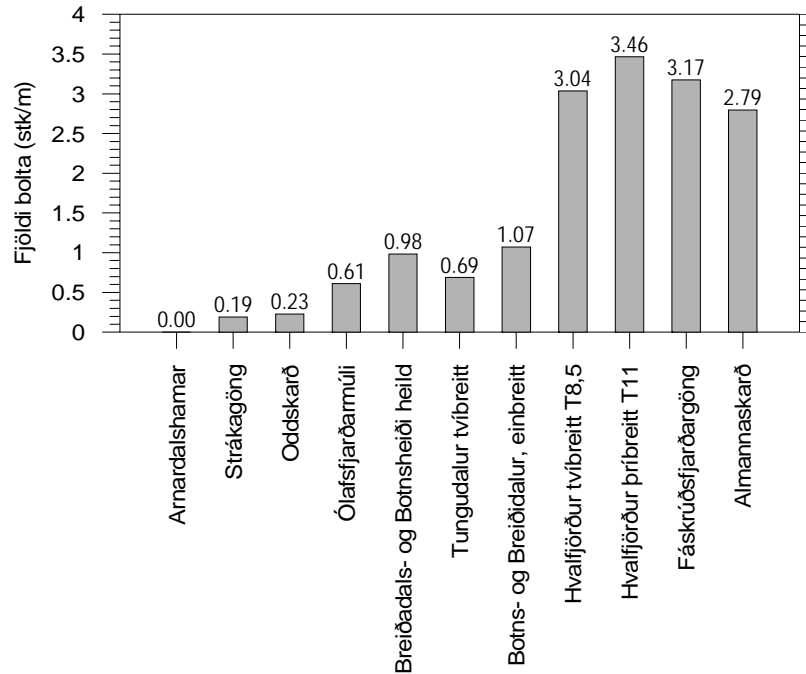


Figure 4-12: Amount of rock bolts used per length meter in different road tunnels in Iceland [46].

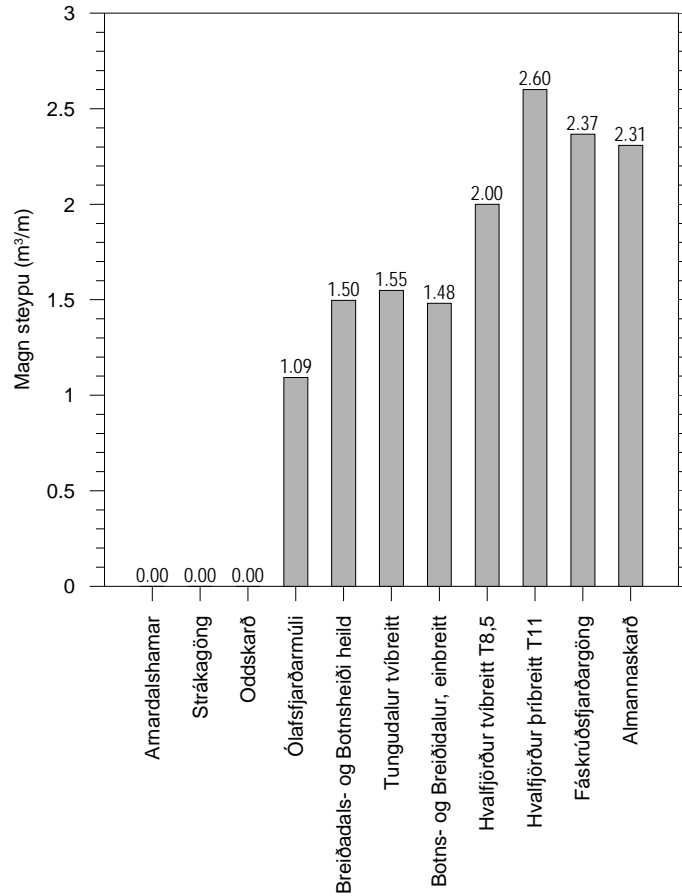


Figure 4-13: Amount of shotcrete used per length meter in different road tunnels in Iceland [46].

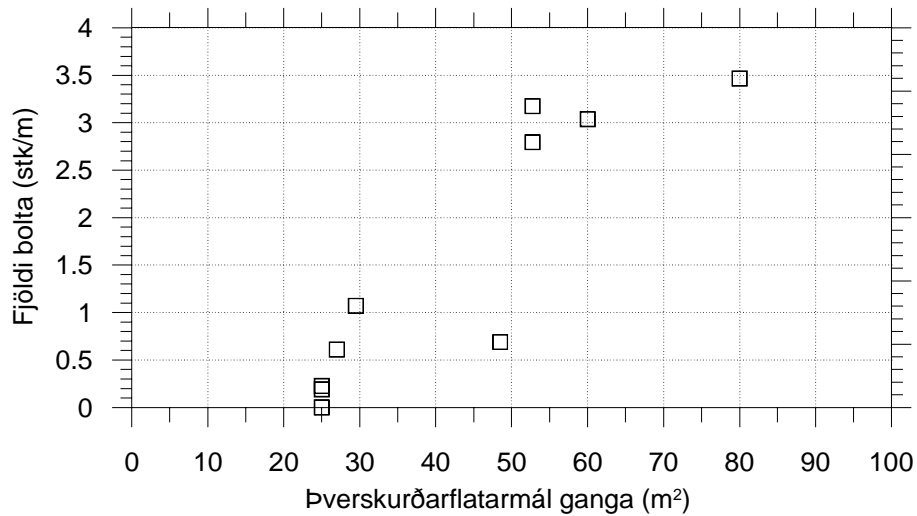
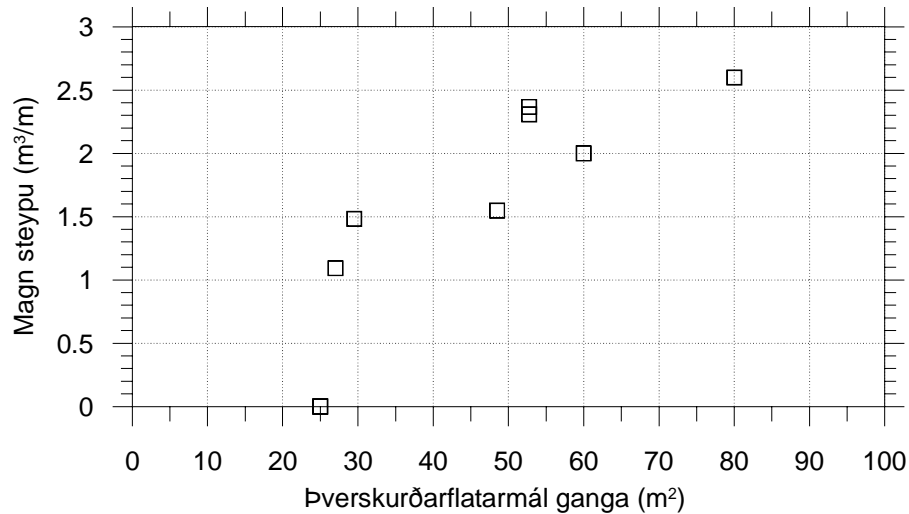


Figure 4-14: Average amount of rock bolts used against cross section area for different road tunnels in Iceland [46].



**Figure 4-15: Average amount of shotcrete used against cross section area for different road tunnels in Iceland [46].**

Experience for modern tunneling in Iceland for a 50 m<sup>2</sup> tunnel face calls for six rock bolts with approximately two meters spacing in between and in excess of 10 cm thickness of shotcrete.

### 4.3 Stresses Around Underground Openings

As mentioned before, after excavation a stress relief of the rock mass occurs and the rock mass nearest to the tunnel opening has to take more load. During this process the rock mass expand into the tunnel opening. Therefore it is very important to gather as much information about the stress conditions before the excavation takes place to minimize all uncertainty. In this subchapter the analysis of stress determination on underground openings will be described.

Figure 4-16 and Figure 4-17 presents a section of a tunnel, the figures presents how the rock mass surrounding the tunnel deforms after an excavation. The rock mass starts to deform about one half a tunnel diameter ahead of the advancing face and reaches its maximum value about one and one half diameters behind the face [19].

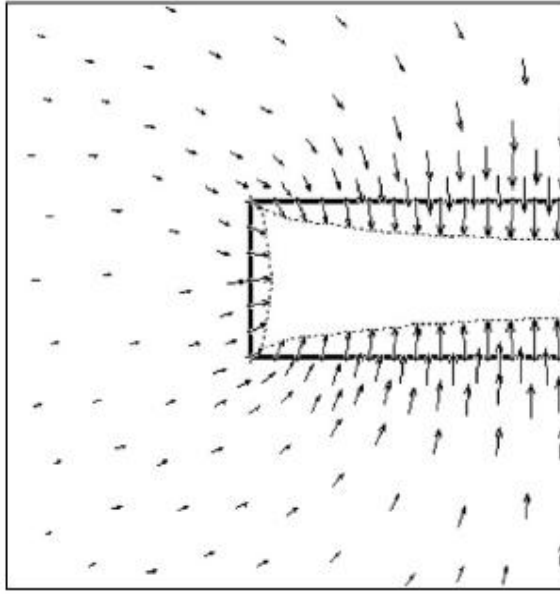


**Figure 4-16:** A section from a finite element model for a circular tunnel, the figure presents the displacement vectors as well as the shape of the deformed tunnel profile [19].

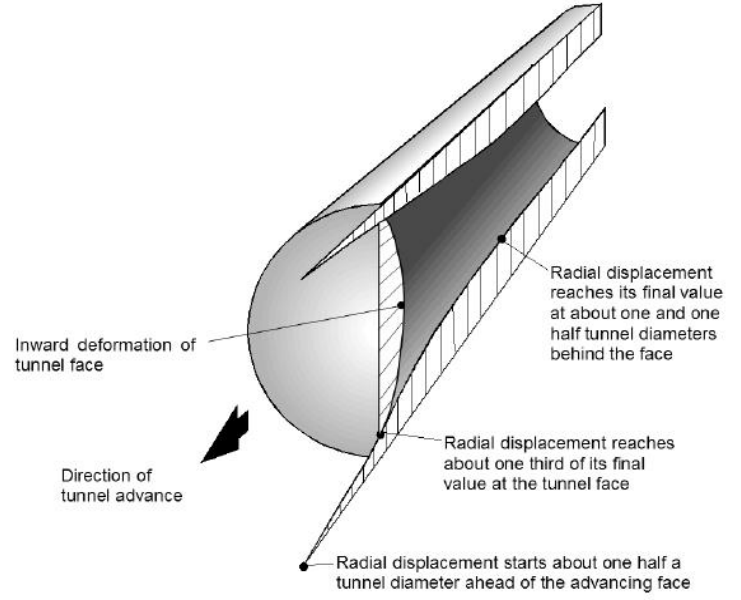


**Figure 4-17:** The deformation in the rock mass surrounding an advancing tunnel [19].

Where the stress distribution is not isotropic, i.e. where the horizontal and the vertical stresses differs, the Kirsch equations can be applied. The Kirsch equations for a circular openings gives the radial, tangential and shear stresses at any point in an infinite plate with polar coordinates. Linear elastic behaviour of the rock mass where  $k$  ( $K_0$ ) is the stress ratio in the original rock is assumed [34]

$$\sigma_r = \frac{\sigma_v}{2} \left[ (1+k) \left( 1 - \frac{r_i^2}{r^2} \right) + (1-k) \left( 1 - 4 \cdot \frac{r_i^2}{r^2} + 3 \cdot \frac{r_i^4}{r^4} \right) \cdot \cos 2\theta \right] \quad (4.23)$$

$$\sigma_\theta = \frac{\sigma_v}{2} \left[ (1+k) \left( 1 + \frac{r_i^2}{r^2} \right) - (1-k) \left( 1 + 3 \cdot \frac{r_i^4}{r^4} \right) \cdot \cos 2\theta \right] \quad (4.24)$$

$$\tau_{r,\theta} = \frac{\sigma_v}{2} \cdot \left[ (-1+k) \cdot \left( 1 + 2 \cdot \frac{r_i^2}{r^2} - 3 \cdot \frac{r_i^4}{r^4} \right) \cdot \sin 2\theta \right] \quad (4.25)$$

where  $r_i$  is the radius of the tunnel,  $r$  is the distance from the axis and  $\theta$  is the angle, which is referenced to the vertical stress, see Figure 4-18. At the excavation surface  $\sigma_r$  and  $\tau_{r,\theta}$  are 0. In all cases  $r \geq r_i$ . The displacements can be calculated

$$u_r = -\frac{\sigma_v \cdot r_i^2}{4 \cdot G_r} \cdot \left[ (1+k) - (1-k) \cdot \left( 4 \cdot (1-\nu) - \frac{r_i^2}{r^2} \right) \cdot \cos 2\theta \right] \quad (4.26)$$

$$u_\theta = -\frac{\sigma_v \cdot r_i^2}{4 \cdot G_r} \cdot \left[ (1-k) \cdot \left( 2 \cdot (1-2 \cdot \nu) + \frac{r_i^2}{r^2} \right) \cdot \sin 2\theta \right] \quad (4.27)$$

where  $G_r$  is the shear stiffness of the rock expressed as

$$G_r = \frac{E}{2 \cdot (1+\nu)} \quad (4.28)$$

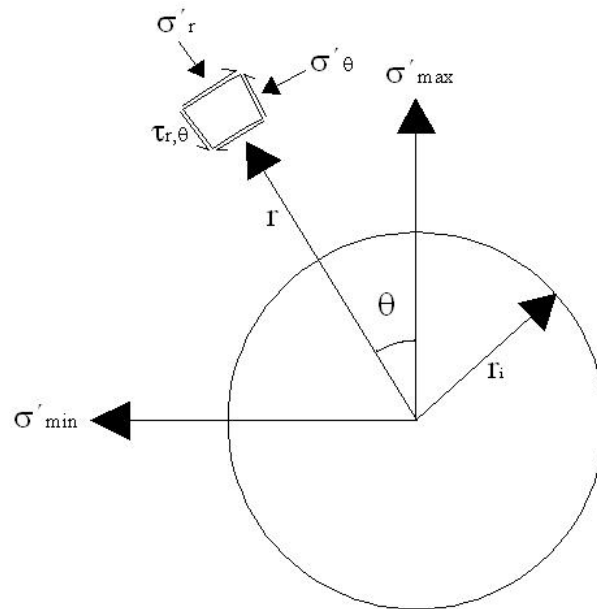


**Figure 4-18: Radial, tangential and shear stresses given at any point with polar coordinates [34].**

An elliptical form has also given a good approximation for stress determination around excavation openings [34]. In a biaxial stress field, the tangential boundary stresses are given as



$$\sigma_{\theta}^A = \sigma_v \cdot \left( 1 + 2 \cdot \frac{W}{H} - k \right) \quad (4.29)$$

$$\sigma_{\theta}^C = \sigma_v \cdot \left( k \cdot \left( 1 + 2 \cdot \frac{H}{W} \right) - 1 \right) \quad (4.30)$$

where  $W$  and  $H$  are the elliptical opening width and height, and the location of  $A$  and  $C$  are at the tunnel wall and roof locus respectively, see Figure 4-19.

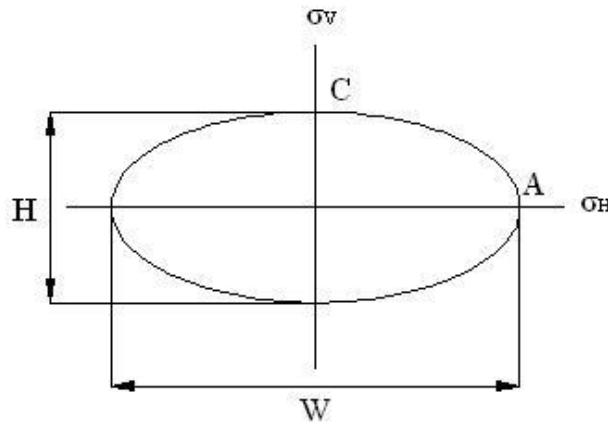


**Figure 4-19: Tangential stresses for an elliptical opening [34].**

Many underground excavations are too complex in cross section to be analyzed by closed form solutions based on the mathematical theory of elasticity, e.g. horseshoe geometry. For these cases numerical models are used to calculate stress distributions with aid of numerical methods. Many methods are available for numerical modelling and choices are made to accommodate material properties and geometry and to keep the numerical effort at a minimum. In the modelling phase of this thesis the finite element program *Phase2* will be used.

## 5 The Fáskrúðsfjörður Tunnel

### 5.1 The Project

The Fáskrúðsfjörður tunnel is 5,7 km long road tunnel. The construction is to improve the transportation system in eastern Iceland. The distance between Reyðarfjörður and Fáskrúðsfjörður before the tunnel was 52 km but after the construction the distance is 21 km. The construction started in April 2003 and the tunnel opened in September 2005, a month before scheduled [35]. Figure 5-1 presents the Fáskrúðsfjörður tunnel construction area.

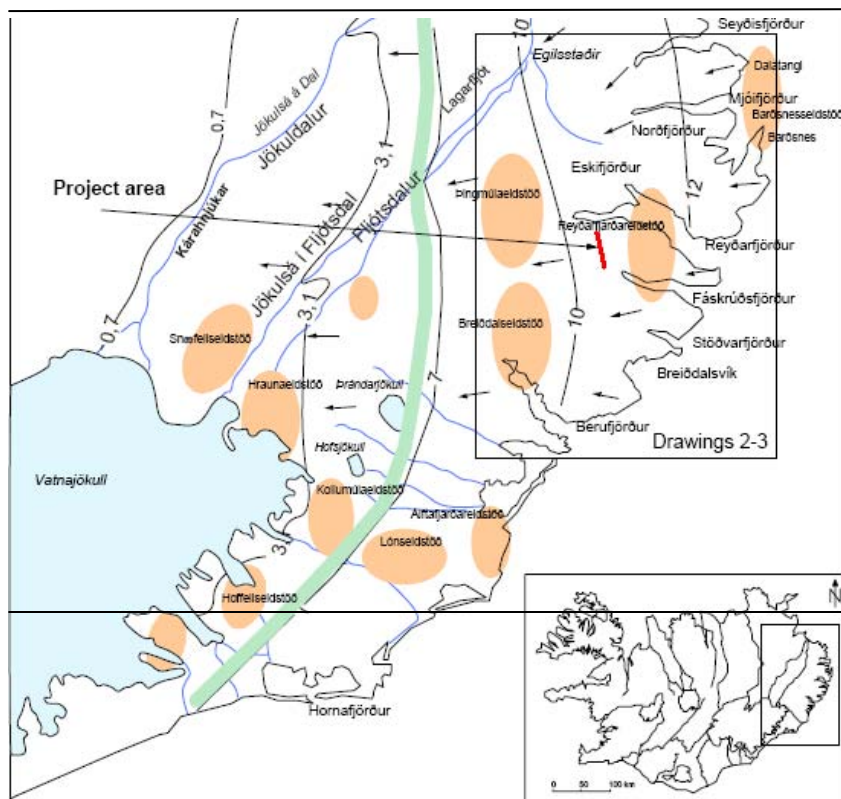
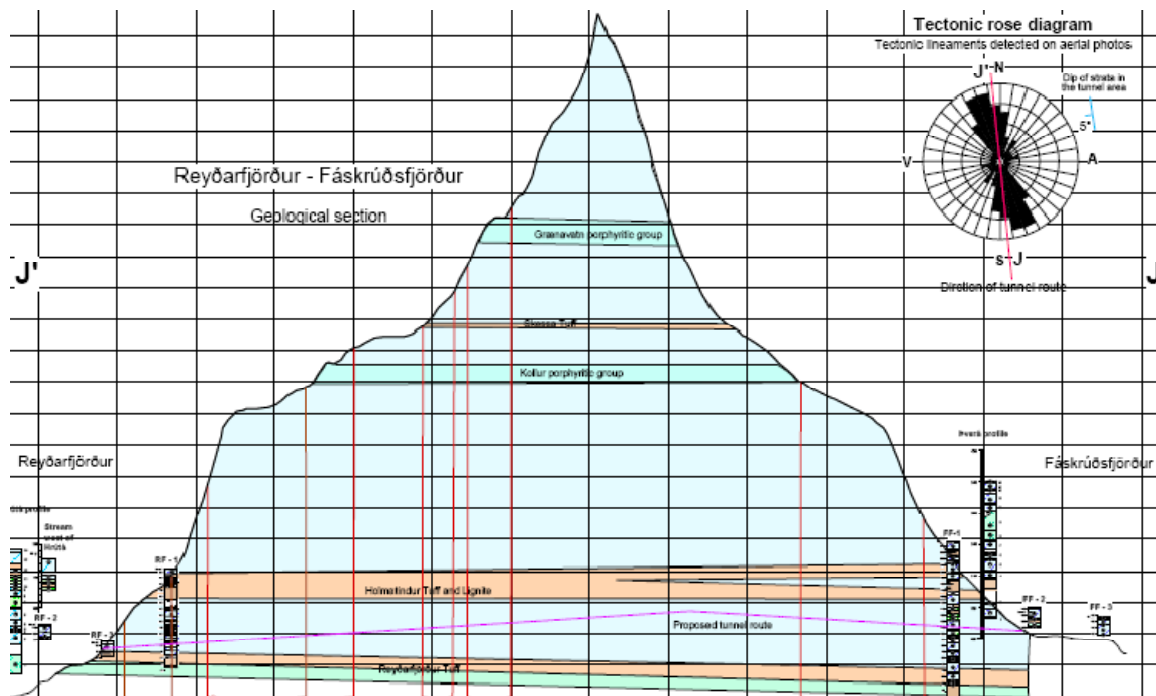


Figure 5-1: Project area for the Fáskrúðsfjörður tunnel [36].

In December 2002 the Icelandic Road Administration tendered the Fáskrúðsfjörður tunnel. A construction contract was made to the lowest bid which came from Ístak ehf. and Pihl & Søn A/S. The supervision was taking care by GeoTek Ltd. The key figures for the project are in Appendix 2. The tunnel was excavated using drill and blast technique [35].

The construction of the tunnel was according to the preliminary studies of the construction area, except in the middle of the excavation time during January 2004. The contractor estimated that the rock stratum were different than according to the given sections. So two boreholes were drilled inside the tunnel to confirm the surrounding rock mass [37].



**Figure 5-2: Cross section of the mountain ridge, the tunnel route is marked as a violet line [36]. Scale 1:50.000**

The location of the tunnel depends on the geological condition in the bedrock, being in the tholeiite basalt series in between the thick sediments of the Reyðarfjörður acidic tuff below and the Hólmatindur tuffs and lignite above. The tunnel runs from a portal at El. 75 m a.s.l. from Hróteyri at Sléttuströnd in Reyðarfjörður to a portal at El. 105 m a.s.l. near Þverá in the Dalir area in the innermost part of Fáskrúðsfjörður. The tunnel route through the mountain, Kollufjall, crossed approximately 100 m thick rock series of basalt layers

comprising relatively thin sedimentary interbeds. Thick sediments of relatively unfavourable tunnelling conditions mark the upper and lower boundaries of this part of the basalt strata. The tunnel route almost line up along the strike of the gently dipping strata so the tunnel crosses relatively few massive basalt layers and thin interbeds. The tectonic activity and dyke intensity is at minimum in this area compared to the conditions few kilometres towards east and west. Figure 5-2 presents the cross section of the mountain ridge where the tunnel runs [36].

Exploratory drilling was carried out near Hróteyri and Dalir in June and July 2000. Six cored boreholes, three on each side of the mountain ridge, with a cumulative length 530 m were drilled to establish the stratigraphical model previously based on field mapping and to evaluate technical properties of the rock. Additionally, 31 percussion boreholes were drilled to find resistance of surficial sediments and to measure depth to solid bedrock. The boreholes confirmed the existing stratigraphical model with a interesting tunnel route in the tholeiite series located in between the Reyðarfjörður acidic tuff and the Hólmatindur tuff and lignite [36], see drawing 6 in Appendix 2.

## **5.2 Geology at Fáskrúðsfjörður and Reyðarfjörður**

The geology at the construction site has been assessed by gathering information from a scientific geological reports by G.P.L. Walker. He and his team mapped the bedrock of the Eastern Fjords, from field mapping, inspection of aerial photographs and description of geological profiles as well as from core drilling, core logs and permeability tests.

The mountains around Fáskrúðsfjörður and Reyðarfjörður are part of the tertiary basalt of Iceland. The mountainous ridge which divide Reyðarfjörður and Fáskrúðsfjörður is narrow at the outer end, relatively broad in the middle part and again a bit narrower at the inner end, see Figure 5-3. The bedrock may be divided into three sections; the lower basalt series, the central volcano and upper series.

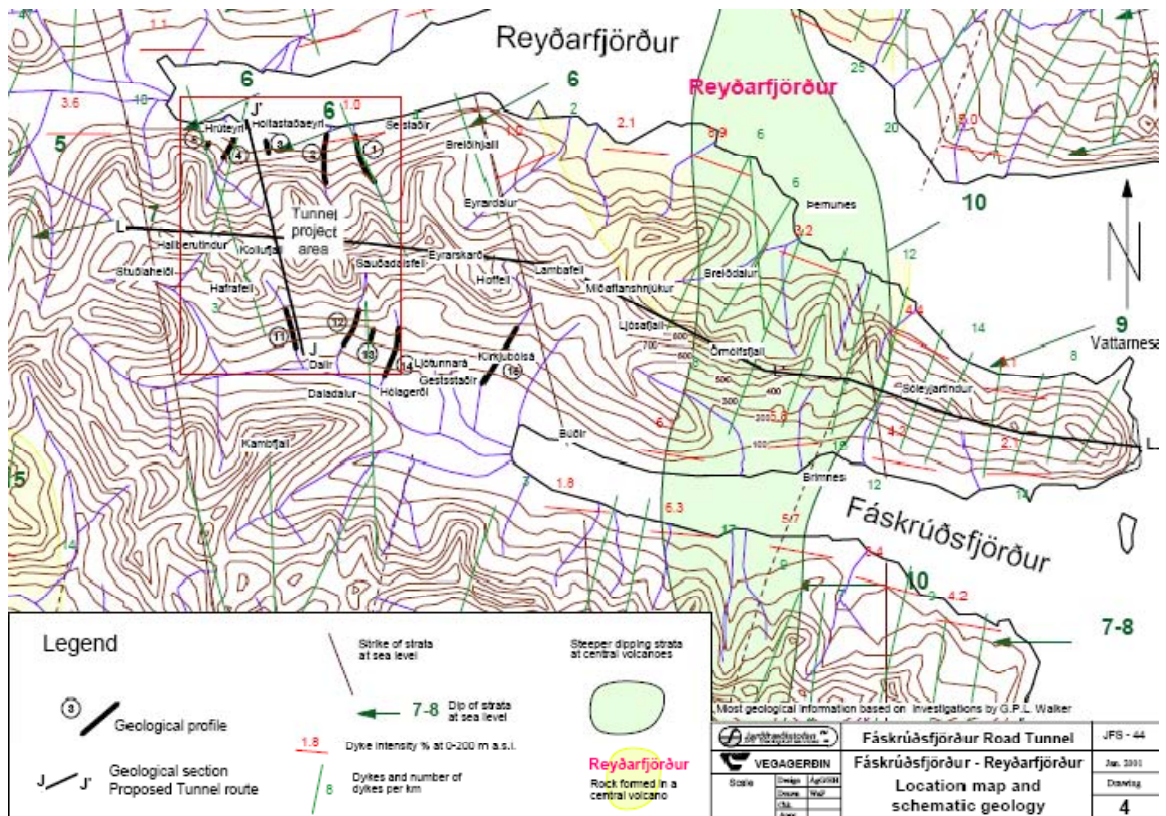


Figure 5-3: A map over Fáskrúðsfjörður tunnel closest area [36]. Scale 1:200.000

The lower series consist of basalt and sedimentary interbeds forming cumulative thickness of approximately 1000 m from Vattarnes in the east up to Sóleyjartindur west of Staðarskarð. The dip of the regional strata is relatively high due to local down sagging under the relict central volcano in addition to the regional dip of the bedrock, see drawing 5 in Appendix 2.

On both sides of Reyðarfjörður there are signs of a big relict central volcano which is designated to Reyðarfjörður and was rising at least several hundred meters over the basalt plateau some 11 million years ago. The southern part of the volcano transect the eastern part of the peninsula between Reyðarfjörður and Fáskrúðsfjörður exhibiting irregular rock units of various type and dip direction. The rock consists of basalt and different acidic rock and sediments of various types and thickness. All rocks in the area of Reyðarfjörður volcano are unfavorable as tunneling rocks [36].

The most suitable area for tunnel between Reyðarfjörður and Fáskrúðsfjörður are located west of the rock series belonging to the Reyðarfjörður central volcano. West of the Reyðarfjörður central volcano the strata was built up by regional volcanism where the basalt layers were buried and wedged out against the sides of

the central volcano. In the lowest part near Búðir in Fáskrúðsfjörður presented series of thin tholeiite lavas belonging to the flanks of the central volcano are. Above the central volcano tholeiites there exists two series of olivine basalt which also belong to the existence of the volcano, which was almost buried in the regional volcanism at this time. These olivine basalt series are compound flow series, above these series the influence of the Reyðarfjörður central volcano disappears in the strata toward west of the old mountain. Above the compound series are approximately 150-200 m thick series of tholeiite basalt layer, frequently intercalated with 1,3 – 2 m thick sediments of red sandstone. On the top of the tholeiite series is approximately 15-30 m thick sediment of acidic tuff, named Reyðarfjörður acidic tuff. This sediment is unfavourable as a tunnelling rock. On the top of the Reyðarfjörður acidic tuff are almost 100 m thick series of relatively massive tholeiite lavas intercalated with thin beds of reddish sandstone and tuff. In this series the tunnel between Fáskrúðsfjörður and Reyðarfjörður is located. Resting on this tholeiite series are very thick sediments containing sandstone and tuff and lignite, named Hólmatindur acidic tuff. Above the Hólmatindur acidic tuff, the basalt lava pile continues with 200 – 300 m thick series of tholeiite basalts within thin sedimentary interbeds [36].

Joints detected in the rock are mainly discontinuous joints formed by cooling of the lava flows forming the basalts. Dikes are relatively few compared to average dike intensity in the bedrock of the East fjords and common dike thickness is 2 – 8 m.

A rose diagram of tectonic features (faults, dike and tectonic joints) detected in the mountains between Fáskrúðsfjörður and Reyðarfjörður show the main trend towards NNW-SSE, 340°-360° see Figure 5-4. Additional tectonic trend is heading NE-SW, 40°. The tunnel route between Hróteyri and Dalir is located approximately in the middle of the low dike intensity between the dike swarms of the Reyðarfjörður and Breiðdalur central volcanoes, approximately 7 – 8 % dike intensity. The tunnel route is almost parallel to the main tectonic direction in the area. The dip of strata in the tunnel area is 5° [36].

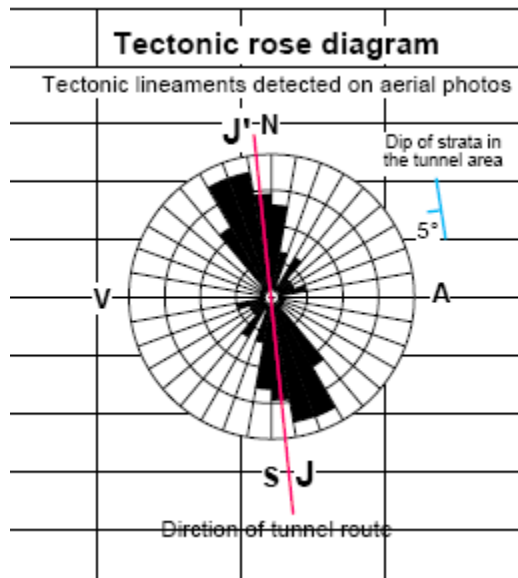


**Figure 5-4: A Rose diagram for the construction area, J-J' presents the tunnel route [36].**

A vertical section through the basalt layers on the tunnel route normally shows approximately 20-25 % of compressed consolidated scoria at the top, 75-80 % of the thickness is massive crystalline rock in the middle of the basalt and less than 5 % of well compressed scoria at the base. The crystalline middle part exhibits normally a relatively high uniaxial breaking strength, or frequently 5-10 times higher than the scoria at the top and bottom and sediments, which show similar range of breaking strengths. Figure 5-5 presents the geotechnical properties of the different layers on the tunnel route [36].

### Typical sequence of rock units in Tertiary basaltic successions in eastern Iceland

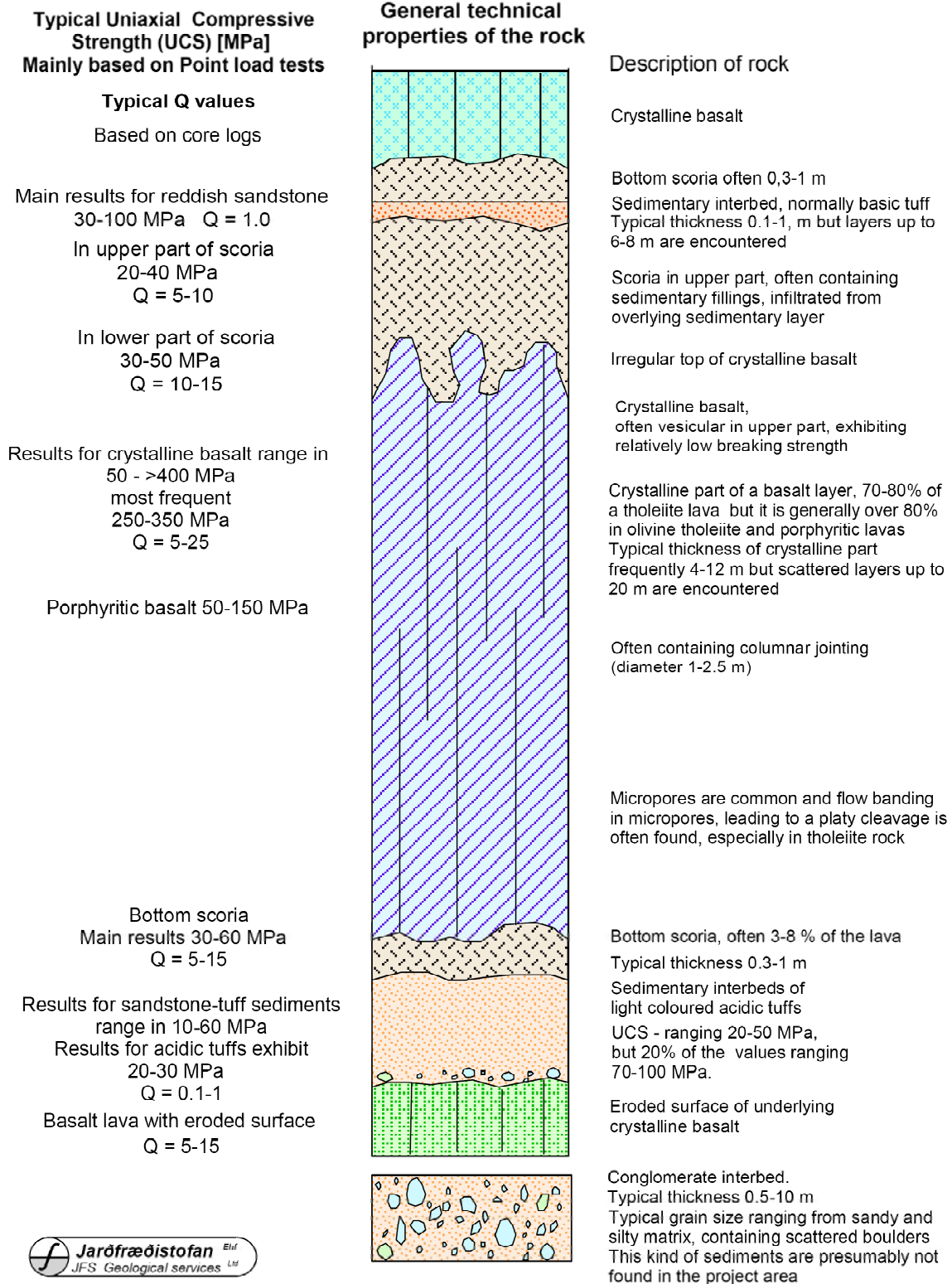


Figure 5-5: Typical properties of a basaltic lava section [36].



### 5.3 Rock Support Systems in Fáskrúðsfjörður Tunnel

The Fáskrúðsfjörður tunnel was supported with shotcrete with and without steel fibres and rock bolts, mainly grouted rebar rock bolts, but also CT-bolts and rock bolts with a chemical anchor. At some places chain links were used between rock bolts to increase the stability. The length of the rock bolts varies from 2,4–8 meters [27].

Circumstances in the Fáskrúðsfjörður tunnel are quite special due to the great overburden above and the orientation of fault zones is parallel to the tunnel route. Because of this the Fáskrúðsfjörður tunnel is most the supported road tunnel in Iceland except for the Hvalfjörður tunnel, which is located undersea [35].

The amount of rock bolts used in the Fáskrúðsfjörður tunnel after secondary support phase were 18.076 or 3,2 rock bolts per length meter. Estimated use of rock bolts according to construction contract were 14.700 rock bolts or 2,6 rock bolts per length meter which is a rise of 23%, see Figure 5-6. The estimated amount of shotcrete used according the construction contract were 10.000 m<sup>3</sup> or 1,8 m<sup>3</sup>/m, but used shotcrete was 13.477 m<sup>3</sup> which is a rise of 35% [35], see Figure 5-7.

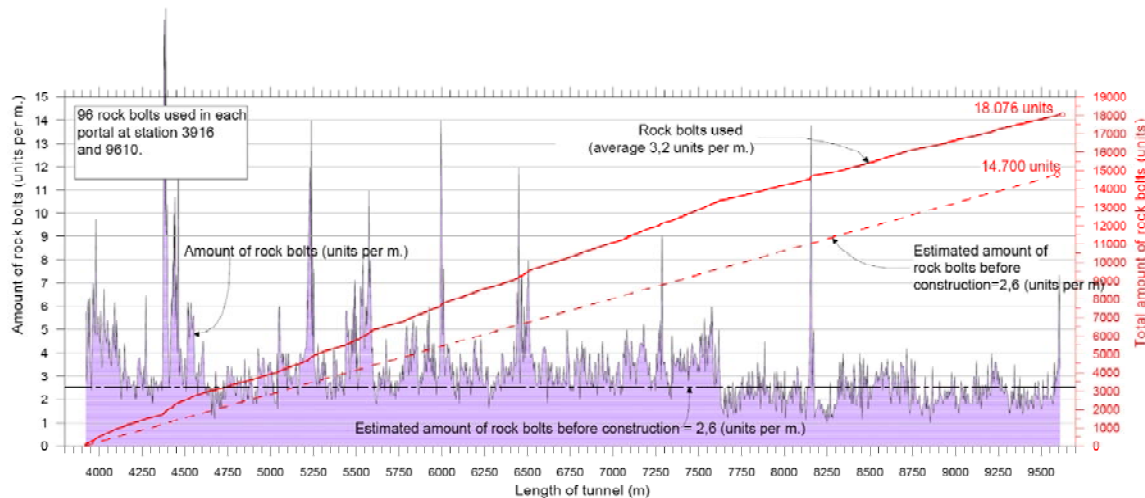


Figure 5-6: Amount of rock bolts used in the Fáskrúðsfjörður tunnel [35].

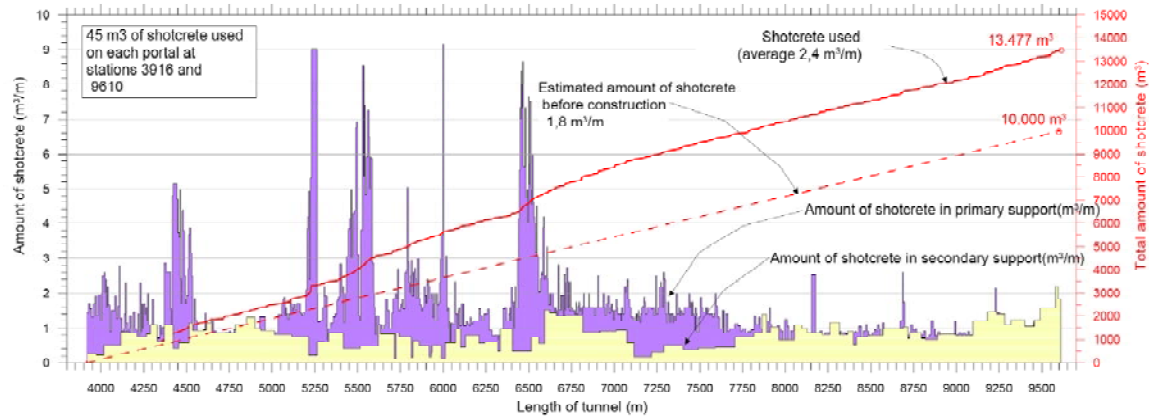


Figure 5-7: Amount of shotcrete used in the Fáskrúðsfjörður tunnel [35].

## 5.4 Stress Measurements in Fáskrúðsfjörður Tunnel

During excavation of the Fáskrúðsfjörður tunnel, explicit signs of high rock stress was encountered, the stress indications was exposed as rock spalling in stiff layers and squeezing/collapse in weak sediments layers. The reason is great overburden above the tunnel, where the mountain ridges rises to El. 1100 m a.s.l. at highest point. The orientation of fault zones is also parallel to the tunnel route. To get better understanding of the behaviour of the rock mass during excavation, in situ rock stress measurements were carried out by SINTEF Ltd. at selected locations in the tunnel [35].

Two different types of methods were applied to get an indication of actual stress concentration near the tunnel, 2D (doorstopper) and 3D, overcoring methods. In Appendix 2 a description of these two tests is given. The stress measurements were performed at four different station in niches where the diameter of the tunnel is about 11 meters. Borehole 1 (2D and 3D) is located at station 6530, borehole 2 (2D) at station 7085, borehole 3 (2D and 3D) at station 7615 and borehole 4 (2D) at station 4208. In borehole 2 at station 7085 no stress measurements were performed due to extremely poor rock quality [38]. Table 5-1 and Table 5-2 presents the results from the stress measurements and theoretical calculations of stress values from the Fáskrúðsfjörður tunnel. In Table 5-1 the dip of the vertical stresses is given for stations 6530 and 7615, also the trend of the horizontal stresses from north for same stations.

**Table 5-1: Results from stress measurements in the Fáskrúðsfjörður tunnel [38].**

Station	$\sigma_v$ [MPa]	$\sigma_{h,max}$ [MPa]	$\sigma_{h,min}$ [MPa]	$K_0^{max}$	$K_0^{min}$
4208 (2D)	7,2	16,1	1,2	2,24	0,17
6530 (2D,3D)	23/68°	11/170°	3/89°	0,48	0,13
7615 (2D,3D)	15/14°	22/6°	2/96°	1,47	0,13

From Figure 5-4 it can be seen the orientation of the maximum horizontal stresses is N-S, which is parallel to the tunnel route, that secure more stability inside the tunnel. If the tunnel route had crossed the maximum horizontal stresses plan, a very problematic condition would have occurred especially at tunnel roof [35]. The difference between  $K_0^{max}$  and  $K_0^{min}$  states that the stress condition is anisotropic.

**Table 5-2: Theoretical stress values [38].**

Station	$\sigma_{v,theo}$ [MPa]	$\sigma_{h,theo}$ [MPa]	Depth [m]
4208 (2D)	3	0,6	100
6530 (2D,3D)	19	4	670
7615 (2D,3D)	14,5	2,5	510

The theoretical stress values were calculated from

$$\sigma_{v,theo} = \rho \cdot g \cdot h \quad (5.1)$$

$$\sigma_{h,theo} = \frac{\nu}{1-\nu} \cdot \sigma_{v,theo} \quad (5.2)$$

where the parameters are

$h$  = vertical overburden (m)

$\nu$  = 0,16

$g$  = 9,81 m/s<sup>2</sup>

$\rho$  = 2900 kg/m<sup>3</sup>

Table 5-1 and Table 5-2 states that vertical stresses coincides well, especially stations 6530 and 7615, which were measured with both methods. The measured maximum horizontal stresses give much higher values than the theoretical stresses

for all three stations. However, the measured minimum horizontal stresses fits quite well with the theoretically values.

According to the results from the stress measurement the most accurate outcome were from stations 6530 and 7615. Consequently, these stations will be modelled using the finite element program *Phase2*.

## 6 Laboratory Tests

To have any idea about the behaviour of the rock mass due to external load the mechanical properties have to be known. To gather these mechanical properties core samples were transported from the Icelandic Road Administration at Reyðarfjörður to Denmark for laboratory testing. The core samples are from borehole FF-04, which is 111,5 m deep and is located at station 7870 inside the tunnel, see Figure 6-1. The borehole was drilled to map the situation of sediment layers below the tunnel.

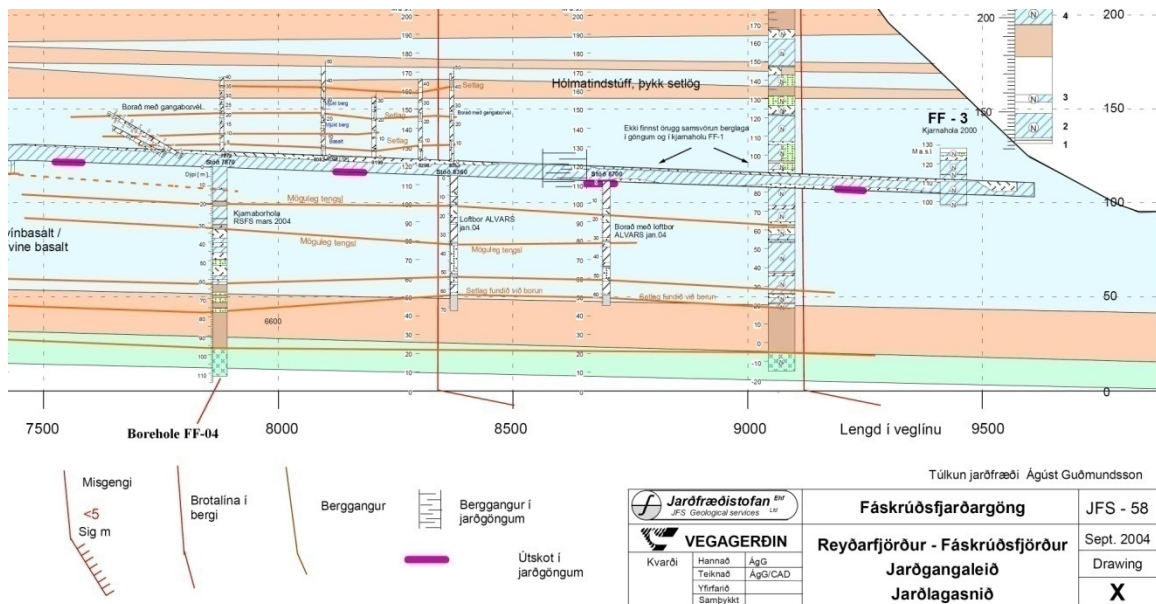


Figure 6-1: Location of the borehole FF-04. Appendix 3 displays a larger figure [36].

Laboratory tests were performed at DTU and GEO. The collected core samples were mainly scoria and sediments, and amount to twelve core pieces. Core pictures and core logs are presented in Appendix 3, where rock cores are classified according to lithology. Laboratory tests performed were brazil test, unconfined compression test and triaxial test. The first two named were performed at GEO and the triaxial test at DTU under guidance of PhD student Katrine Alling Andreason. A master

student at DTU Hallgrímur Örn Arngrímsson was a participant in the laboratory tests, writing a special project about volcanic rocks in Iceland.

## 6.1 Preparation for Laboratory Testing

The core samples from borehole FF-04 have the diameter 45 mm. The samples were cut at GEO using a diamond disc. All core samples were cut according to ISRM standard, the height of Brazil samples were cut half a diameter, approximately 22 mm and for the Unconfined compression and Triaxial samples the height was two times larger than the diameter, or 90 mm.



**Figure 6-2: Core samples measured**

All cores were measured and inspected to get as many good samples as possible. Height for Brazil samples is 22 mm and 90 mm for Unconfined Compression and Triaxial tests.

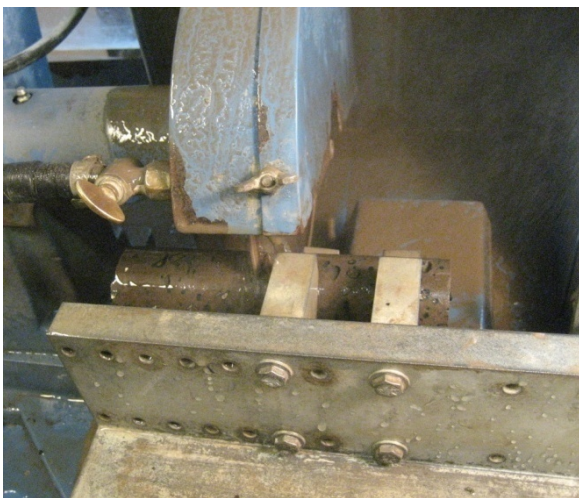


**Figure 6-3: Core sample cut in pieces**

The core is installed in between steel jaws to secure its stability. The diamond disc is cooled down with cold water during the action. The platform with the sample can be controlled by turning a winch.

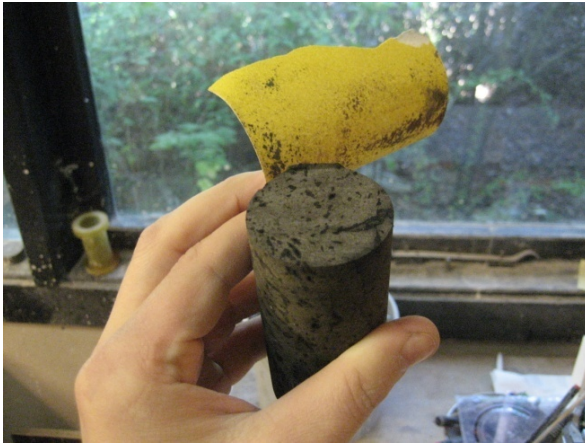


**Figure 6-4: Sample polished**

During cut off, some of the samples got an edge, which must be polished to surface plan by using sandpaper.



**Figure 6-5: Sample compare with a setsquare**

Both ends of the sample must be cut at right angle to the longitudinal axis, so the load will distribute equally on the whole surface.



**Figure 6-6: Samples marked**

All samples were marked according to the borehole and the depth they were taken.



**Figure 6-7: Siltstone waste away during cut off**

Almost all the fine grained siltstones core samples got ruined during the cut off, due to a contact to water.



**Figure 6-8: Workshop at GEO**

Thesis author and Hallgrímur Örn cutting rock cores in workshop at GEO.



**Figure 6-9: Samples water saturated**

After all the process the test samples were put into a bowl with closed lid which was attached to a vacuum instrument. The purpose was to get the samples saturated, in order to simulate in-situ conditions.



## 6.2 Brazil Test

The Brazil tests were performed at GEO. The test samples were mainly scoria and sediments, but also some basalt samples. A total number of 25 samples were tested. The test is used for indirect determination of the tensile strength of intact rock. If a circular cylindrical sample is compressed along its diameter and strain measured, failure occurs by an extension fracture in the loaded diametric plane at some value of the applied load. The uniaxial tensile strength in MPa can be estimated from

$$\sigma_t = 0,636 \cdot \frac{P}{D \cdot t} \quad (6.1)$$

where  $P$  is the applied load at failure in Newtons,  $D$  is the diameter and  $t$  is the thickness of the sample in mm. The test samples were handled according to ISRM standard (Suggested Methods for Defining Tensile Strength of Rock Matreials, pp:177-183) before and after testing [39]. Figure 6-10 and Figure 6-11 presents the test setup.



**Figure 6-10: Test setup for Brazil test, includes a loading frame, a data logger, a load cell, a vertical strain gauge and a computer.**

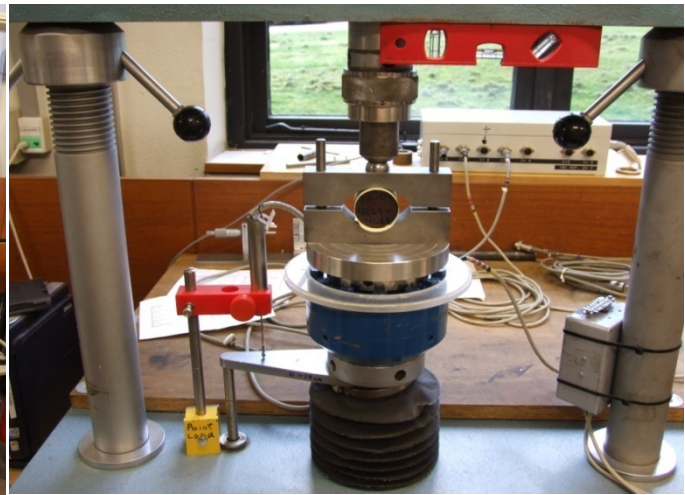


**Figure 6-11: Scoria sample placed in between the two jaws, ready for testing.**

Pictures of the test samples and the test results are presented in Appendix 4. For further detailed descriptions of the test interpretations, reference is given to Hallgrímur Örn Arngrímsson's report [40].

### 6.3 Unconfined Compression Test

The unconfined compression tests were performed at GEO. The test samples were 12, mainly scoria and sediments, but also some basalts samples. The vertical compression load,  $P$ , is applied to the sample and the vertical strain,  $\varepsilon_t$ , is recorded. The estimated parameters are unconfined compressive strength  $\sigma_c$  and Young's modulus  $E$ .

$$\sigma_c = \frac{P}{A} \quad (6.2)$$

$$E = \frac{\Delta\sigma_1}{\Delta\varepsilon_1} \cdot 100 \quad (6.3)$$

where  $P$  is load at failure in Newtons and  $A$  is the cross section area in square millimetres. The test samples were handled according to ISRM standard (Suggested Methods for Defining the Uniaxial Compression Strength and Deformability of Rock Materials, pp:151-156) before and after testing [39]. The test setup is the same as in the brazil test except for the disc shape jaws, instead the specimen ends are connected to a vertical axis and a load cell, see Figure 6-12.

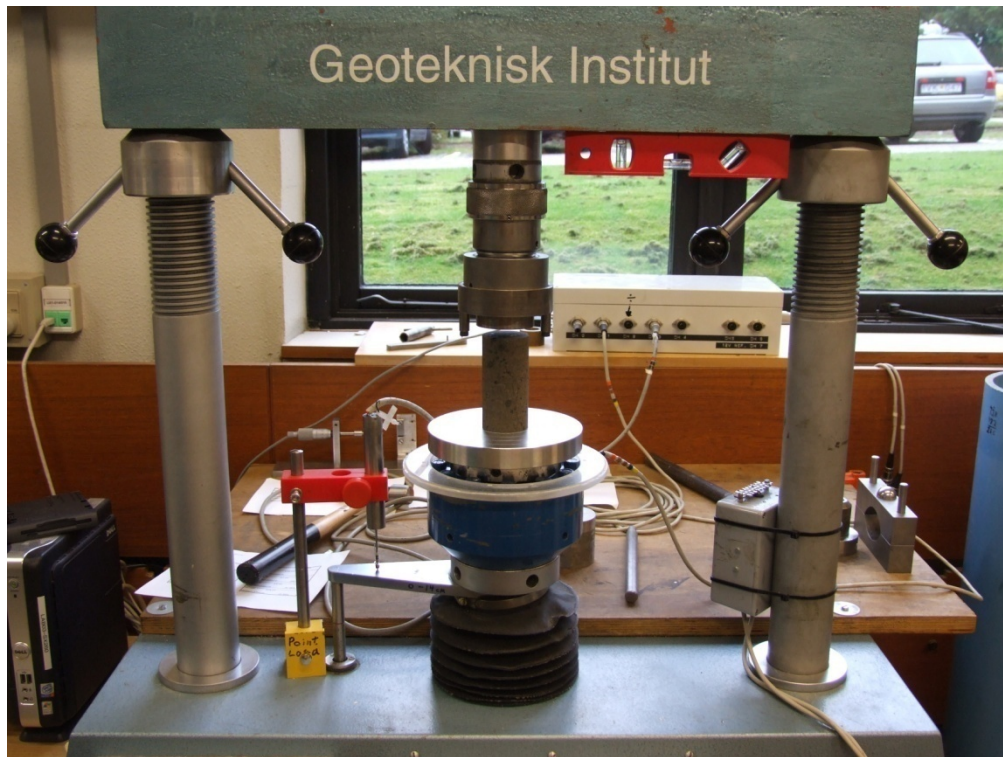
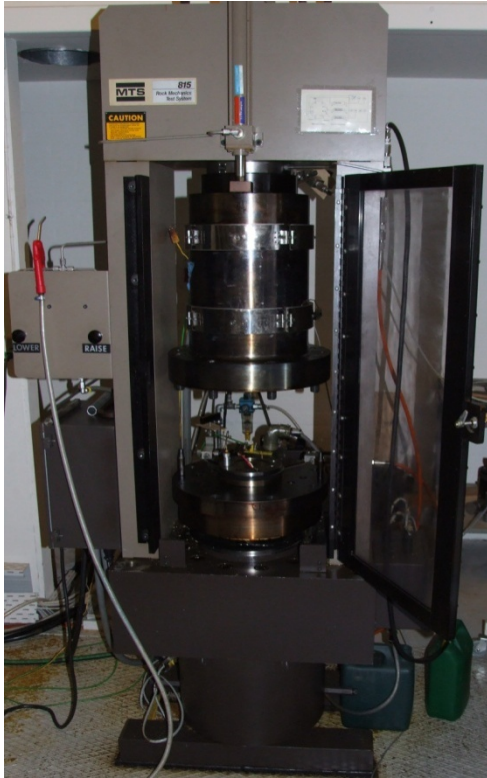


Figure 6-12: The test setup is same as for Brazil test except for the disc shape jaws.

Pictures of the test samples and the test results are presented in Appendix 4. Further detailed descriptions of the test interpretations, reference is given to Hallgrímur Örn Arngrímsson's report [40].

## 6.4 Triaxial Test

The triaxial tests were performed at DTU under guidance of Katrine Alling Olufsen. The amount of test samples were four, but one of them failed during the loading at the start so no results are available for that sample. The MTS compression machine can provide a confining pressure up to 83 MPa, which is applied with special oil in the test cell, see Figure 6-13. The test samples were handled according to ISRM standard (Suggested Methods for Defining the Strength of Rock Materials in Triaxial Compression, pp: 157-164 and Suggested Methods for Defining the Complete Stress-Strain Curve for Intact Rock in Uniaxial Compression, pp: 217-229) before and after testing, see Figure 6-14 [39].



**Figure 6-13: The MTS compression machine used for the triaxial testing.**

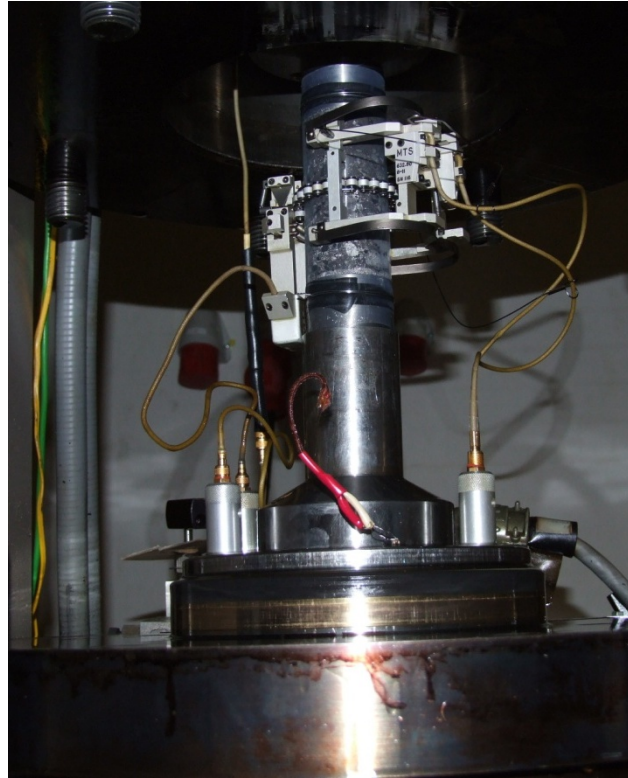


**Figure 6-14: Sandstone sample installed in the cell, ready for testing. Extensometers positioned at each side of the sample to measure radial and axial strains.**

Test procedure is as follows: The samples were loaded vertically with  $K_\sigma$ -loading where lateral strains  $\Delta\varepsilon_2$  and  $\Delta\varepsilon_3$  are kept constant till the vertical stress ( $\sigma_l$ ) reaches 15 MPa which is approximately the in-situ stress condition. Then the load is decreased down to 3-5 MPa and reloaded with constant  $K_\sigma$ -loading up to 15 MPa. At that point the confining pressure ( $\sigma_3$ ) were kept constant and vertical stress driven towards failure.

Sample nr.5 fractured during the vertical  $K_\sigma$ -loading in the start so limited results are available for that. Various parameters are interpreted from test results. Pictures of the test samples and the test results are presented in Appendix 4. For further detailed descriptions of the test interpretations, reference is given to Hallgrímur Örn Arngrímsson's report [40].

## 6.5 Comparison to Dataset from Kárahnjúkar

A large laboratory test dataset from the headrace tunnel in the Kárahnjúkar hydroelectric project was analysed as an intimation for strength properties of the rock mass surrounding the Fáskrúðsfjörður tunnel. Kárahnjúkar is also located in the eastern part of Iceland. The bedrock from Kárahnjúkar area is only about 6,5 million years old. However, the Fáskrúðsfjörður bedrock is approximately 10 million years old, so the analyses should give a satisfactory approximation. In the selection of the rock cores from the Fáskrúðsfjörður tunnel the attention was kept on scoria or porous basalts and sediments.

The method used for comparison was applied on limestone during preparation for the studies in construction of the Citytunnel in Malmö [41], but has never been applied to volcanic rock as known. The method comprehends plotting of various strength properties; tensile strength, unconfined compression strength and Young's modulus on a logarithmic scale against bulk density for different rock types. Then, strength parameters from different tests were combined using a method proposed by Merete V. Madland [42]. The friction angle  $\varphi$  and the cohesion  $c$  are calculated according to

$$\varphi = \arcsin \left( \frac{\frac{\sigma_c}{\sigma_t} - 4}{\frac{\sigma_c}{\sigma_t} - 2} \right) \quad (6.4)$$

$$c = \sqrt{3} \cdot \sigma_t \quad (6.5)$$

**Table 6-1: Strength parameters from rock cores tested from the Fáskrúðsfjörður tunnel**

Rock type	$\sigma_c$ [MPa]	$\sigma_t$ [MPa]	E [MPa]	$\phi$ [°]	c [MPa]
Tholeiite basalt	30	3,7	10621	42,5	6,4
Olivine basalt	24,5	2,2	9692	51,7	3,8
Scoria	16,1	1,7	7413	47,4	2,9
Sandstone	11,7	1,7	4190	35,9	3

**Table 6-2: Strength parameters from Kárahnjúkar project analysis [5].**

Rock type	$\sigma_c$ [MPa]	$\sigma_t$ [MPa]	E [MPa]	$\phi$ [°]	c [MPa]
Tholeiite basalt	193,4	13,5	34088	56,9	23,4
Olivine basalt	168	12	29859	56,4	20,8
Scoria	23	4,7	4025	24,4	9,1
Sandstone	43,6	4	5000	42,9	7,1

Appendix 4 presents plots of the comparison between laboratory test results for the Kárahnjúkar headrace tunnel and the Fáskrúðsfjörður tunnel. As seen from the tables above and the plots, almost all strength parameters for the Fáskrúðsfjörður tunnel are much lower, e.g. unconfined compression strength for various basalts is more than six times larger from Kárahnjúkar than Fáskrúðsfjörður. On the other hand, there is not so much difference between scorias. Also, the bulk density is much lower for samples from Fáskrúðsfjörður. The reasons for high differences in strength and bulk density may be related to the selection of porous rock cores from Fáskrúðsfjörður tunnel, but the rock mass there is also older and its strength has been reduced due to weathering and high stress conditions. Comparing the laboratory test results from various sites with the values in Table 2-2, the unconfined compression strength for different basalts from Kárahnjúkar suits well to the fresh basalt given, but basalts from Fáskrúðsfjörður are showing much lower strength.

## 7 Numerical Analysis

### 7.1 Introduction

Initially, *Plaxis V8* was planned to be used in the modelling phase, but soon some problems appeared when modelling various support systems. Then in cooperation with Oddur Sigurðsson, a decision was made to use *Phase2*, which can be used parallel with *RocLab*. *Phase2* is a 2-dimensional elastic-plastic finite element program for calculating stresses and displacements around underground or surface excavations in rock or soil. *Phase2* offers a wide range of support modelling options e.g. rock bolts and shotcrete. The program consists of three modules; model, compute and interpret.

A basic model will be set up for a typical Icelandic mixed face tunnel in elastic and elastic-plastic conditions to see how the program computes compared to the theory, and also to give a clue for selection of mechanical properties for various rock types and need of support. Then two different cross sections, station 6530 and 7615, from the Fáskrúðsfjörður tunnel will be modelled and analysed. The rock mass properties will be determined using the Kárahnjúkar properties discussed in section 6.5, by use of *RocLab*, which will be used as input parameters in *Phase2*.

Displacement measurements in Icelandic tunnels have never been recorded before and after excavation. A limited knowledge is available about this term, but according to Icelandic geotechnical tunnel engineers the maximum displacement should not exceed 10 mm [28],[43]. Consequently, the working goal has been that a fully supported (rock bolt and shotcrete) model should not have more than 10 mm in maximum total displacements.

### 7.2 Typical Icelandic Mixed Face Tunnel

Basic model of a typical Icelandic mixed face tunnel will be modelled for both elastic and plastic conditions. A normal cross section from the Fáskrúðsfjörður tunnel will be used, according to rock types, depth, dimensions of tunnel and geometry of rock stratum etc. The same parameters will be used for the different

models, except in the plastic phase, where some additional parameters will be introduced. A plain strain model with three nodes was chosen. The amount of mesh elements and nodes are 3625 and 1866 respectively. The failure criteria for defining the strength of the rock mass is Mohr-Coulomb. A gravity field stress is used, then initial element loading for each rock type will be field stress and body force. Due to various  $K_0$  values from stress measurements in the Fáskrúdsfjörður tunnel, the  $K_0$  value is estimated from Figure 3-9, and is set as 0,39.

The rock mass consists of basalt layer interbedded with relatively thin layers of scoria and sandstone, which crosses the tunnel. The dip of the stratum is 5-7° and the depth is 650 m. The tunnels width is 8,5 m and its height is 6,5 m, see Figure 7-1.

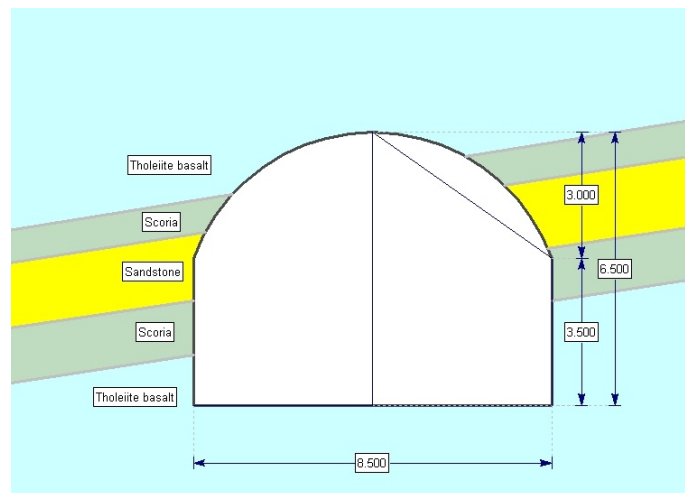


**Figure 7-1: Cross section of the basic model, the dimensions are in meters.**

To evaluate the input parameters used in *Phase2* the strength parameters from the Kárahnjúkar project analysis, see Table 6-2, were processed in *RocLab*. This is because the test samples are almost intact rock. Therefore it is preferable to reduce the strength parameters in order to simulate rock mass conditions. Strength parameters were evaluated for three different GSI values (75, 50, 25). In Table 7-1 other important input parameters used in *RocLab* are presented.

**Table 7-1: Additional parameters in *RocLab***

Rock type	$m_i$	$\gamma$ [MN/m <sup>3</sup> ]
Tholeiite basalt	25	0,028
Scoria	10	0,02141
Sandstone	17	0,01834

Other important input features for *RocLab* are following: The application is tunnel,  $D$  is set to 0 as for undisturbed rock mass and the tunnel depth is 650 m. The unit weight is almost in saturated condition.

### 7.2.1 Calculation Based on Elastic Model

One of the purpose of defining failure criterion parameters for an elastic rock type, is to allow the calculation and plotting of strength factor. Even though an elastic rock type in *Phase2* does not “fail”, the failure criterion allows a degree of overstress to be calculated.

Strength factor represents the ratio of available rock mass strength to induced stress, at a given point. Consequently, rock element which has a strength factor less than 1 will fail if left unsupported. The elastic model used for defining the rock elastic properties is isotropic, which only requires Young's modulus and Poisson's ratio. In Table 7-2, the input parameters from *RocLab* used in the elastic modelling part are presented.

**Table 7-2: Input parameters for elastic part modelled in *Phase2*.**

GSI=75					
Rock type	E [MPa]	$\nu$	$\sigma_t$ [MPa]	$\phi$ [°]	c [MPa]
Tholeiite basalt	27828	0,16	1,17	57,73	7,43
Scoria	3286	0,35	0,3492	36,95	1,92
Sandstone	4082	0,3	0,393	47,65	2,66
GSI=50					
Rock type	E [MPa]	$\nu$	$\sigma_t$ [MPa]	$\phi$ [°]	c [MPa]
Tholeiite basalt	10471	0,16	0,18	52,02	4,11
Scoria	1236	0,35	0,053	30,07	1,186
Sandstone	1536	0,3	0,06	40,86	1,63
GSI=25					
Rock type	E [MPa]	$\nu$	$\sigma_t$ [MPa]	$\phi$ [°]	c [MPa]
Tholeiite basalt	2040	0,16	0,027	44,38	2,57
Scoria	241	0,35	0,00805	22,95	0,73
Sandstone	299	0,3	0,009	33,02	1,03



It is clear, from Table 7-2, that a decrease in the strength parameters occurs with lower GSI value, by using *RocLab*. The output from the modelling phase is presented in Figure 7-2 - Figure 7-10. Strength factors, displacements and deformations for different GSI values are compared.

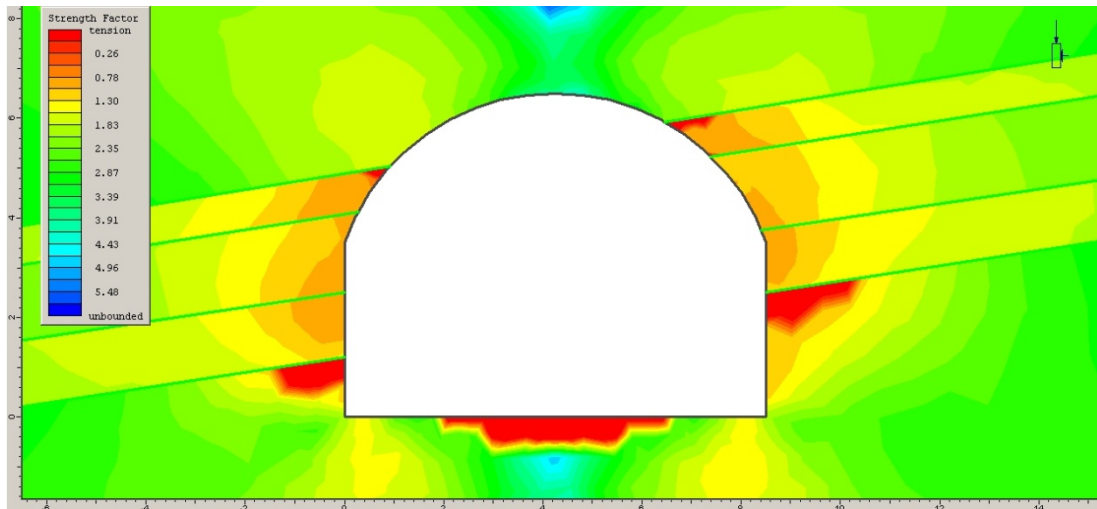


Figure 7-2: Strength factor for GSI=75.

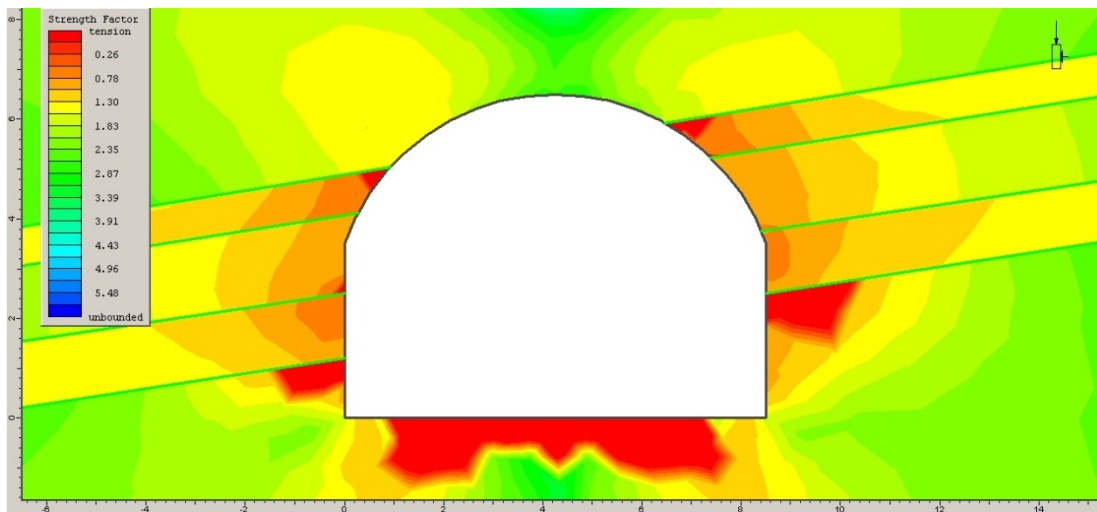


Figure 7-3: Strength factor for GSI=50.

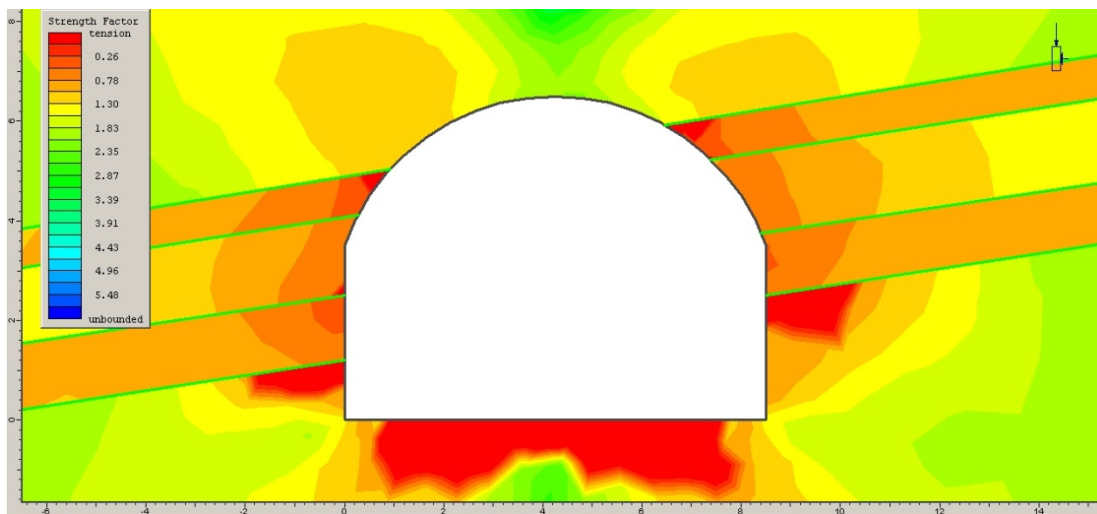
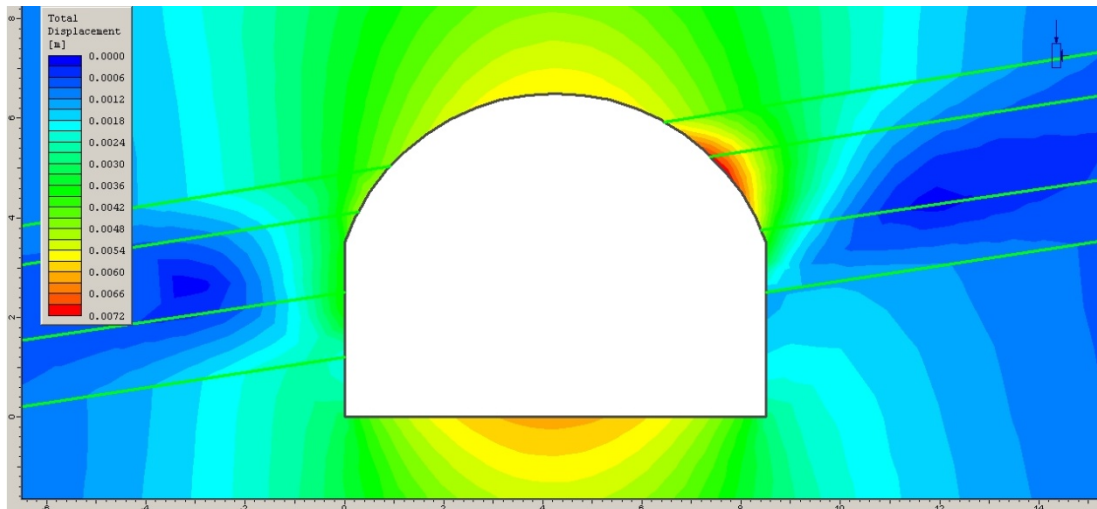
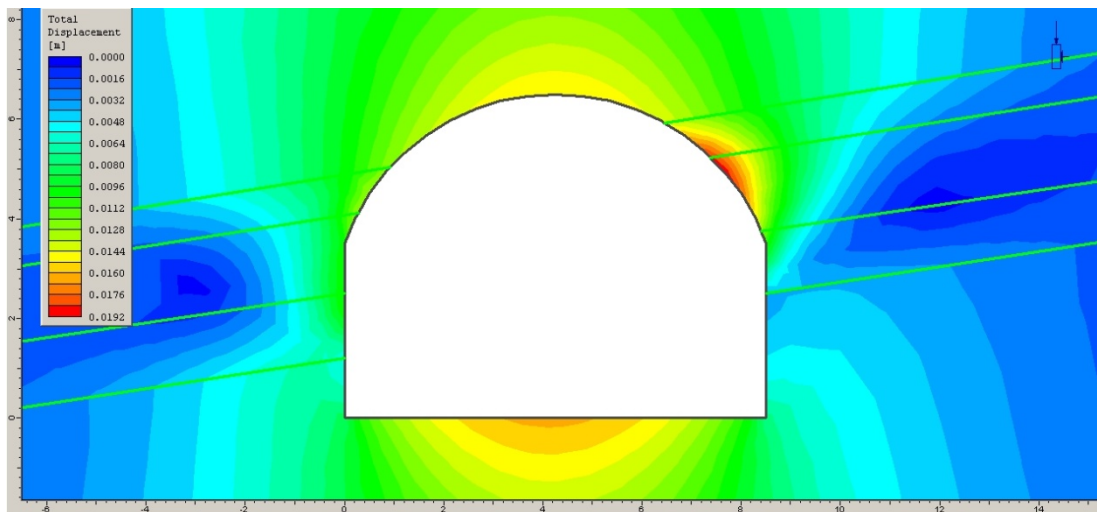


Figure 7-4: Strength factor for GSI=25.



**Figure 7-5: Total displacements for GSI=75, largest displacement is 7,1 mm.**



**Figure 7-6: Total displacements for GSI =50, largest displacement is 19 mm.**

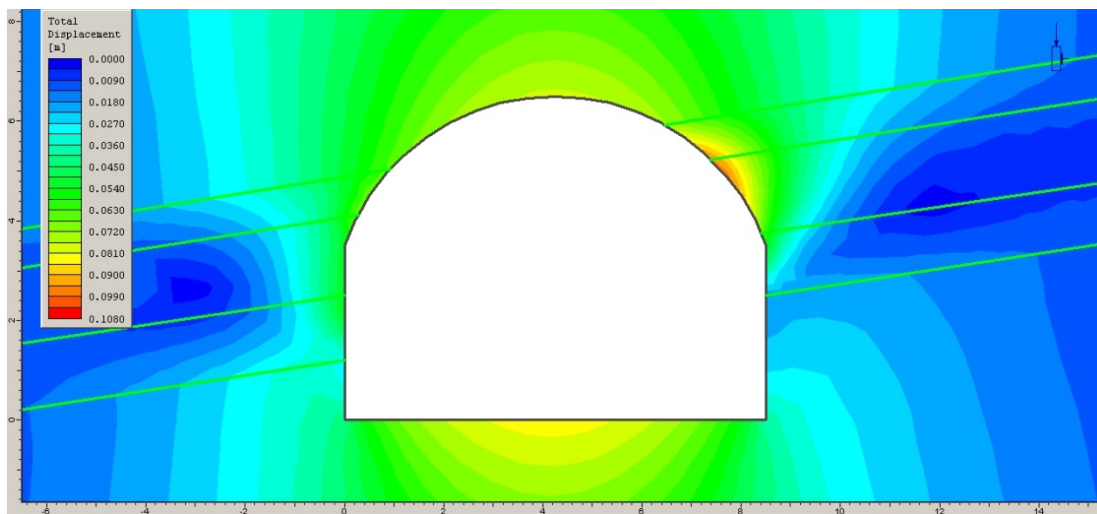


**Figure 7-7: Total displacements for GSI =25, largest displacement is 97 mm.**

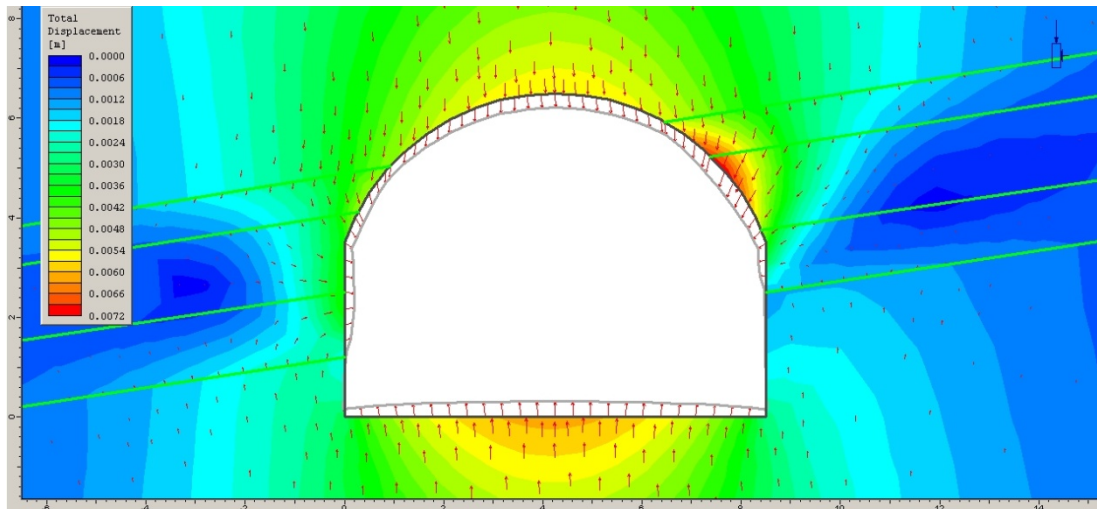


**Figure 7-8: Deformed boundaries and deformation vectors for GSI=75 (scale: x50).**

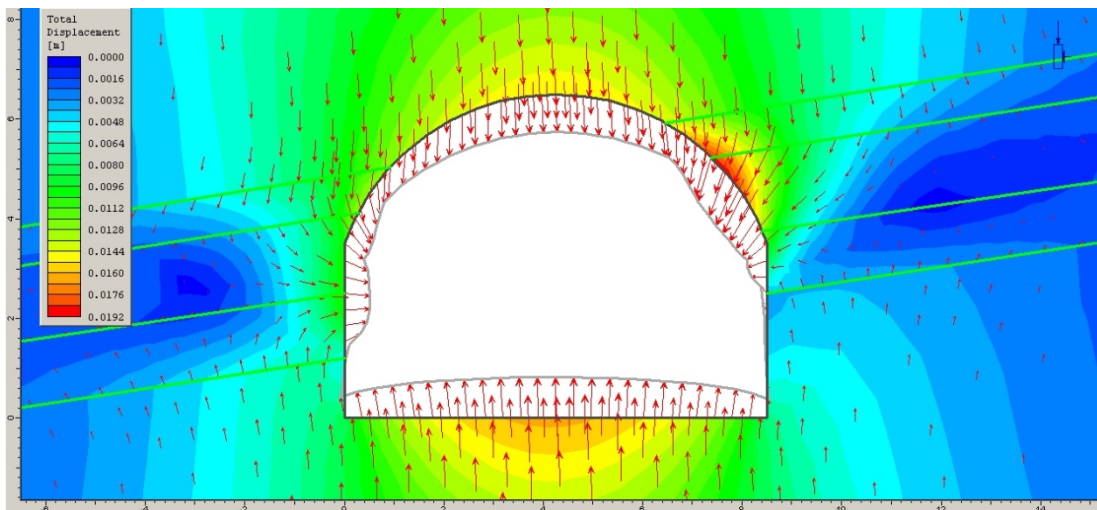


**Figure 7-9: Deformed boundaries and deformation vectors for GSI=50 (scale: x50).**

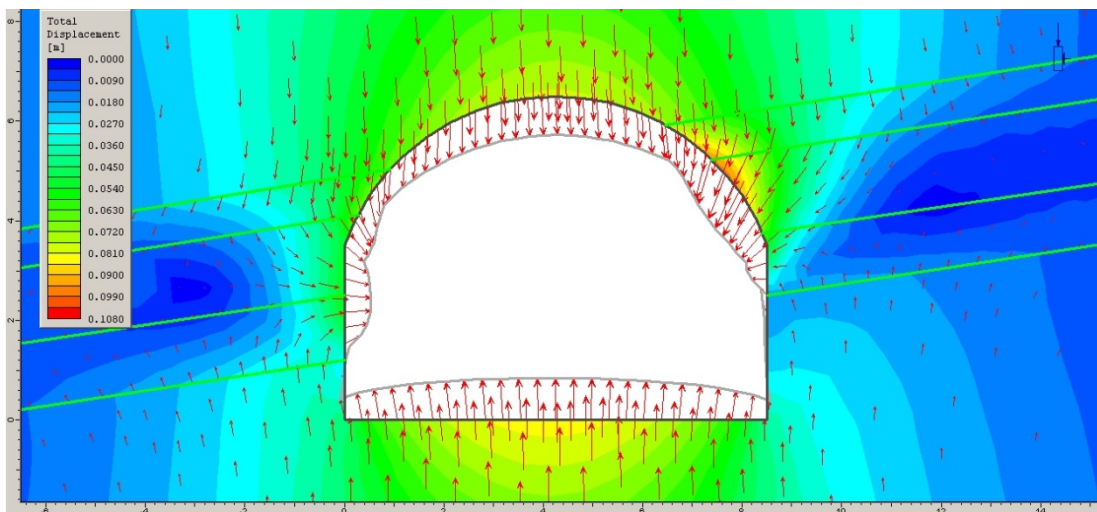


**Figure 7-10: Deformed boundaries and deformation vectors for GSI=25 (scale: x10).**

From Figure 7-2 to Figure 7-4, of the strength factor analysis, stability problems are expected in the tunnel floor and the tunnel walls in the sandstone and the scoria. No stability problems are visible in the tunnel roof and in the lower parts of the walls in the tholeiite basalt region according to the strength factor analysis.

Largest displacements of the tunnel boundary are expected in the upper right corner, in the barrier between the scoria and the sandstone, where displacements vary from 7,1 mm to 97 mm for different GSI values. Considerable displacements are visible in the roof and the floor.

With regards to deformations, see Figure 7-8 to Figure 7-10, the obvious problematic zones are visible, the scoria and the sandstone layers will squeeze into the tunnel. Considerable deformation will also occur as expected in the tholeiite zones in the roof and the floor. No deformation occurs in the lower parts of the walls.

### 7.2.2 Calculation Based on Elastic-Plastic Model

For the elastic-plastic model part, same models as used in the elastic model part will be analysed, for GSI 75, 50 and 25. Now, yielding is allowed and rock elements can reach the plastic zones, so no rock elements can have strength factor less than 1, when yielding (failure) occurs. The strength factor is by definition equal to one. So the yielded zone corresponds roughly to the zone where the strength factor is less than 1 from the elastic analysis. Some additional parameters are used in the elastic-plastic model part, dilation angle  $\psi$ , residual friction angle  $\phi_{resid}$  and residual cohesion  $c_{resid}$ .

**Table 7-3: Input parameters for elastic-plastic part modelled in *Phase2*.**

<b>GSI=75</b>								
<b>Rock type</b>	<b>E [MPa]</b>	<b><math>\nu</math></b>	<b><math>\sigma_t</math> [MPa]</b>	<b><math>\phi</math> [°]</b>	<b>c [MPa]</b>	<b><math>\psi</math> [°]</b>	<b><math>\phi_{resid}</math> [°]</b>	<b><math>c_{resid}</math> [MPa]</b>
Tholeiite basalt	27828	0,16	1,17	57,73	7,43	15	49	3
Scoria	3286	0,35	0,3492	36,95	1,92	4	32	0,5
Sandstone	4082	0,3	0,393	47,65	2,66	7	41	0,5
<b>GSI=50</b>								
<b>Rock type</b>	<b>E [MPa]</b>	<b><math>\nu</math></b>	<b><math>\sigma_t</math> [MPa]</b>	<b><math>\phi</math> [°]</b>	<b>c [MPa]</b>	<b><math>\psi</math> [°]</b>	<b><math>\phi_{resid}</math> [°]</b>	<b><math>c_{resid}</math> [MPa]</b>
Tholeiite basalt	10471	0,16	0,18	52,02	4,11	10	45	1
Scoria	1236	0,35	0,053	30,07	1,186	2	25	0,2
Sandstone	1536	0,3	0,06	40,86	1,63	5	35	0,2
<b>GSI=25</b>								
<b>Rock type</b>	<b>E [MPa]</b>	<b><math>\nu</math></b>	<b><math>\sigma_t</math> [MPa]</b>	<b><math>\phi</math> [°]</b>	<b>c [MPa]</b>	<b><math>\psi</math> [°]</b>	<b><math>\phi_{resid}</math> [°]</b>	<b><math>c_{resid}</math> [MPa]</b>
Tholeiite basalt	2040	0,16	0,027	44,38	2,57	10	35	0,25
Scoria	241	0,35	0,00805	22,95	0,73	0	17	0,1
Sandstone	299	0,3	0,009	33,02	1,03	0	27	0,1

Since all rock elements will now follow elastic-plastic behaviour, much larger displacements are expected than from the elastic model part. The stress distribution will also be more expansive. The output from the modelling phase is presented in Figure 7-11 to Figure 7-19. There yielded elements, displacements and deformations for the three different GSI values are compared.

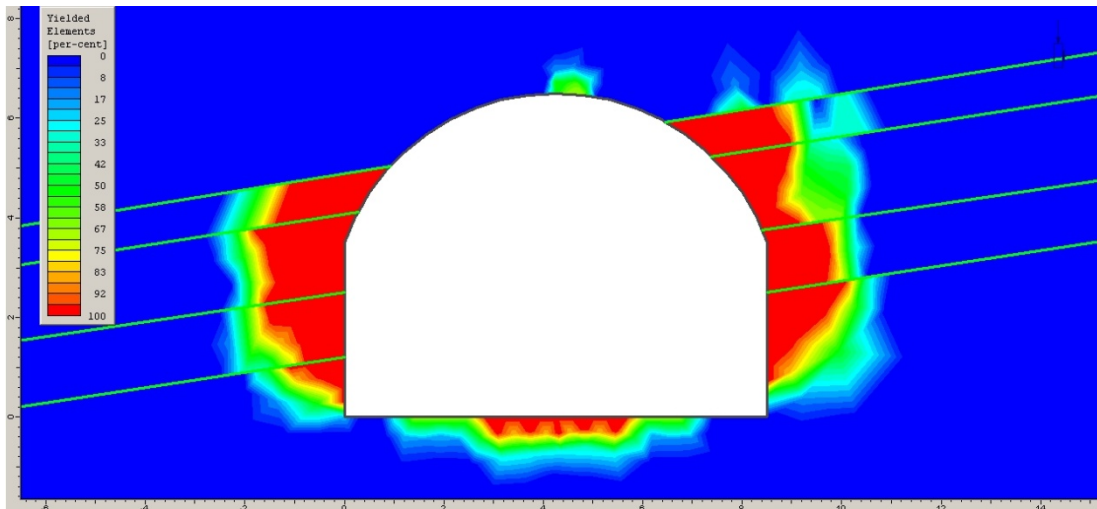


**Figure 7-11: Yielded elements for GSI=75, total number of yielded elements=244.**

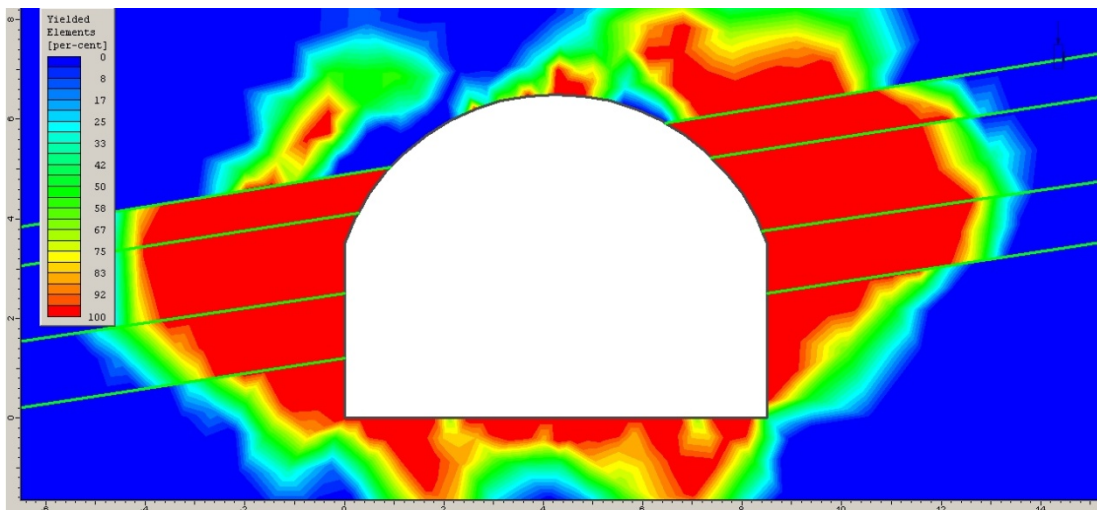


**Figure 7-12: Yielded elements for GSI=50, total number of yielded elements=536.**

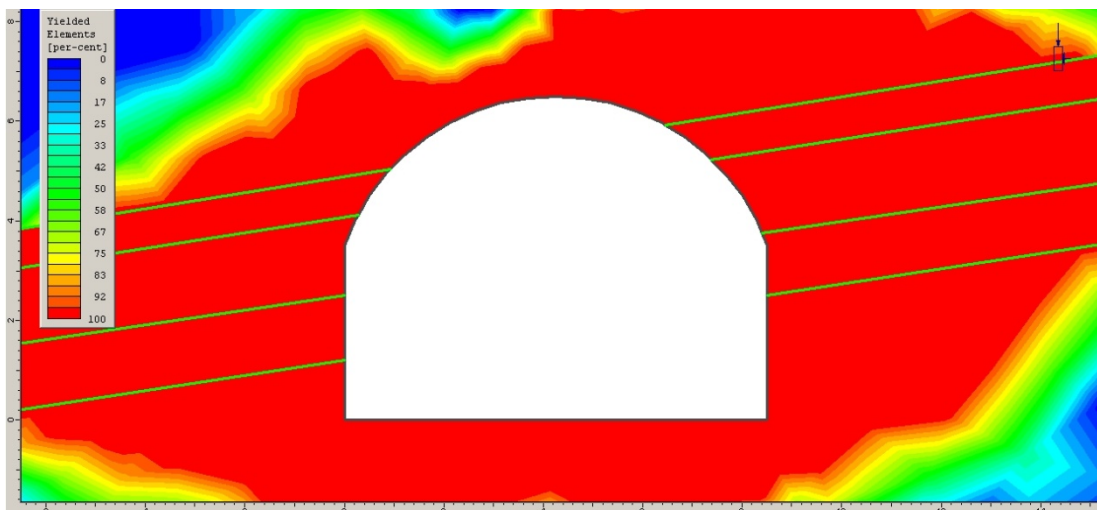


**Figure 7-13: Yielded elements for GSI=25, total number of yielded elements=961.**

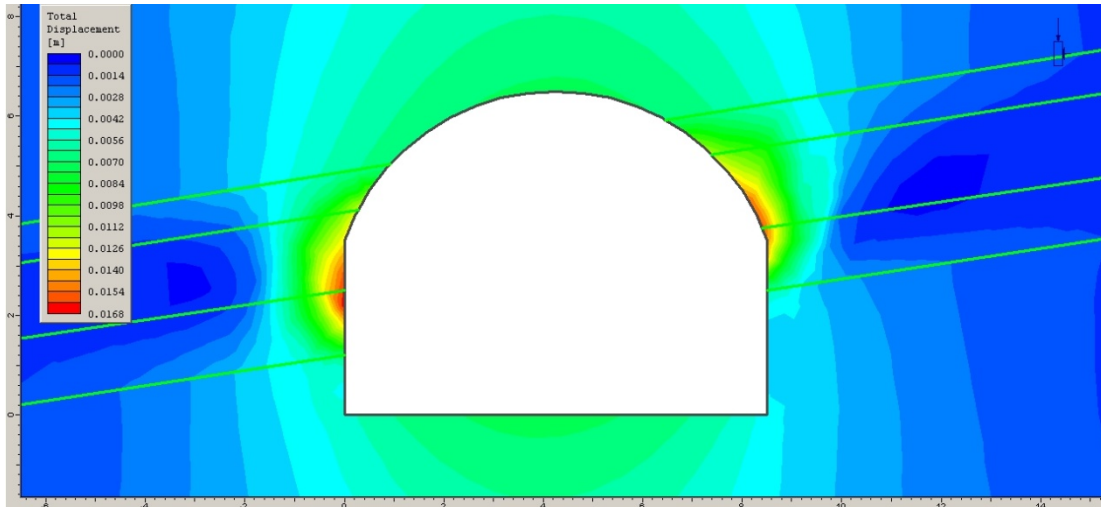


Figure 7-14: Total displacements for GSI=75, largest displacement is 16 mm.

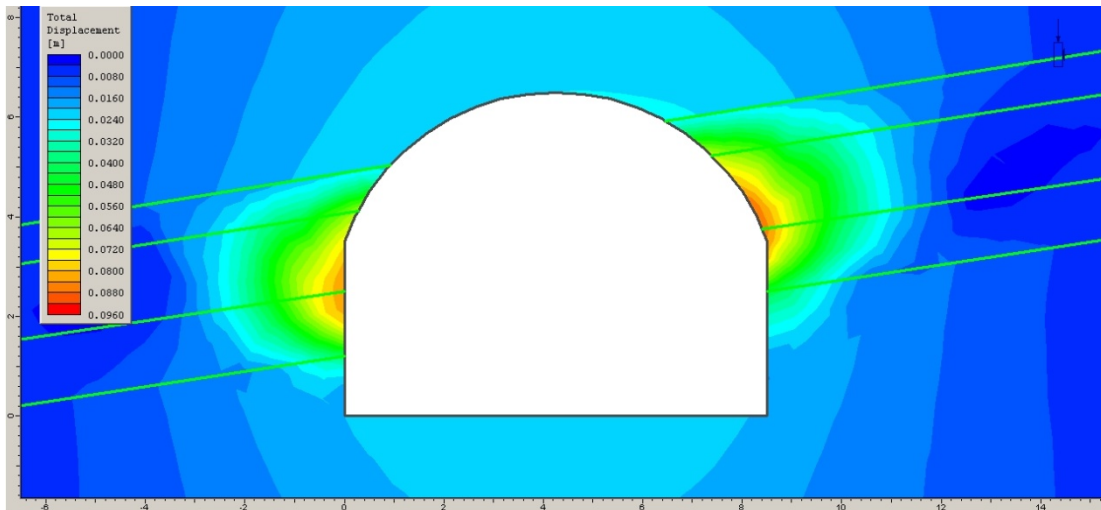


Figure 7-15: Total displacements for GSI=50, largest displacement is 88 mm.

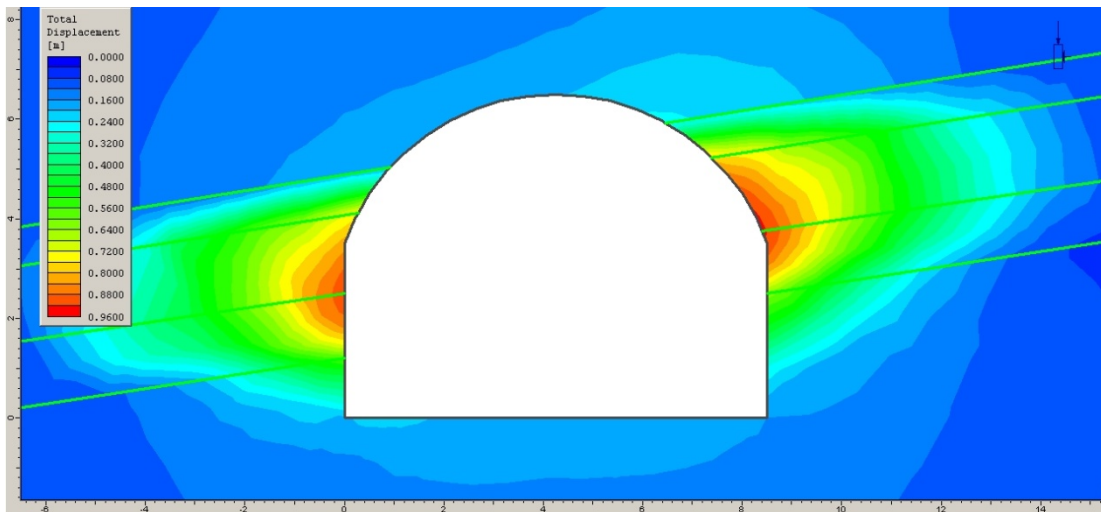


Figure 7-16: Total displacements for GSI=25, largest displacement is 933 mm.



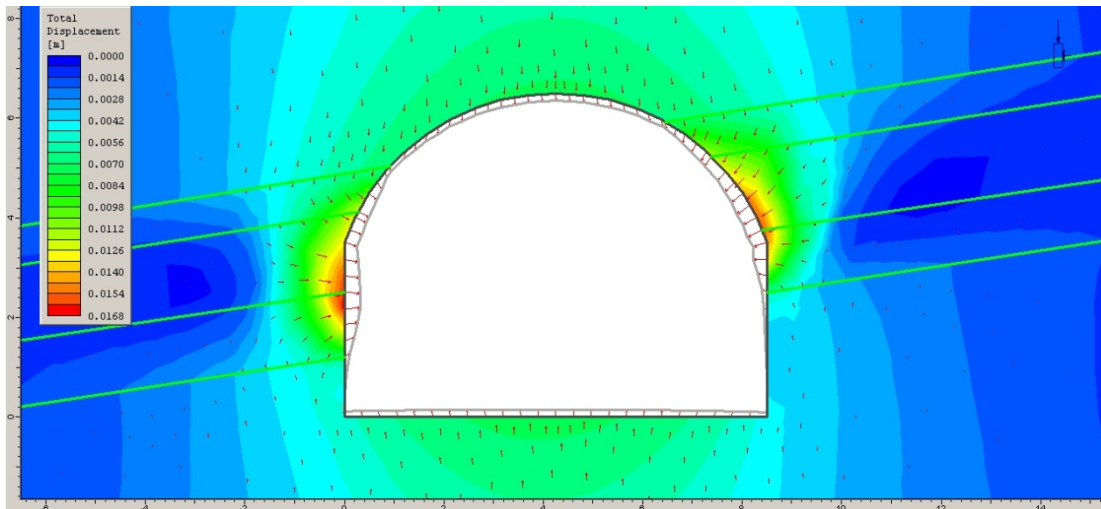


Figure 7-17: Deformed boundaries and deformation vectors for GSI=75 (scale: x20).

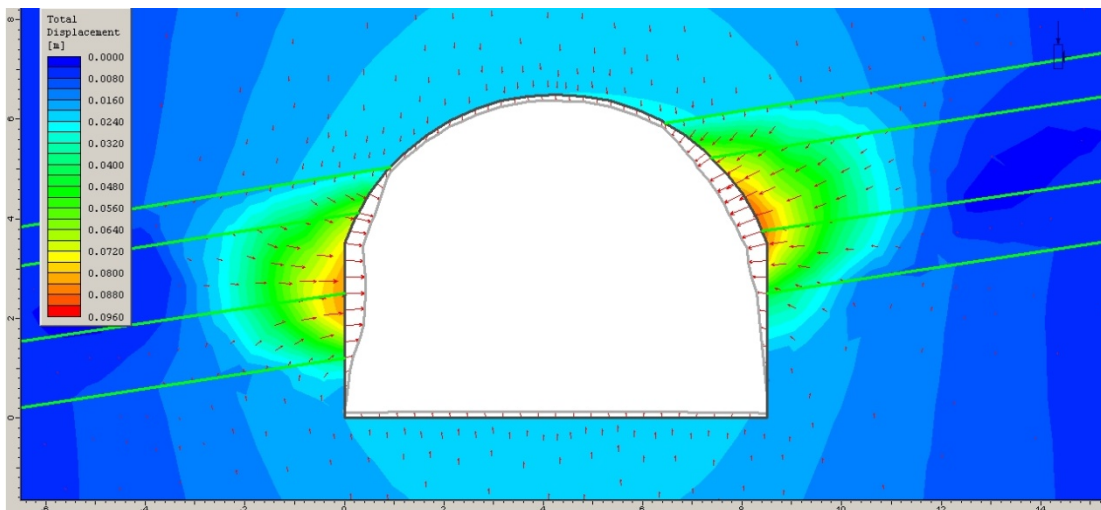


Figure 7-18: Deformed boundaries and deformation vectors for GSI=50 (scale: x5).

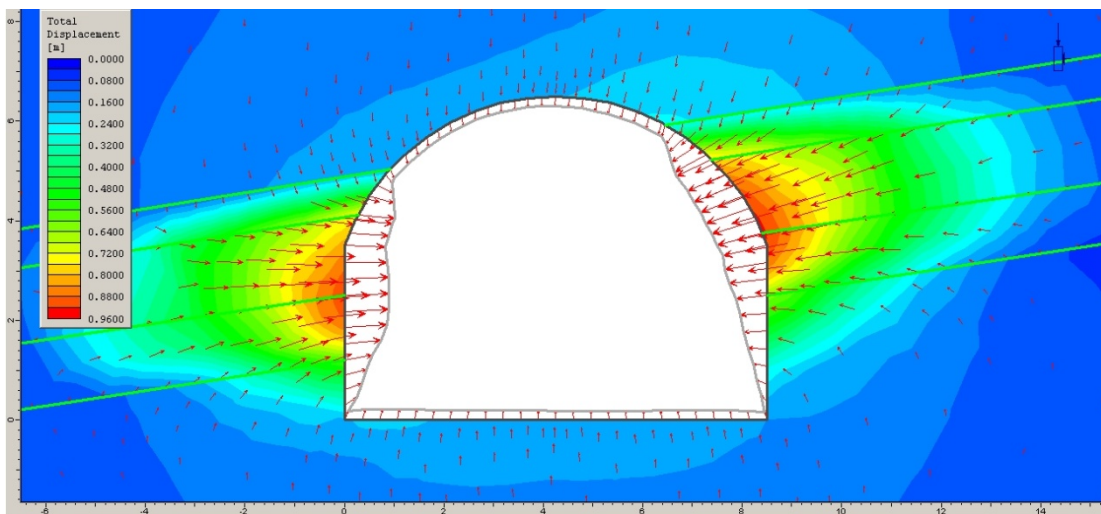


Figure 7-19: Deformed boundaries and deformation vectors for GSI=25 (scale: x1).

For GSI=75 and GSI=50 the tunnel wall regions are completely yielded, where the sandstone and scoria crosses the tunnel opening, reaching few meters from the tunnel walls into the rock mass. The tunnel floor has also yielded, but the tunnel roof and the floor corners seems to have no yielding. For GSI=25 the whole rock mass surrounding the tunnel opening is yielded, and the yielded zones stretch almost 10 meters from the tunnel walls. This will cause severe problems during supporting, e.g. installation of rock bolts, which have to be connected into a stable rock to secure enough stability.

For both GSI=75 and GSI=50 the largest total displacements are in the tunnel walls, in the barrier between the lower scoria and the sandstone. The displacements for GSI=25 are 933 mm, which is very unrealistic in hard rock and it indicates that collapse will occur, see Table 7-4.

It can be stated, from the figures above it is stated that the weaker rock types, the scoria and the sandstone, will be problematic, since they will squeeze into the tunnel opening. No special problems are related to the tunnel roof and the floor. Figure 7-19 presents serious stability problems from the tunnel walls, which is probably unworkable to support using rock bolts and shotcrete.

**Table 7-4: Yielded elements and total displacements for various GSI values.**

<b>GSI</b>	<b>Yielded elements</b>	<b>Total displacement [mm]</b>
75	244	16
50	536	88
25	961	933

From this analysis it is clear that the GSI=25 parameter set is describing too poor strength parameters for plastic conditions, causing it to be infeasible to excavate tunnel in such kind of rock mass. In the next subchapters GSI=75 and GSI=50 will be model in elastic-plastic condition and supported using rock bolts and shotcrete.

### **7.2.1 Supported Elastic-Plastic GSI=75 Model**

The tunnel will be supported with systematic bolting and full cover shotcrete, see Figure 7-20. The material properties of rock bolts and shotcrete used in this model are the same as used in the Fáskrúðsfjörður tunnel, see Table 7-5 and Table 7-6. Grouted rebar rock bolts are used, suitable length is 6 m in order to ensure connection to a stable rock. The rock bolt pattern is radial which is generated from the tunnel's centre point, with 1 meter spacing in between. The amount of rock

bolts is 27. The whole tunnel border is covered with 15 cm thick shotcrete, which is very thick compared to normal use in Iceland.

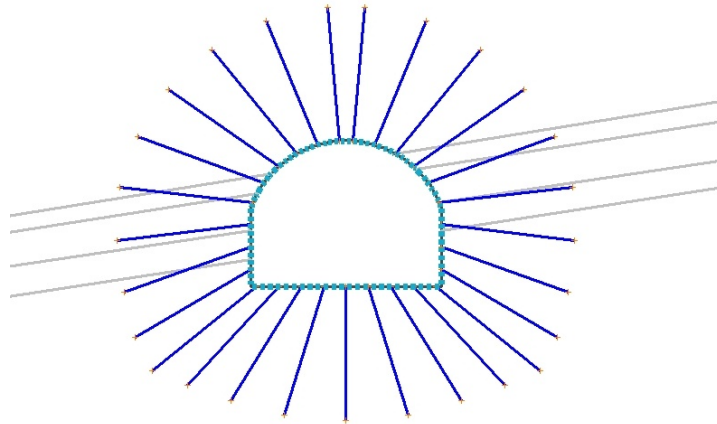


**Figure 7-20: Rock bolt pattern and shotcrete application.**

**Table 7-5: Material properties for the grouted rebar rock bolt.**

Parameter	Value
Bolt type	Fully bonded
Diameter [mm]	20
Young's modulus [GPa]	200
Peak capacity [MN]	0,15
Residual capacity [MN]	0,12

**Table 7-6: Material properties for the shotcrete.**

Parameter	Value
Thickness [m]	0,15
Young's modulus [MPa]	7875
Poisson ratio	0,2
Compressive strength , peak [MPa]	40
Compressive strength, residual [MPa]	5,6
Tensile strength, peak [MPa]	5,6
Tensile strength, residual [MPa]	0

From Figure 7-21 to Figure 7-29 the output for unsupported, systematic bolt supported and combined support with systematic bolts and shotcrete (fully support) are presented. Yielded elements, total displacements and deformation will be compared for various support. Red colour in rock bolts and shotcrete elements present yielding.

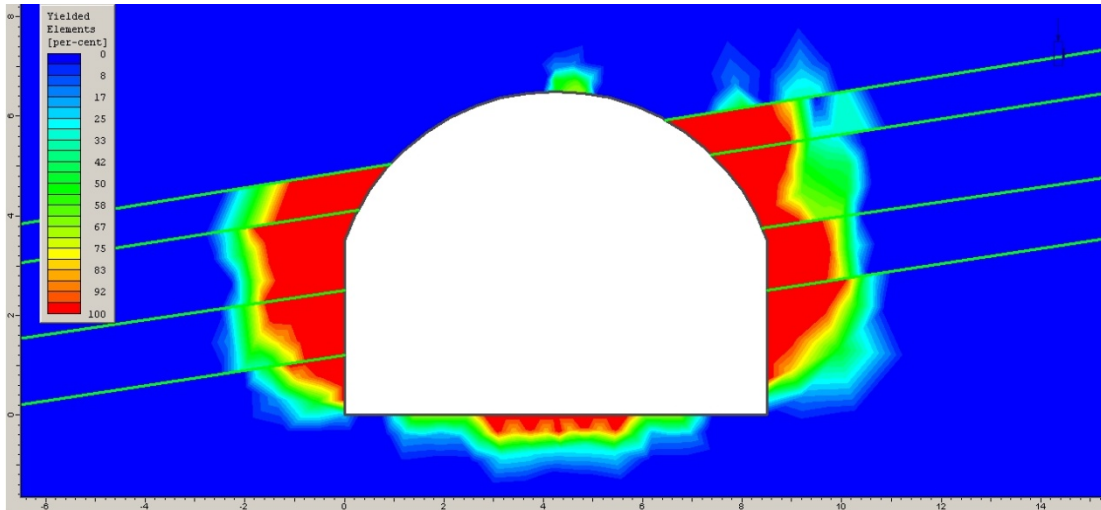


Figure 7-21: Yielded elements for unsupported tunnel. Model GSI=75.

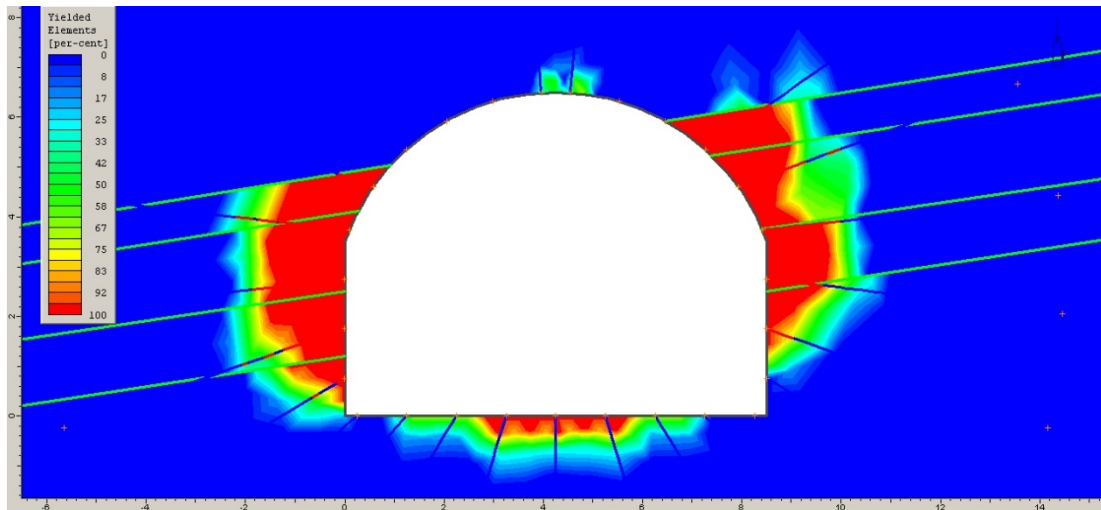


Figure 7-22: Yielded elements for bolt supported tunnel. Model GSI=75.

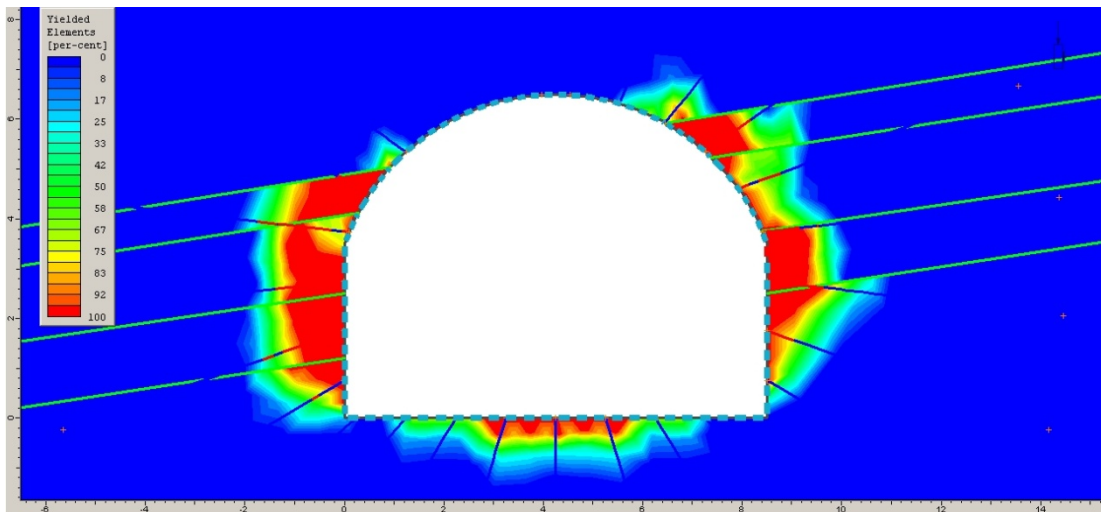
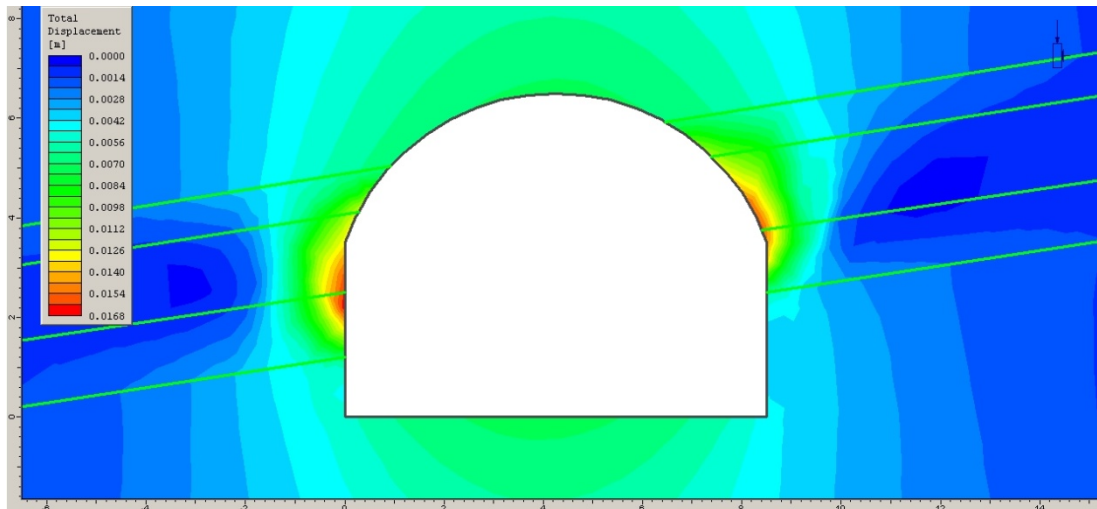
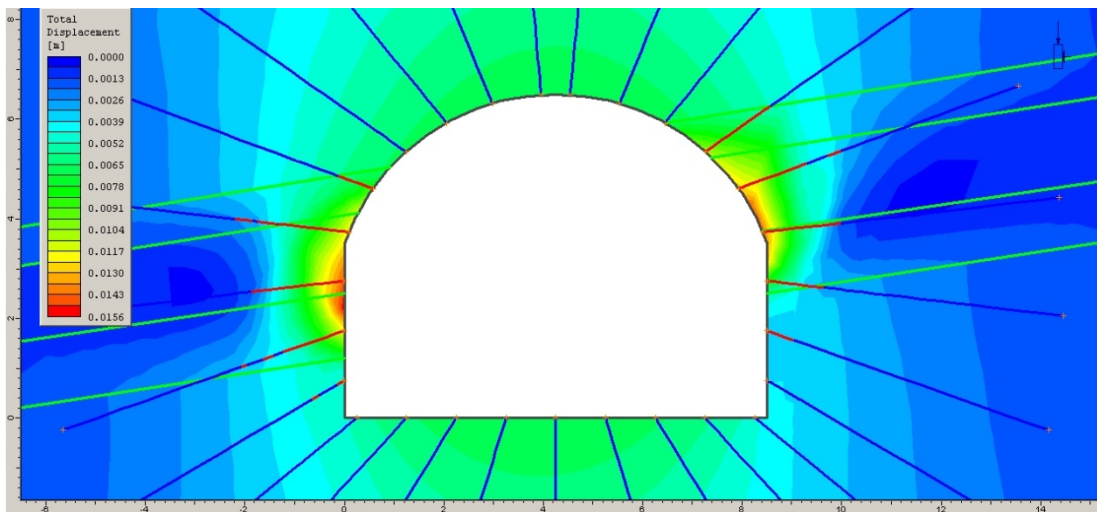


Figure 7-23: Yielded elements for bolt and shotcrete supported tunnel. Model GSI=75.



**Figure 7-24: Total displacements for unsupported tunnel. Model GSI=75.**



**Figure 7-25: Total displacements for bolt supported tunnel. Model GSI=75.**

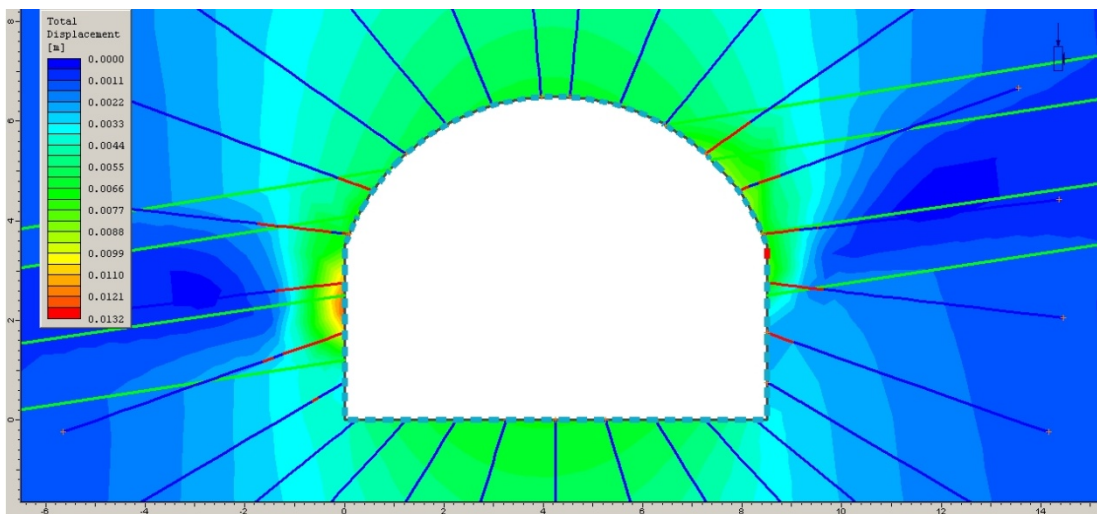


**Figure 7-26: Total displacements for bolt and shotcrete supported tunnel. Model GSI=75.**

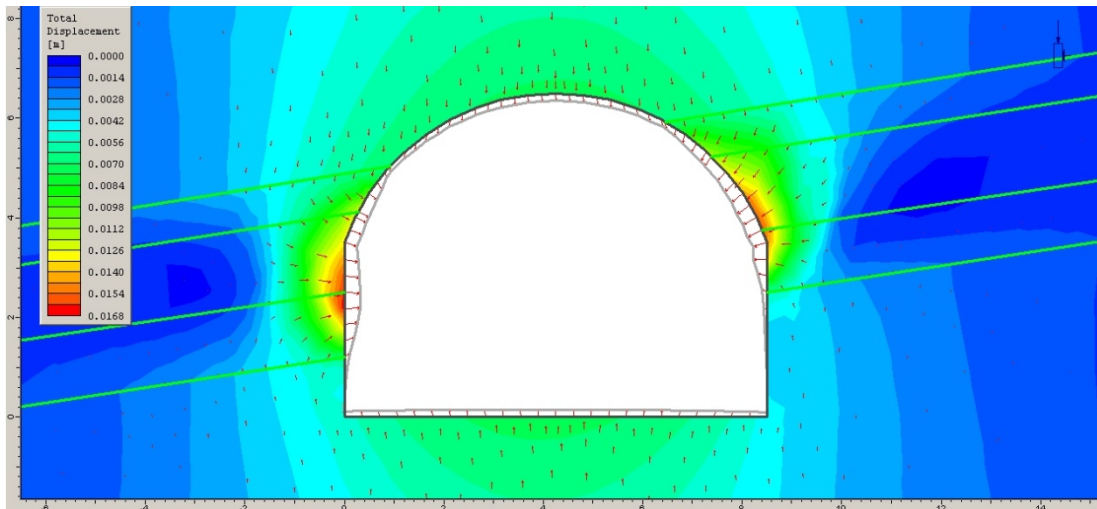


Figure 7-27: Deformed geometry for unsupported tunnel. Model GSI=75 (scale: x20).

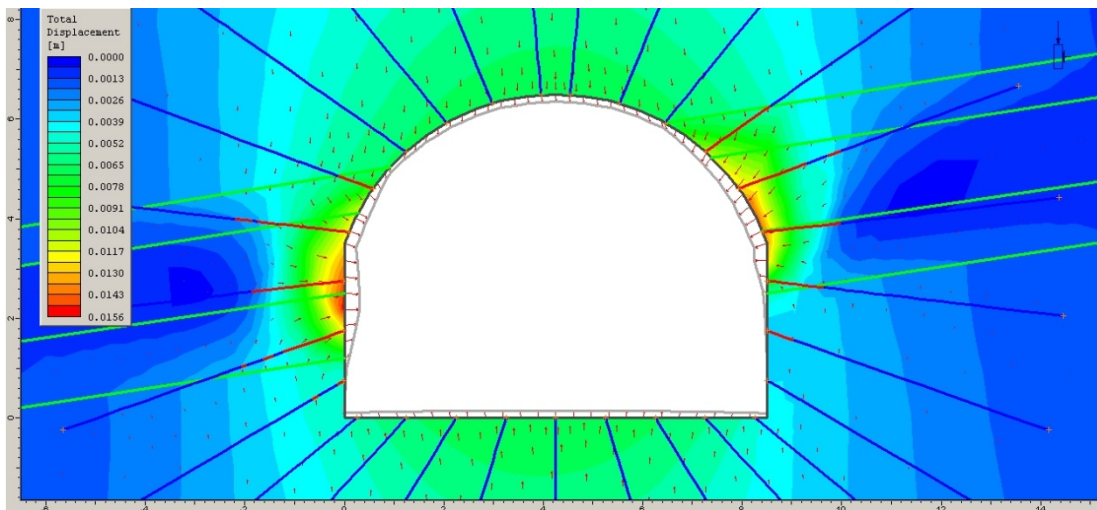


Figure 7-28: Deformed geometry for bolt supported tunnel. Model GSI=75 (scale: x20).

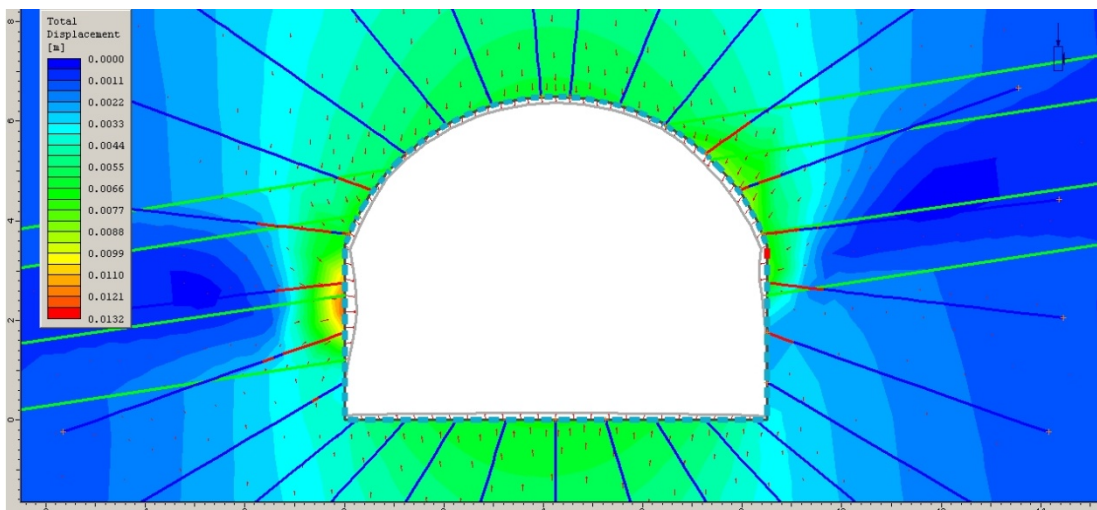


Figure 7-29: Deformed geometry for bolt and shotcrete supported tunnel. GSI=75 (scale: x20).

Minor yielding is expected in the roof and floor corners. However, major yielding is visible in the center of the floor and in the tunnel walls in the weaker rock layers, the scoria and the sandstone. Yielded rock elements reach 2 meters from the tunnel walls into the rock mass. From unsupported to systematic bolt supported, the number of yielded elements decreases from 244 to 235, application of shotcrete reduces the amount of yielded elements to 201. Yielded rock bolts presented in the tunnel walls, show that the number of rock bolts in these regions is not sufficient. Four rock bolts should be applied in each of the walls to minimize yielding. Only one shotcrete element in upper right wall presents yielding, so additional 2-5 cm of shotcrete on that spot would probably prevent yielding.

It is clear that the largest total displacements are in the tunnel walls, in the lower scoria and the sandstone. For unsupported tunnel the total displacements are 16,4 mm in the tunnel walls but in and at other regions, the total displacements are somewhere below 10 mm. For fully supported tunnel the maximum total displacement is 12,4 mm on the left wall between the scoria and the sandstone. By applying additional rock bolts in that region, the total displacement could be reduced to 10 mm.

From Figure 7-27 to Figure 7-29, it can clearly be seen how the deformations decreases between different support stages.

**Table 7-7: Yielded elements and total displacements for various support types for GSI=75.**

<b>GSI=75</b>	<b>Yielded elements</b>	<b>Total displacement [mm]</b>
Unsupported	244	16,4
System bolted	235	15,3
System bolted + shotcrete	201	12,4

### **7.2.2 Supported Elastic-Plastic GSI=50 Model**

In the elastic-plastic GSI=50 model the same presuppositions are used as in the elastic-plastic GSI=75 model, except mechanical properties for various rock types differs, see Table 7-3. From Figure 7-30 to Figure 7-38, the output from the modelling is presented.



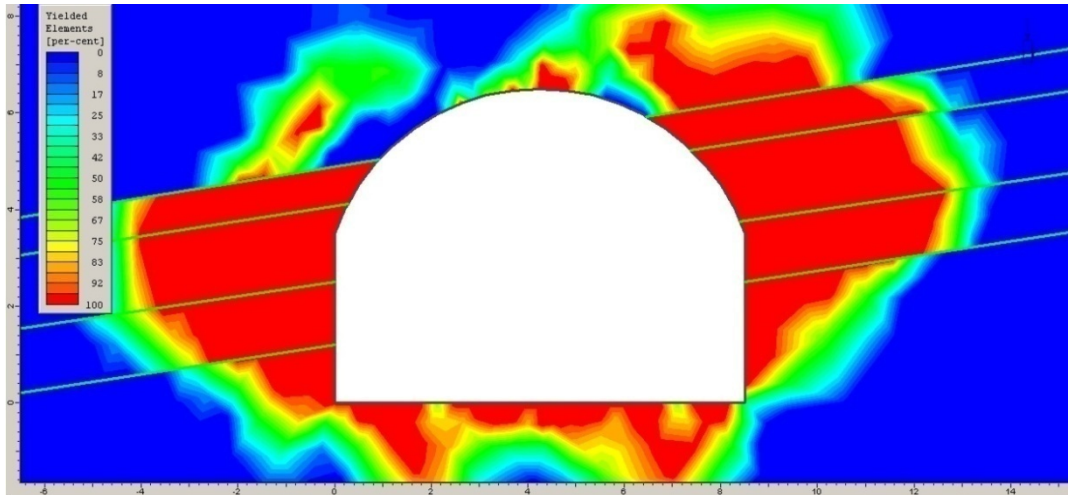


Figure 7-30: Yielded elements for unsupported tunnel, GSI=50.

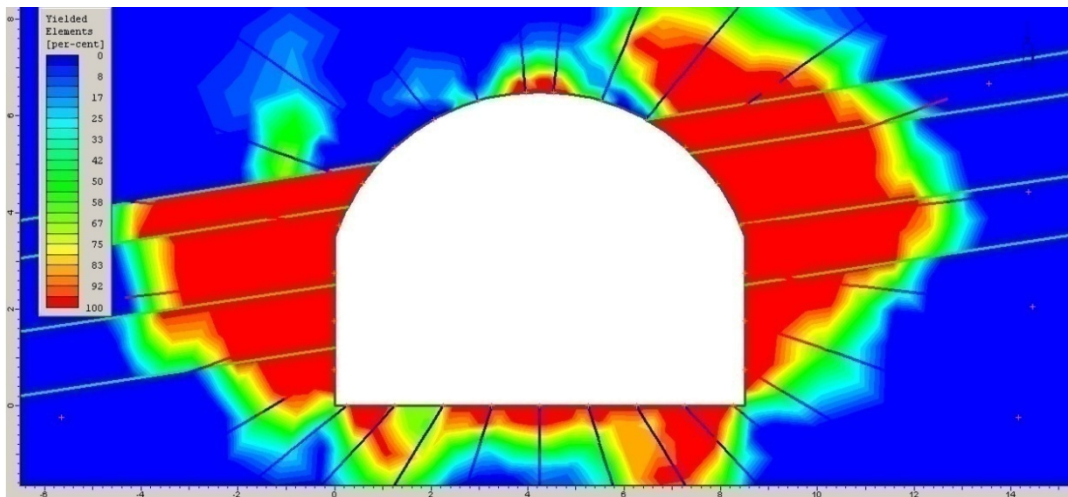


Figure 7-31: Yielded elements for bolt supported tunnel, GSI=50.

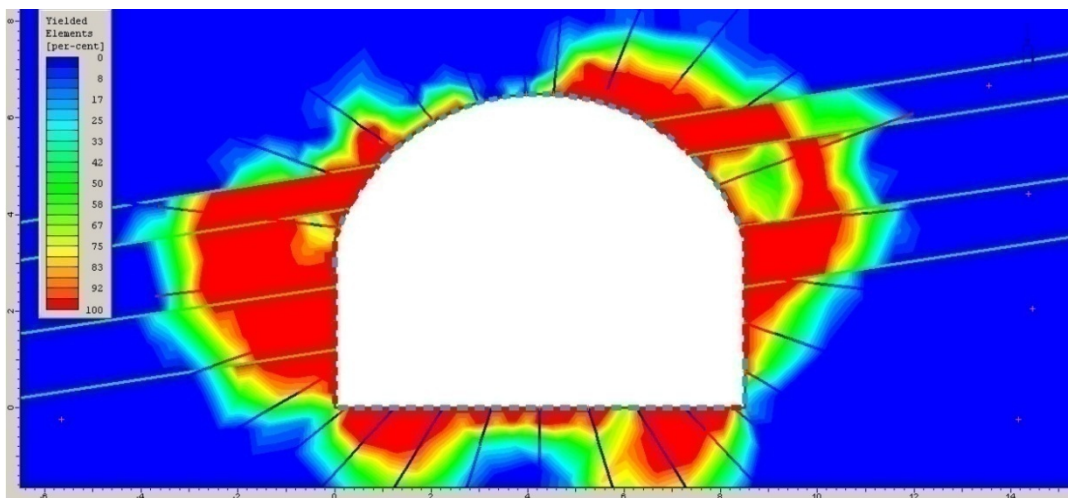
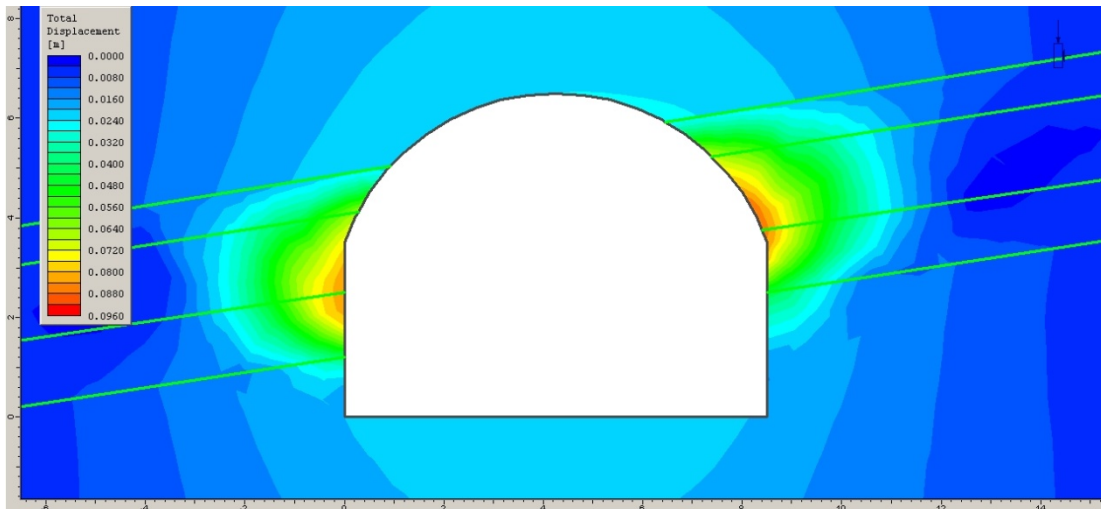
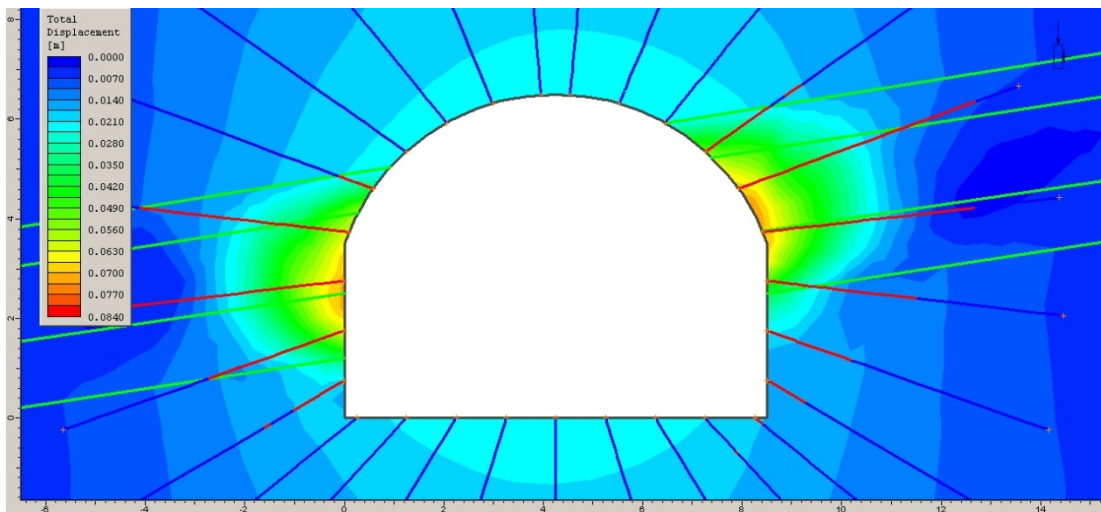


Figure 7-32: Yielded elements for bolt and shotcrete supported tunnel, GSI=50.



**Figure 7-33: Total displacements for unsupported tunnel, GSI=50.**



**Figure 7-34: Total displacements for bolt supported tunnel, GSI=50.**

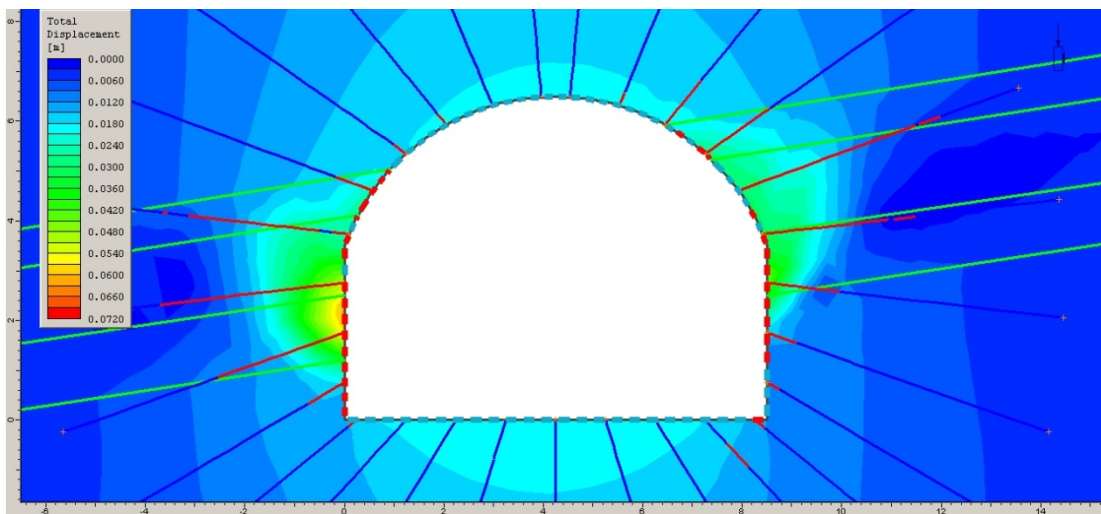


**Figure 7-35: Total displacements for bolt and shotcrete supported tunnel, GSI=50.**

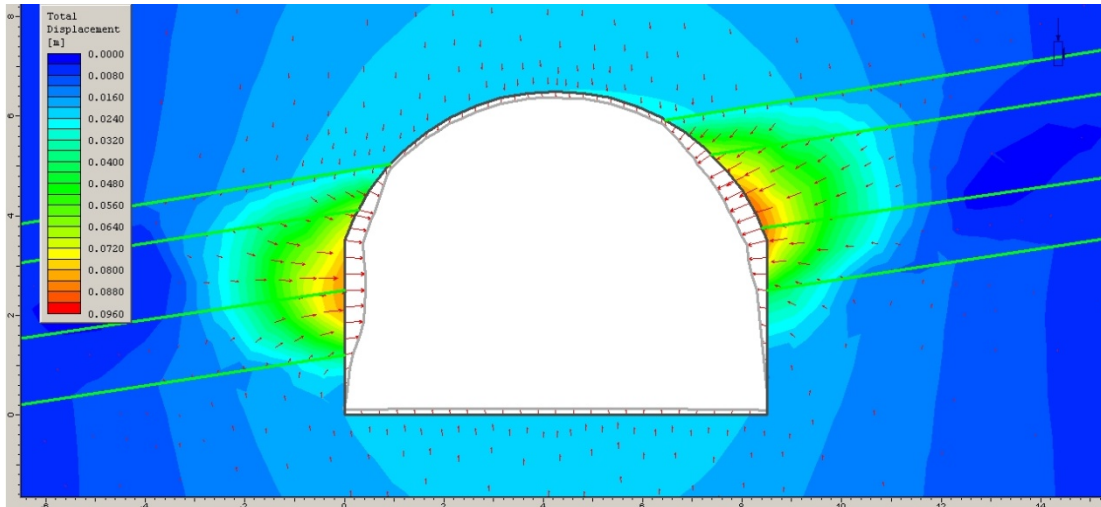


Figure 7-36: Deformed geometry for unsupported tunnel, GSI=50 (scale: x5).

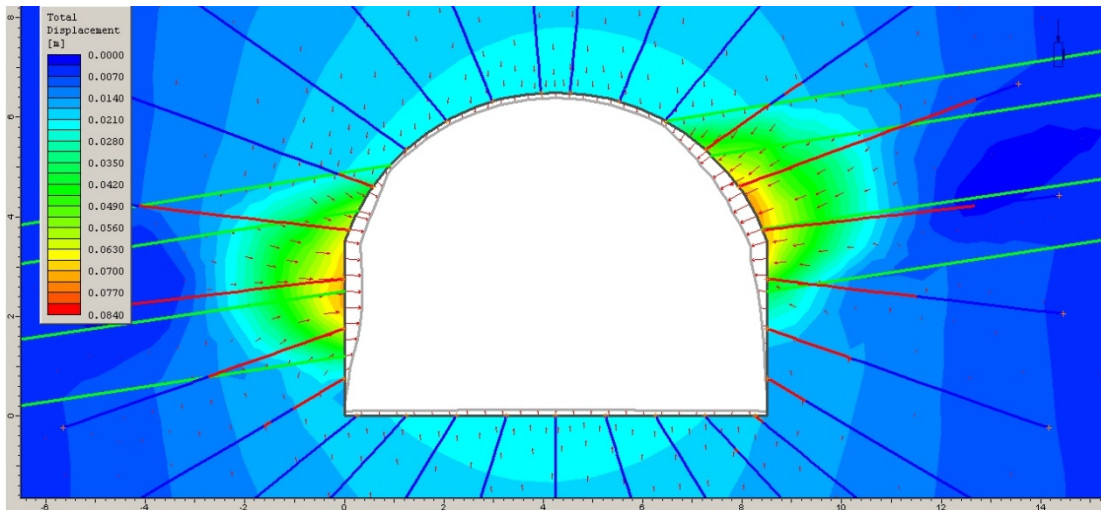


Figure 7-37: Deformed geometry for bolt supported tunnel, GSI=50 (scale: x5).

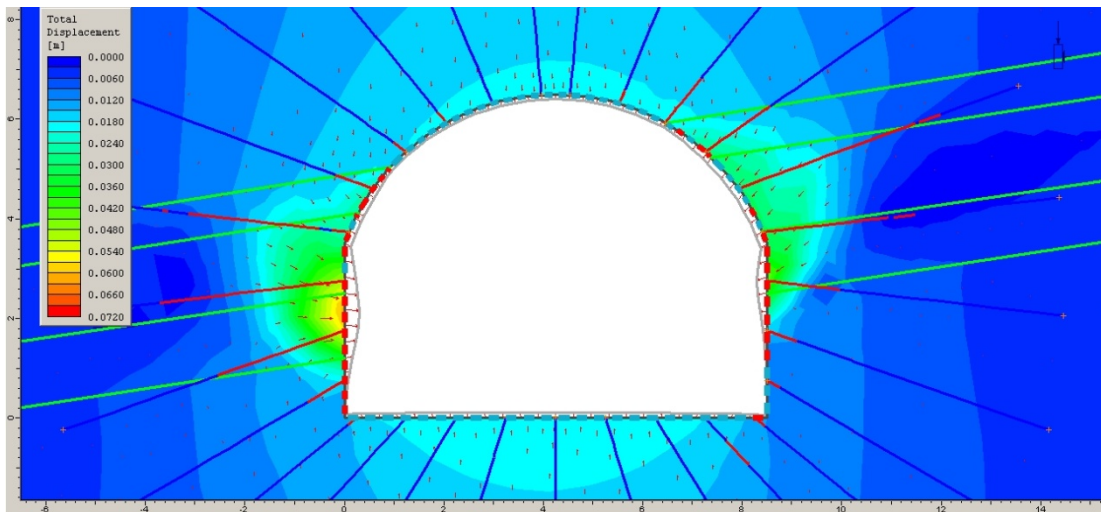


Figure 7-38: Deformed geometry for bolt and shotcrete supported tunnel, GSI=50 (scale: x5).

Yielded elements are widely surrounding the tunnel opening. However, some spots on the tunnel roof presents no yielding. The longest distance from a tunnel wall through yielded zone is 5 meters, in the scoria and the sandstone. Yielded elements reduces from 536 for the unsupported model to 440 for the fully supported model. Almost all the support elements in the walls are yielding, marked in red colour. This states that the number of rock bolts and the thickness of shotcrete is insufficient and/or more stiffness is needed in the support elements.

The locations of the total displacements are the same as for the elastic-plastic GSI=75 model but they are much larger. The total displacements decreases from 88 mm for the unsupported model to 61,4 mm for the fully supported model. According to Figure 7-35, the largest displacements are expected in the left wall at the lower scoria layer. It seems quite unrealistic to minimise the maximum total displacement below 10 mm for elastic-plastic GSI=50 model.

From Figure 7-36 to Figure 7-38 a reduction of the deformation is clear. A great refinement is presented at the roof corners.

**Table 7-8: Yielded elements and total displacements for various support types for GSI=50.**

<b>GSI=50</b>	<b>Yielded elements</b>	<b>Total displacement [mm]</b>
Unsupported	536	88,0
System bolted	490	74,8
System bolted + shotcrete	440	61,4

The results from the elastic-plastic GSI=75 and GSI=50 models states that a combined use of *Phase2* and *RocLab* might give a reliable results for a typical Icelandic tunnel conditions. According to acceptable maximum total displacements of 10 mm and below, the elastic-plastic GSI=50 gives too large displacements and therefore the rock mass properties are not sufficient. In the next subchapters, two different cross sections from the Fáskrúðsfjörður tunnel will be modelled with elastic-plastic GSI=75.

### 7.3 The Fáskrúðsfjörður Tunnel – Station 6530

Station 6530 is located approximately 2,6 km inside the tunnel from Reyðarfjörður portal at El. 113 m a.s.l, see Figure 7-39. A regular cross section of the Fáskrúðsfjörður tunnel is 52 m<sup>2</sup>, but at station 6530 a niche is placed giving an area of 75 m<sup>2</sup> with approximately 11 m wide and 6,5 m high tunnel, see Figure 7-40. The geology at station 6530 consist of tholeiite basalt at the roof underlain by red sediment interbedded between scoria, and then tholeiite basalt from the middle of the cross section to the floor, see Figure 7-40. No visual joints or fault systems were shown in the geological mapping from the contractor, which supports the use of GSI=75, see Appendix 5.

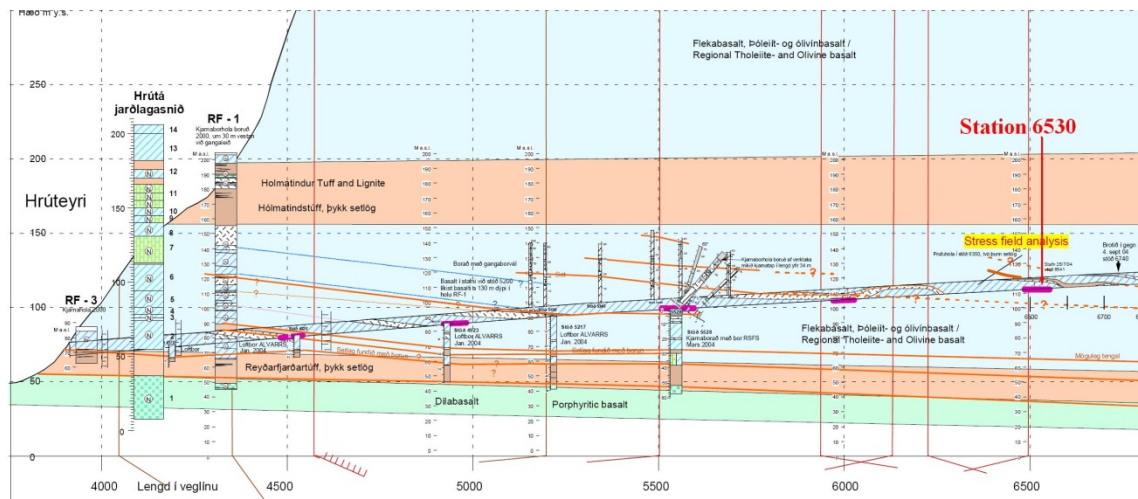


**Figure 7-39: Cross section part of the Fáskrúðsfjörður tunnel from Reyðarfjörður side, station 6530 is located on the right side of the figure [36].**

The cross section used in the modelling is made from design drawings and cross section measurements from the contractor, see Appendix 5. The model setup is the same as for the typical Icelandic mixed face tunnel model for plastic condition, except for the amount of mesh elements and nodes, 2331 and 1197 respectively. A constant stress condition will also be applied with a load splitting between two stages. According to stress measurement made by SINTEF a large anisotropy stress conditions appears, so a constant stress condition will be applied, see Table 5-1. In the typical Icelandic mixed face tunnel model the installation of supports is carried out immediately after excavation so no displacements take place prior to the installation of supports, which is not realistic. Installation of supports starts usually two to four hours after blasting. Then, most of the deformations have

already occurred [27]. In this model the load splitting is divided between two stages. In the first stage, 80% of the field stress induced load is applied, then rock bolts and shotcrete are applied. Finally in the second stage, 20% residual field stress induced load is applied. This application gives an approximation, see Figure 4-6. The input parameters used for this model are presented in Table 7-9.

**Table 7-9: Input parameters for station 6530 in *Phase2*.**

Rock type	GSI=75							
	E [MPa]	$\nu$	$\sigma_t$ [MPa]	$\phi$ [°]	c [MPa]	$\psi$ [°]	$\phi_{resid}$ [°]	$c_{resid}$ [MPa]
Tholeiite basalt	27828	0,16	1,17	57,73	7,43	15	49	3
Scoria	3286	0,35	0,3492	36,95	1,92	4	32	0,5
Sandstone	4082	0,3	0,393	47,65	2,66	7	41	0,5

The material properties for rock bolts and shotcrete used in this model are the same as used in the typical Icelandic mixed face tunnel model, see Table 7-5 and Table 7-6. Figure 7-40 presents the tunnel cross section at station 6530.

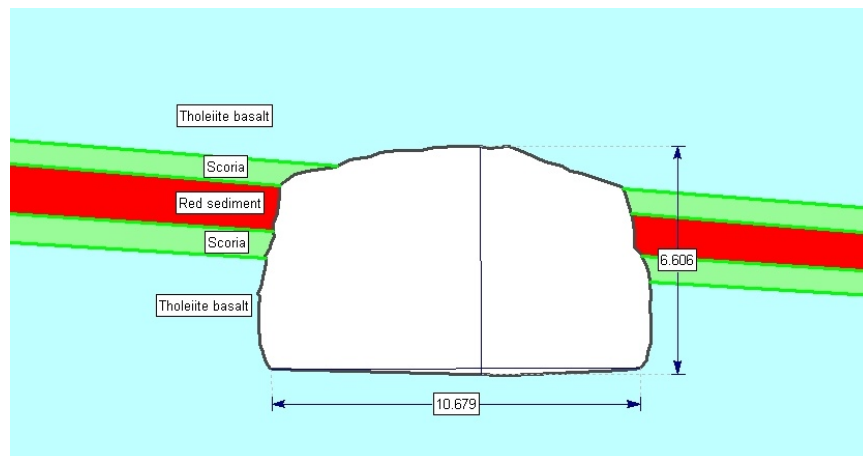


**Figure 7-40: Tunnel cross section of station 6530, the dimensions are in meters.**

### 7.3.1 Practical Support at Station 6530 in Fáskrúðsfjörður Tunnel

By utilizing rock bolts and shotcrete reports from the contractor and the supervisor, the cross section from station 6530 with various supports will be modelled. Appropriate pages from the support reports can be found in Appendix 5.

The grouted rebar rock bolts were installed using spot bolting, not systematic bolting as in the typical Icelandic mixed face tunnel model. A total amount of 10 rock bolts were used. Eight of them were 5 meters long and two of them were 2 meters long. The thickness of the shotcrete was 11,4 cm, based on calculations from the shotcrete report, see Figure 7-41.

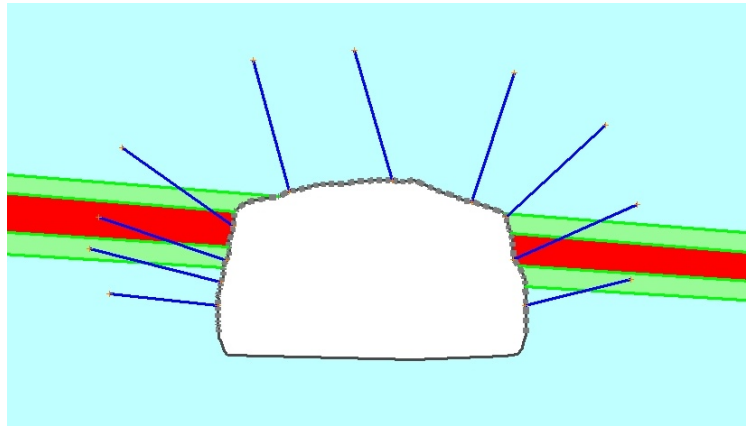


**Figure 7-41: Support setup for station 6530, based on rock bolts and shotcrete reports.**

From Figure 7-42 to Figure 7-50 a comparison is made of three various models; unsupported model, model with 80% of the stress relief and full supported model with full stress relief. The comparison is based on yielded elements, total displacements and deformations.

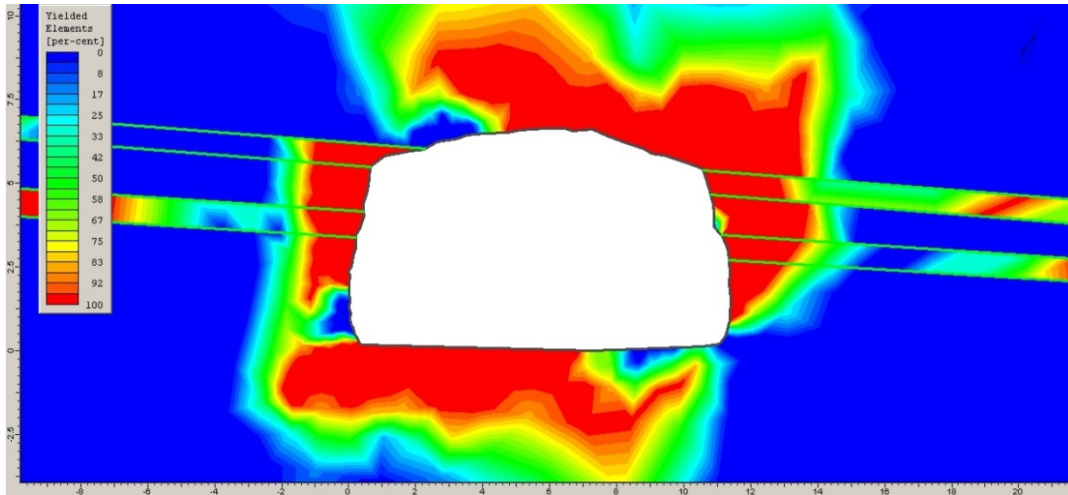


Figure 7-42: Yielded elements for unsupported model from station 6530.

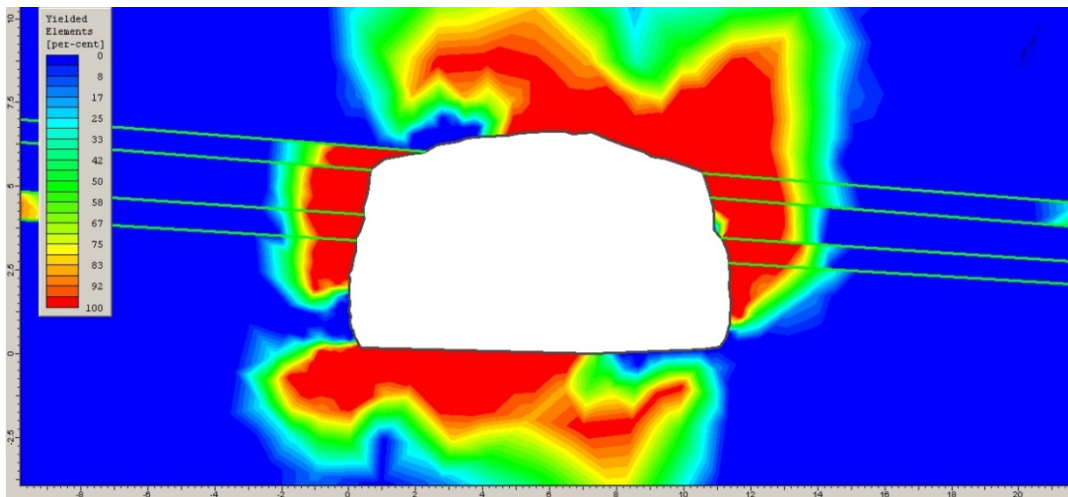


Figure 7-43: Yielded elements for 80% stress relief model from station 6530.

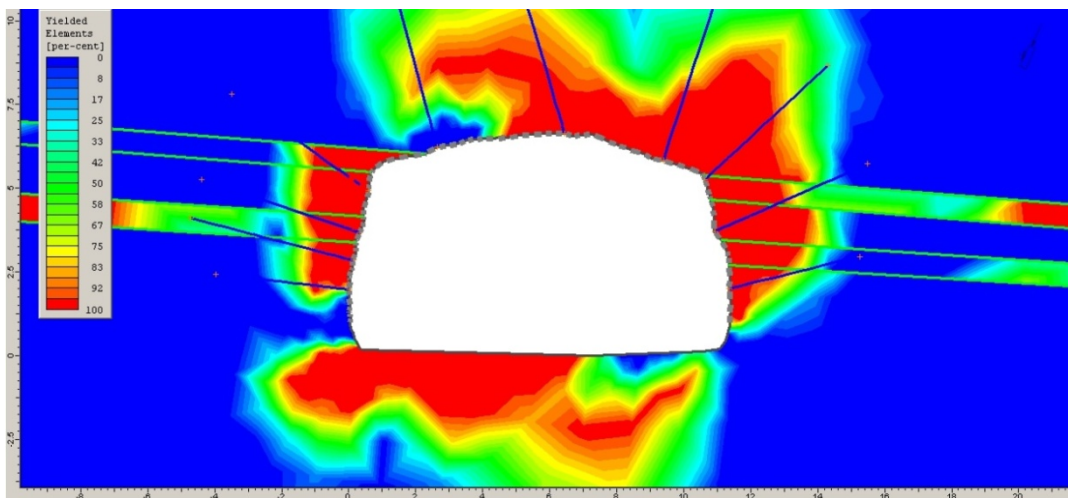


Figure 7-44: Yielded elements for full supported and full stress relieved model from station 6530.



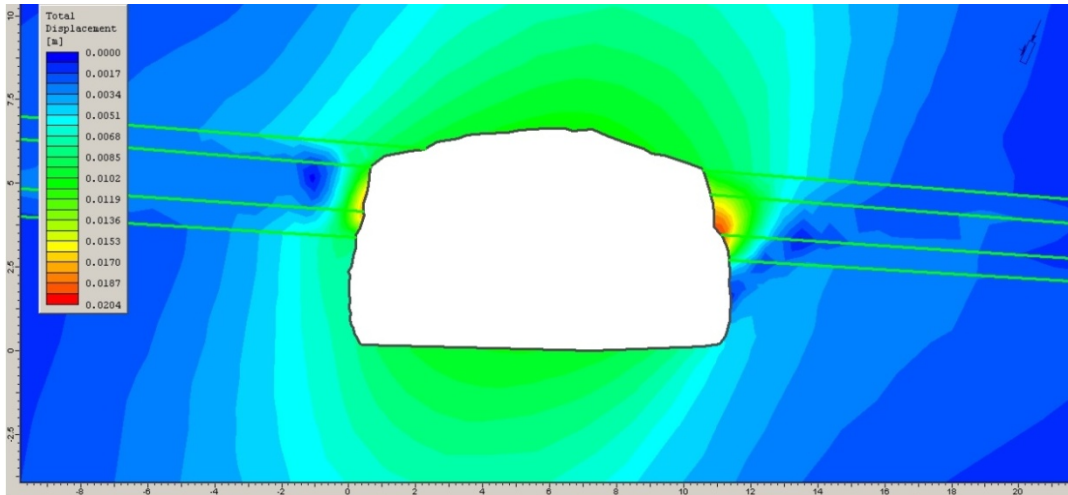


Figure 7-45: Total displacements for unsupported model from station 6530.

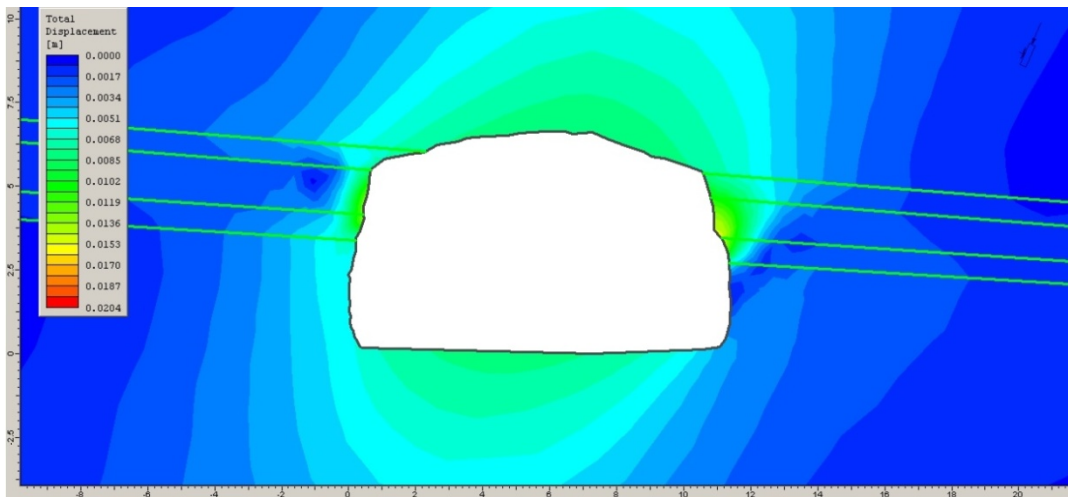


Figure 7-46: Total displacements for 80% stress relief model from station 6530.

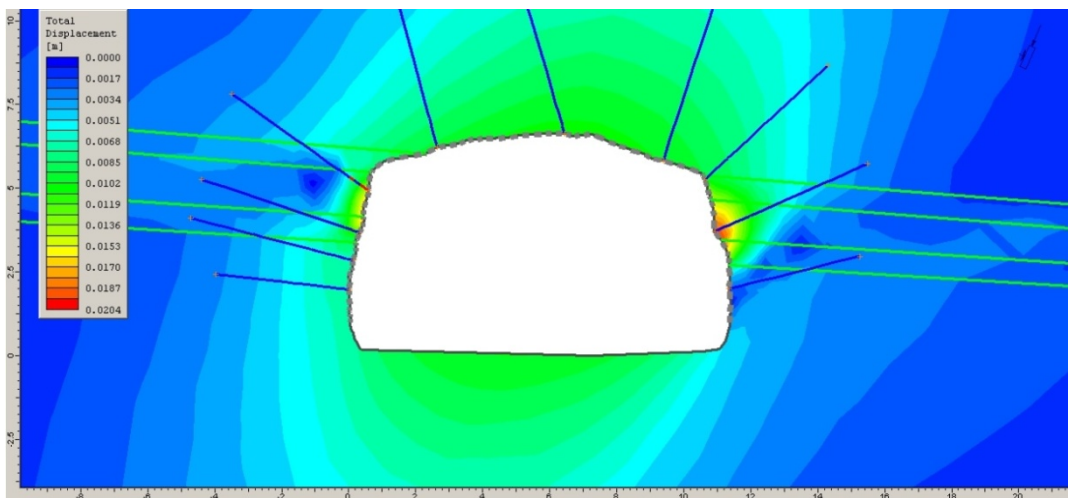


Figure 7-47: Total displacements for full supported and full stress relieved model from station 6530.

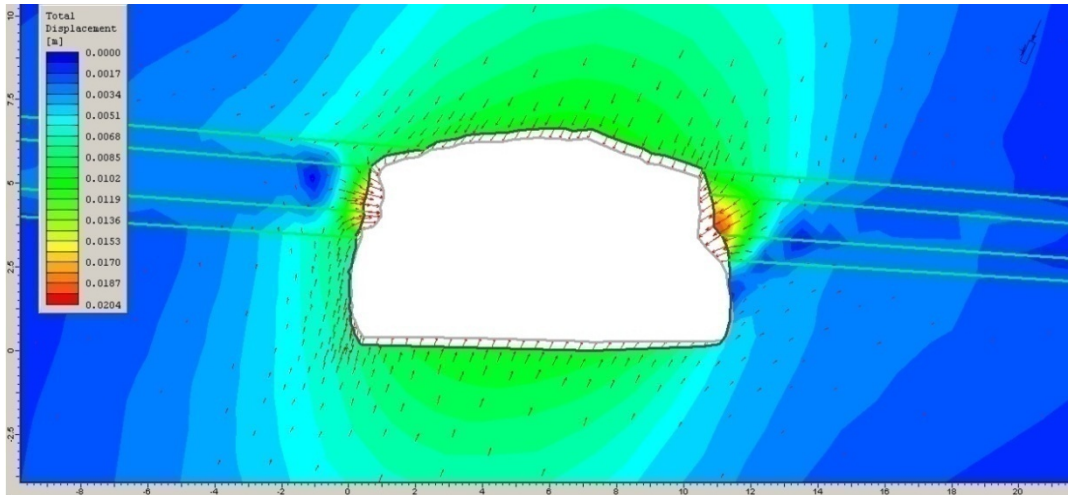


Figure 7-48: Deformed geometry for unsupported model from station 6530 (scale: x30).

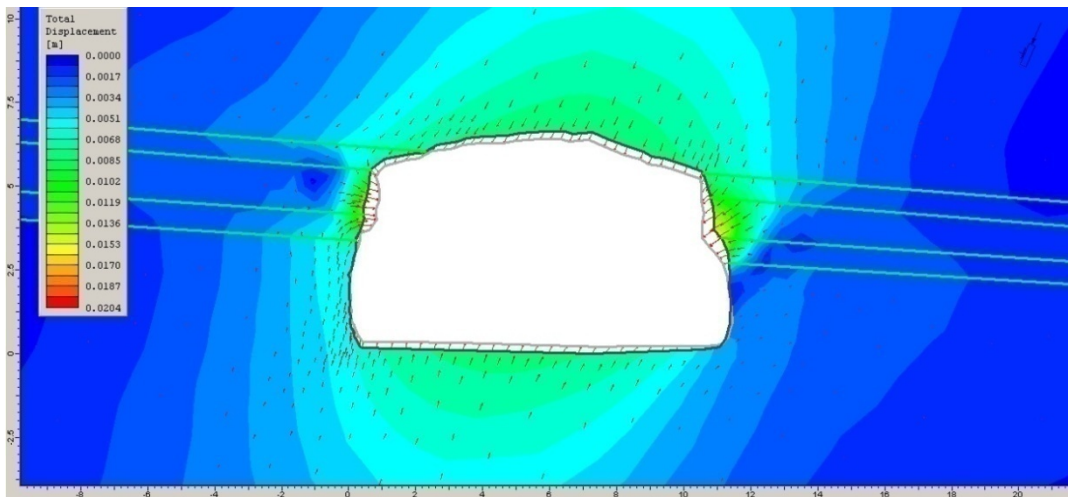


Figure 7-49: Deformed geometry for 80% stress relief model from station 6530 (scale: x30).

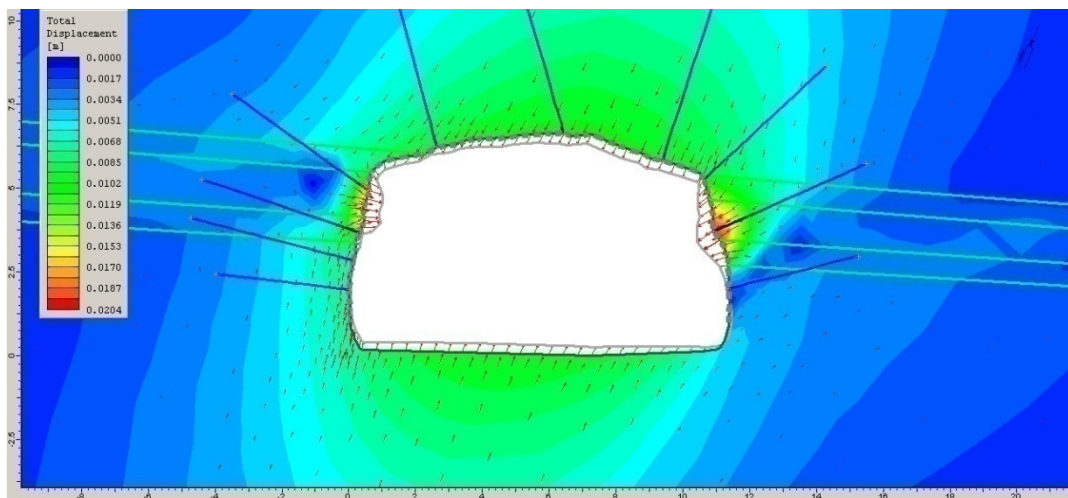


Figure 7-50: Deformed geometry for full supported and full stress relieved model from station 6530 (scale: x30).

The tunnel opening is covered with yielded elements, except for some spots near the floor corners and the left side of the roof. In the worst case the yielded elements reaches seven meters from the tunnel walls into the surrounding rock mass. A sign of a yielded rock bolt on the left wall states that more rock bolts are needed in that wall. There are no signs of yielded shotcrete elements which secures stability of the tunnel.

The maximum total displacement is expected in the red sediment layer. The displacement becomes 19,7 mm for unsupported model, but 19,6 mm for full supported and full stress relieved model. Only 0,1 mm difference is quite small and states that there is insufficient support in that region, but other regions around the tunnel range from 8 mm to 10 mm which to be seems sufficient.

The deformation on the tunnel opening is parallel to the total displacements, Figure 7-48 to Figure 7-50 presents how the weaker layers, the scoria and the red sediment, squeeze into the tunnel like in the typical Icelandic mixed face tunnel model. The tholeiite basalt is very stable, as seen at the roof and the floor.

**Table 7-10: Yielded elements and total displacements for various models from station 6530.**

<b>Station 6530</b>	<b>Yielded elements</b>	<b>Total displacement [mm]</b>
Unsupported	668	19,7
80% stress relieved	609	14,9
Full supported and full stress relieved	639	19,6

### **7.3.2 Supplementary Support for Station 6530**

After further analysis of the practical supports at station 6530 in the Fáskrúðsfjörður tunnel it is clear that three rock bolts yielded but none shotcrete element, see Appendix 6. This states that some supplementary support is needed and will be added in the model to prevent large total displacements. The tunnel segments which need additional supports are located in the red sediment layer below the tunnel roof, other segments are about 10 mm or lower. The same rock bolts and shotcrete will be used as in previous models, but the amount of rock bolts and the thickness of the shotcrete will be increased. An attempt is made to install the rock bolts in stable rock, avoiding installation in the yielded zone. Two different supplement models will be modeled.

### Supplementary Support Model 1

The model consist of three additional rock bolts in each tunnel wall and two additional rock bolts in the roof. The thickness of the shotcrete is kept the same, or 11,4 mm. Figure 7-51 presents the rock bolts from the practical support (1-10) and the additional rock bolts (11-18).

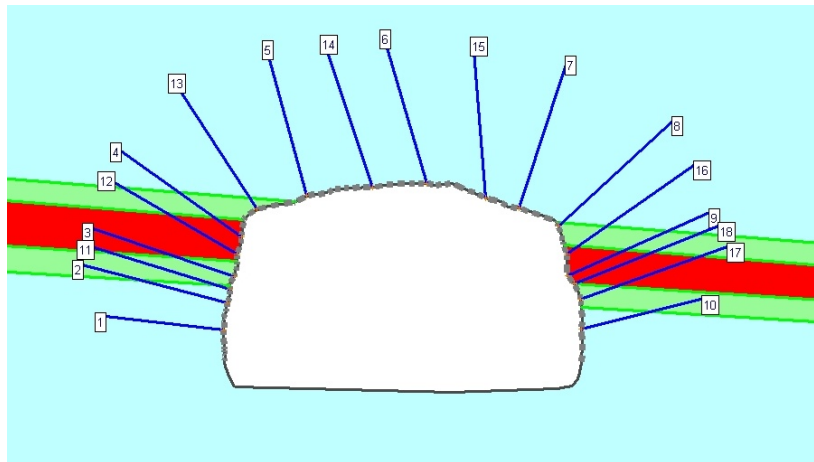


**Figure 7-51: Rock bolts from the practical support (1-10) and additional rock bolts (11-18).**

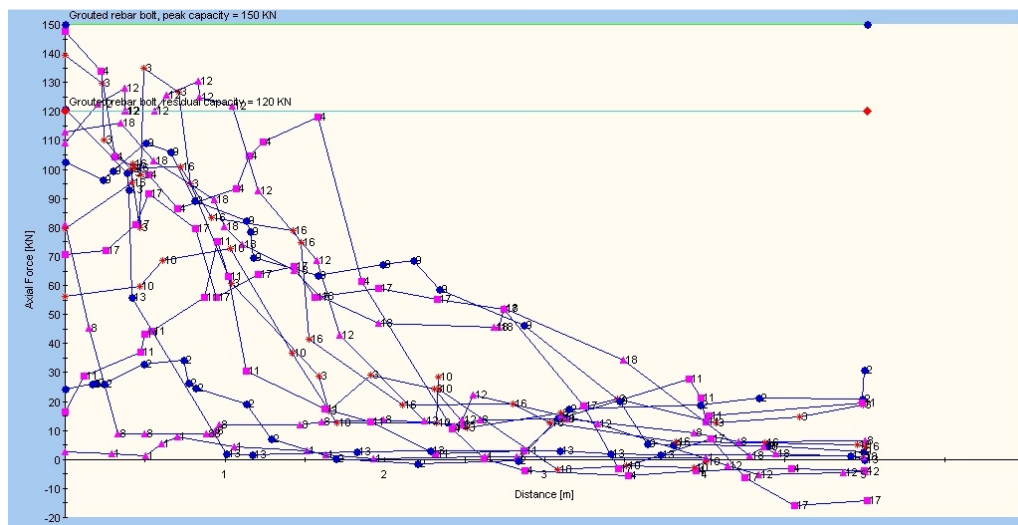


**Figure 7-52: Axial force in rock bolts in the tunnel walls in supplementary support model 1.**

The axial force in the rock bolts in the tunnel walls is displayed in Figure 7-52. It is seen on the figure bolts nr. 3, 4, 12, 13 presents yielding. The maximum total displacement decreases down to 19,2 mm in the right tunnel wall from 19,6 mm in the practical supported model. For the left wall the total displacement decreases from 16,2 mm to 15,2 mm. In Appendix 6 the bending moment for the shotcrete liner is displayed.

## Supplementary Support Model 2

The supplementary supported model 2 will be extended from supplementary supported model 1. Two rock bolts will be installed in the red sediment layer at each tunnel wall and the thickness of the shotcrete will be increased from 11,4 mm to 15 mm. That amount of shotcrete is rarely used, unless where conditions are very poor.

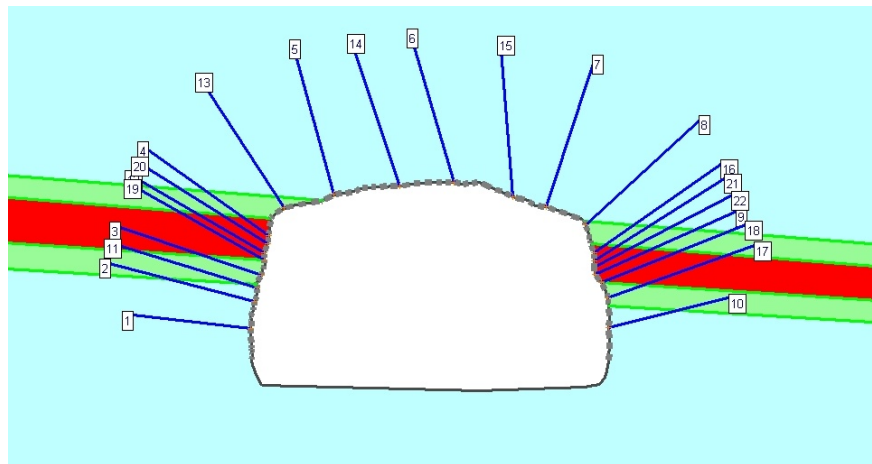


Figure 7-53: Rock bolt setup, additional rock bolts (19-22).

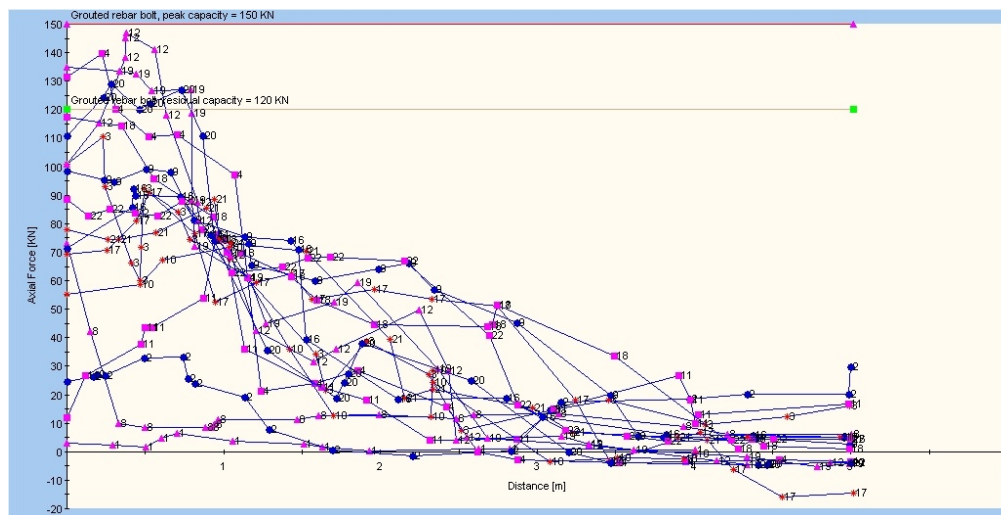


Figure 7-54: Axial force in rock bolts in the tunnel walls in supplementary support model 2

As seen in Figure 7-54 yielding occurs in rock bolts nr. 4, 12, 19 and 20. All these bolts are installed in the left tunnel wall. No bolt is yielding in the right tunnel wall where the maximum total displacement is 19,0 mm. The maximum total displacement is 14,4 mm for the left wall. Table 7-11 presents the maximum

total displacement in the red sediment layer in each tunnel wall. In Appendix 6 the bending moment for the shotcrete liner is displayed.

**Table 7-11: Maximum total displacements in red sediment layer in left and right wall.**

<b>Model</b>	<b>Disp. in left wall [mm]</b>	<b>Disp. in right wall [mm]</b>
Practical support model	16,2	19,6
Supplementary support model 1	15,2	19,2
Supplementary support model 2	14,4	19,0

The difference in maximum total displacement is not large, especially for the red sediment in the right tunnel wall, additionally, it is impracticable to minimize the displacement using current rock bolts and shotcrete. There are many possible reasons for this little difference they will be presented in the discussion chapter.



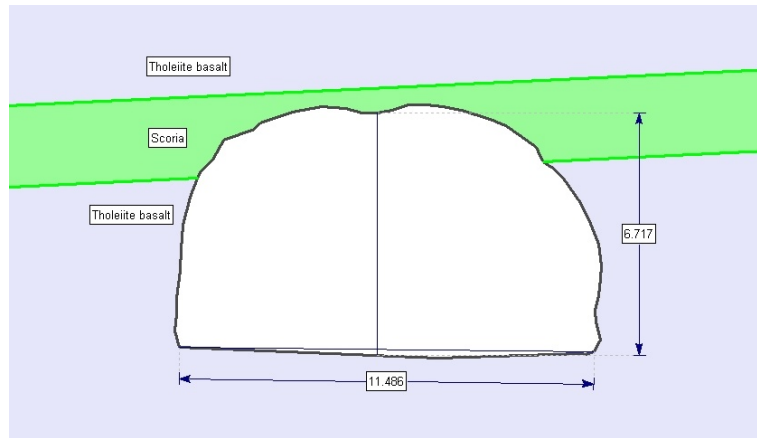


**Figure 7-56: Tunnel cross section of station 7615, the dimensions are in meters.**

#### 7.4.1 Practical Support at Station 7615 in Fáskrúðsfjörður Tunnel

By utilizing rock bolts and shotcrete reports from the contractor and the supervisor, a cross section from station 7615 with various supports will be modelled. Appropriate pages from the support reports can be find in Appendix 5.

Nine grouted rebar rock bolts were installed with spot bolting, the length of each of them is four meters. The thickness of the shotcrete is 5,1 cm, based on calculations from the shotcrete report, see Figure 7-57.

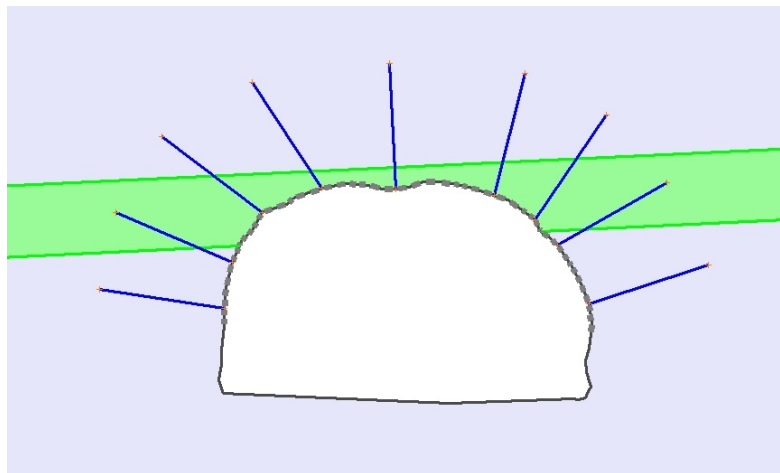


**Figure 7-57: Support setup for station 7616, based on rock bolts and shotcrete reports.**

From Figure 7-58 to Figure 7-66 a comparison of three various models; unsupported model, model with 80% of the stress relief and full supported model with full stress relief is presented. The comparison is based on yielded elements, total displacement and deformation.



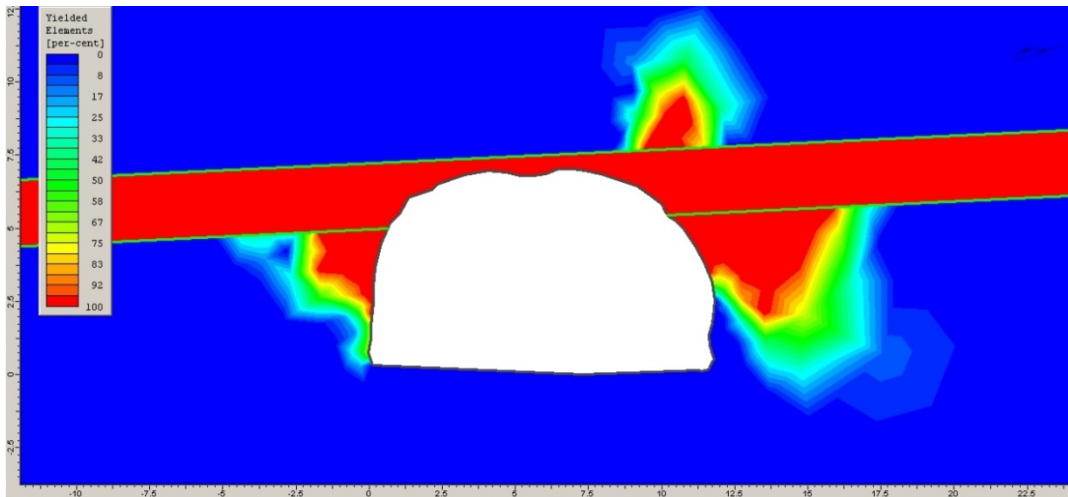


Figure 7-58: Yielded elements for unsupported model from station 7615.

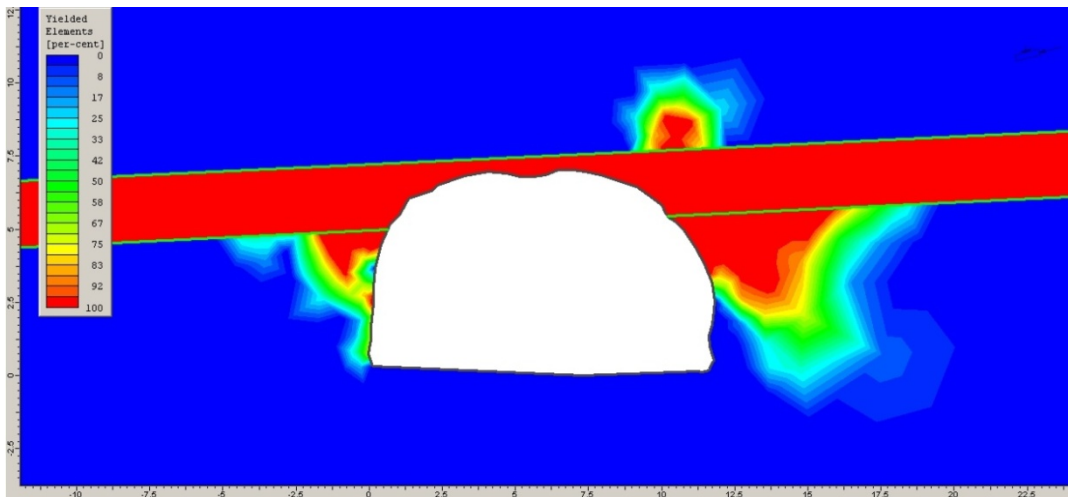


Figure 7-59 Yielded elements for 80% stress relief model from station 7615.

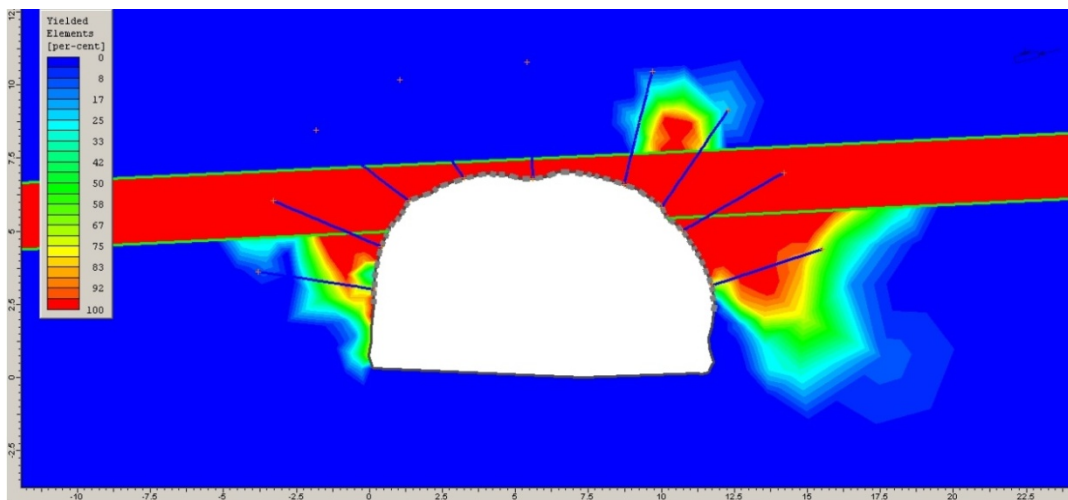


Figure 7-60: Yielded elements for full supported and full stress relieved model from station 7615.

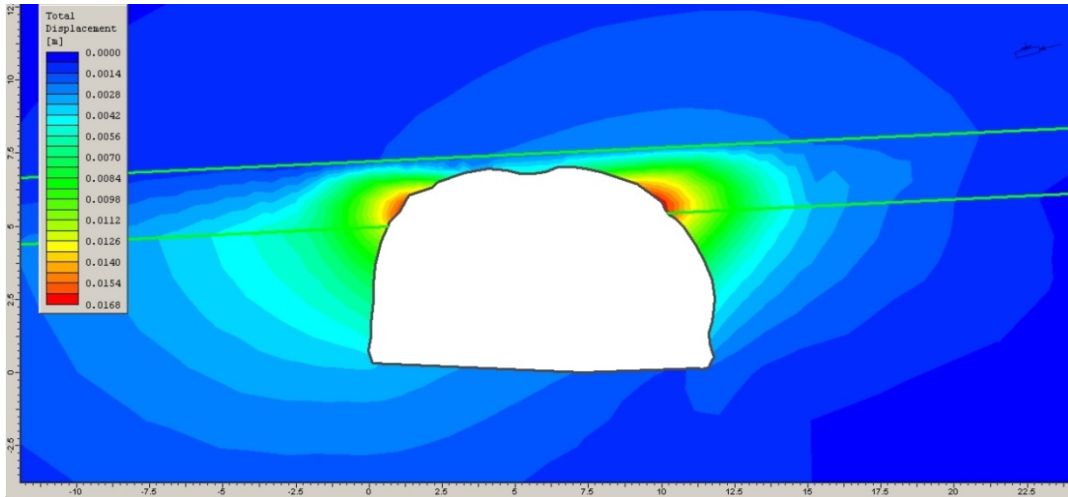


Figure 7-61: Total displacements for unsupported model from station 7615.

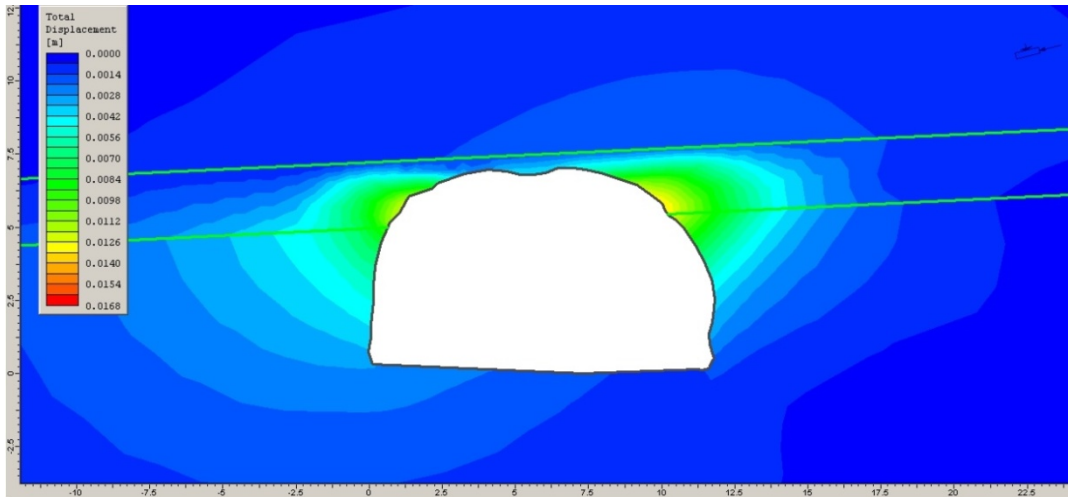


Figure 7-62: Total displacements for 80% stress relief model from station 7615.

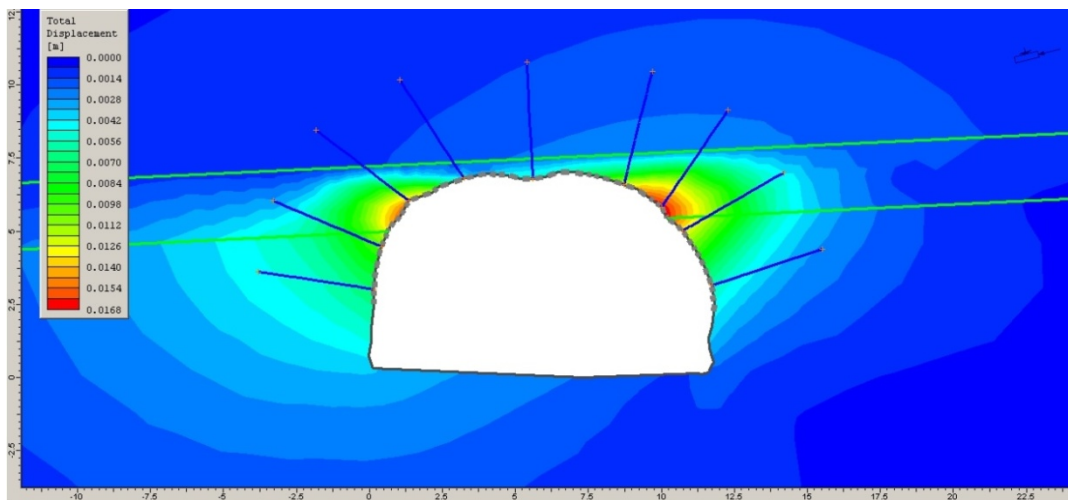


Figure 7-63: Total displacements for full supported and full stress relieved model from station 7615.

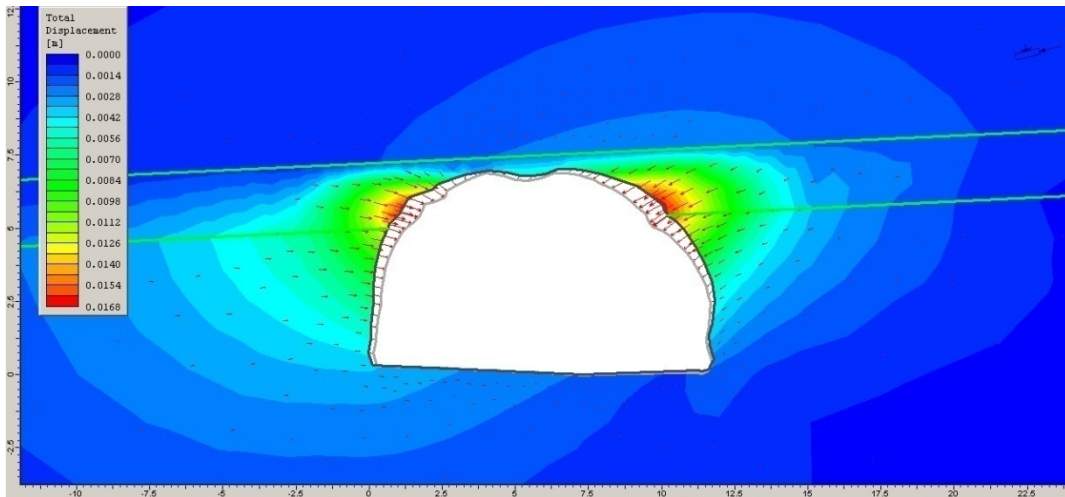


Figure 7-64: Deformed geometry for unsupported model from station 7615 (scale: x40).

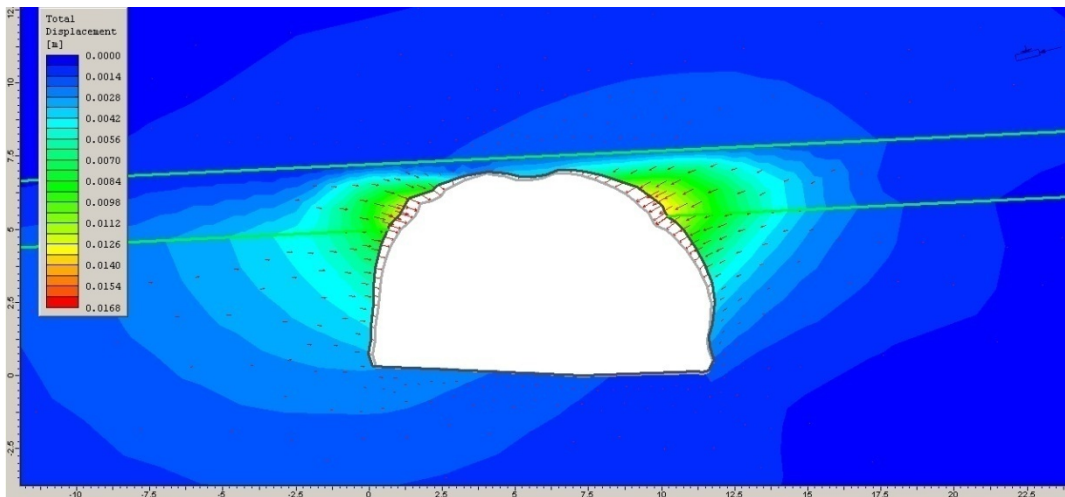


Figure 7-65: Deformed geometry for 80% stress relief model from station 7615 (scale: x40).

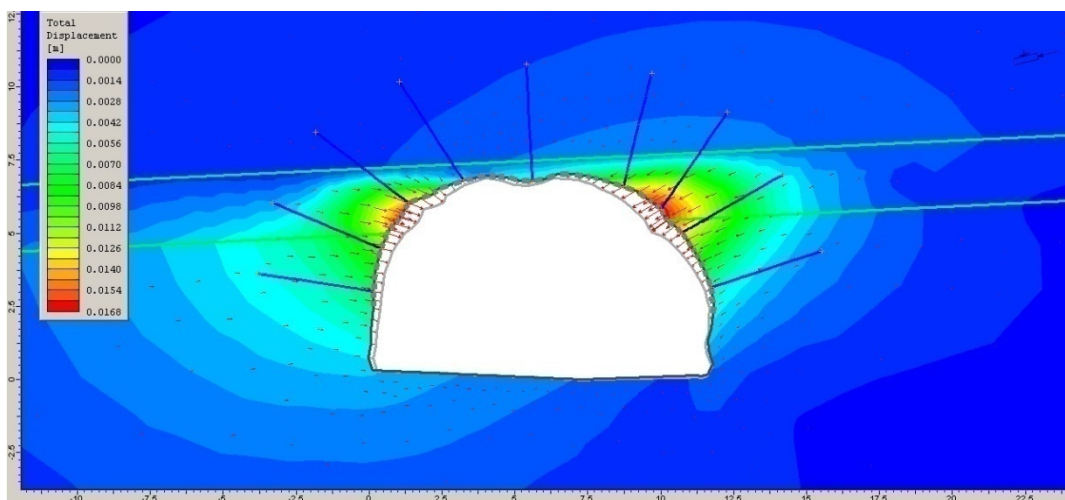


Figure 7-66: Deformed geometry for full supported and full stress relieved model from station 7615 (scale: x40).

The scoria layer in the tunnel roof has completely yielded, same as for upper part of the tunnel walls. A condition like this could have serious risk of downfall from the roof. No yielding zones appear in the tunnel floor. No rock bolts or shotcrete elements are yielding which secure the stability of the tunnel. The number of yielded elements decrease from 366 for unsupported to 354 for fully supported.

The maximum total displacement are expected in the corners of the tunnel roof, from the scoria. Other tunnel parts have maximum total displacement lower than 10 mm. But maximum total displacement in the unsupported model is 16,5 mm and 16,7 mm for the fully supported model, which looks a bit confusing but could be caused by the 80/20 load splitting.

The deformation figures state how the scoria layer in the roof and the tunnel walls “falls” into the tunnel. Little as none deformation seems to be in the centre tunnel roof and the tunnel floor.

**Table 7-12: Yielded elements and total displacements for various models from station 7615.**

<b>Station 7615</b>	<b>Yielded elements</b>	<b>Total displacement [mm]</b>
Unsupported	366	16,5
80% stress relieved	351	13,3
Full supported and full stress relieved	354	16,7

#### **7.4.2 Supplementary Support for Station 7615**

The same problem is in station 7615 as in station 6530 where weak rock layer is resulting in too large displacements, in this case a scoria layer in the tunnel roof. After further analysis on the practical support model, rock bolt nr. 3 presents yielding, see Appendix 6. In order to decrease the maximum total displacement, some supplementary support is needed. The attention will be on the roof corners in the scoria layer. Since other tunnel segments displayed total displacement below 10 mm. The same rock bolts and shotcrete will be used as in the practical supported model, but the amount of rock bolts and the thickness of the shotcrete will be increased. An attempt is made to install the rock bolts in stable rock, in order to avoid installation in yielded zone. Two different supplementary models will be modeled.

### Supplementary Support Model 1

The additional rock bolts were all installed in the roof corners where the largest displacements took place in the practical support model. The number of rock bolts is six, three in each roof corner, and the length is unchanged, or four meters. The shotcrete thickness is still 5,1 mm. Figure 7-67 presents the rock bolt setup.

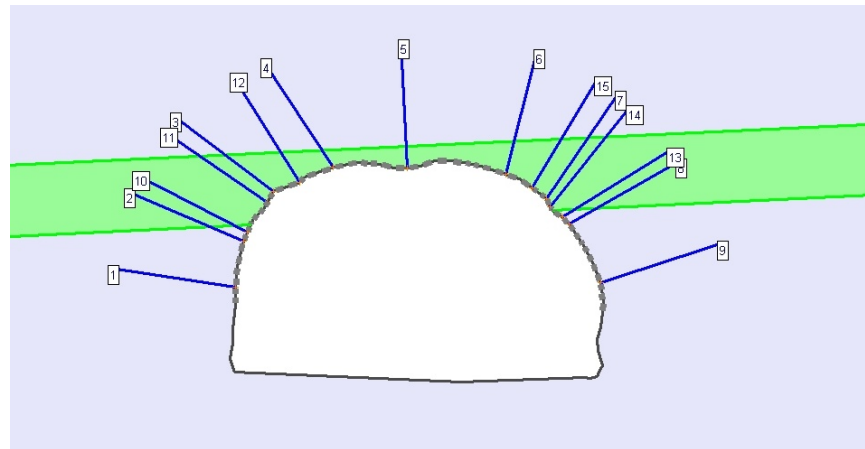


**Figure 7-67: Rock bolts from the practical support (1-9) and additional rock bolts (10-15).**

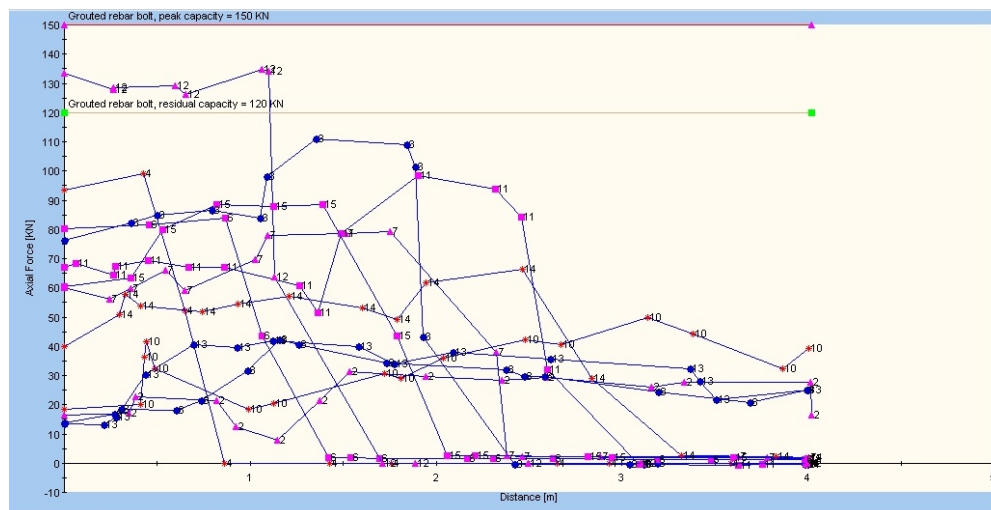


**Figure 7-68: Axial force in rock bolts in the tunnel roof corners in supplementary support model 1.**

According to Figure 7-68, rock bolt nr.12 yields from tunnel wall to approximately one meter into the rock mass. The rock bolt is located in the left corner which states that more rock bolts are needed at that region. Rock bolt nr.12, which is placed beside rock bolt nr.3 in the left tunnel wall, has obviously taking some of the load from rock bolt nr.3 in the practical support model. The maximum total displacement reduces to 16,5 mm in the right tunnel roof corner from 16,7

mm in the practical supported model. For the left roof corner the total displacement decreases from 15,2 mm to 14,7 mm.

### Supplementary Support Model 2

The supplementary supported model 2 will be extended from supplementary supported model 1. Two additional rock bolts will be installed in each corner of the tunnel roof and the thickness of the shotcrete will be increased from 5,1 cm to 15,0 cm. That amount of shotcrete is rarely used, unless where conditions are very poor.

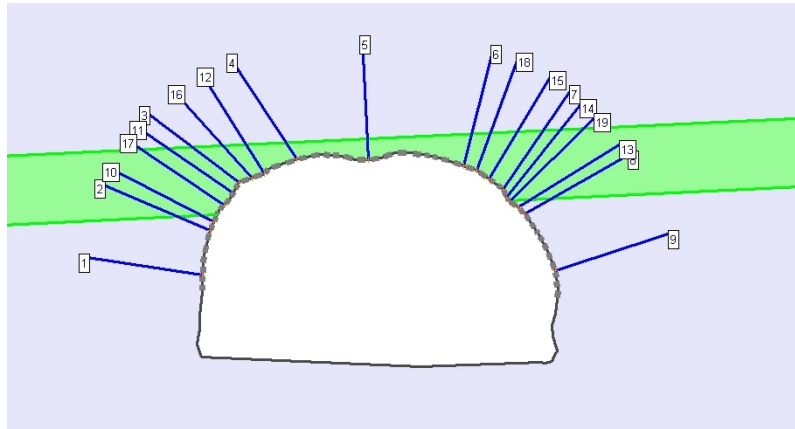


Figure 7-69: Rock bolt setup, additional rock bolts (16-19).

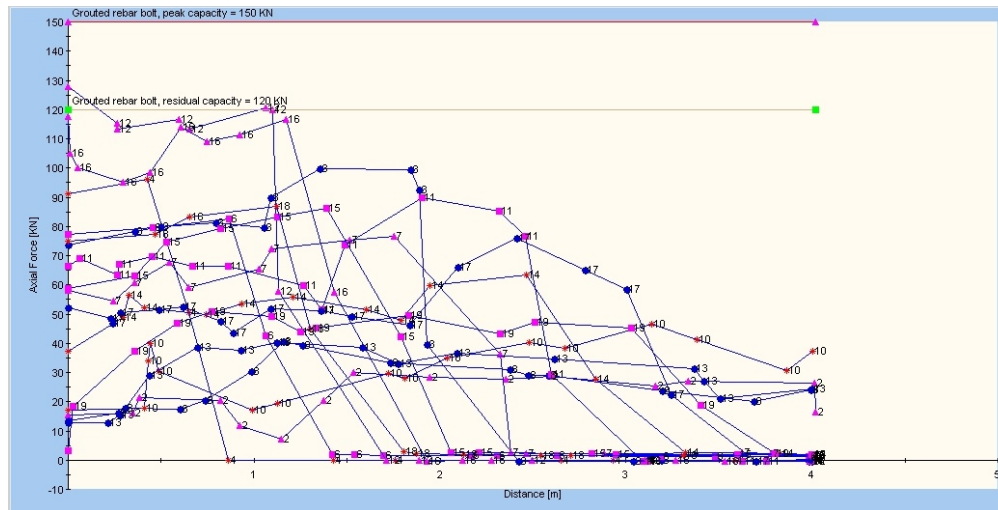


Figure 7-70: Axial force in rock bolts in the roof corners for supplementary support model 2.

As seen in Figure 7-70, bolt nr.12 does still yield, even though additional rock bolts have been installed. The maximum total displacement in the right roof corner tunnel is 16,4 mm and 14,7 mm for the left roof corner.

Table 7-13 presents the maximum total displacement in the scoria layer in each roof corner.

**Table 7-13: Maximum total displacements in scoria layer in left and right roof corner.**

Model	Disp. in left roof corner [mm]	Disp. in right roof corner [mm]
Practical support model	15,4	16,7
Supplementary support model 1	14,7	16,5
Supplementary support model 2	14,7	16,4

The total displacements in the roof corners are following the same pattern as the red sediment in the tunnel walls from station 6530. The decrease in displacements is very small and against expectations. The possible reasons for this little differences can be many and will be discussed in next chapter.

## 7.5 Discussion

All models states that weaker rock types, scoria and sediments, surrounding the tunnel do not support the desired load and deform and squeezes into the tunnel opening.

The decrease in maximum displacements for supplementary support models for stations 6530 and 7615, are not as expected. Especially when taken into consideration that the results from the typical Icelandic mixed face tunnel model for elastic-plastic conditions and GSI=75 gave difference of 4 mm between unsupported and fully supported models. Some modifications were made on the supplementary supported models to explore this little difference in displacements. Strength and stiffness properties for rock bolts and shotcrete were put as high as possible, but the change in displacements did not exceed half a millimetre. Different ratios of load splitting were also utilized but gave same outcome.

The main difference between the practical supported models from stations 6530 and 7615 and the typical Icelandic mixed face tunnel model is the tunnel width and the surface shape. The tunnel opening for practical support models are made from cross section measurements causing rough surface but the typical Icelandic mixed face tunnel model has an arc-shaped roof which will distribute the stress field more equally over the whole tunnel surface.

The large deformations obtained may relate to underestimated choice of  $\psi$ ,  $\varphi_{resid}$  and  $c_{resid}$  for the weaker rock types, especially for scoria. Compared to laboratory test results from the Fáskrúðsfjörður tunnel, the strength properties for scoria are



much higher than the values used in the modelling. This shows that further work is needed in parameter evaluation for the weaker rock types.

The practical support used in stations 6530 and 7615 is sufficient, despite the modelling showed 19,6 mm and 16,7 mm as maximum displacements. Some rock bolts obtained yielding but at both sites the shotcrete liner carried the rest of the load and secured safe stability. It suggests that the upper limit of 10 mm for maximum displacement may be an underestimated choice.

In the supplementary support models for stations 6530 and 7615 the maximum displacements did not decrease according to expectations, which state that the practical support used is the optimal support according to this analyses. The cost of the additional support in supplementary support models is more than two times higher than in the practical supported models and did not reduce the displacements.



## 8 Conclusion

All models state that weaker rock types, scoria and sediments, surrounding the tunnel, do not support the desired load and react to deform and squeeze into the tunnel opening. This, of course, can cause serious instability problems, especially if such layers are placed in tunnel walls and roof. As seen from models with GSI=75, the total displacements for tholeiite basalt are quite small and do rarely exceed 10 mm, which states that excavation in pure basalt would only need minimum of support.

The parameters used for elastic-plastic models must be taken with precaution, due to uncertainty of  $\psi$ ,  $\varphi_{\text{resid}}$  and  $c_{\text{resid}}$ . Due to the lack of hard data, the limitation of important input parameters is great and further parameter analyses are needed, especially for scoria.

From the comparison of laboratory test results from the headrace tunnel of Kárahnjúkar hydroelectric project and the Fáskrúðsfjörður tunnel, the difference is obvious. Strength and stiffness parameters for different rock types from the Fáskrúðsfjörður tunnel are much lower, particularly for the various basalts where unconfined compression strength is more than six times larger in the samples from Kárahnjúkar than Fáskrúðsfjörður. For scoria, the difference is not much which underlines that the used strength and stiffness properties in the modelling were too low. The possible reason for this gap between the two sites, is a selection of porous rock cores from the Fáskrúðsfjörður tunnel and older rock mass in Fáskrúðsfjörður which has reduced its strength cause of weathering and high stress conditions.

It can be stated that the practical support used in the Fáskrúðsfjörður tunnel, for both stations 6530 and 7615, is well optimised despite of the maximum displacements exceeding 10 mm. Some rock bolts presented yielding but at both sites the shotcrete liner carried the rest of the load and secured safe stability. The supplementary support models for both stations did not decrease the maximum displacements as expected. The cost for the additional support is more than two

times higher than in the practical supported models. The use of additional bolts gives no significant reduction in convergence.

In general it is the conclusion of the modelling work that *Phase2* works well. It is recommended for future works to emphasise on more rock stress measurements and more rock mechanical testing to provide better data for the convergence modelling work. Especially, the used GSI evaluation and definition of residual values calls for concurrent calibration of actual tunnelling sites with face logging and support strategy applied.

Using numerical analyses in estimation of the need of acceptable support can be profitable. But as always in modelling, the input data has to be as in-situ like as possible, to get reliable results. In every model there is always a certain amount of important factors needed, which are obtained by conservative guessing or taken from practical point of view due to the lack of hard data. Rock support needs in Icelandic underground structures are estimated from visual inspection at site and use of the NGI tunnel quality index. Using a finite element program, similar to *Phase2*, can give an invaluable findings in the preliminary studies which can prevent unforeseen situations. But however, some improvements are still needed in adjusting the rock classification systems and the finite element programs to Icelandic circumstances.

## 9 Future work

- ✓ Use *Phase2* in cooperation with responsible engineering geologist concurrently at site in order to optimise bolt position and bolt alignment.
- ✓ Make further triaxial tests on weaker rock types, scoria and sediments, to obtain more reliable residual values after peak value of compression strength using constant deformation rate.
- ✓ Use measuring points set up by surveyors for the tunnel alignment to obtain time series of convergence in order to refine the load splitting support strategies.
- ✓ Make an analysis on how different load splitting ratio affects the same cross section.



## 10 References

- [1] Harðarson, B. A.: "Icelandic Rock Tunneling Quality". ITA and ITS Tunneling Conference 1991.
- [2] Höskuldsson, Á.; Þórðarson, Þ.: "Classic Geology in Europe 3 – Iceland". Terra Publishing 2002. Hertfordshire, England.
- [3] Nature explorer. <http://www.natureexplorer.is/page.asp?id=613>. Accessed: 05/05/2008
- [4] Einarsson, Þ.: "Geology of Iceland: Rocks and Landscape". Published by Mál og Menning 1994. Reykjavík, Iceland.
- [5] Landsvirkjun: Kárahnjúkar Hydroelectric Project. "Contract Documents KAR-14: Headrace tunnel – Volume 5". Kárahnjúkar Engineering Joint Venture, 2003.
- [6] Jónsson, B.: "Geotechnical Field Classification of Basalts in Iceland". Nordic Geotechnical Conference 1996, pp.469-473.
- [7] Sent from Bjarney Guðbjörnsdóttir at the National Land Survey of Iceland. The figure is owned by ©Landmælingar Íslands/©National Land Survey of Iceland. 2008.
- [8] Erlingsson, S.: "Seismic Design of Subsea Tunnels with Special Emphasizes to the Hvalfjörður Tunnel in Iceland". Proceedings of the International Symposium on Rock Support – Applied Solutions for Underground Structures, Lillehammer, 1997. PP. 804-811.

- [9] Jóhannsson, Æ.: “Mechanical Properties of Rock in an Icelandic Lava Stratum – measurements in Laboratory”. Master’s Thesis at University of Iceland, 1997.
- [10] Loftsson, M.: “Blanda Hydroelectric Project – Groundwater Conditions and Related Excavation Problems”. ITA and ITS Tunneling Conference 1991.
- [11] Jónsson, B.: “Undirbúningsrannsóknir vegna jarðganga við vatnsaflsvirkjanir á Íslandi”. Tímarit Verkfræðingafélags Íslands 69.árg. 1984, 21-43.
- [12] Das, B. M.: “Principle of Geotechnical Engineering”. Fifth edition 2002, California State University, Sacramento, USA.
- [13] Ingimarsson, A. K.; Jóhannsson, Æ.; Loftsson, M.: “In situ rock Mass Stresses in Iceland and Rock Mass Deformation of Underground Caverns in the Kárahnjúkar and Blanda Hydroelectric Projects”. Proceedings of the International Symposium on In-situ Rock Stress. Trondheim, Norway 19<sup>th</sup> – 21<sup>st</sup> June 2006.
- [14] Erlingsson, S.: “Lecture notes in the course 08.13.58 Rock Mechanics and Blasting Techniques”. University of Iceland, Faculty of Engineering, 2007.
- [15] Rennen, M.; Sigurðsson, Þ.; Valsson, G.: “Campaign ISNET2004 - Remeasurement of the Icelandic reference network”. The 17<sup>th</sup> Nordic GIS Conference 2005. Reykjavík 2005
- [16] Nelson, S.: “Deformation of rock” <http://pulse.tcs.tulane.edu/~sanelson/geol111/deform.htm>. Accessed 27/07/2008.
- [17] Wang, J.: “Seismic Design of Tunnels”, published 1991. <http://www.pbworld.com/library/fellowship/wang/>. Accessed 15.08.2008.
- [18] Íslenskur staðall. “Þjóðarskjal með FS ENV 1998-1-1:1994”. Staðlaráð Íslands, 2002.
- [19] Hoek, E.: “Practical Rock Engineering”. Evert Hoek Consulting Engineer Inc. Vancouver, Canada, 2007.



- 
- [20] Wikipedia. <http://en.wikipedia.org/wiki/RQD>. Accessed 16/07/2008.
- [21] Pade, E.: "Parameter study based on jointed limestone". Master's Thesis at Technical University of Denmark, 2006.
- [22] Wikipedia. [http://en.wikipedia.org/wiki/Rock\\_Mass\\_Rating\\_system](http://en.wikipedia.org/wiki/Rock_Mass_Rating_system). Accessed 18/07/2008.
- [23] Simon Fraser University. [http://www.sfu.ca/~tafgrc/Courses/Easc313/Frock\\_Mass\\_Classification](http://www.sfu.ca/~tafgrc/Courses/Easc313/Frock_Mass_Classification). Accessed 23/07/2008.
- [24] US Army Corps of Engineers. <http://www.usace.army.mil/publications/engineering-manuals/em1110-2-2901/c-7.pdf>. Accessed 23/07/2008.
- [25] Løset, F.: "The Q-Method and its Application-A Method for Describing Rock Mass Stability in Tunnels". Norwegian Tunnelling Technology, publication no.2. 1983, 76-78.
- [26] Harðarson, B. H.: "Jarðgöng á Íslandi: Berggæðamat". Orkustofnun Vatnsorkudeild OS-84080/VOD-21, 1984.
- [27] Sigurdsson, O.: Oral reference. Accessed 29/07/2008.
- [28] Palmstrom, A.; Stille, H.: "Ground behaviour and rock engineering tools for underground excavation". Norconsult AS. Norway, 2006.
- [29] Carranza-Torres, C.; Corkum, B.; Hoek, E.: "Hoek-Brown Failure Criterion-2002 Edition". Canada, 2002.
- [30] Sigursteinsdóttir, A. K.: "Berggæðamatskerfi í jarðgöngum". B.Sc Thesis at University of Reykjavík, 2006.
- [31] Pusch, R.: "Rock Mechanics on a Geological Base". Elsevier Science B.V. Netherland, 1995.
- [32] Wisegeek. <http://www.wisegeek.com/what-is-shotcrete.htm>. Accessed 18/07/2008.

- 
- [33] Erlingsson, S.: "Lecture notes in the course 08.41.48 Sprengitækni". University of Iceland, Faculty of Engineering, 2007.
- [34] Herget, G.: "Stresses in Rock". Published by A.A Balkema, Rotterdam, Netherland 1988.
- [35] Harðarson, B. H.; Sigurðsson, O.: "Fáskrúðsfjarðargöng - Framkvæmdaskýrsla". GeoTek Ltd, 2006.
- [36] Guðmundsson, Á.; Hallsteinsson, H.: "Fáskrúðsfjörður – Road Tunnel, Geological Report". JFS Geological services Ltd, December 2000.
- [37] Guðmundsson, Á.: Written reference by e-mail. Accessed 23/04/2008.
- [38] Dahle, H.: "In Situ Rock Stress in Layered Icelandic Volcanic Rocks- Fáskrúðsfjörður tunnel". SINTEF Technology and Society-Rock and Soil Mechanics, Norway, 2005.
- [39] Hudson, J.A.; Ulusay, R.: "The Complete ISRM Suggested Methods for Rock Characterization, Testing and Monitoring: 1974-2006". ISRM, 2007.
- [40] Arngrímsson, H. Ö.: "Mechanical testing on Icelandic volcanic rocks". Special course at Technical University of Denmark, 2008.
- [41] Foged, N.; Hartlén, J.; Jackson, P.G.; Steenfelt, J.S.: "Evaluation of Bryozoan limestone properties based on in-situ and laboratory elements tests". Proceedings of ISC (International Conference on Site Characterisation) in Porto, Portugal 2004.
- [42] Korsnes, R. I.; Madland, M. V.; Risnes, R.: "Temperature effects in Brazilian, uniaxial and triaxial compressive tests with high porosity chalk". SPE (Society of Petroleum Engineers Inc.) annual technical conference and exhibition, San Antonio, Texas, 29<sup>th</sup> September – 2<sup>nd</sup> October 2002.
- [43] Guðmundsson, H.: Written reference by e-mail. Accessed 06/10/2008.

- [44] Ísaksdóttir, H.: “Rock mechanical studies of volcanic tephra for hydroelectric power station”. Master's Thesis at Technical University of Denmark, 2004.
  
- [45] Ernstsóttir, K. K.: “Rock mechanical studies for a hydroelectric power station.” Master's Thesis at Technical University of Denmark, 2003.
  
- [46] Sigurðsson, O.: Pictures and other materials sent by e-mails.





Master's Thesis

# Rock Mass Characterisation and Reinforcement Strategies for Tunnels in Iceland

---

## Fáskrúðsfjörður Tunnel

## Appendixes

Gunnar Arnar Gunnarsson

October, 2008

In corporation with:





## 1. Appendix

This appendix contains a parameter description of various types of rock classification system from chapter 4.1. in the thesis and also figure from *RocLab*

- ✓ Parameter description of RSR, rock structure rating.
- ✓ Parameter description of RMR, rock mass rating.
- ✓ Parameter description of NGI tunnelling quality index.
- ✓ Determination of GSI for heterogeneous rock.
- ✓ Figure from the computer program *RocLab*.

**Table 1-1: Parameter description of RSR, rock structure rating.**

Table 4.1: Rock Structure Rating: Parameter A: General area geology

	Basic Rock Type				Geological Structure			
	Hard	Medium	Soft	Decomposed				
Igneous	1	2	3	4		Slightly	Moderately	Intensively
Metamorphic	1	2	3	4		Folded or	Folded or	Folded or
Sedimentary	2	3	4	4	Massive	Faulted	Faulted	Faulted
Type 1					30	22	15	9
Type 2					27	20	13	8
Type 3					24	18	12	7
Type 4					19	15	10	6

Table 4.2: Rock Structure Rating: Parameter B: Joint pattern, direction of drive

Average joint spacing	Strike ⊥ to Axis					Strike    to Axis			
	Direction of Drive								
	Both	With Dip			Against Dip		Either direction		
	Dip of Prominent Joints <sup>a</sup>								
	Flat	Dipping	Vertical	Dipping	Vertical	Flat	Dipping	Vertical	
1. Very closely jointed, < 2 in	9	11	13	10	12	9	9	7	
2. Closely jointed, 2-6 in	13	16	19	15	17	14	14	11	
3. Moderately jointed, 6-12 in	23	24	28	19	22	23	23	19	
4. Moderate to blocky, 1-2 ft	30	32	36	25	28	30	28	24	
5. Blocky to massive, 2-4 ft	36	38	40	33	35	36	24	28	
6. Massive, > 4 ft	40	43	45	37	40	40	38	34	

Table 4.3: Rock Structure Rating: Parameter C: Groundwater, joint condition

Anticipated water inflow gpm/1000 ft of tunnel	Sum of Parameters A + B					
	13 - 44			45 - 75		
	Joint Condition <sup>b</sup>					
	Good	Fair	Poor	Good	Fair	Poor
None	22	18	12	25	22	13
Slight, < 200 gpm	19	15	9	23	19	14
Moderate, 200-1000 gpm	15	22	7	21	16	12
Heavy, > 1000 gp	10	8	6	18	14	10

<sup>a</sup> Dip: flat: 0-20°; dipping: 20-50°; and vertical: 50-90°

<sup>b</sup> Joint condition: good = tight or cemented; fair = slightly weathered or altered; poor = severely weathered, altered or open



**Table 1-2: Parameter description of RMR, rock mass rating.**

Table 4.4: Rock Mass Rating System (After Bieniawski 1989).

A. CLASSIFICATION PARAMETERS AND THEIR RATINGS								
Parameter		Range of values						
1	Strength of intact rock material	Point-load strength index	>10 MPa	4 - 10 MPa	2 - 4 MPa	1 - 2 MPa	For this low range - uniaxial compressive test is preferred	
		Uniaxial comp. strength	>250 MPa	100 - 250 MPa	50 - 100 MPa	25 - 50 MPa	5 - 25 MPa	1 - 5 MPa
	Rating	15	12	7	4	2	1	0
2	Drill core Quality RQD		90% - 100%	75% - 90%	50% - 75%	25% - 50%	< 25%	
	Rating		20	17	13	8	3	
3	Spacing of discontinuities		> 2 m	0.6 - 2 . m	200 - 600 mm	60 - 200 mm	< 60 mm	
	Rating		20	15	10	8	5	
4	Condition of discontinuities (See E)		Very rough surfaces Not continuous No separation Unweathered wall rock	Slightly rough surfaces Separation < 1 mm Slightly weathered walls	Slightly rough surfaces Separation < 1 mm Highly weathered walls	Slickensided surfaces or Gouge < 5 mm thick or Separation 1-5 mm Continuous	Soft gouge >5 mm thick or Separation > 5 mm Continuous	
	Rating		30	25	20	10	0	
5	Ground water	Inflow per 10 m tunnel length (l/m)	None	< 10	10 - 25	25 - 125	> 125	
		(Joint water press)/ (Major principal $\sigma$ )	0	< 0.1	0.1, - 0.2	0.2 - 0.5	> 0.5	
		General conditions	Completely dry	Damp	Wet	Dripping	Flowing	
	Rating		15	10	7	4	0	
B. RATING ADJUSTMENT FOR DISCONTINUITY ORIENTATIONS (See F)								
Strike and dip orientations		Very favourable	Favourable	Fair	Unfavourable	Very Unfavourable		
Ratings	Tunnels & mines	0	-2	-5	-10	-12		
	Foundations	0	-2	-7	-15	-25		
	Slopes	0	-5	-25	-50			
C. ROCK MASS CLASSES DETERMINED FROM TOTAL RATINGS								
Rating		100 ← 81	80 ← 61	60 ← 41	40 ← 21	< 21		
Class number		I	II	III	IV	V		
Description		Very good rock	Good rock	Fair rock	Poor rock	Very poor rock		
D. MEANING OF ROCK CLASSES								
Class number		I	II	III	IV	V		
Average stand-up time		20 yrs for 15 m span	1 year for 10 m span	1 week for 5 m span	10 hrs for 2.5 m span	30 min for 1 m span		
Cohesion of rock mass (kPa)		> 400	300 - 400	200 - 300	100 - 200	< 100		
Friction angle of rock mass (deg)		> 45	35 - 45	25 - 35	15 - 25	< 15		
E. GUIDELINES FOR CLASSIFICATION OF DISCONTINUITY conditions								
Discontinuity length (persistence)		< 1 m	1 - 3 m	3 - 10 m	10 - 20 m	> 20 m		
Rating		6	4	2	1	0		
Separation (aperture)		None	< 0.1 mm	0.1 - 1.0 mm	1 - 5 mm	> 5 mm		
Rating		6	5	4	1	0		
Roughness		Very rough	Rough	Slightly rough	Smooth	Slickensided		
Rating		6	5	3	1	0		
Infilling (gouge)		None	Hard filling < 5 mm	Hard filling > 5 mm	Soft filling < 5 mm	Soft filling > 5 mm		
Rating		6	4	2	2	0		
Weathering Ratings		Unweathered	Slightly weathered	Moderately weathered	Highly weathered	Decomposed		
Rating		6	5	3	1	0		
F. EFFECT OF DISCONTINUITY STRIKE AND DIP ORIENTATION IN TUNNELLING**								
Strike perpendicular to tunnel axis				Strike parallel to tunnel axis				
Drive with dip - Dip 45 - 90°		Drive with dip - Dip 20 - 45°		Dip 45 - 90°		Dip 20 - 45°		
Very favourable		Favourable		Very unfavourable		Fair		
Drive against dip - Dip 45-90°		Drive against dip - Dip 20-45°		Dip 0-20 - Irrespective of strike°				
Fair		Unfavourable		Fair				

\* Some conditions are mutually exclusive . For example, if infilling is present, the roughness of the surface will be overshadowed by the influence of the gouge. In such cases use A.4 directly.

\*\* Modified after Wickham et al (1972).

**Table 1-3: Guidelines for excavation and support of 10 m span rock tunnels in accordance with the RMR system (After Bieniawski 1989).**

Rock mass class	Excavation	Rock bolts (20 mm diameter, fully grouted)	Shotcrete	Steel sets
I - Very good rock <i>RMR</i> : 81-100	Full face, 3 m advance.	Generally no support required except spot bolting.		
II - Good rock <i>RMR</i> : 61-80	Full face , 1-1.5 m advance. Complete support 20 m from face.	Locally, bolts in crown 3 m long, spaced 2.5 m with occasional wire mesh.	50 mm in crown where required.	None.
III - Fair rock <i>RMR</i> : 41-60	Top heading and bench 1.5-3 m advance in top heading. Commence support after each blast. Complete support 10 m from face.	Systematic bolts 4 m long, spaced 1.5 - 2 m in crown and walls with wire mesh in crown.	50-100 mm in crown and 30 mm in sides.	None.
IV - Poor rock <i>RMR</i> : 21-40	Top heading and bench 1.0-1.5 m advance in top heading. Install support concurrently with excavation, 10 m from face.	Systematic bolts 4-5 m long, spaced 1-1.5 m in crown and walls with wire mesh.	100-150 mm in crown and 100 mm in sides.	Light to medium ribs spaced 1.5 m where required.
V – Very poor rock <i>RMR</i> : < 20	Multiple drifts 0.5-1.5 m advance in top heading. Install support concurrently with excavation. Shotcrete as soon as possible after blasting.	Systematic bolts 5-6 m long, spaced 1-1.5 m in crown and walls with wire mesh. Bolt invert.	150-200 mm in crown, 150 mm in sides, and 50 mm on face.	Medium to heavy ribs spaced 0.75 m with steel lagging and forepoling if required. Close invert.

**Table 1-4: Parameter description of NGI tunnelling quality index.**

Table 4.6: Classification of individual parameters used in the Tunnelling Quality Index  $Q$  (After Barton et al 1974).

DESCRIPTION	VALUE	NOTES
<b>1. ROCK QUALITY DESIGNATION</b>	<b><math>RQD</math></b>	
A. Very poor	0 - 25	1. Where $RQD$ is reported or measured as $\leq 10$ (including 0), a nominal value of 10 is used to evaluate $Q$ .
B. Poor	25 - 50	
C. Fair	50 - 75	
D. Good	75 - 90	2. $RQD$ intervals of 5, i.e. 100, 95, 90 etc. are sufficiently accurate.
E. Excellent	90 - 100	
<b>2. JOINT SET NUMBER</b>	<b><math>J_n</math></b>	
A. Massive, no or few joints	0.5 - 1.0	
B. One joint set	2	
C. One joint set plus random	3	
D. Two joint sets	4	
E. Two joint sets plus random	6	
F. Three joint sets	9	1. For intersections use $(3.0 \times J_n)$
G. Three joint sets plus random	12	
H. Four or more joint sets, random, heavily jointed, 'sugar cube', etc.	15	2. For portals use $(2.0 \times J_n)$
J. Crushed rock, earthlike	20	
<b>3. JOINT ROUGHNESS NUMBER</b>	<b><math>J_r</math></b>	
<b>a. Rock wall contact</b>		
<b>b. Rock wall contact before 10 cm shear</b>		
A. Discontinuous joints	4	
B. Rough and irregular, undulating	3	
C. Smooth undulating	2	
D. Slickensided undulating	1.5	1. Add 1.0 if the mean spacing of the relevant joint set is greater than 3 m.
E. Rough or irregular, planar	1.5	
F. Smooth, planar	1.0	
G. Slickensided, planar	0.5	2. $J_r = 0.5$ can be used for planar, slickensided joints having lineations, provided that the lineations are oriented for minimum strength.
<b>c. No rock wall contact when sheared</b>		
H. Zones containing clay minerals thick enough to prevent rock wall contact	1.0 (nominal)	
J. Sandy, gravely or crushed zone thick enough to prevent rock wall contact	1.0 (nominal)	
<b>4. JOINT ALTERATION NUMBER</b>	<b><math>J_a</math></b>	$\phi_r$ degrees (approx.)
<b>a. Rock wall contact</b>		
A. Tightly healed, hard, non-softening, impermeable filling	0.75	1. Values of $\phi_r$ , the residual friction angle, are intended as an approximate guide to the mineralogical properties of the alteration products, if present.
B. Unaltered joint walls, surface staining only	1.0	25 - 35
C. Slightly altered joint walls, non-softening mineral coatings, sandy particles, clay-free disintegrated rock, etc.	2.0	25 - 30
D. Silty-, or sandy-clay coatings, small clay-fraction (non-softening)	3.0	20 - 25
E. Softening or low-friction clay mineral coatings, i.e. kaolinite, mica Also chlorite, talc, gypsum and graphite etc., and small quantities of swelling clays. (Discontinuous coatings, 1 - 2 mm or less)	4.0	8 - 16

**Table 1-5: Parameter description of NGI tunnelling quality index.**Table 4.6: (cont'd.) Classification of individual parameters used in the Tunnelling Quality Index  $Q$  (After Barton et al 1974).

DESCRIPTION	VALUE	NOTES
<b>4. JOINT ALTERATION NUMBER</b>	$J_a$	$\phi_r$ degrees (approx.)
<b>b. Rock wall contact before 10 cm shear</b>		
F. Sandy particles, clay-free, disintegrating rock etc.	4.0	25 - 30
G. Strongly over-consolidated, non-softening clay mineral fillings (continuous < 5 mm thick)	6.0	16 - 24
H. Medium or low over-consolidation, softening clay mineral fillings (continuous < 5 mm thick)	8.0	12 - 16
J. Swelling clay fillings, i.e. montmorillonite, (continuous < 5 mm thick). Values of $J_a$ depend on percent of swelling clay-size particles, and access to water.	8.0 - 12.0	6 - 12
<b>c. No rock wall contact when sheared</b>		
K. Zones or bancs of disintegrated or crushed rock and clay (see G, H and J for clay conditions)	6.0	
L. Zones or bands of silty- or sandy-clay, small clay fraction, non-softening	5.0	
M. Thick continuous zones or bands of clay	10.0 - 13.0	
N. Zones or bands of silty- or sandy-clay, small clay fraction, non-softening	5.0	
O. Thick continuous zones or bands of clay	10.0 - 13.0	
P. & R. (see G,H and J for clay conditions)	6.0 - 24.0	
<b>5. JOINT WATER REDUCTION</b>	$J_w$	approx. water pressure (kgf/cm <sup>2</sup> )
A. Dry excavation or minor inflow i.e. < 5 l/m locally	1.0	< 1.0
B. Medium inflow or pressure, occasional outwash of joint fillings	0.66	1.0 - 2.5
C. Large inflow or high pressure in competent rock with unfilled joints	0.5	2.5 - 10.0
D. Large inflow or high pressure	0.33	2.5 - 10.0
E. Exceptionally high inflow or pressure at blasting, decaying with time	0.2 - 0.1	> 10
F. Exceptionally high inflow or pressure	0.1 - 0.05	> 10
		1. Factors C to F are crude estimates; increase $J_w$ if drainage installed.
		2. Special problems caused by ice formation are not considered.
<b>6. STRESS REDUCTION FACTOR</b>		<b>SRF</b>
<b>a. Weakness zones intersecting excavation, which may cause loosening of rock mass when tunnel is excavated</b>		
A. Multiple occurrences of weakness zones containing clay or chemically disintegrated rock, very loose surrounding rock (any depth)	10.0	1. Reduce these values of SRF by 25 - 50% but only if the relevant shear zones influence do not intersect the excavation
B. Single weakness zones containing clay, or chemically disintegrated rock (excavation depth < 50 m)	5.0	
C. Single weakness zones containing clay, or chemically disintegrated rock (excavation depth > 50 m)	2.5	
D. Multiple shear zones in competent rock (clay free), loose surrounding rock (any depth)	7.5	
E. Single shear zone in competent rock (clay free). (depth of excavation < 50 m)	5.0	
F. Single shear zone in competent rock (clay free). (depth of excavation > 50 m)	2.5	
G. Loose open joints, heavily jointed or 'sugar cube', (any depth)	5.0	

**Table 1-6: Parameter description of NGI tunnelling quality index.**






Table 4.6: (cont'd.) Classification of individual parameters in the Tunnelling Quality Index  $Q$  (After Barton et al 1974).

DESCRIPTION	VALUE		NOTES
<b>6. STRESS REDUCTION FACTOR</b>			<b>SRF</b>
<b>b. Competent rock, rock stress problems</b>			
	$\sigma_c/\sigma_1$	$\sigma_t/\sigma_1$	2. For strongly anisotropic virgin stress field
H. Low stress, near surface	> 200	> 13	(if measured): when $5 \leq \sigma_1/\sigma_3 \leq 10$ , reduce $\sigma_c$
J. Medium stress	200 - 10	13 - 0.66	to $0.8\sigma_c$ and $\sigma_t$ to $0.8\sigma_t$ . When $\sigma_1/\sigma_3 > 10$ ,
K. High stress, very tight structure (usually favourable to stability, may be unfavourable to wall stability)	10 - 5	0.66 - 0.33	reduce $\sigma_c$ and $\sigma_t$ to $0.6\sigma_c$ and $0.6\sigma_t$ , where $\sigma_c$ = unconfined compressive strength, and $\sigma_t$ = tensile strength (point load) and $\sigma_1$ and $\sigma_3$ are the major and minor principal stresses.
L. Mild rockburst (massive rock)	5 - 2.5	0.33 - 0.16	
M. Heavy rockburst (massive rock)	< 2.5	< 0.16	3. Few case records available where depth of crown below surface is less than span width. Suggest SRF increase from 2.5 to 5 for such cases (see H).
<b>c. Squeezing rock, plastic flow of incompetent rock under influence of high rock pressure</b>			
N. Mild squeezing rock pressure			5 - 10
O. Heavy squeezing rock pressure			10 - 20
<b>d. Swelling rock, chemical swelling activity depending on presence of water</b>			
P. Mild swelling rock pressure			5 - 10
R. Heavy swelling rock pressure			10 - 15
<b>ADDITIONAL NOTES ON THE USE OF THESE TABLES</b>			
When making estimates of the rock mass Quality ( $Q$ ), the following guidelines should be followed in addition to the notes listed in the tables:			
1. When borehole core is unavailable, $RQD$ can be estimated from the number of joints per unit volume, in which the number of joints per metre for each joint set are added. A simple relationship can be used to convert this number to $RQD$ for the case of clay free rock masses: $RQD = 115 - 3.3 J_v$ (approx.), where $J_v$ = total number of joints per $m^3$ ( $0 < RQD < 100$ for $35 > J_v > 4.5$ ).			
2. The parameter $J_n$ representing the number of joint sets will often be affected by foliation, schistosity, slaty cleavage or bedding etc. If strongly developed, these parallel 'joints' should obviously be counted as a complete joint set. However, if there are few 'joints' visible, or if only occasional breaks in the core are due to these features, then it will be more appropriate to count them as 'random' joints when evaluating $J_n$ .			
3. The parameters $J_f$ and $J_a$ (representing shear strength) should be relevant to the weakest significant joint set or clay filled discontinuity in the given zone. However, if the joint set or discontinuity with the minimum value of $J_f/J_a$ is favourably oriented for stability, then a second, less favourably oriented joint set or discontinuity may sometimes be more significant, and its higher value of $J_f/J_a$ should be used when evaluating $Q$ . The value of $J_f/J_a$ should in fact relate to the surface most likely to allow failure to initiate.			
4. When a rock mass contains clay, the factor $SRF$ appropriate to loosening loads should be evaluated. In such cases the strength of the intact rock is of little interest. However, when jointing is minimal and clay is completely absent, the strength of the intact rock may become the weakest link, and the stability will then depend on the ratio rock-stress/rock-strength. A strongly anisotropic stress field is unfavourable for stability and is roughly accounted for as in note 2 in the table for stress reduction factor evaluation.			
5. The compressive and tensile strengths ( $\sigma_c$ and $\sigma_t$ ) of the intact rock should be evaluated in the saturated condition if this is appropriate to the present and future in situ conditions. A very conservative estimate of the strength should be made for those rocks that deteriorate when exposed to moist or saturated conditions.			

Table 1-7: Determination of GSI for heterogeneous rock mass such as flysch.

GSI FOR HETEROGENEOUS ROCK MASSES SUCH AS FLYSCH (Marinos, P and Hoek, E, 2000)		SURFACE CONDITIONS OF DISCONTINUITIES (Predominantly bedding planes)				
<p>From a description of the lithology, structure and surface conditions (particularly of the bedding planes), choose a box in the chart. Locate the position in the box that corresponds to the condition of the discontinuities and estimate the average value of GSI from the contours. Do not attempt to be too precise. Quoting a range from 33 to 37 is more realistic than giving GSI = 35. Note that the Hoek-Brown criterion does not apply to structurally controlled failures. Where unfavourably oriented continuous weak planar discontinuities are present, these will dominate the behaviour of the rock mass. The strength of some rock masses is reduced by the presence of groundwater and this can be allowed for by a slight shift to the right in the columns for fair, poor and very poor conditions. Water pressure does not change the value of GSI and it is dealt with by using effective stress analysis.</p> <p>COMPOSITION AND STRUCTURE</p>	<p><b>A. Thick bedded, very blocky sandstone</b> The effect of pelitic coatings on the bedding planes is minimized by the confinement of the rock mass. In shallow tunnels or slopes these bedding planes may cause structurally controlled instability.</p>	70	VERY GOOD - Very rough, fresh unweathered surfaces			
	<p><b>B. Sandstone with thin inter-layers of siltstone</b></p>	60	GOOD - Rough, slightly weathered surfaces			
	<p><b>C. Sandstone and siltstone in similar amounts</b></p>	50	FAIR - Smooth, moderately weathered and altered surfaces			
	<p><b>D. Siltstone or silty shale with sandstone layers</b></p>	40	POOR - Very smooth, occasionally slickensided surfaces with compact coatings or fillings with angular fragments			
	<p><b>E. Weak siltstone or clayey shale with sandstone layers</b></p>	30	VERY POOR - Very smooth slickensided or highly weathered surfaces with soft clay coatings or fillings			
	<p><b>F. Technically deformed, intensively folded/faulted, sheared clayey shale or siltstone with broken and deformed sandstone layers forming an almost chaotic structure</b></p>	20				
	<p><b>G. Undisturbed silty or clayey shale with or without a few very thin sandstone layers</b></p>	10				
	<p><b>H. Technically deformed silty or clayey shale forming a chaotic structure with pockets of clay. Thin layers of sandstone are transformed into small rock pieces.</b></p>					
<p>C, D, E and G - may be more or less folded than illustrated but this does not change the strength. Tectonic deformation, faulting and loss of continuity moves these categories to F and H.</p>						
<p>↘ : Means deformation after tectonic disturbance</p>						

**Table 1-8: Guideline for estimating disturbance factor *D*.**

Appearance of rock mass	Description of rock mass	Suggested value of <i>D</i>
	Excellent quality controlled blasting or excavation by Tunnel Boring Machine results in minimal disturbance to the confined rock mass surrounding a tunnel.	<i>D</i> = 0
	Mechanical or hand excavation in poor quality rock masses (no blasting) results in minimal disturbance to the surrounding rock mass.  Where squeezing problems result in significant floor heave, disturbance can be severe unless a temporary invert, as shown in the photograph, is placed.	<i>D</i> = 0  <i>D</i> = 0.5 No invert
	Very poor quality blasting in a hard rock tunnel results in severe local damage, extending 2 or 3 m, in the surrounding rock mass.	<i>D</i> = 0.8
	Small scale blasting in civil engineering slopes results in modest rock mass damage, particularly if controlled blasting is used as shown on the left hand side of the photograph. However, stress relief results in some disturbance.	<i>D</i> = 0.7 Good blasting  <i>D</i> = 1.0 Poor blasting
	Very large open pit mine slopes suffer significant disturbance due to heavy production blasting and also due to stress relief from overburden removal.  In some softer rocks excavation can be carried out by ripping and dozing and the degree of damage to the slopes is less.	<i>D</i> = 1.0 Production blasting  <i>D</i> = 0.7 Mechanical excavation

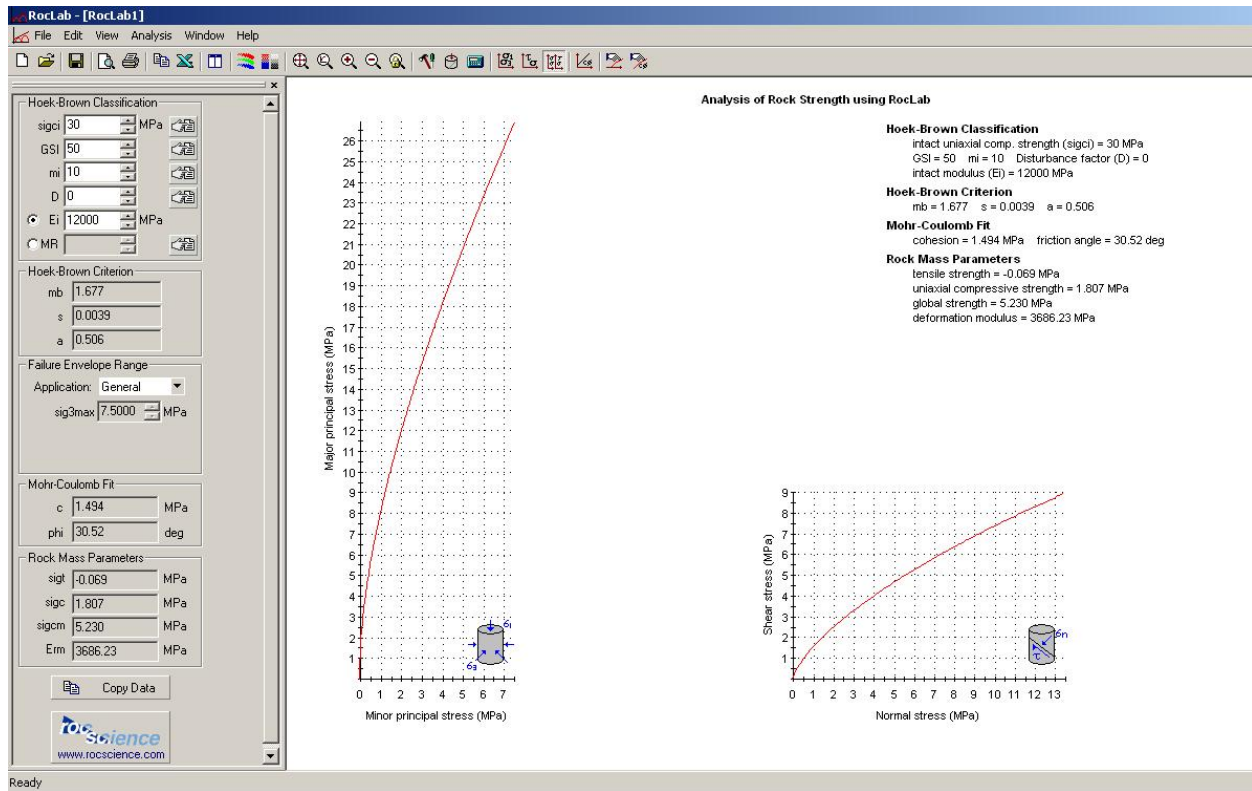


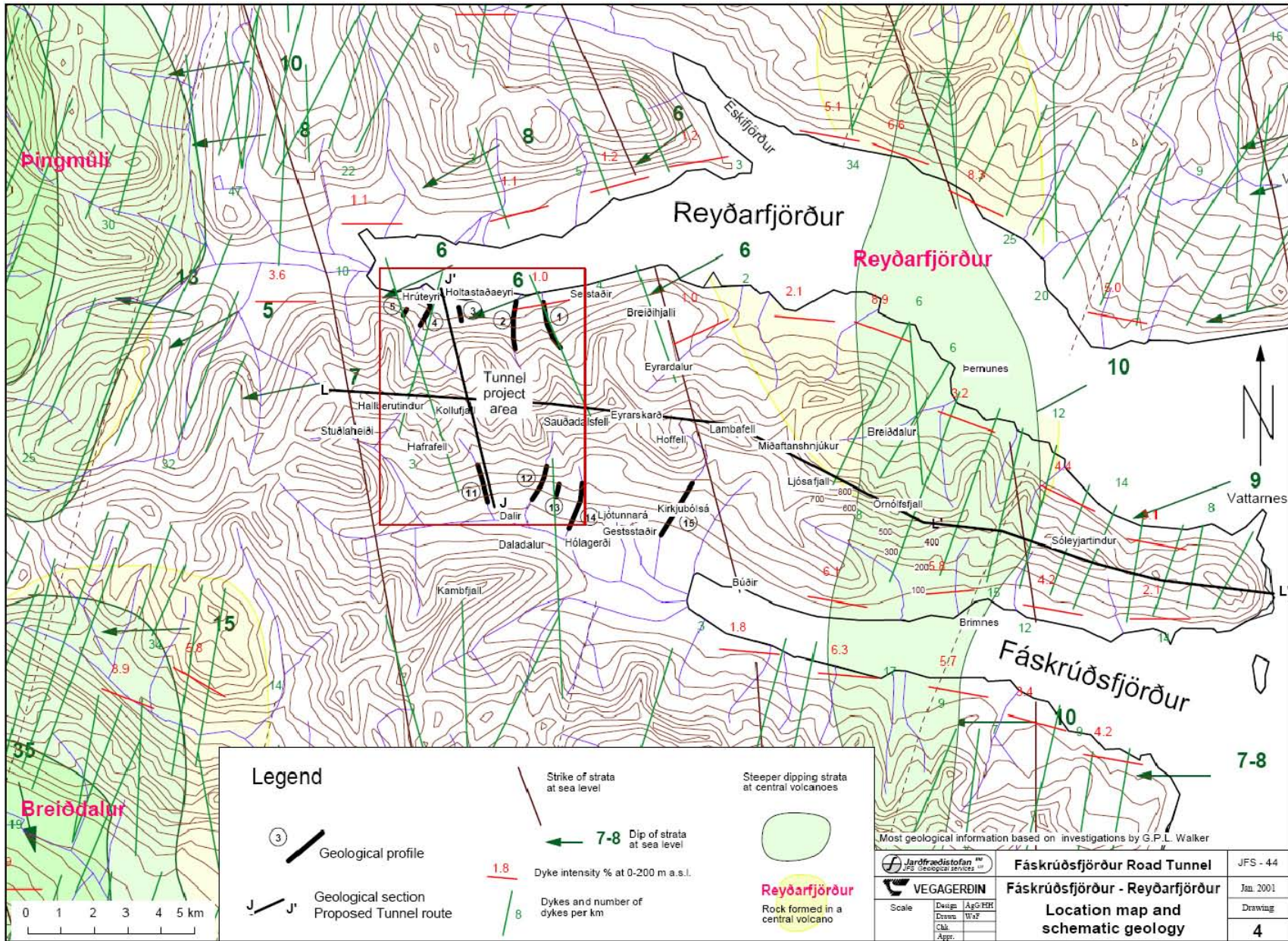
Figure 1-1: Picture from *RocLab*.



## 2. Appendix

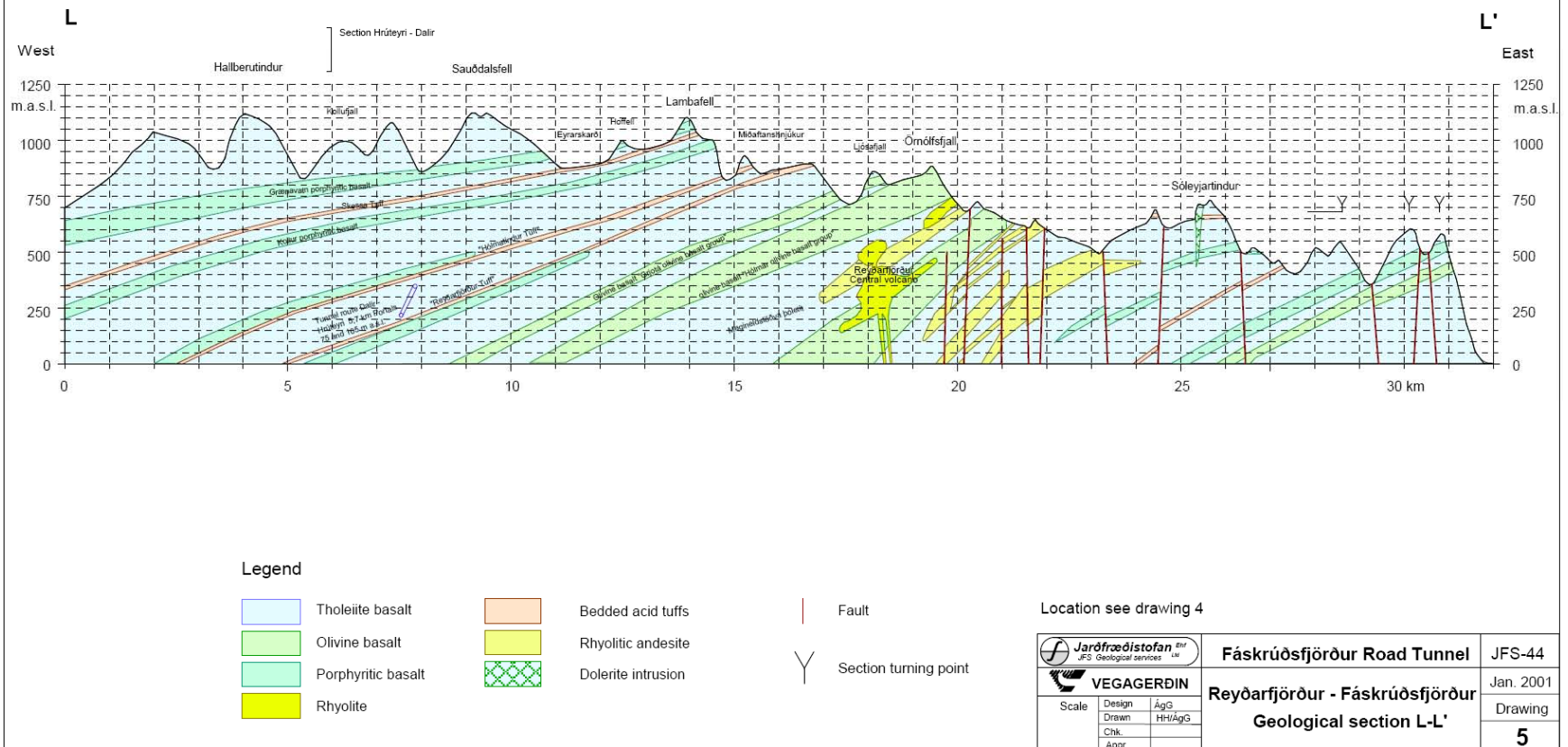
This appendix contains maps, long sections and cross sections from the construction area of the Fáskrúðsfjörður tunnel. Also a descriptions of two different types of overcoring rock stress measurement tests and key figures for the Fáskrúðsfjörður tunnel.

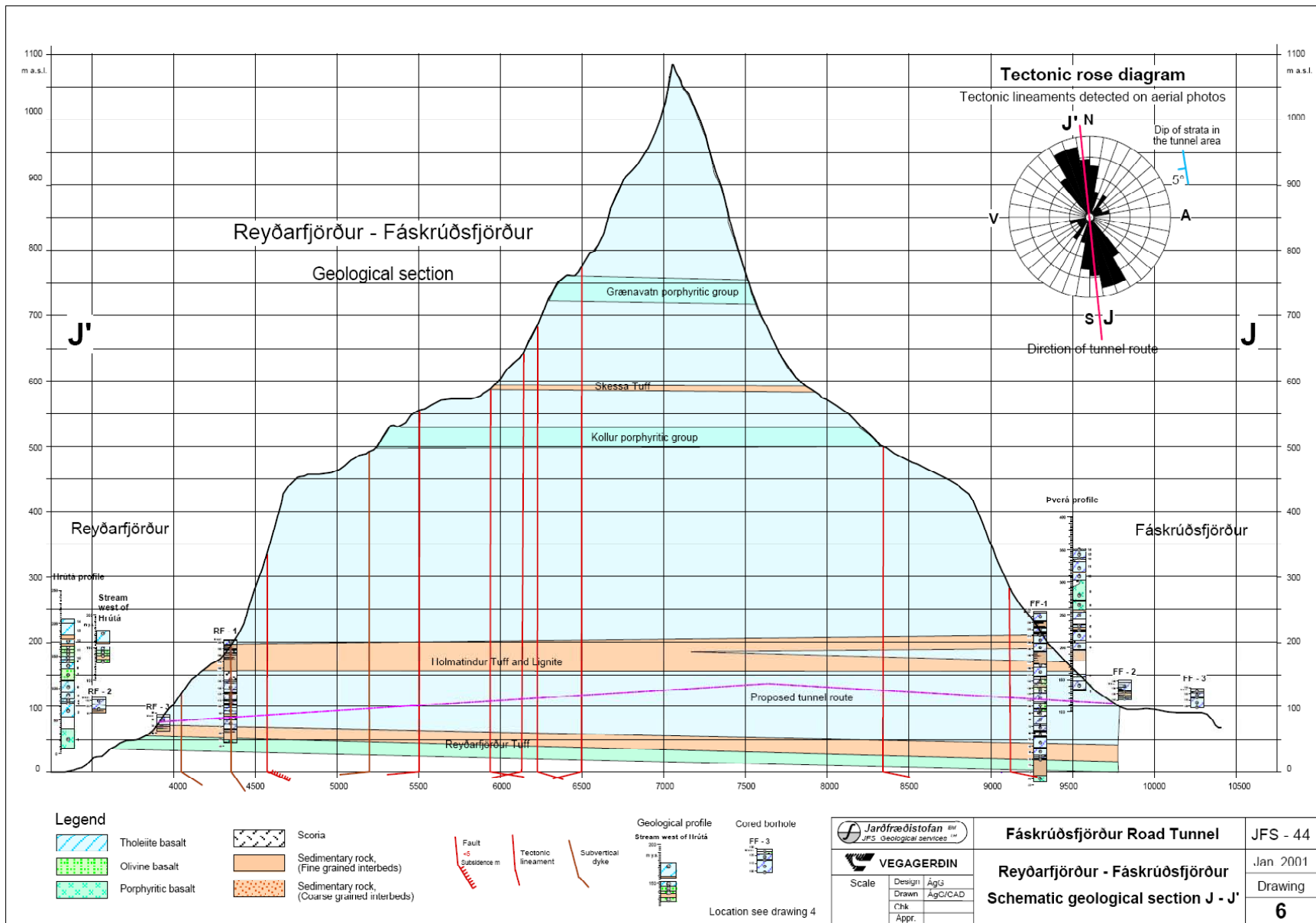
- ✓ Map of locations and geology at the neighbourhood closes to the construction area.
- ✓ Geological longitudinal section of Fáskrúðsfjörður-Reyðarfjarðar peninsula.
- ✓ Geological cross section of Fáskrúðsfjörður-Reyðarfjarðar peninsula where the tunnel are excavated.
- ✓ Detailed geological cross section from Reyðarfjörður side of the tunnel route.
- ✓ Detailed geological cross section from Fáskrúðsfjörður side of the tunnel route.
- ✓ Description of 2D rock stress measurements by overcoring.
- ✓ Description of 3D rock stress measurements by overcoring.
- ✓ Key figures for Fáskrúðsfjörður tunnel.

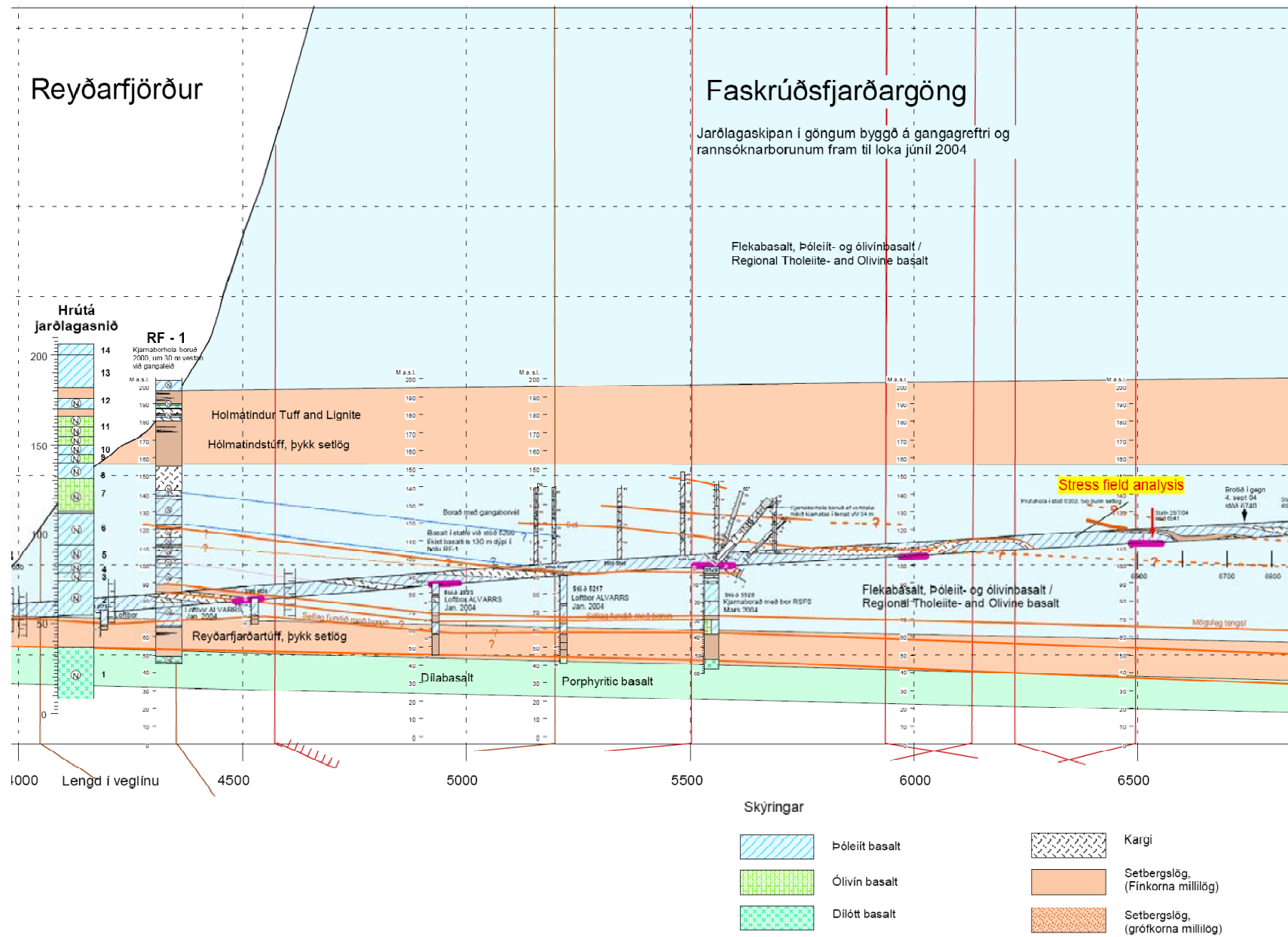


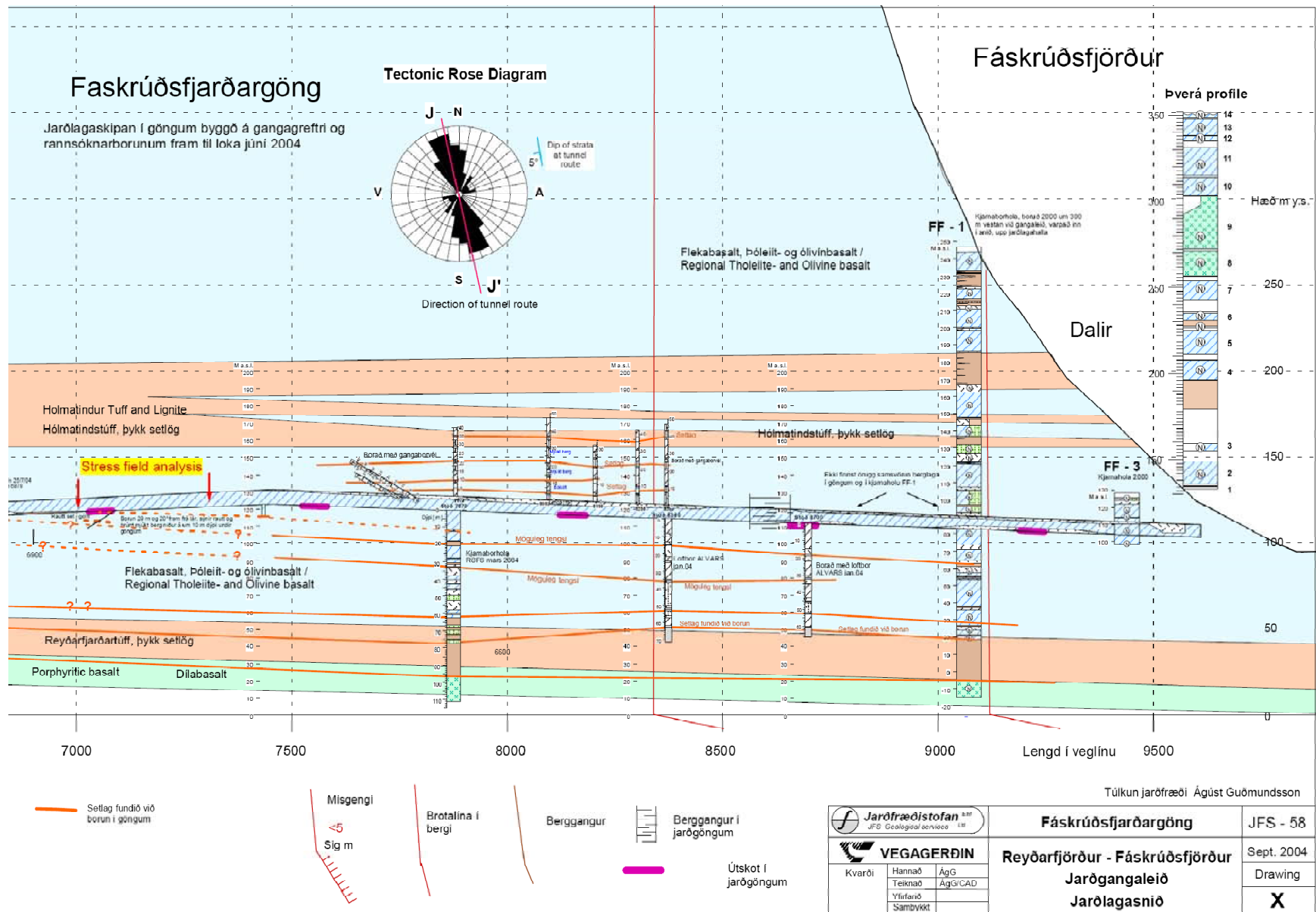
### Fáskrúðsfjörður - Reyðarfjörður peninsula

### Geological longitudinal section

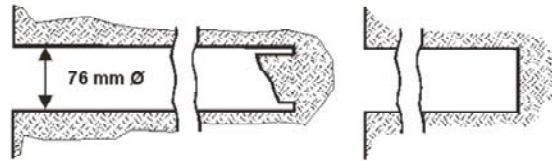




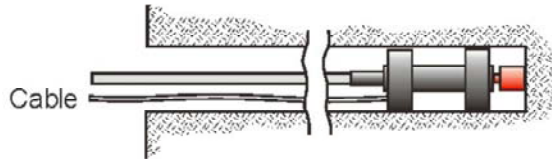




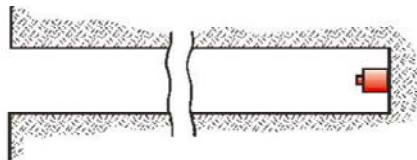
## 2-dimensional Rock Stress Measurements by Overcoring



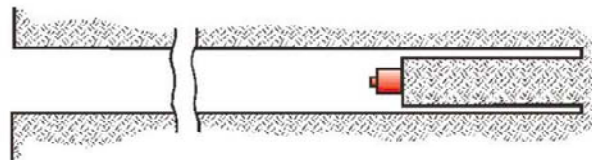
A diamond drill hole (76 mm outer diameter) is drilled to wanted depth. The core is removed and the hole bottom is flattened with a special drill bit.



A two dimensional measuring cell (doorstopper) that contains a strain gauge rosette, is inserted into the hole with a special installing tool and glued to the bottom of the hole.



The doorstopper is now fixed to the hole and initial reading (0 recording) is done. The installing tool is removed and the cell is ready for overcoring.

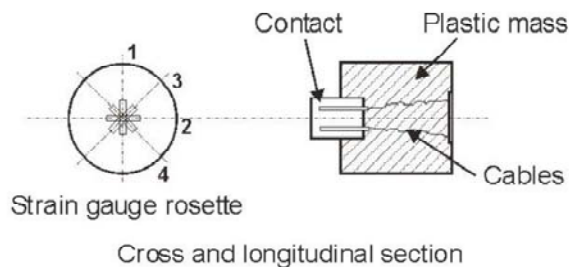


A new core is drilled with the 76 mm  $\varnothing$  diamond drill, thus stress relieving the bottom of the borehole. The corresponding strains at the end of the core are recorded by the strain gauge rosette.



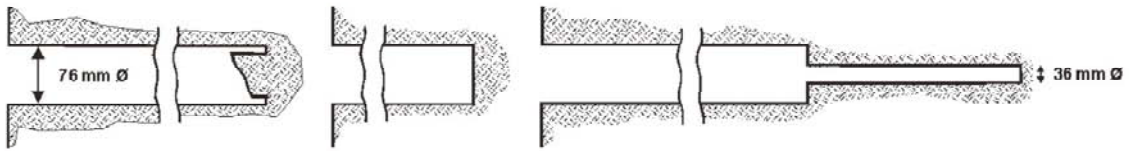
The core is caught with a special core catcher, and immediately after removal from the hole the second recording is done. From the recorded strains the stresses in the plane normal to the borehole, may be calculated when the elastic parameters determined from laboratory tests are known.

Measuring cell  
"Doorstopper"

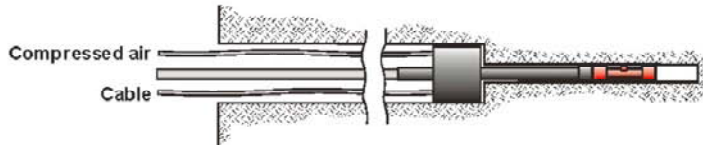


Cross and longitudinal section

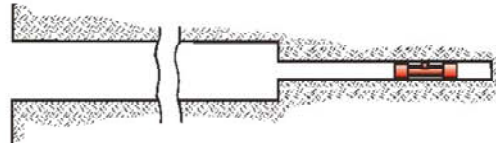
### 3-D IN-SITU ROCK STRESS MEASUREMENTS BY OVERCORING



A diamond drill hole (76 mm outer diameter) is drilled to wanted depth. The hole bottom is flattened with a special drill bit, and a concentric hole with smaller diameter (36 mm o.d.) is drilled approximately 30 cm further.



The measuring cell is inserted with a special installing tool containing an orienting device and a cable to read-out unit. The instrument head is put in place with detachable aluminium rods. Compressed air is used to expand the cell in the hole, and the strain gauges are cemented to the hole wall.



The measuring cell is now fixed to the hole and initial reading (0 recording) is done. The installing tool is removed and the cell is ready for overcoring.



The small hole is overcored by the larger diameter bit, thus stress relieving the core. The corresponding strains are recorded by the strain gauge rosettes.



The core is caught with a special core catcher, and immediately after removal from the hole the second recording is done. From the recorded strains the stresses may be calculated when the elastic parameters determined from biaxial- and laboratory tests are known.

#### MEASURING CELL

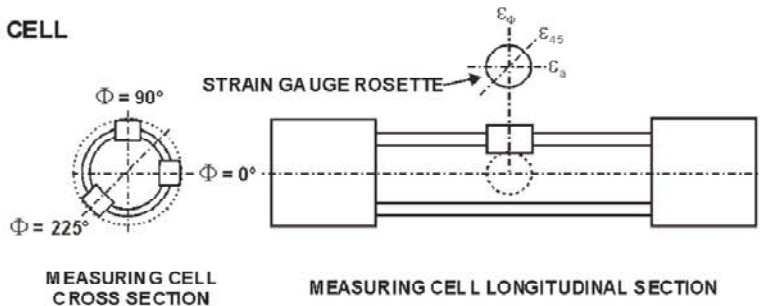




**Table 2-1: Summation of different construction parts for Fáskrúðsfjörður tunnel [35].**

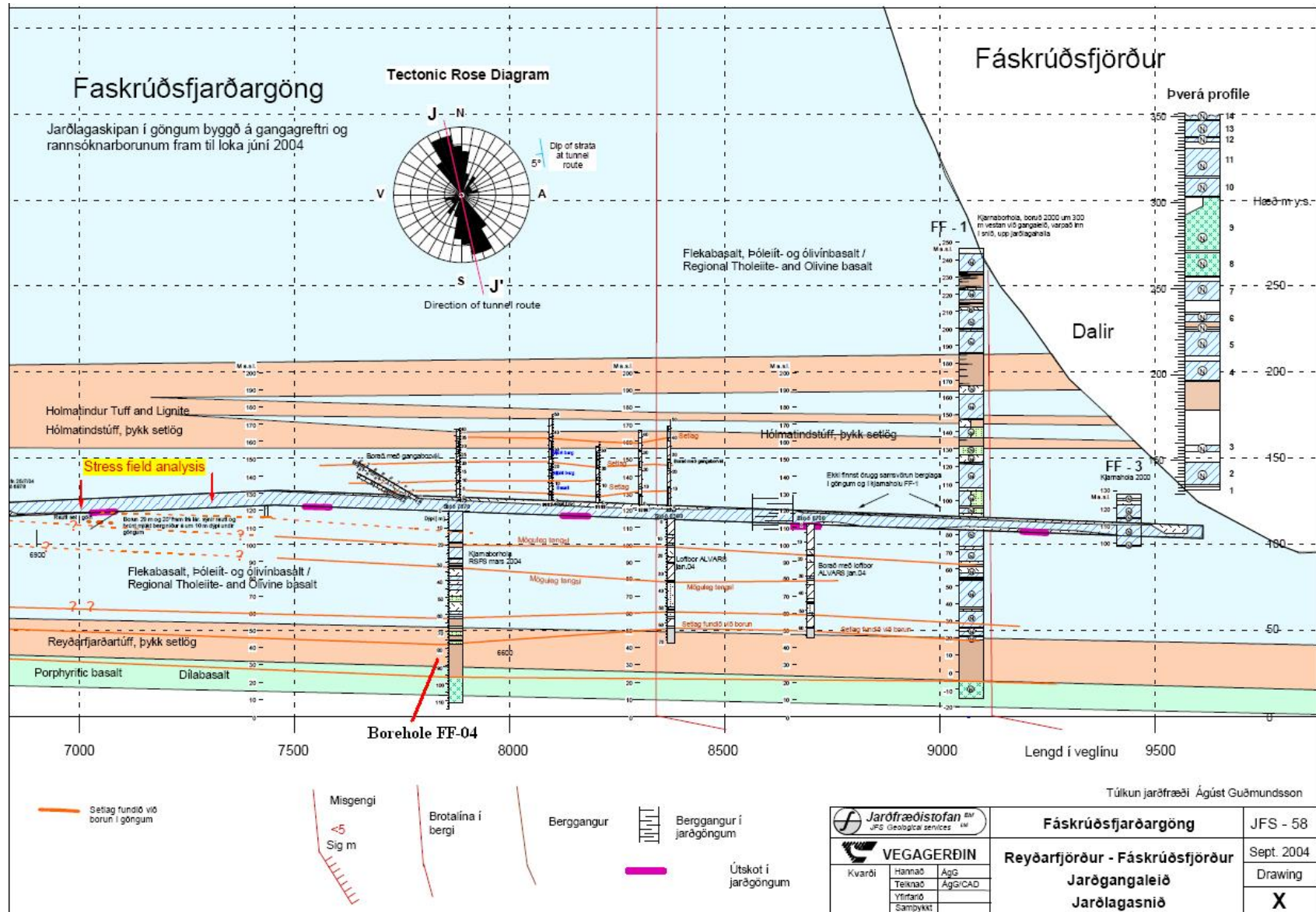
<b>Part</b>	<b>Amount</b>	<b>Unit</b>
Road fill layer	392.000	m <sup>3</sup>
Road top layer	106.000	m <sup>3</sup>
Drain	770	m
Excavate for portals	18.000	m <sup>3</sup>
Excavate tunnel	330.000	m <sup>3</sup>
Rock bolts	18.000	piece
Shotcrete	13.600	m <sup>3</sup>
Water lining	15.400	m <sup>2</sup>
Concrete in portals	1.910	m <sup>3</sup>
Framework in portals	9.400	m <sup>2</sup>
Cast iron in portals	205.000	kg
Pipes	55.300	m
Electric wires	70.700	m
Lights	550	piece
Lining	67.700	m <sup>2</sup>



### 3. Appendix

This appendix contains a geological cross section map of borehole FF-04, also pictures of rock cores from borehole FF-04.

- ✓ Cross section of the mountain ridge, display the location of the borehole FF-04.
- ✓ Core log from FF-04 and RF-04.
- ✓ Pictures of core boxes from borehole FF-04.
- ✓ Pictures of selected rock cores for the laboratory tests.



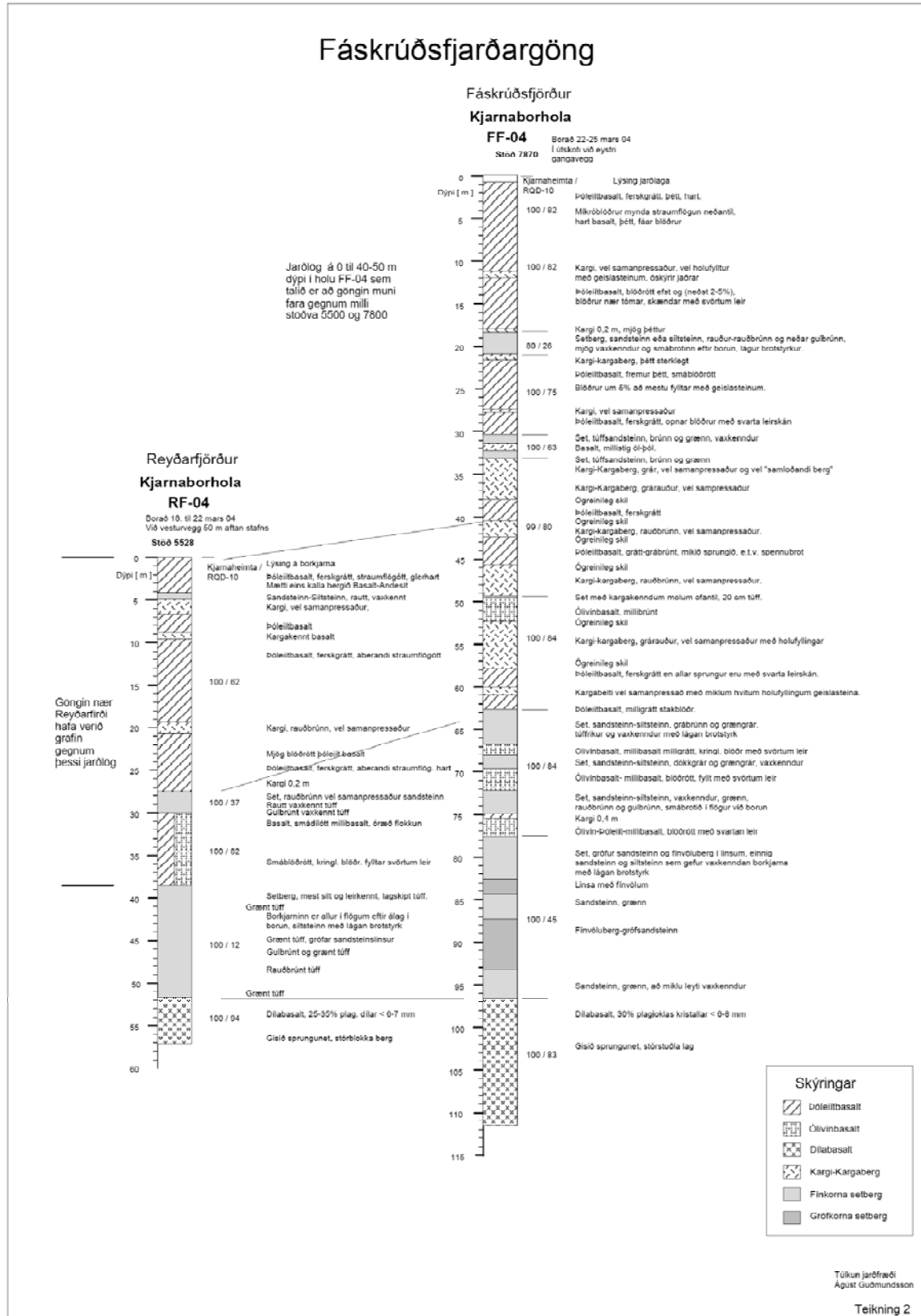


Figure 3-1: Core logs from FF-04 and RF-04.



Figure 3-2: Core boxes 1-2.



Figure 3-3: Core boxes 3-4.



Figure 3-4: Core boxes 5-6.



Figure 3-5: Core boxes 7-8.

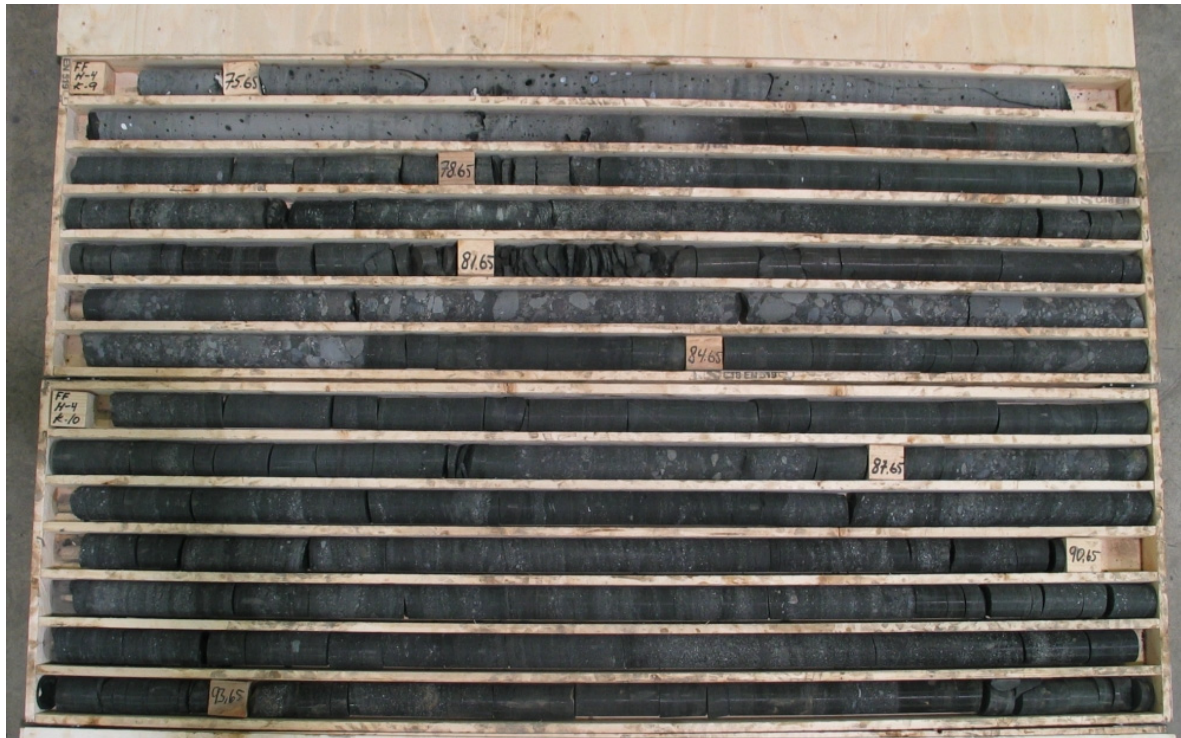


Figure 3-6: Core boxes 9-10.



Figure 3-7: Core boxes 11-12.



**Selected cores for laboratory testing.**



**Selected cores for laboratory testing.**



**Selected cores for laboratory testing.**



**Selected cores for laboratory testing.**



## 4. Appendix

This appendix contains results from laboratory tests from headrace tunnel in Kárahnjúkar hydroelectric project and laboratory testing on rock cores from borehole FF-04 drilled in the Fáskrúðsfjörður tunnel.

- ✓ Scope and number of laboratory testing from Kárahnjúkar headrace tunnel, tests standards and legends for test tables.
- ✓ Laboratory test results from borehole FF-04 drilled in the Fáskrúðsfjörður tunnel.
- ✓ Laboratory test results from headrace tunnel in Kárahnjúkar hydroelectric project.
- ✓ Pictures from brazil test.
- ✓ Plots from unconfined compression test.
- ✓ Pictures from unconfined compression test.
- ✓ Plots from triaxial test.
- ✓ Pictures from triaxial test.
- ✓ Comparison of laboratory test results from Kárahnjúkar headrace tunnel and Fáskrúðsfjörður tunnel.

**Table 4-1: Scope and number of laboratory testing from Kárahnjúkar headrace tunnel.**

	Sandstone /Siltstone	Conglo-merate	Tholeiitic basalt	Olivine basalt	Porphyritic basalt	Andesite	Scoria	
Unconfined compressive strength	37	40	34	71	50	7	24	
Tensile strength	18	14	8	17	13	1	3	
Specific gravity	34	39	24	37	26	7	7	
Bulk density	34	39	31	66	48	7	24	
Porosity	34	39	24	37	26	7	7	
Slake durability	1	15		0	0	0	0	
Young modulus	10	3	18	36	25	0	18	
Poisson's ratio	7	1	5	14	9	0	6	
			0					
Drill rate index			5 basalt samples from FS-30, FS-31, FS-32, Fs-33, FV-1 (old borehole)					
CERCHAR	70	2	6	8	11	3		
LCPC	4	0	3	4	5	3		

Few further testing, including CERCHAR and LCPC was performed on various móberg types (pillow lava, breccia, cube jointed basalt, agglomerate).

**Table 4-2: Tests standards from Kárahnjúkar headrace tunnel.**

TEST	STANDARD
Unconfined compression	ASTM D 3148-86
Young's modulus and Poisson's ratio	ASTM D 3148-86 and D 4543-85
Schmidt hammer	ISRM
Tensile strength	ASTM D 3967-86 and ASTM D 4543-85
Bulk density, apparent specific gravity and porosity	ASTM D127 and ISRM
Slake durability	Manufacturer's (ELE) operating instructions and ISRM
Point load tests	ISRM

**Table 4-3: Legends to following tables.**

<b>TB:</b>	Tholeiite basalt
<b>OB:</b>	Olivine basalt
<b>PB:</b>	Porphyritic basalt
<b>AN:</b>	Andesite
<b>PW:</b>	Pillow lava
<b>BRC:</b>	Breccia
<b>SC:</b>	Scoria
<b>MB:</b>	Móberg
<b>AGG:</b>	Agglomerate
<b>CG:</b>	Conglomerate
<b>SD:</b>	Sandstone
<b>ST:</b>	Siltstone

<b>fgr:</b>	fine grained
<b>mgr:</b>	medium grained
<b>cgr:</b>	coarse grained
<b>d:</b>	dense
<b>flw:</b>	flow banded
<b>h:</b>	homogeneous
<b>irr:</b>	irregular
<b>j:</b>	jointed
<b>mp:</b>	microporous
<b>mss:</b>	massive
<b>p:</b>	porous

<b>cgl:</b>	conglomeratic
<b>hy:</b>	hyaloclastic matrix
<b>ph:</b>	porphyritic
<b>ph:</b>	porphyritic
<b>pum:</b>	pumiceous
<b>sd:</b>	sandy
<b>st:</b>	silty
<b>tff:</b>	tuffaceous

**Table 4-4: Laboratory test results for borehole FF-04.**

Lab	Core	Sample nr.	Depth	Lithology	Height	Diameter	D/H	Bulk specific gravity	Bulk specific gravity (SSD)	Water content	Porosity	Tensile strength	UCS	Elasticity modulus E	Elasticity modulus E (50%)	Poisson ratio v	Poisson ratio v (50%)	K0	Creep index	Brazil	Uniax	Triax
[-]	[-]	[-]	[m]	[-]	[cm]	[cm]	[-]	[g/cm3]	[g/cm3]	[%]	[%]	[MPa]	[MPa]	[GPa]	[GPa]	[-]	[-]	[-]	[%/time log cycle]	[-]	[-]	[-]
GEO2008	FF04	39	18,0-18,02	OB	2,215	4,469	2,02	2,608	2,740	4,63	12,7	6,011								X		
GEO2008	FF04	38	18,05-18,07	SC	1,946	4,469	2,30	2,443	2,620	6,55	17,2	1,981								X		
GEO2008	FF04	27	18,15-18,17	SC	2,289	4,457	1,95	2,021	2,325	12,94	30,2	0,000								X		
GEO2008	FF04	23	18,17-18,20	SC	2,321	4,466	1,92	2,021	2,326	12,93	30,1	0,878								X		
GEO2008	FF04	31	18,4-18,42	SC	2,272	4,474	1,97	2,011	2,309	12,67	29,5	1,849								X		
GEO2008	FF04	40	18,45-18,47	SC	2,206	4,469	2,03	1,948	2,196	10,92	24,3	1,335								X		
GEO2008	FF04	35	31,61-31,63	SC	2,256	4,462	1,98	2,350	2,543	7,18	18,4	1,619								X		
GEO2008	FF04	24	31,81-31,83	SC	2,302	4,462	1,94	2,281	2,497	8,47	21,2	2,213								X		
GEO2008	FF04	42	32,09-32,11	SC	2,307	4,462	1,93	2,311	2,499	7,13	18,0	1,554								X		
GEO2008	FF04	26	33,52-33,54	SC	2,284	4,463	1,95	2,152	2,393	9,83	23,7	0,789								X		
GEO2008	FF04	34	33,5-33,52	SC	2,257	4,461	1,98	2,149	2,403	10,30	24,8	1,079								X		
GEO2008	FF04	32	40,37-40,39	TB	2,304	4,459	1,94	2,509	2,657	5,33	14,3	4,301								X		
GEO2008	FF04	41	40,39-40,41	TB	2,274	4,464	1,96	2,500	2,661	5,67	15,2	3,052								X		
GEO2008	FF04	22	41,67-41,69	SC	2,319	4,463	1,92	2,348	2,535	7,61	19,3	4,205								X		
GEO2008	FF04	25	41,69-41,71	SC	2,236	4,463	2,00	2,133	2,361	9,38	22,3	2,218								X		
GEO2008	FF04	29	50,24-50,26	SC	2,302	4,457	1,94	2,270	2,485	8,43	21,0	1,677								X		
GEO2008	FF04	37	50,26-50,28	SC	2,262	4,473	1,98	2,243	2,430	7,40	18,3	0,868								X		
GEO2008	FF04	43	50,37-50,39	SC	2,254	4,459	1,98	2,170	2,407	9,59	23,2	3,048								X		
GEO2008	FF04	28	51,19-51,21	OB	2,293	4,464	1,95	2,450	2,604	5,67	14,9	2,083								X		
GEO2008	FF04	30	51,21-51,23	OB	2,282	4,465	1,96	2,282	2,493	8,26	20,7	0,521								X		
GEO2008	FF04	33	51,37-51,39	OB	2,257	4,462	1,98	2,293	2,485	7,40	18,7	1,133								X		
GEO2008	FF04	36	51,39-51,41	OB	2,360	4,459	1,89	2,334	2,521	7,16	18,3	1,111								X		
GEO2008	FF04	20	83,25-83,27	SD	2,411	4,471	1,85	2,294	2,479	7,22	18,0	1,224								X		
GEO2008	FF04	21	83,4-83,42	SD	2,451	4,472	1,82	2,261	2,459	8,57	21,1	1,527								X		
GEO2008	FF04	44	84,0-84,02	SD	2,309	4,468	1,94	2,311	2,472	6,21	15,7	2,383								X		
GEO2008	FF04	12	18,03-18,12	SC	8,992	4,468	0,50	2,001	2,301	12,94	29,8	4,745		2,004							X	
GEO2008	FF04	8	31,63-31,72	SC	9,008	4,462	0,50	2,331	2,536	8,05	20,1	12,711		5,804							X	
GEO2008	FF04	11	31,72-31,81	SC	8,986	4,463	0,50	2,269	2,495	8,73	22,2	8,978		7,099							X	
GEO2008	FF04	4	32,0-32,09	SC	9,046	4,465	0,49	2,344	2,546	7,78	19,8	14,048		8,002							X	
GEO2008	FF04	2	32,20-32,31	SC	9,013	4,460	0,49	2,080	2,336	10,84	25,4	7,492		3,750							X	
GEO2008	FF04	7	40,41-40,50	TB	8,998	4,459	0,50	2,594	2,742	5,30	14,5	30,022		10,621							X	
GEO2008	FF04	6	41,71-41,80	SC	8,983	4,452	0,50	2,280	2,500	8,36	20,9	44,500		16,385							X	
GEO2008	FF04	10	50,31-50,40	SC	8,990	4,451	0,50	2,256	2,485	9,10	22,6	20,498		8,847							X	
GEO2008	FF04	13	51,10-51,19	OB	9,010	4,464	0,50	2,612	2,756	4,64	12,8	40,853		17,045							X	
GEO2008	FF04	19	51,28-51,37	OB	8,998	4,460	0,50	2,314	2,542	8,85	22,5	8,176		2,340							X	
GEO2008	FF04	15	83,35-83,44	SD	9,034	4,468	0,49	2,299	2,498	7,82	19,5	13,041		5,134							X	
GEO2008	FF04	17	84,1-84,19	SD	9,046	4,468	0,49	2,360	2,544	7,11	18,1	10,335		3,245							X	
DTU2008	FF04	5	18,1-18,19	SC	8,643	4,462	0,50	1,952	2,292	14,83	34,0											X
DTU2008	FF04	3	31,52-31,61	SC	8,943	4,454	0,50	2,324	2,535	8,30	21,1		16,393	13,333	0,132	0,194	0,107	0,00852				X
DTU2008	FF04	14	50,28-50,37	SC	9,023	4,463	0,49	2,261	2,488	9,11	22,6		14,925	12,048	0,184	0,199	0,110	0,00668				X
DTU2008	FF04	16	84,20-84,29	SD	9,011	4,466	0,50	2,281	2,482	7,90	19,6		14,706	13,699	0,167	0,194	0,070	0,00299				X



**Table 4-5: Laboratory test results for Kárahnjúkar headrace tunnel.**

Lab	DH-No	From	To	Suite	Lithology	Remarks to lithology	Core Diam.	L/D	UCS lab	Tensile strength	Water content	Apparent specific gravity	Bulk specific gravity	Bulk specific gravity (SSD)	Porosity	Slake durability	Phi	Poisson ratio	Elasticity modulus E	Triax	Uniax
-	-	m	m	-	-	-	mm	-	MPa	MPa	%	kg/m <sup>3</sup>	kg/m <sup>3</sup>	kg/m <sup>3</sup>	%	%	°	-	GPa	-	-
BRI2001	FV-46	36,60	36,92	TB	PB		44,60	2,23	117		1,68	2882,2	2740,5	2789,7	4,9						X
BRI2001	FV-46	74,10	74,40	TB	TB		44,66	2,21	217		0,71	2972,5	2920,3	2937,9	1,8						X
BRI2001	FV-46	131,60	131,80	TB	OB		44,20	2,25	133		1,63	3003,1	2812,2	2875,8	6,4						X
BRI2001	FV-46	136,20	136,45	TB	SC		44,64	2,23	38		3,15	2718,1	2278,3	2440,7	16,3						X
BRI2001	FV-46	175,80	176,20	ML	TB		44,39	2,22	249		1,90	3014,9	2764,1	2847,2	8,3						X
BRI2001	FV-46	208,85	209,10	ML	SC		44,27	2,24	13		3,74	2872,4	2284,0	2488,8	20,5						X
BRI2001	FV-46	222,40	222,70	ML	TB		44,42	2,23	264		1,06	3043,5	2952,4	2982,4	3,0						X
BRI2001	FV-46	236,95	237,25	ML	SD		44,28	2,25	49		21,96	2778,6	1558,0	1997,3	44,2						X
BRI2001	FV-46	308,60	308,95	ML	CG		44,42	2,24	37		9,74	3001,9	2194,1	2463,2	27,0						X
BRI2001	FV-46	330,90	331,10	ML	TB		44,51	2,23	264		1,35	3038,8	2937,6	2970,9	3,3						X
BRI2001	FV-46	340,45	340,65	ML	SD		44,43	2,23	52		17,65	2802,1	1706,6	2097,7	39,2						X
BRI2001	FV-46	385,70	385,90	ML	SD		44,46	2,23	35		26,05	2728,7	1481,7	1938,7	46,0						X
BRI2001	FV-46	456,00	456,27	ML	TB		44,47	2,23	199		0,86	3032,1	2934,2	2966,5	3,2						X
BRI2001	FV-46	475,35	475,55	ML	TB		44,52	2,23	123		1,43	3023,0	2890,2	2934,2	4,4						X
BRI2001	FV-46	489,60	489,80	ML	CG	fgr	44,64	2,24	29		6,66	2753,9	2034,9	2295,6	26,0						X
BRI2001	FV-46	555,24	555,50	ML	TB		44,74	2,22	203		1,79	3001,5	2828,6	2886,2	5,7						X
BRI2001	FV-46	585,40	585,60	ML	TB		44,71	2,22	278		1,04	2973,3	2895,6	2921,7	2,6						X
BRI2001	FV-47	21,35	21,65	LA	PB	fgr.d.h	44,77	2,23	245		0,11	3072,2	2934,9	2979,6	4,5						X
BRI2001	FV-47	56,10	56,50	LA	TB	fgr.flw.irr	44,76	2,23	138		1,09	3024,3	2909,0	2947,1	3,8						X
BRI2001	FV-47	68,45	68,65	LA	OB	fgr.d.h	44,75	2,22	248		0,54	3011,0	2926,5	2954,6	2,8						X

**Table 4-6: Laboratory test results for Kárahnjúkar headrace tunnel.**

Lab	DH-No	From	To	Suite	Lithology	Remarks to lithology	Core Diam.	L/D	UCS lab	Tensile strength	Water content	Apparent specific gravity	Bulk specific gravity	Bulk specific gravity (SSD)	Porosity	Slake durability	Phi	Poisson ratio	Elasticity modulus E	Triax	Uniax	
-	-	m	m	-	-	-	mm	-	MPa	MPa	%	kg/m <sup>3</sup>	kg/m <sup>3</sup>	kg/m <sup>3</sup>	%	%	°	-	GPa	-	-	
BRI2001	FV-47	96,65	96,90	HA	OB	fgr,irr.mp	44,78	2,21	138		1,53	3020,6	2868,5	2918,8	5,0						X	
BRI2001	FV-47	129,00	129,30	IIA	TB	d.mp	44,66	2,23	186		0,55	3038,4	2968,0	2991,2	2,3							X
BRI2001	FV-47	148,10	148,30	HA	TB	p	44,62	2,23	183		0,46	3004,2	2930,8	2955,2	2,4							X
BRI2001	FV-47	184,45	185,00	SA	CG	h	44,57	2,23	35		8,80	2978,9	2133,2	2417,1	28,3							X
BRI2001	FV-47	225,65	226,00	SA	CG	h	44,61	2,25	71		13,02	2769,5	1865,2	2191,7	32,5							X
BRI2001	FV-47	245,45	245,70	SA	CG	h	44,57	2,24	25		4,00	2929,3	2487,3	2638,2	15,1							X
BRI2001	FV-47	265,70	266,00	SA	CG	h	44,57	2,22	17		4,63	2931,1	2325,4	2531,3	20,3							X
BRI2001	FV-47	271,10	273,30	SA	PB	p,h	44,59	2,24	227		1,67	2903,8	2721,2	2784,1	6,2							X
BRI2001	FV-54	14,55	15,00	FA	TB		44,55	2,23	172		0,46	2985,2	2890,3	2922,1	3,2							X
BRI2001	FV-54	40,10	40,40	FA	TB		44,69	2,22	174		0,53	2976,6	2837,1	2883,9	4,7							X
BRI2001	FV-54	66,90	67,30	FA	OB	ph	44,69	2,22	129		0,51	2978,2	2819,1	2872,5	5,3							X
BRI2001	FV-54	79,05	79,45	FA	OB		44,64	2,22	148		1,60	3010,2			5,4							X
BRI2001	FV-54	85,60	86,00	FA	SD		44,62	2,24	48		21,69	2800,0	1599,3	2028,1	43,8							X
BRI2001	FV-54	85,60	86,00	FA	SD		44,62	2,23	46		18,97	2832,0	1675,3	2084,0	40,9							X
BRI2001	FV-54	89,30	89,70	FA	CG		44,67	2,17	26		5,64	2876,5	2327,9	2518,8	19,1							X
BRI2001	FV-54	112,90	113,30	TB	PB		44,61	2,23	103		1,84	2861,6	2643,5	2719,7	7,6							X
BRI2001	FV-54	125,30	125,60	TB	PB		44,61	2,23	93		2,12	2871,2	2672,4	2741,5	6,9							X
BRI2001	JB-02	28,50	28,75	HdeS	CG		44,58	2,22	14		8,07	2768,3	1687,4	2077,9	38,9							X
BRI2001	JB-02	59,77	60,27	HdeS	CG	mgr	44,38	2,18	14		14,60	2775,5	1692,1	2082,4	39,2							X
BRI2001	JB-02	59,77	60,27	HdeS	CG	mgr	44,48	2,21	8		13,20	2747,0	1660,6	2056,0	38,6							X
BRI2001	JB-02	70,20	70,50	HdeS	SD		44,59	2,23			12,07	2790,6	1816,4	2165,4	34,8							X
BRI2001	JB-02	74,25	74,52	HdeS	CG	tff	44,57	2,22	63		10,23	2820,9	1954,2	2261,5	30,8							X
BRI2001	JB-03	42,30	42,70	UTB	OB	mss	47,38	2,10	117		0,28	3010,9	2671,2	2783,9	11,1							X

**Table 4-7: Laboratory test results for Kárahnjúkar headrace tunnel.**

Lab	DH-No	From	To	Suite	Lithology	Remarks to lithology	Core Diam.	L/D	UCS lab	Tensile strength	Water content	Apparent specific gravity	Bulk specific gravity	Bulk specific gravity (SSD)	Porosity	Slake durability	Phi	Poisson ratio	Elasticity modulus E	Triax	Uniax
-	-	m	m	-	-	-	mm	-	MPa	MPa	%	kg/m <sup>3</sup>	kg/m <sup>3</sup>	kg/m <sup>3</sup>	%	%	°	-	GPa	-	-
BRI2001	JB-03	54,43	54,80	UTB	OB	mss	45	2,21	109		0,34	2964,1	2716,4	2800,0	8,2						X
BRI2001	JB-03	95,77	96,03	UTB	OB		44,92	2,22	161		0,12	3052,2	2933,0	2971,9	3,9						X
BRI2001	JB-03	101,95	102,25	UTB	OB		44,9	2,22	174		0,22	3033,4	2859,2	2916,6	5,7						X
BRI2001	JB-03	103,66	103,87	UTB	OB		44,95	2,21	150		0,20	3056,6	2852,2	2919,1	6,6						X
BRI2001	JB-23	85,13	85,30	KM	BRC	p,h	44,92	2,19	103		0,12	2568,6	2314,5	2413,6	9,4						X
BRI2001	JB-23	106,70	106,86	KM	BRC	p,h	44,75	2,24	83		0,11	2546,2	2351,0	2427,2	10,1						X
BRI2001	JB-23	123,04	123,24	KM	BRC	p,h	44,7	2,22	112		0,30	2570,8	2343,2	2431,8	8,6						X
BRI2001	JB-23	124,73	124,95	KM	BRC	p,h	44,68	2,23	114		0,17	2605,5	2425,0	2494,2	6,8						X
BRI2001	JB-23	144,31	144,52	KM	BRC	p,h	44,72	2,22	66		0,20	2552,2	2377,9	2445,9	6,7						X
BRI2001	JB-23	166,90	167,25	KM	BRC	p,h	44,8	2,22	111		0,19	2603,4	2355,1	2450,4	9,3						X
BRI2001	JB-37	91,40	91,85	HdM	BRC	tff,d	44,87	2,16	35		7,40	2570,5	1961,4	2198,3	23,5						X
BRI2001	JB-37	102,50	102,80	HdM	BRC	tff,d	44,85	2,13	24		7,97	2457,0	1909,3	2131,9	22,3						X
BRI2001	JB-37	106,05	106,47	HdM	BRC	tff,d	44,84	2,20	30		7,63	2621,9	2059,8	2274,2	22,2						X
BRI2001	JB-37	140,00	140,22	HdM	PW	p	44,92	2,21	44		3,52	2774,6	2263,5	2447,6	17,7						X
BRI2001	JB-37	145,65	146,00	HdM	PW	p	44,86	2,20	35		4,22	2745,0	2158,0	2372,0	21,2						X
BRI2001	JB-37	174,32	174,62	HdM	PW	p	44,98	2,22	65		2,72	2867,1	2580,4	2680,2	9,7						X
BRI2001	JB-37	181,70	182,15	IIdnS	CG	st	44,87	2,22	90		9,06	2804,0	2119,6	2363,6	24,4						X
BRI2001	JB-37	181,70	182,15	HdnS	CG	st	44,48	2,25	82		9,04	2762,5	2095,4	2336,9	25,1						X
BRI2001	JB-37	193,60	193,80	HdnS	SD	fgr	43,83	2,23	16		11,62	2606,5	1695,2	2044,8	34,9						X
BRI2001	JB-37	205,85	206,10	HdnS	SD	fgr,tff,pum	44,88	2,19	24		9,61	2613,9	1747,6	2078,9	33,0						X
BRI2001	JB-37	214,10	214,40	HdnS	SD	egl						2479,6	1664,9	1993,5	31,9						X
BRI2001	JB-37	232,50	232,80	HdnS	SD	tff,egr	44,82	2,21	29		9,39	2556,8	1800,1	2096,0	31,5						X
BRI2001	JB-38	70,06	70,25	RA	SC	d	44,87	2,14	31		2,12	2786,8	2143,4	2374,5	22,6						X

**Table 4-8: Laboratory test results for Kárahnjúkar headrace tunnel.**

Lab	DH-No	From	To	Suite	Lithology	Remarks to lithology	Core Diam.	L/D	UCS lab	Tensile strength	Water content	Apparent specific gravity	Bulk specific gravity	Bulk specific gravity (SSD)	Porosity	Slake durability	Phi	Poisson ratio	Elasticity modulus E	Triax	Uniax
-	-	m	m	-	-	-	mm	-	MPa	MPa	%	kg/m <sup>3</sup>	kg/m <sup>3</sup>	kg/m <sup>3</sup>	%	%	°	-	GPa	-	-
BRI2001	JB-38	99,65	99,92	RA	PB		44,84	2,22	171		0,97	3017,7	2952,0	2973,8	2,2						X
BRI2001	JB-38	102,65	101,98	RA	PB		44,86	2,22	158		0,94	3023,5	2952,5	2976,0	2,3						X
BRI2001	JB-38	127,10	127,30	RA	PB		44,89	2,22	149		0,84	3017,7	2955,4	2976,1	2,0						X
BRI2001	JB-40	53,05	53,30	EY	AN		44,64	2,23	305		0,52	2890,6	2831,4	2851,8	2,0						X
BRI2001	JB-40	81,10	81,34	EY	AN		44,68	2,22	229		0,63	2926,2	2831,7	2864,0	3,2						X
BRI2001	JB-40	117,72	118,00	LA	PB		44,8	2,22	254		0,25	2971,7	2871,8	2905,4	3,5						X
BRI2001	JB-40	126,25		LA	SD	e <sub>gr</sub> .p <sub>um</sub> .d									54,4						X
BRI2001	JB-40	173,30	173,55	LA	OB		44,76	2,21	252		0,55	3019,4	2890,7	2933,3	4,2						X
BRI2001	JB-40	220,10	220,36	LA	OB		44,77	2,22	216		0,93	3003,5	2894,1	2930,5	3,6						X
BRI2001	JB-40	224,00	224,26	LA	OB		44,78	2,22	215		0,78	2991,8	2912,8	2939,2	2,6						X
BRI2001	JB-40	243,10	243,40	LA	PB		44,72	2,22	185		0,78	3004,0	2912,0	2942,6	3,1						X
BRI2001	JB-41	74,60	74,92	RA	PB		44,56	2,24	216		1,01	2983,0	2873,9	2910,5	3,7						X
BRI2001	JB-41	113,00	113,30	EY	AN	f <sub>gr</sub> .m <sub>ss</sub>	44,49	2,24	148		0,77	2860,6	2775,5	2805,3	3,0						X
BRI2001	JB-41	127,90	128,12	EY	OB	f <sub>gr</sub> .m <sub>ss</sub> .f <sub>w</sub>	44,58	2,24	210		0,60	2908,0	2825,0	2853,6	2,8						X
BRI2001	JB-41	165,37		EYa	AN		44,74	2,23	220		0,66	2909,8	2838,0	2862,7	2,5						X
BRI2001	JB-41	211,00	211,40	EY	SD	m <sub>gr</sub> .l <sub>am</sub>	44,53	2,23	25		8,10	2578,8	1786,3	2093,5	30,8						X
BRI2001	JB-41	281,70	282,00	EY	AGG	m <sub>gr</sub>	44,48	2,24	24		7,51	2580,9	1888,9	2157,0	26,9						X
BRI2001	JB-41	289,20	289,50	EY	AGG	e <sub>gr</sub>	44,54	2,23	36		6,10	2615,7	2010,9	2241,9	23,1						X
BRI2001	JB-42	40,90	41,20	HdnS	CG		44,78	2,18	43		15,22	2729,0	1801,9	2141,5	33,9						X
BRI2001	JB-42	113,30	113,60	RA	SD		44,62	2,23	70		16,67	2688,0	1678,6	2054,2	37,6						X
BRI2001	JB-42	124,70	125,00	RA	PB		44,68	2,22	220		0,32	3010,9	2907,5	2941,8	3,4						X
BRI2001	JB-42	128,10	128,38	RA	PB		44,64	2,22	262		0,32	3004,0	2898,3	2933,5	3,5						X
BRI2001	JB-42	181,50	181,73	EY	CG		44,66	2,20	22		3,87	2998,7	2424,4	2615,9	18,7						X

**Table 4-9: Laboratory test results for Kárahnjúkar headrace tunnel.**

Lab	DH-No	From	To	Suite	Lithology	Remarks to lithology	Core Diam.	L/D	UCS lab	Tensile strength	Water content	Apparent specific gravity	Bulk specific gravity	Bulk specific gravity (SSD)	Porosity	Slake durability	Phi	Poisson ratio	Elasticity modulus E	Triax	Uniax
-	-	m	m	-	-	-	mm	-	MPa	MPa	%	kg/m <sup>3</sup>	kg/m <sup>3</sup>	kg/m <sup>3</sup>	%	%	°	-	GPa	-	-
BRI2001	JB-42	200,05	200,50	EY	CG		44,65	2,21	57		7,09	2850,6	2127,1	2380,9	25,3						X
BRI2001	JB-42	219,27	219,60	EY	AN		44,73	2,21	280		0,54	3057,8	2981,1	3006,2	2,5						X
BRI2001	JB-42	224,80	225,20	EY	AN		44,75	2,24	212		0,90	3050,5	2922,4	2964,4	4,2						X
BRI2001	JB-51	11,95	12,20	HdeS	MB	h	44,64	2,23	62		3,89	2619,7	2191,6	2355,7	16,6						X
BRI2001	JB-51	15,80	16,10	HdeS	MB	i	44,69	2,24	64		7,24	2777,4	2300,3	2472,2	17,1						X
BRI2001	JB-51	29,10	29,30	HdeS	OB	ph,p	44,42	2,25	150		2,00	2998,5	2764,7	2842,7	7,7						X
BRI2001	JB-51	33,10	33,40	HdeS	MB	d	44,64	2,23	34		4,34	2736,5	2294,9	2456,2	16,3						X
BRI2001	JB-51	38,80	39,10	HdeS	CG	mgr	44,65	2,25	43		10,31	2840,0	2012,3	2303,7	29,3						X
BRI2001	JB-51	42,00	42,30	IIdes	CG	mgr	44,66	2,24	44		10,49	2828,7	2092,4	2352,5	26,0						X
BRI2001	JB-52B	7,60	7,90	HdeS	MB	d,hy	44,64	2,23	63		5,72	2843,4	2357,2	2528,2	17,1						X
BRI2001	JB-52B	14,30	14,55	HdeS	MB	d,hy	44,67	2,24	57		6,05	2774,3	2347,3	2501,3	15,4						X
BRI2001	JB-52B	20,10	20,40	HdeS	MB	d,hy	44,72	2,23	30		10,89	2795,5	2094,0	2344,9	25,0						X
BRI2001	JB-52B	25,45	25,70	HdeS	OB	ph	44,79	2,22	98		2,44	2825,8	2548,3	2646,6	9,7						X
BRI2001	JB-54	24,15	24,40	UTB	TB	fgr	44,68	2,24	135		0,20	3041,8	2919,8	2959,9	4,0						X
BRI2001	JB-54	42,30	42,60	UTB	TB	fgr,d,h	44,62	2,24	304		0,56	3046,0	2962,7	2990,1	2,7						X
BRI2001	JB-54	49,15	49,40	UTB	TB	fgr,d,h	44,63	2,24	330		0,50	3059,0	2961,5	2993,4	3,2						X
BRI2001	JB-54	79,20	79,40	UTB	OB	flw,mp	44,62	2,24	183		1,48	3057,7	2887,3	2943,0	5,5						X
BRI2001	JB-54	113,40	113,80	UTB	OB	flw,mp	44,74	2,22	124		1,83	3061,7	2800,4	2885,7	8,4						X
BRI2001	JB-54	120,30	120,60	UTB	OB		44,75	2,23	175		0,70	3036,3	2871,5	2925,8	5,4						X
BRI2001	JB-54	139,60	139,85	UTB	OB	mp	44,75	2,22	169		0,89	3064,6	2957,2	2992,2	3,5						X
BRI2001	JB-54	162,00	162,30	HdeS	CG	fgr,sd	44,69	2,23	73		12,80	2813,8	1941,3	2251,4	31,2						X
BRI2001	JB-54	163,70	163,90	HdeS	SD	fgr,mss,h	44,68	2,22	72		18,74	2722,2	1696,1	2073,1	37,9						X
BRI2001	JB-54	180,35	180,72	HdeS	CG	fgr,mss	44,34	2,25	111		8,87	2789,4	2215,2	2421,0	20,5						X

**Table 4-10: Laboratory test results for Kárahnjúkar headrace tunnel.**

Lab	DH-No	From	To	Suite	Lithology	Remarks to lithology	Core Diam.	L/D	UCS lab	Tensile strength	Water content	Apparent specific gravity	Bulk specific gravity	Bulk specific gravity (SSD)	Porosity	Slake durability	Phi	Poisson ratio	Elasticity modulus E	Triax	Uniax
-	-	m	m	-	-	-	mm	-	MPa	MPa	%	kg/m <sup>3</sup>	kg/m <sup>3</sup>	kg/m <sup>3</sup>	%	%	°	-	GPa	-	-
BRI2001	JB-54	180,35	180,72	HdeS	CG	fgr.mss	44,34	2,24	112		8,83	2751,0	2172,0	2382,5	21,0						X
BRI2001	JB-54	180,70	181,00	HdeS	SD	fgr.mss.h	44,35	2,25	117		8,72	2757,8	2183,4	2391,7	20,8						X
BRI1990	FS-31	11,4	11,7	SA	OB	p		2,1	77	9,5		2980,0	2550,8		8,8						X
BRI1990	FS-31	15,6	15,9	SA	OB	p		2,1	189	13,9		3005,0	2834,5		4,4						X
BRI1990	FS-31	38,7	39,0	SA	SC			2,1	88			2855,0	2523,6		8,8						X
BRI1990	FS-31	48,1	48,4	SA	SD			2,1	39	3,1		2765,0	2004,6		38,5	97,0					X
BRI1990	FS-31	52,2	52,5	SA	CG			2,1	18	2,1		2780,0	2052,8		32,3	98,0					X
BRI1990	FS-31	57,9	58,2	SA	SD			2,1	41	3,6		2750,0	2003,3		37,5	98,0					X
BRI1990	FS-31	60,0	60,3	SA	CG			2,1	77			2830,0	2098,0		36,1						X
BRI1990	FS-31	61,2	61,5	SA	CG			2,1	85			2780,0	1981,3		36,3						X
BRI1990	FS-31	61,8	62,1	SA	SD			2,1		5,0		2780,0	2011,9		33,5						X
BRI1990	FS-31	70,4	70,7	PF	SC			2,1	17	4,0		2870,0	2256,8		16,8						X
sintef1990	FS-31	87,6	87,9	PF	PB	d		2,1	223	19,0		3000,0	2895,5		4,0						X
BRI1990	FS-31	127,5	127,8	PF	TB	flw. p		2,1	178	13,0		2936,7	2654,5		6,9						X
BRI1990	FS-31	146,2	146,5	PF	PB	flw		2,1	145	14,1		3045,0	2905,7		2,9						X
BRI1990	FS-31	172,3	172,6	FA	OB	p		2,1	173	13,8		2970,0	2851,8		4,2						X
BRI1990	FS-31	192,3	192,6	FA	OB	d		2,1	262	17,5		2975,0	2883,1		3,3						X
BRI1990	FS-31	239,6	239,9	FA	TB	d. flw		2,1	165	13,8		2990,0	2846,2		4,1						X
BRI1990	FS-32	12,1	12,4	HA	OB	d		2,1	247	13,2		3050,0	2940,0		2,2						X
BRI1990	FS-32	39,9	40,2	HA	PB	d		2,1	230	14,7		3010,0	2873,3		2,9						X
BRI1990	FS-32	56,4	56,7	SA	SD			2,1	64	4,7		2830,0	2043,3		37,9	98,0					X
BRI1990	FS-32	61,4	61,7	SA	SD			2,1	22	5,4		2660,0	1773,3		39,2	99,0					X
BRI1990	FS-32	72,9	73,2	SA	CG			2,1	35			3030,0	2395,0		21,1	98,0					X

**Table 4-11: Laboratory test results for Kárahnjúkar headrace tunnel.**

Lab	DH-No	From	To	Suite	Lithology	Remarks to lithology	Core Diam.	L/D	UCS lab	Tensile strength	Water content	Apparent specific gravity	Bulk specific gravity	Bulk specific gravity (SSD)	Porosity	Slake durability	Phi	Poisson ratio	Elasticity modulus E	Triax	Uniax
-	-	m	m	-	-	-	mm	-	MPa	MPa	%	kg/m <sup>3</sup>	kg/m <sup>3</sup>	kg/m <sup>3</sup>	%	%	°	-	GPa	-	-
BRI1990	FS-34	201,1	201,4	HA	OB	d		2,1	275	12,5		2850,0	2800,4		1,6						X
BRI1990	FS-35	17,2	17,5	LA	OB	p		2,1	160	11,7		3030,0	2800,0		6,6						X
BRI1990	FS-35	39,5	39,8	LA	OB	flw		2,1	172	11,7		3010,0	2916,7		2,9						X
BRI1990	FS-35	46,3	46,6	LA	OB	flw		2,1	212	10,7		3070,0	2916,7		3,4						X
BRI1990	FS-35	76,0	76,3	LA	OB	p		2,1	50	6,5		2410,0	2260,0		13,1						X
BRI1990	FS-35	98,3	98,6	LA	PB	d		2,1	209	10,9		2960,0	2873,3		3,1						X
BRI1990	FS-35	120,4	120,7	LA	OB	p		2,1	110	8,0		2910,0	2656,7		10,3						X
BRI1990	FS-35	127,1	127,4	LA	TB	p		2,1	68	6,4		3040,0	2563,3		11,7						X
BRI1990	FS-35	145,0	145,3	LA	TB	d		2,1	271	14,4		2990,0	2960,0		1,4						X
BRI1990	FS-36	12,9	13,2	HD	AN	d		2,1	284	19,7		2830,0	2750,0		2,0						X
BRI1990	FS-36	49,8	50,1	LA	PB	d		2,1	211	13,1		3030,0	2850,0		5,5						X
BRI1990	FS-36	75,6	75,9	LA	OB	d		2,1	330	7,6		2970,0	2903,3		1,1						X
BRI1990	FS-36	79,1	79,4	LA	OB	d		2,1	201	10,9		3010,0	2943,3		2,3						X
BRI1990	FS-37	13,4	13,7	SA	CG			2,1	15	4,1		2780,0	2276,7		24,3						X
BRI1990	FS-37	20,2	20,5	SA	CG			2,1	53	6,6		2950,0	2363,3		25,1	98,0					X
BRI1990	FS-37	36,9	37,2	SA	ST			2,1	47	3,9		2890,0	2090,0		35,6	99,0					X
BRI1990	FS-37	48,0	48,3	SA	SD			2,1	34	3,1		2870,0	2013,3		37,9	98,0					X
BRI1990	FS-37	64,0	64,3	SA	SD			2,1	71	3,4		2700,0	2143,3		24,5	98,2					X
BRI1990	FS-37	79,4	79,7	SA	SD			2,1	51	5,4		2680,0	2100,0		31,7	98,0					X
BRI1990	FS-37	84,3	84,6	SA	SD			2,1	41	3,8		2760,0	2090,0		36,2	98,0					X
BRI1990	FS-37	90,7	91,0	SA	SD			2,1	66	4,5		2750,0	2133,3		33,9	98,0					X
BRI1990	FS-37	104,2	104,5	SA	SD			2,1	70	6,7		2700,0	2186,7		28,0	97,9					X
BRI1990	FS-37	112,7	113,0	SA	SD			2,1	16	2,7		2690,0	2000,0		38,4	98,0					X

**Table 4-12: Laboratory test results for Kárahnjúkar headrace tunnel.**

Lab	DH-No	From	To	Suite	Lithology	Remarks to lithology	Core Diam.	L/D	UCS lab	Tensile strength	Water content	Apparent specific gravity	Bulk specific gravity	Bulk specific gravity (SSD)	Porosity	Slake durability	Phi	Poisson ratio	Elasticity modulus E	Triax	Uniax
-	-	m	m	-	-	-	mm	-	MPa	MPa	%	kg/m <sup>3</sup>	kg/m <sup>3</sup>	kg/m <sup>3</sup>	%	%	°	-	GPa	-	-
BRI1990	FS-38	4,4	4,7	PF	PB	flw, p		2,1	154	13,1		3000,0	2880,0		3,8						X
BRI1990	FS-38	28,4	28,7	PF	TB	d		2,1	217	14,9		3050,0	2876,7		5,0						X
BRI1990	FS-38	45,9	46,2	PF	PB	p		2,1	145	10,8		3040,0	2820,0		6,3						X
BRI1990	FS-38	47,2	47,5	PF	PB	p		2,1	99	6,8		2900,0	2593,3		6,2						X
BRI1990	FS-38	54,3	54,6	FA	SD			2,1	22	1,0		2660,0	1980,0		26,8	96,4					X
BRI1990	FS-38	55,5	55,8	FA	SD			2,1		1,3		2760,0	1655,0		52,8	94,9					X
BRI1990	FS-38	81,4	81,7	FA	SD			2,1	20			2600,0	1680,0		38,4	9,6					X
BRI1990	FS-38	83,1	83,4	FA	PB	d		2,1	62	9,8		2880,0	2403,3		12,3						X
BRI1990	FS-38	87,9	88,2	FA	PB	d		2,1	224	16,9		3030,0	2933,3		2,4						X
BRI1990	FS-38	103,0	103,3	FA	SD			2,1	29	6,8		2720,0	1963,3		40,1	98,9					X
BRI1990	FS-38	121,8	122,1	FA	SC			2,1	53	6,5		3040,0	2576,7		16,2						X
BRI1990	FS-38	136,5	136,8	FA	TB	d		2,1	227	14,6		3010,0	2940,0		2,1						X
BRI1990	FS-38	154,7	155,0	FA	TB	p		2,1	252	12,9		2990,0	2906,7		3,5						X
BRI1990	FS-38	169,3	169,6	FA	PB	p		2,1	126	9,9		2960,0	2723,3		6,9						X
Kingst84	FV-32	139,6	151,096		OB		47,34	2,4	62				2561,96				47	0,087	13,471	X	
Kingst84	FV-32	139,8	151,408		OB		47,34	2,5	110				2670,43				29		15,725	X	
Kingst84	FV-32	140	151,674		OB		47,34	2,5	-				2687,05				44		17,607	X	
Kingst84	FV-32	140,4	152,645		OB		47,34	2,6	125				2574,45				48		19,734	X	
Kingst84	FV-32	140,6	152,907		OB		47,34	2,6	127				2641,30				48		24,918	X	
Kingst84	FV-32	143,2	155,067		OB		47,34	2,5	135				2586,71				28		21,258	X	
Kingst84	FV-32	143,4	154,896		OB		47,34	2,4	131				2785,27				44	0,088	28,616		X
Kingst84	FV-8	132,8	141,812		OB		36,2	2,5	164				2867,83				24	0,109	30,34		X
Kingst84	FV-8	135,6	144,571		OB		36,17	2,5	210				2906,33				38		24,254	X	

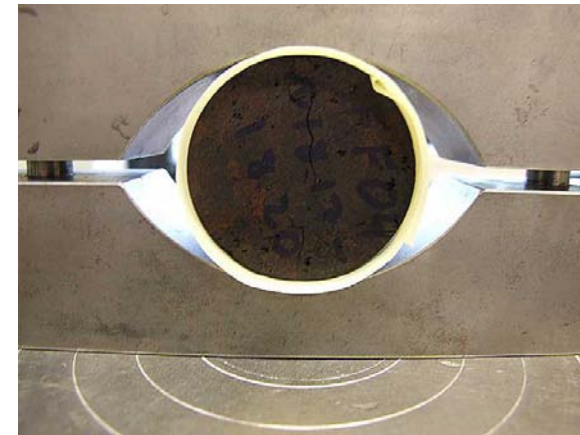


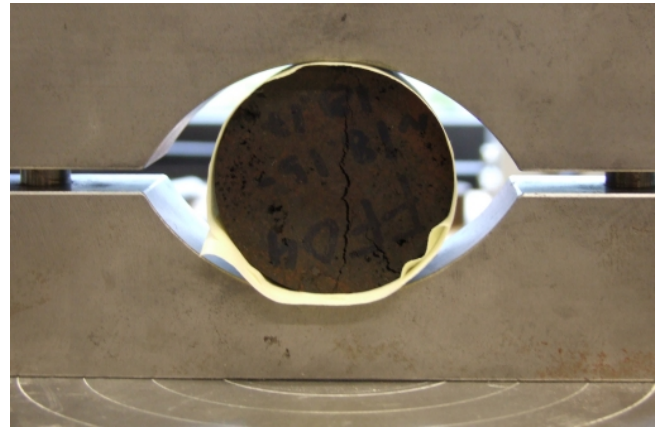
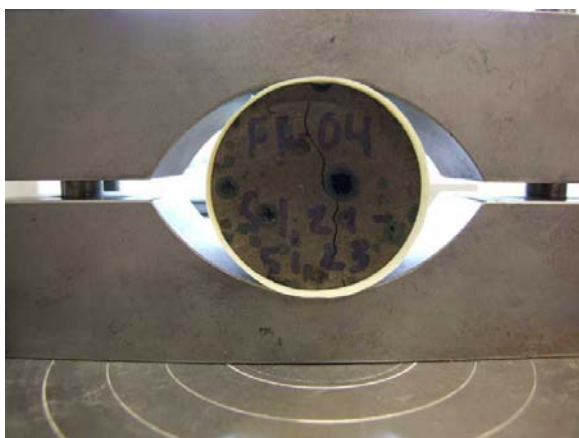
**Table 4-13: Laboratory test results for Kárahnjúkar headrace tunnel.**

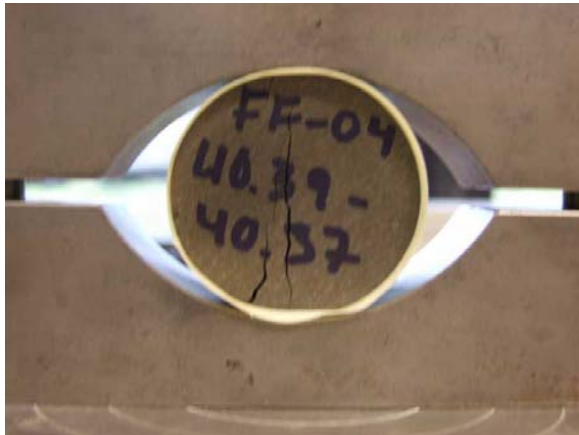
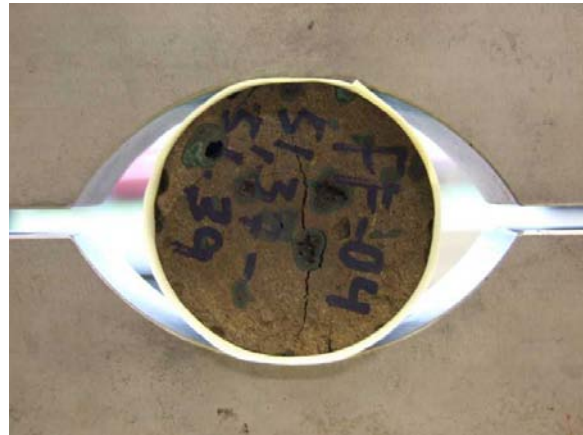
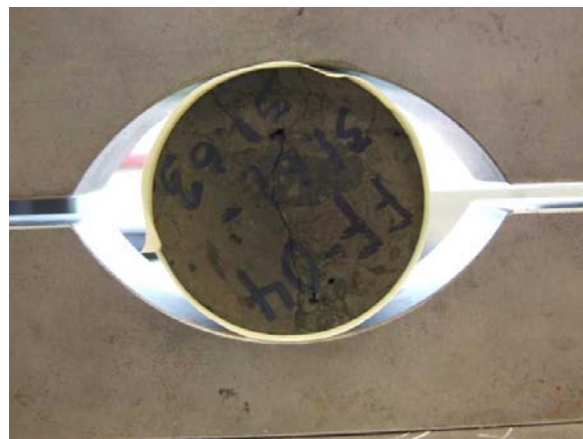
Lab	DH-No	From	To	Suite	Lithology	Remarks to lithology	Core Diam.	L/D	UCS lab	Tensile strength	Water content	Apparent specific gravity	Bulk specific gravity	Bulk specific gravity (SSD)	Porosity	Slake durability	Phi	Poisson ratio	Elasticity modulus E	Triax	Uniax
-	-	m	m	-	-	-	mm	-	MPa	MPa	%	kg/m <sup>3</sup>	kg/m <sup>3</sup>	kg/m <sup>3</sup>	%	%	°	-	GPa	-	-
Kingst84	FV-8	135,8	144,632		OB		36,19	2,4	144				2884,97				44		19,115	X	
Kingst84	FV-8	135,95	144,888		OB		36,22	2,5	209				2880,78				47		26,459	X	
Kingst84	FV-8	136,1	145,584		OB		36,19	2,6	141				2917,27				54		18,74	X	
Kingst84	FV-8	136,2	144,732		OB		36,17	2,4	204				2912,15				34	0,089	35,322	X	
Kingst84	FV-8	136,3	144,822		OB		36,19	2,4	244				2899,79				54		22,056		X
Kingst84	FV-9	95,4	106,97		OB		47,5	2,4	115				2842,07				52	0,151	39,879		X
Kingst84	FV-9	95,7	107,295		OB		47,6	2,4	177				2814,83				44		31,547	X	
Kingst84	FV-9	96,2	107,772		OB		47,5	2,4	126				2829,39				46		29,104	X	
Kingst84	FV-9	97,1	108,685		OB		47,5	2,4	179				2845,21				44		32,786	X	
Kingst84	FV-9	97,4	108,728		OB		47,5	2,4	201				2839,02				42		33,248	X	
Kingst84	FV-9	98,2	109,666		OB		47,5	2,4	151				2858,00				44		35,638	X	
Kingst84	FV-9	98,4	109,69		OB		47,5	2,4	171				2872,07				45	0,161	45,92		X
Kingst84	FV-10	40,1	51,593		OB		47,47	2,4	129				2837,20				34		26,043	X	
Kingst84	FV-10	42,2	53,389		OB		47,49	2,4	111				2884,58				30		30,584	X	
Kingst84	FV-10	42,4	52,171		OB		47,5	2,1	148				2883,09				49	0,137	36,035		X
Kingst84	FV-10	44,5	56,07		OB		47,49	2,4	176				2888,16				54		32,181	X	
Kingst84	FV-10	44,7	55,696		OB		47,47	2,3	173				2890,41				52	0,158	48,524		X
Kingst84	FV-10	48,7	59,868		OB		47,49	2,4	163				2885,46				32		30,527	X	
Kingst84	FV-10	48,9	60,061		OB		47,42	2,4	121				2813,61				48	0,138	38,6		X
Kingst84	FV-10	51,8	63,542		OB		47,47	2,5	235				2904,07				52		38,037	X	
Kingst84	FV-10	54	65,976		OB		47,49	2,5	222				2934,02				54		37,238	X	
Kingst84	FV-8	172,1	172,1		TB			2,4	166				2850,00				52		22,056	X	
Kingst84	FV-8	172,2	172,2		TB			2,4	179				2860,00				38	0,118	26,38		X

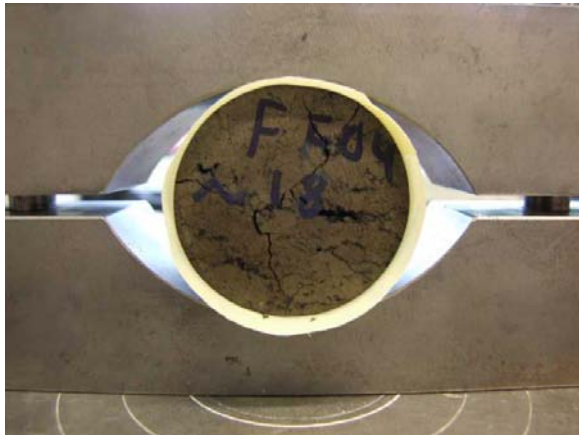
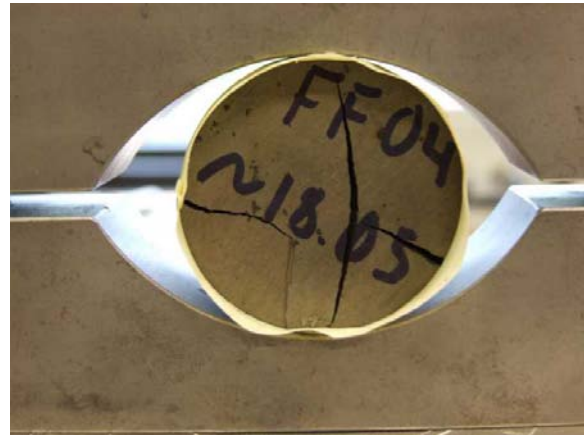
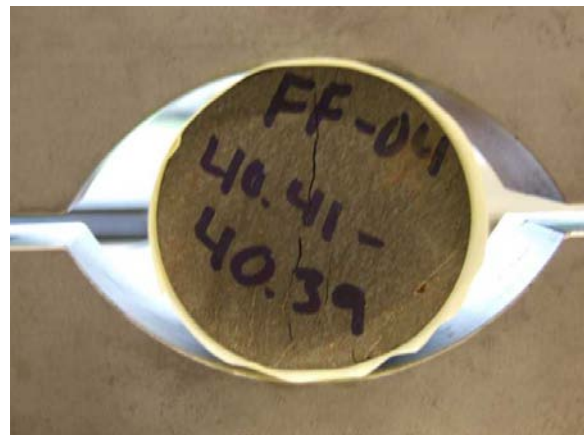
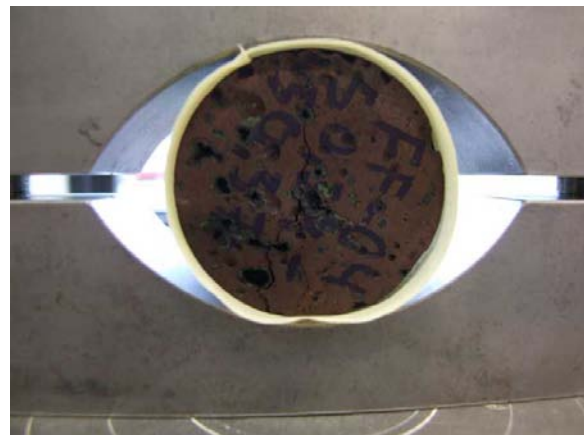
**Table 4-14: Laboratory test results for Kárahnjúkar headrace tunnel.**

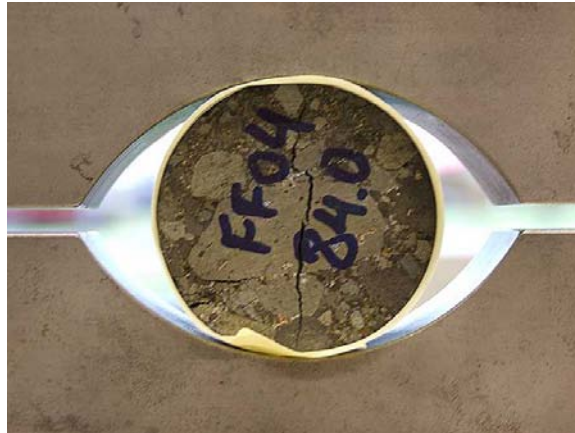
Lab	DH-No	From	To	Suite	Lithology	Remarks to lithology	Core Diam.	L/D	UCS lab	Tensile strength	Water content	Apparent specific gravity	Bulk specific gravity	Bulk specific gravity (SSD)	Porosity	Slake durability	Phi	Poisson ratio	Elasticity modulus E	Triax	Uniax
-	-	m	m	-	-	-	mm	-	MPa	MPa	%	kg/m <sup>3</sup>	kg/m <sup>3</sup>	kg/m <sup>3</sup>	%	%	°	-	GPa	-	-
Kingst84	FV-8	173,6	173,6		TB			2,5	441				2920,00				50		39,14	X	
Kingst84	FV-8	173,8	173,8		TB			2,7	279				2820,00				72		37,47	X	
Kingst84	FV-8	174	174		TB			2,3	389				2910,00				50		35,416	X	
Kingst84	FV-8	174,15	174,15		TB			2,3	396				2940,00				51	0,092	49,492		X
Kingst84	FV-8	176	176		TB			2,3	209				2870,00				40		28,664	X	
Kingst84	FV-x1	135,9	145,491		PB		4,732	2,0	71				2621,06				38		17,196	X	
Kingst84	FV-x1	136	146,665		PB		4,753	2,2	87				2636,50				46		16,374	X	
Kingst84	FV-x1	136,4	147,744		PB		4,735	2,4	101				2717,34				32		20,087	X	
Kingst84	FV-x1	136,5	148,132		PB		4,737	2,5	92				2610,26				47		116,449		X
Kingst84	FV-x2	140,6	152,459		PB		4,744	2,5	94				2742,62				52	0,133	29,901		X
Kingst84	FV-x2	140,8	152,481		PB		4,729	2,5	98				2778,71				26		25,928	X	
Kingst84	FV-x2	141,2	152,526		PB		4,729	2,4	85				2749,68				29	0,125	29,683		X
Kingst84	FV-x2	141,4	153,282		PB		4,678	2,5	94				2823,42				0		20,859	X	
Kingst84	FV-x2	141,6	153,426		PB		4,727	2,5	79				2691,55				25		16,439	X	
Kingst84	FV-x3	299,2	310,96		PB		4,729	2,5	112				2746,00				40		24,093	X	
Kingst84	FV-x3	299,8	310,91		PB		4,737	2,3	192				2811,56				50	0,137	36,141		X
Kingst84	FV-x3	300	311,151		PB		4,742	2,4	213				2824,26				38		31,664	X	
Kingst84	FV-x3	300,3	311,56		PB		4,74	2,4	142				2766,56				46	0,118	32,001		X
Kingst84	FV-x3	300,4	311,594		PB		4,735	2,4	195				2816,66				50		29,751	X	
Kingst84	FV-x4	499,7	510,66		PB		4,752	2,3	98				2636,06				46		18,447	X	
Kingst84	FV-x4	499,9	510,07		PB		4,73	2,2	77				2702,24				47	0,134	26,642		X
Kingst84	FV-x4	500,1	512,084		PB		4,75	2,5	104				2750,01				44		16,215	X	
Kingst84	FV-x4	500,3	511,915		PB		4,747	2,4	159				2764,10				40	0,137	38,411		X

**Table 4-15: Pictures from brazil test.**Sample nr. 20: Sandstone,  $\sigma_t = 1,22$  MPa.Sample nr. 21: Sandstone,  $\sigma_t = 1,53$  MPa.Sample nr. 22: Scoria,  $\sigma_t = 4,21$  MPa.Sample nr. 23: Scoria,  $\sigma_t = 0,88$  MPa.Sample nr. 24: Scoria,  $\sigma_t = 2,21$  MPa.Sample nr. 25: Scoria,  $\sigma_t = 2,22$  MPa.

**Table 4-16: Pictures from brazil test.**Sample nr. 26: Scoria,  $\sigma_t = 0,79$  MPa.Sample nr. 27: Scoria,  $\sigma_t = 0,00$  MPa. (Broke before loading)Sample nr. 28: Olivine tholeiite,  $\sigma_t = 2,08$  MPa.Sample nr. 29: Scoria,  $\sigma_t = 1,68$  MPa.Sample nr. 30: Olivine tholeiite,  $\sigma_t = 0,52$  MPa.Sample nr. 31: Scoria,  $\sigma_t = 1,85$  MPa.

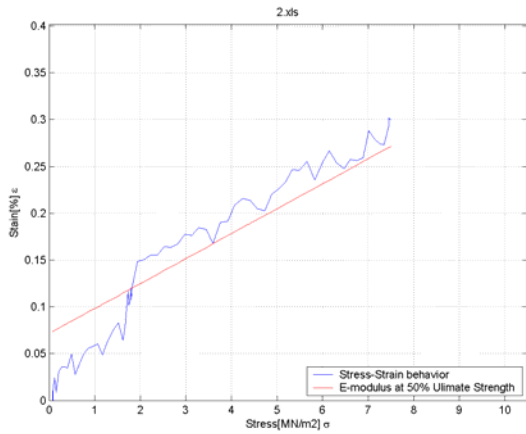
**Table 4-17: Pictures from brazil test.**Sample nr. 32: Tholeiite basalt,  $\sigma_t = 4,30$  MPa.Sample nr. 33: Olivine tholite,  $\sigma_t = 1,13$  MPa.Sample nr. 34: Scoria,  $\sigma_t = 1,08$  MPa.Sample nr. 35: Scoria,  $\sigma_t = 1,62$  MPa.Sample nr. 36: Olivine t tholeiite,  $\sigma_t = 1,11$  MPa.Sample nr. 37: Scoria,  $\sigma_t = 0,87$  MPa.

**Table 4-18: Pictures from brazil test.**Sample nr. 38: Scoria,  $\sigma_t = 1,98$  MPa.Sample nr. 39: Scoria,  $\sigma_t = 6,01$  MPa.Sample nr. 40: Scoria,  $\sigma_t = 1,34$  MPa.Sample nr. 41: Tholeiite basalt,  $\sigma_t = 3,05$  MPa.Sample nr. 42: Scoria,  $\sigma_t = 1,55$  MPa.Sample nr. 43: Scoria,  $\sigma_t = 3,05$  MPa.

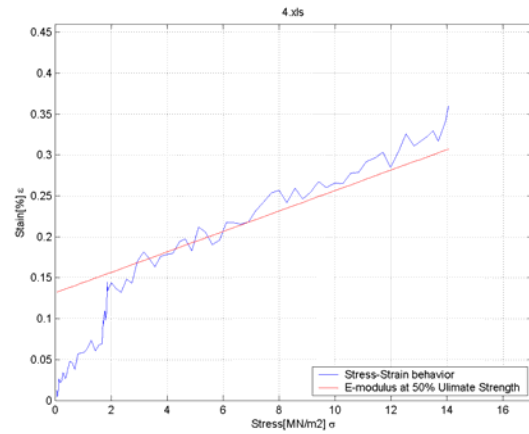


Sample nr. 44: Sandstone,  $\sigma_t = 2,38$  MPa.

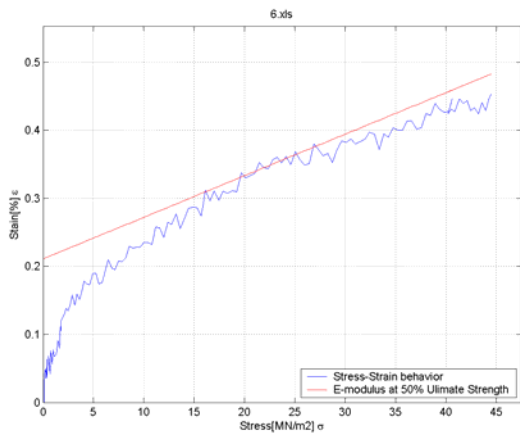
**Table 4-19: Plots from unconfined compression test.**



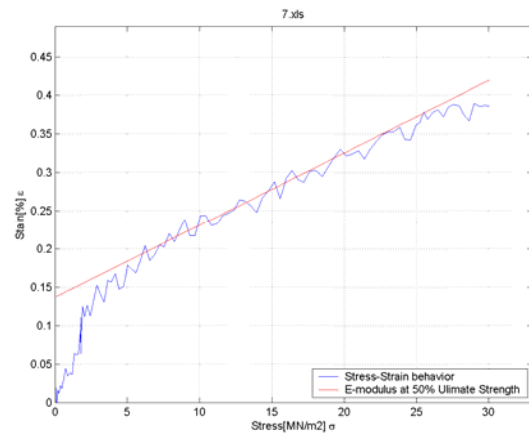
Olivine tholeiite,  $\sigma_c=7,49$  MPa, E-modulus = 3,75 GPa



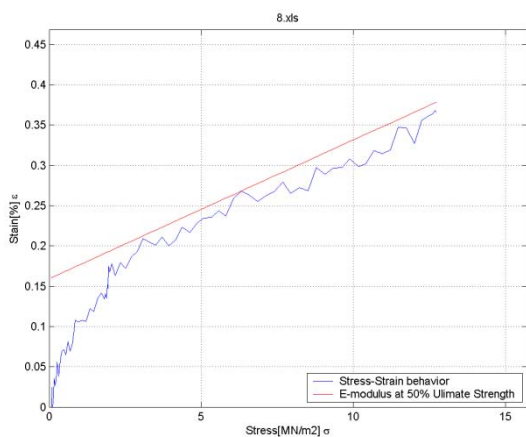
Olivine tholeiite,  $\sigma_c=14,05$  MPa, E-modulus = 8,0 GPa



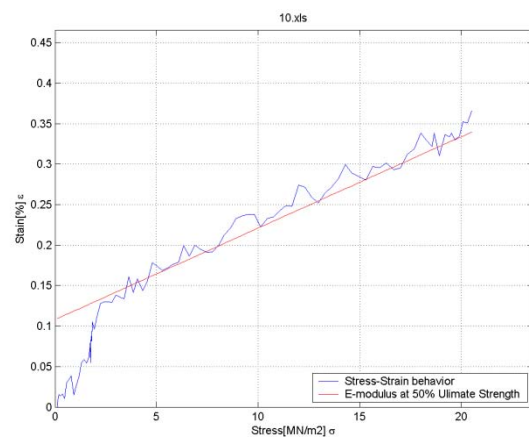
Scoria,  $\sigma_c =44,5$  MPa, E-modulus = 16,39 GPa



Tholeiite basalt,  $\sigma_c =30,02$  MPa, E-modulus = 10,62 GPa



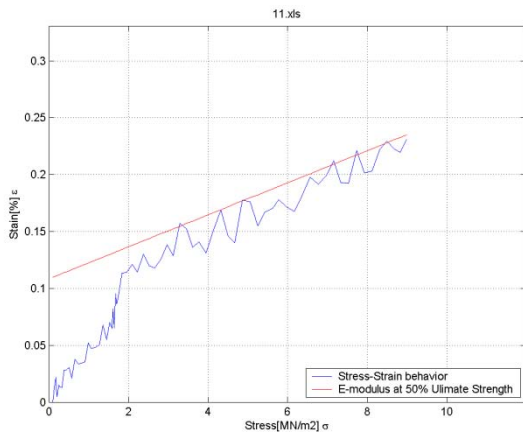
Olivine tholeiite,  $\sigma_c =12,71$  MPa, E-modulus = 5,80 GPa



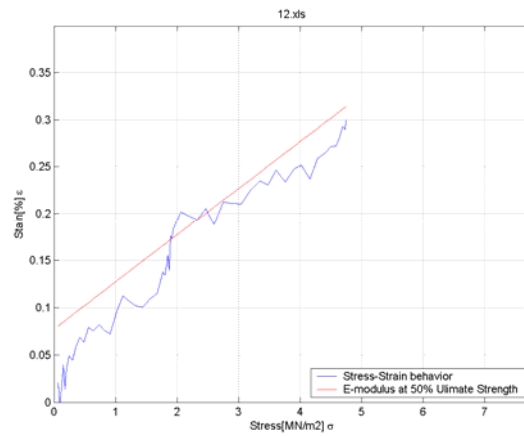
Olivine tholeiite,  $\sigma_c =20,5$  MPa, E-modulus = 8,85 GPa



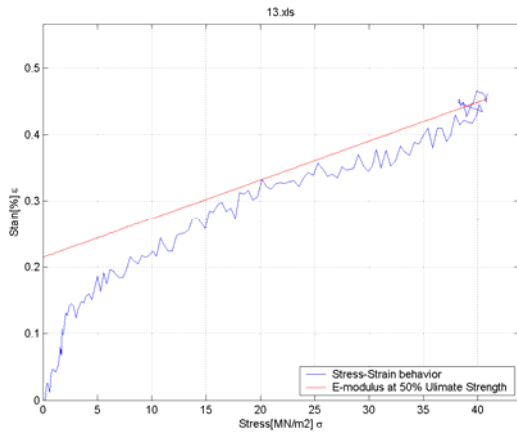
**Table 4-20: Plots from unconfined compression test.**



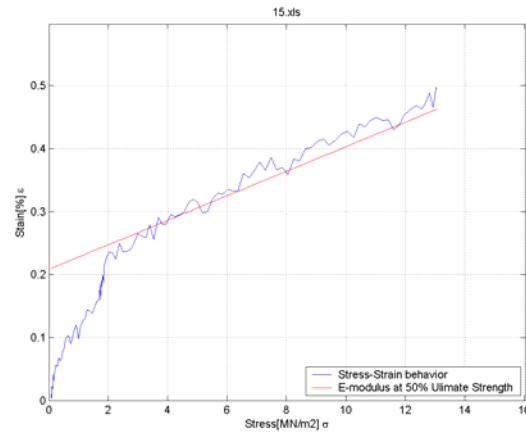
Olivine tholeiite,  $\sigma_c = 8,98$  MPa, E-modulus = 7,10 GPa



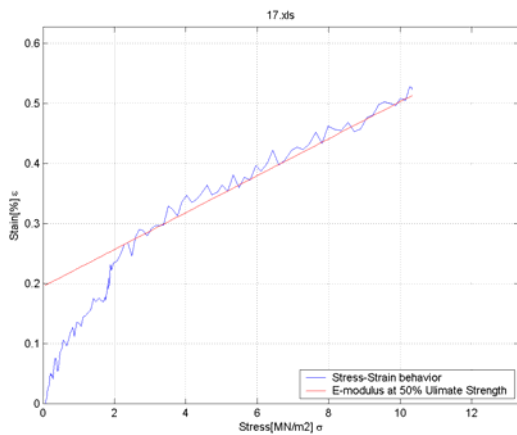
Sandstone,  $\sigma_c = 4,75$  MPa, E-modulus = 2,00 GPa



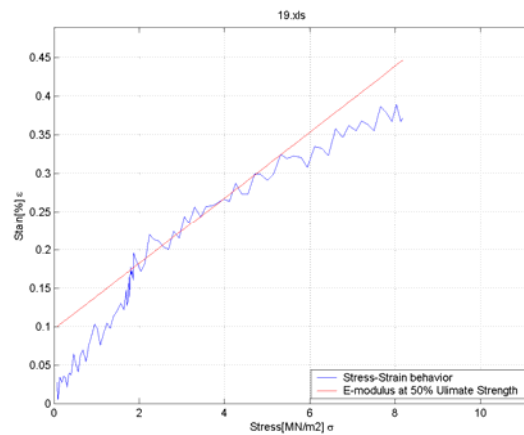
Olivine tholeiite,  $\sigma_c = 40,85$  MPa, E-modulus = 17,05 GPa



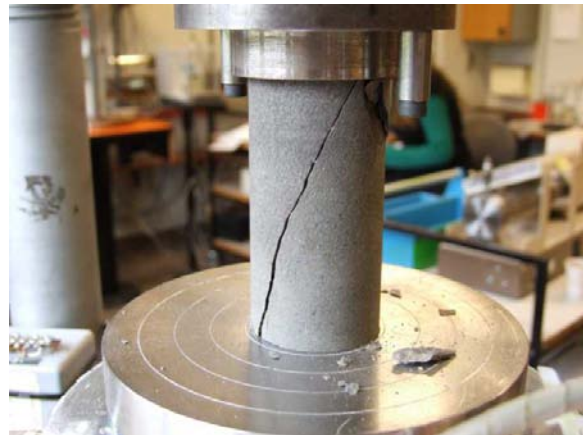
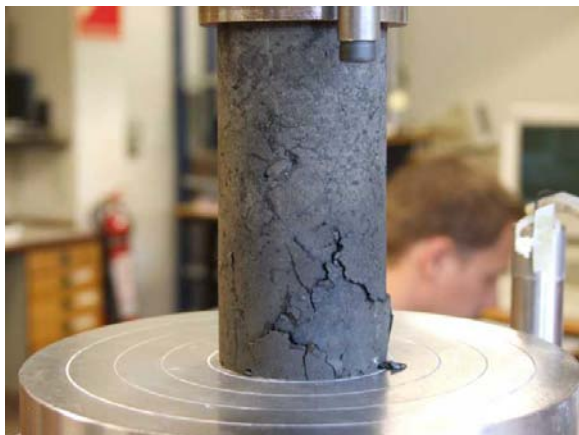
Sandstone,  $\sigma_c = 13,04$  MPa, E-modulus = 5,13 GPa

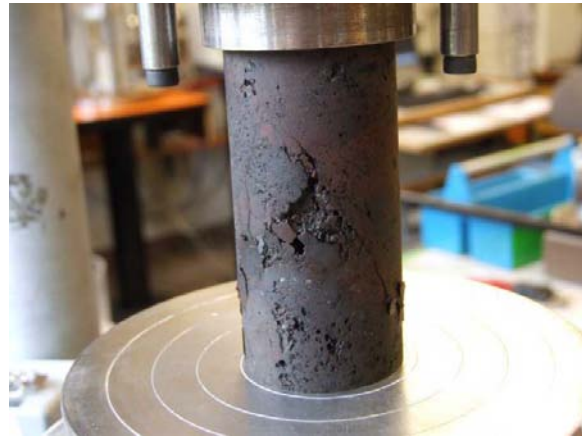
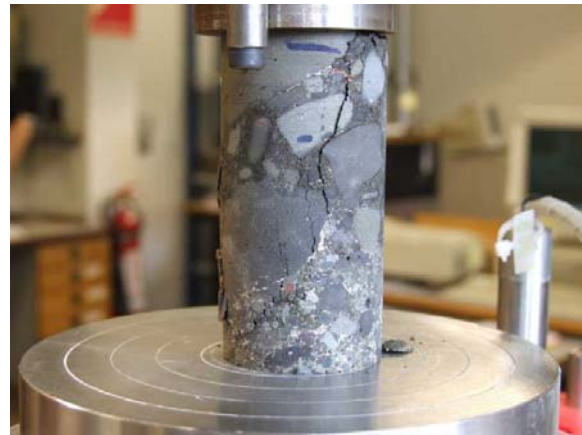
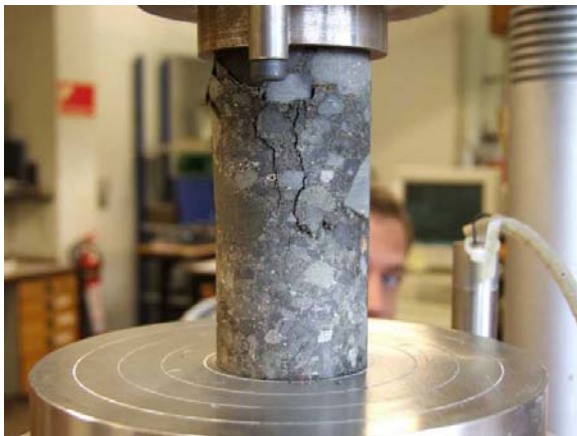
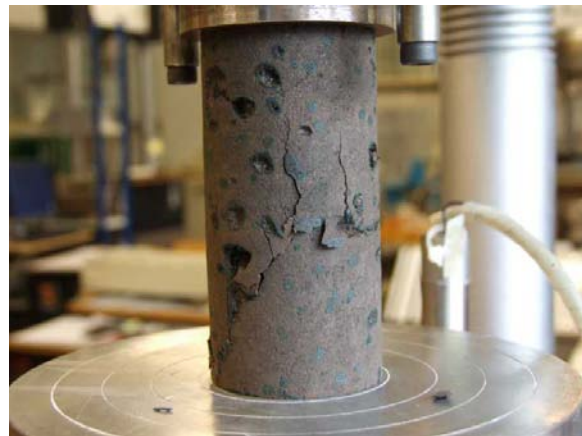


Sandstone,  $\sigma_c = 10,34$  MPa, E-modulus = 3,25 GPa

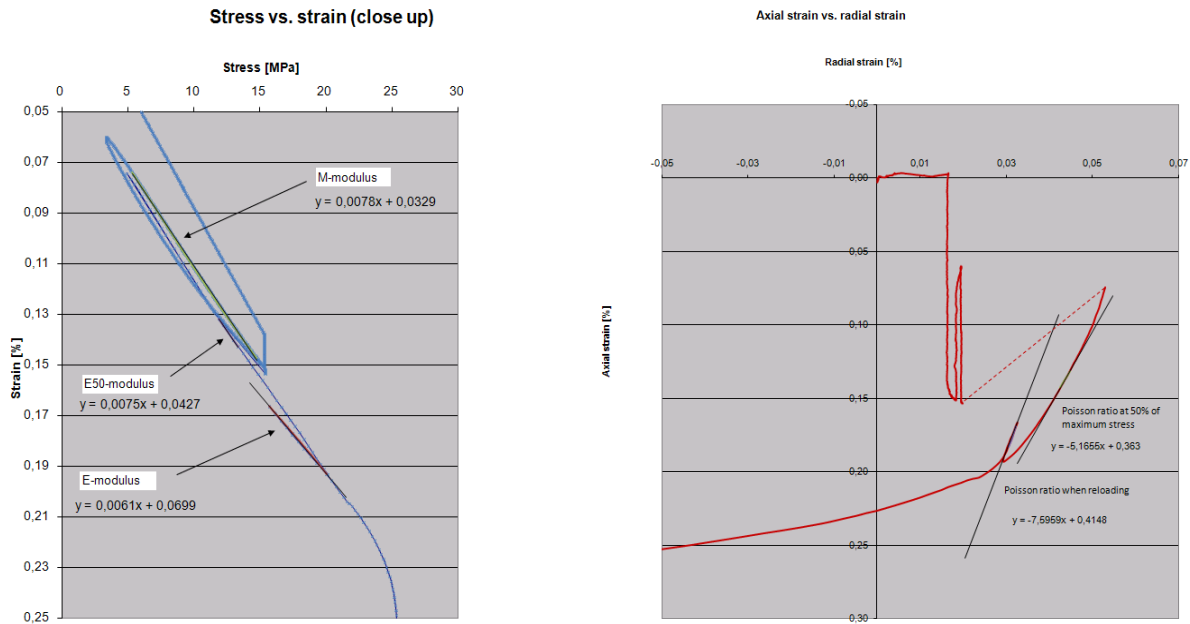


Olivine tholeiite,  $\sigma_c = 8,18$  MPa, E-modulus = 2,34 GPa

**Table 4-21: Pictures from unconfined compression test.**Sample nr. 2: Scoria,  $\sigma_c = 7,49$  MPa.Sample nr. 4: Scoria,  $\sigma_c = 14,05$  MPa.Sample nr. 6: Scoria,  $\sigma_c = 44,50$  MPa.Sample nr. 7: Tholeiite basalt,  $\sigma_c = 30,02$  MPa.Sample nr. 8: Scoria,  $\sigma_c = 12,71$  MPa.Sample nr. 10: Scoria,  $\sigma_c = 20,50$  MPa.

**Table 4-22: Pictures from unconfined compression test.**Sample nr. 11: Scoria,  $\sigma_c = 8,98$  MPa.Sample nr. 12: Scoria,  $\sigma_c = 4,75$  MPa.Sample nr. 13: Olivine tholeiite,  $\sigma_c = 40,85$  MPa.Sample nr. 15: Sandstone,  $\sigma_c = 13,04$  MPa.Sample nr. 17: Sandstone,  $\sigma_c = 10,34$  MPa.Sample nr. 19: Olivine tholeiite,  $\sigma_c = 8,18$  MPa.

**Table 4-23: Plots from triaxial test of sample 3-scoria.**



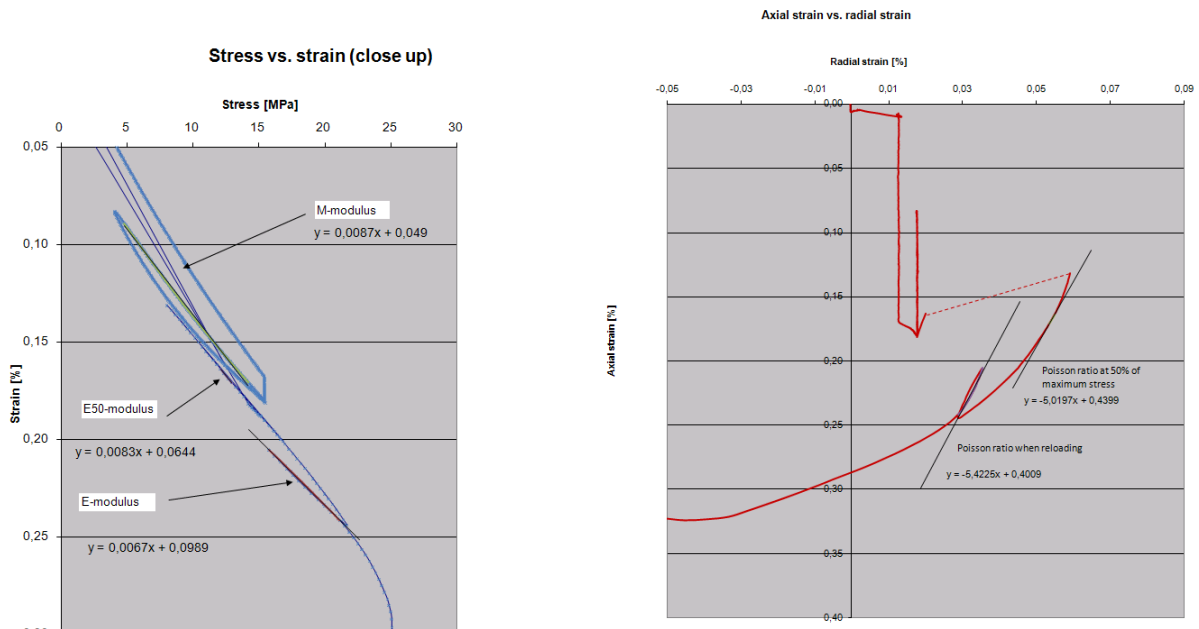
E-modulus = 16,39 GPa.

Poisson ratio = 0,132

E-modulus at 50% of strength = 13,33 GPa

Poisson ratio at 50% of strength = 0,194

**Table 4-24: Plots from triaxial test of sample 14-scoria.**



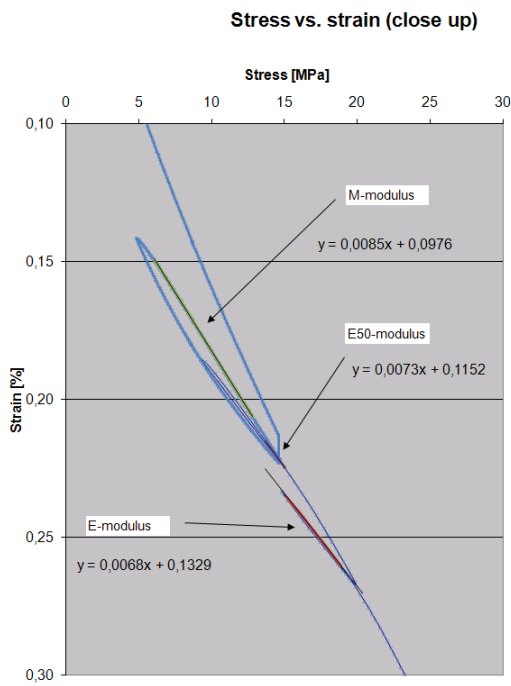
E-modulus = 14,93 GPa.

Poisson ratio = 0,184

E-modulus at 50% of strength = 12,05 GPa

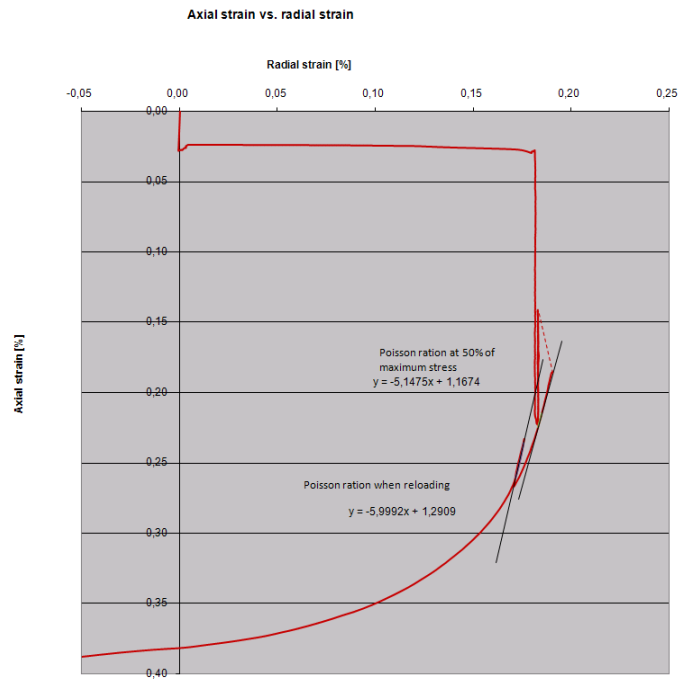
Poisson ratio at 50% of strength = 0,199

**Table 4-25: Plots from triaxial test of sample 16-sandstone.**



E-modulus = 14,71 GPa.

E-modulus at 50% of strength = 13,70 GPa



Poisson ratio = 0,167

Poisson ratio at 50% of strength = 0,194

**Table 4-26: Pictures from triaxial test.**

Sample nr. 3: Scoria  
Failure at:  $\sigma_1 = 25,346$  MPa and  $\sigma_3 = 1,456$  MPa



Sample nr. 14: Scoria  
Failure at:  $\sigma_1 = 25,123$  MPa and  $\sigma_3 = 1,432$  MPa



Sample nr. 16: Sandstone  
Failure at:  $\sigma_1 = 28,624$  MPa and  $\sigma_3 = 0,891$  MPa



Sample nr. 5: Scoria  
Failure at:  $\sigma_1 = 6,321$  MPa and  $\sigma_3 = 0,504$  MPa

**Table 4-27: Comparison of laboratory test results from the Kárahnjúkar headrace tunnel and the Fáskrúðsfjörður tunnel.**

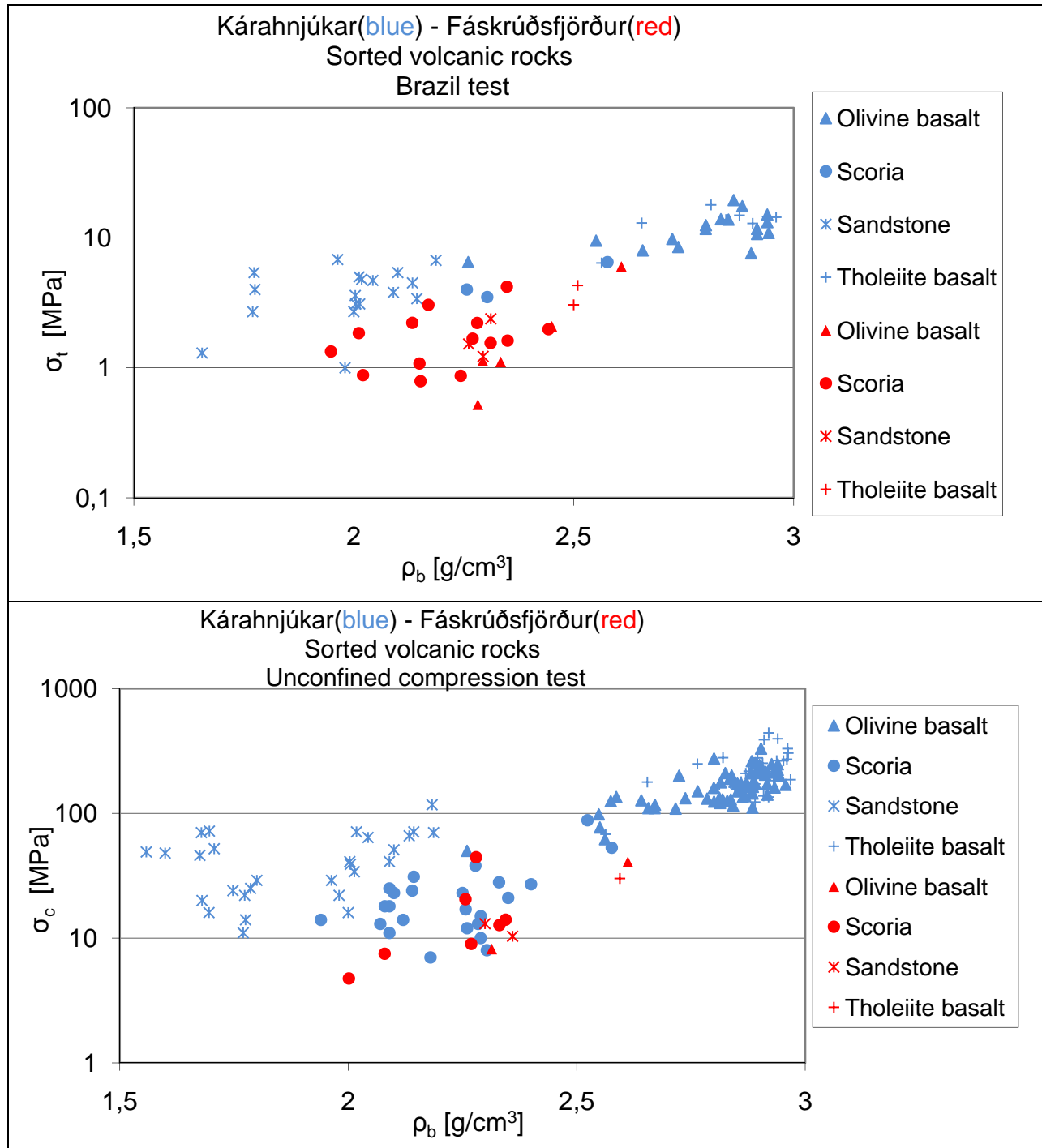
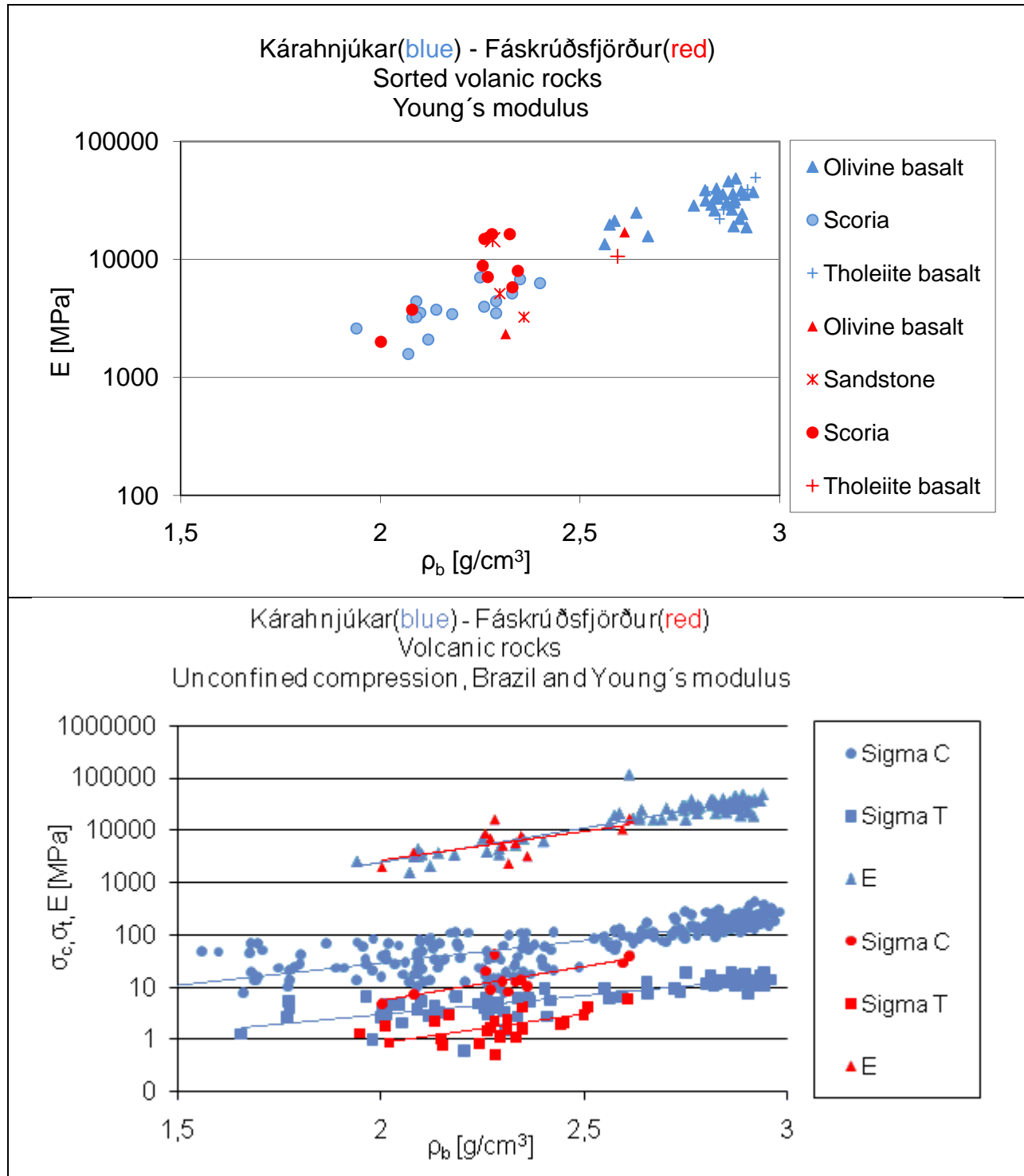


**Table 4-28: Comparison of laboratory test results from the Kárahnjúkar headrace tunnel and the Fáskrúðsfjörður tunnel.**

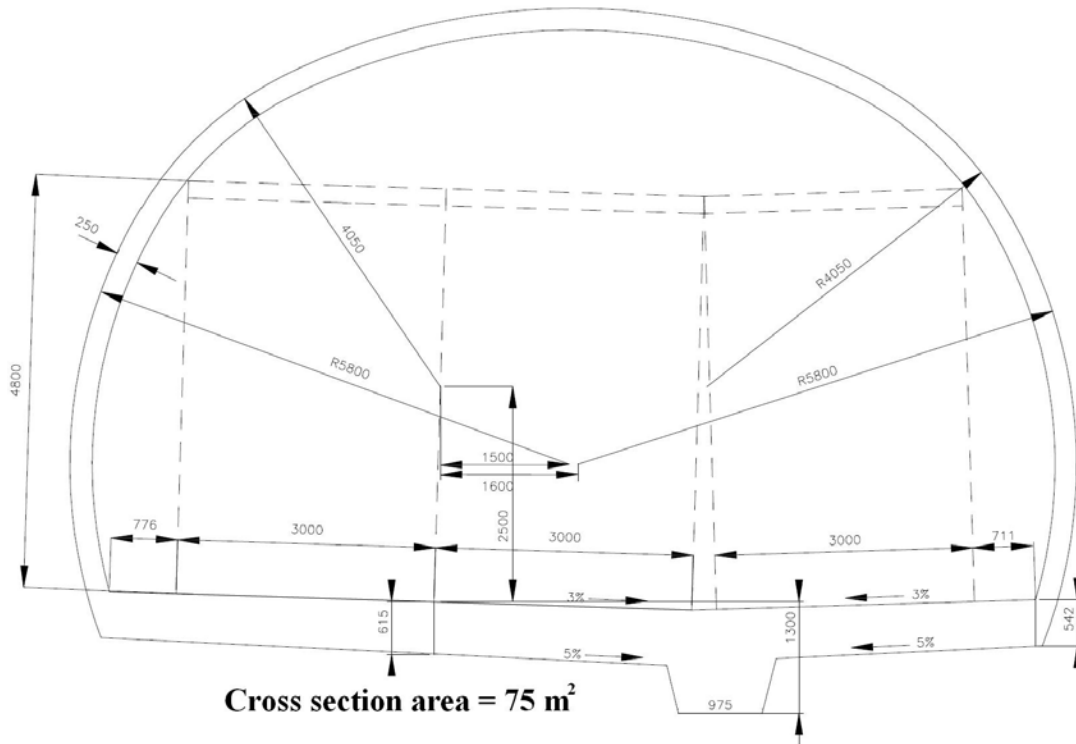




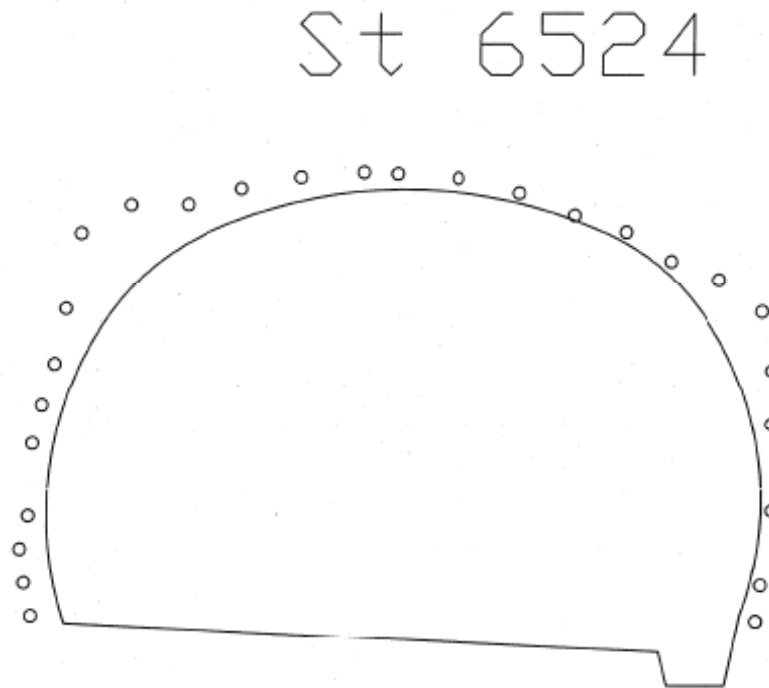
## 5. Appendix

This appendix contains a design cross section, cross section measurements from various stations from the Fáskrúðsfjörður tunnel also other materials used in the modelling phase of the thesis.

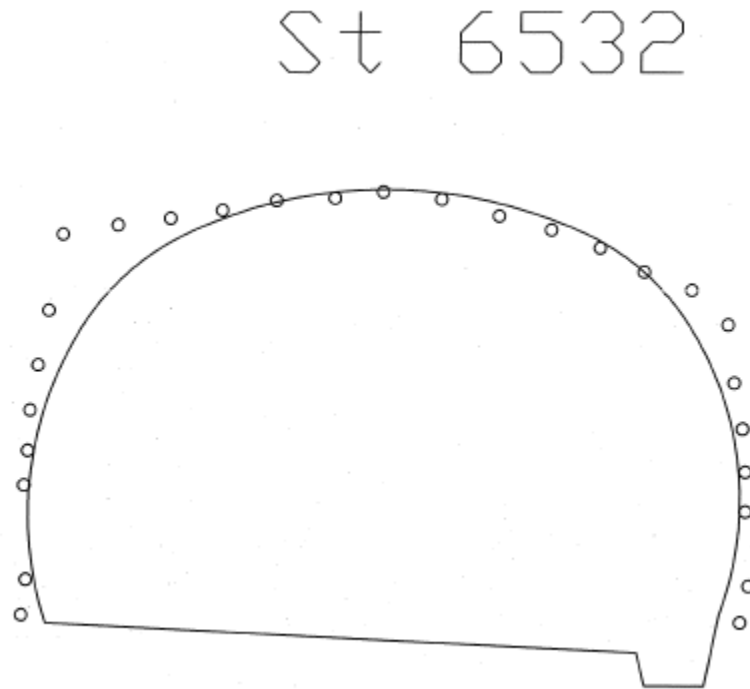
- ✓ Design cross section of the Fáskrúðsfjörður tunnel where niche is placed.
- ✓ Cross section measurement of station 6524 made by Ístak, used to model the cross section for station 6530.
- ✓ Cross section measurement of station 6532 made by Ístak, used to model the cross section for station 6530.
- ✓ Cross section measurement of station 7616 made by Ístak, used to model the cross section for station 7615.
- ✓ Geological mapping and primary support for station 6530 from Ístak.
- ✓ Rock characterisation, geological mapping and bolt support for station 6530 from GeoTek.
- ✓ Rock bolt report for station 6530 from Ístak.
- ✓ Shotcrete report for station 6530 from Ístak.
- ✓ Geological mapping and primary support for station 7615 from Ístak.
- ✓ Rock characterisation and geological mapping for station 7615 from Ístak.
- ✓ Shotcrete reports for station 7615 from Ístak.



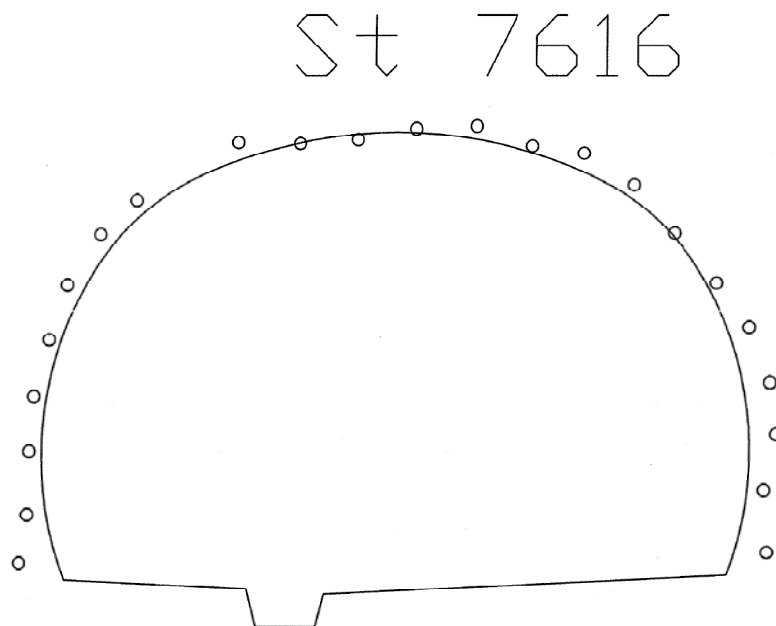
**Figure 5-1: Design cross section of the Fáskrúðsfjörður tunnel where niche is placed, dimensions are in millimetres.**



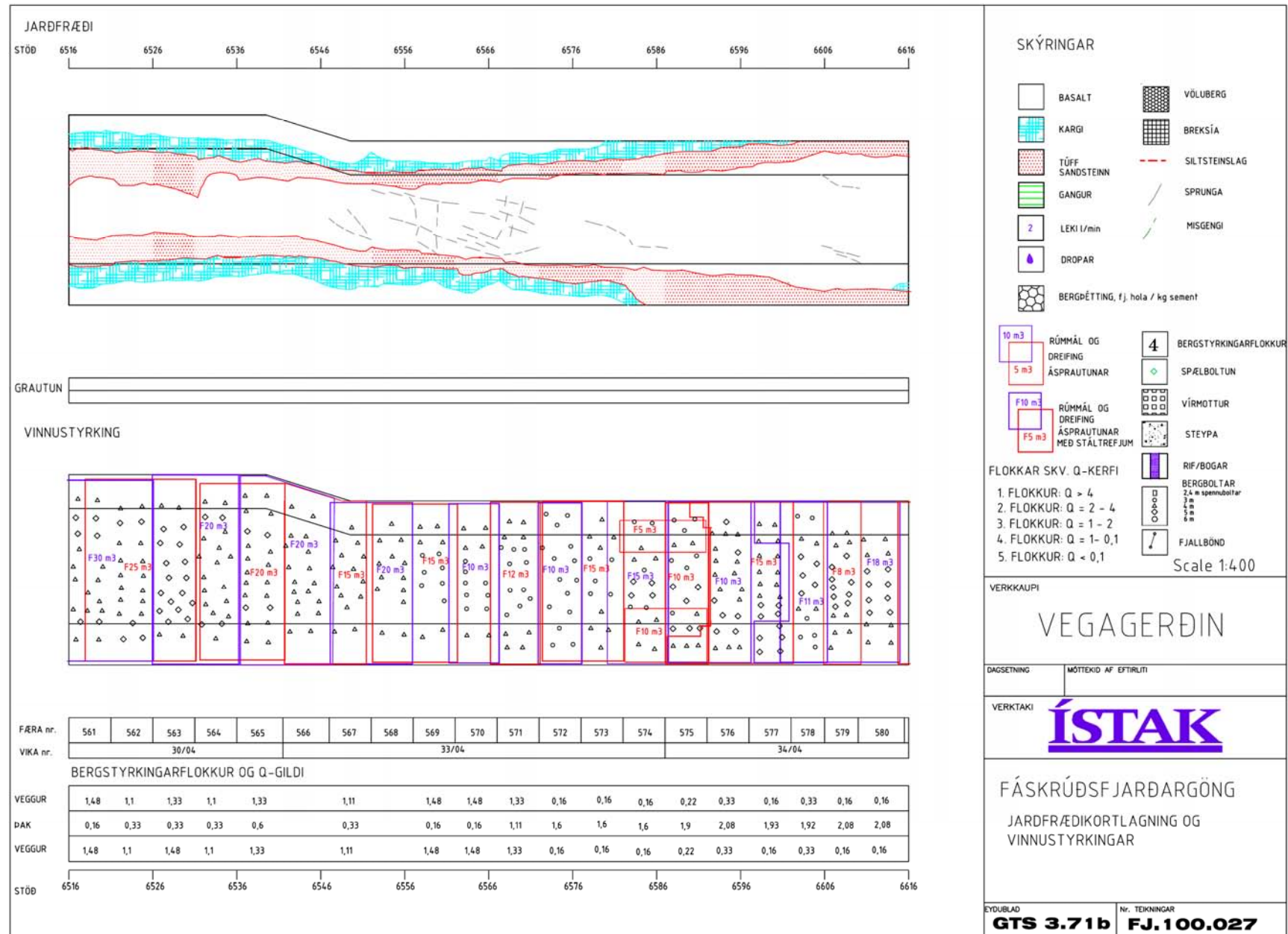
**Figure 5-2: Cross section measurements of station 6524, used to model station 6530.**



**Figure 5-3: Cross section measurements of station 6532, used to model station 6530.**



**Figure 5-4: Cross section measurements of station 7616, used to model station 7615.**



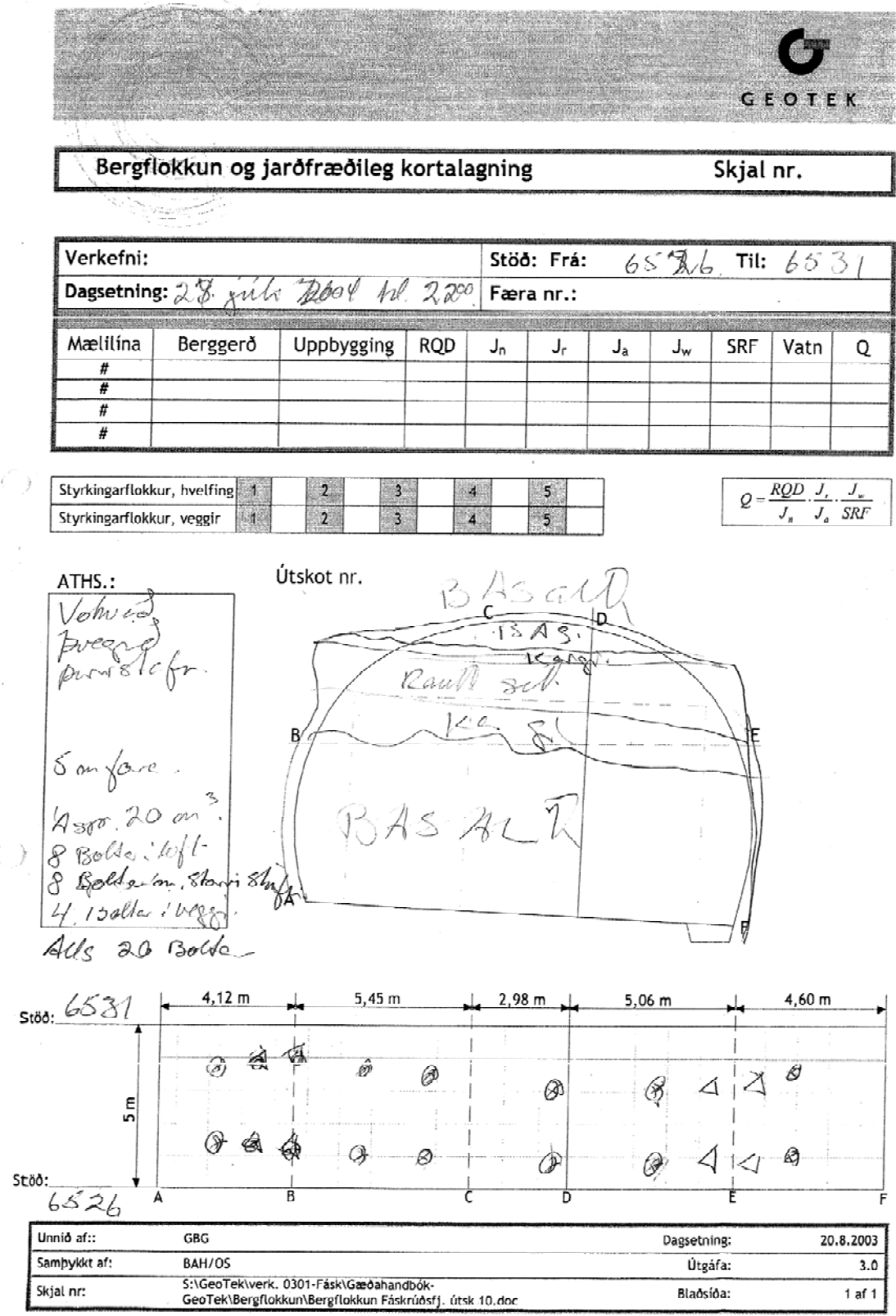


Figure 5-5: Geological mapping and bolt support for station 6530 from GeoTek

**Fáskrúðstjarðargöng** **GTS 3.78a**

---

**ÍSTAK**

## BOLTASKÝRSLA

Dags: 23/7 04 Stöð frá: 6531 til: 6526 Nr. \_\_\_\_\_

Stakboltun Þvermál, Ø  
 Kerfisboltun 16mm  20mm  25mm

		Fjöldi			
Lengd	Gerð	V. Veggur	Hvelfing	H. Veggur	Samtals
3m	Kambst.				
3m	Ankerisb.				
4m	Kambst.	2		2	4
4m	Ankerisb.				
5m	Kambst.		16		16
5m	Ankerisb.				
6m	Kambst.				
2.4m	Endafestir				

Σ = 20

Athugasemdir:

---



---



---



---

Undirskrift:

**Verktaki**

**Verkkaupi**

Figure 5-6: Rock bolt report for station 6530 from Ístak.

Fáskrúðsjarðargöng

GTS 3.71d

**ÍSTAK**

SPRAUTUSTEYPUSKÝRSLA

Dags: 23/7 04

Stafn: Nordur

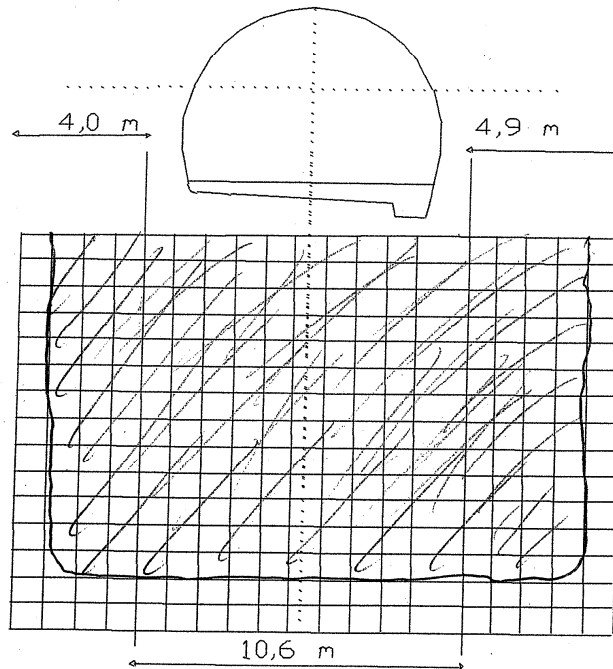
Ásprautun hefst kl: 22<sup>10</sup>

Ásprautun lýkur kl: 01<sup>40</sup>

Sprautari: Kiddi / Dafur

	Stöð:		m <sup>3</sup> með stáltreffjum	m <sup>3</sup> án stáltreffa
	Frá:	Til:		
V. veggur	6531	6518	3 1/2	
Hvelving	—	—	17	
H. veggur	—	—	4 1/2	

Samtals:	25	
Hraðari:	750	lítrar



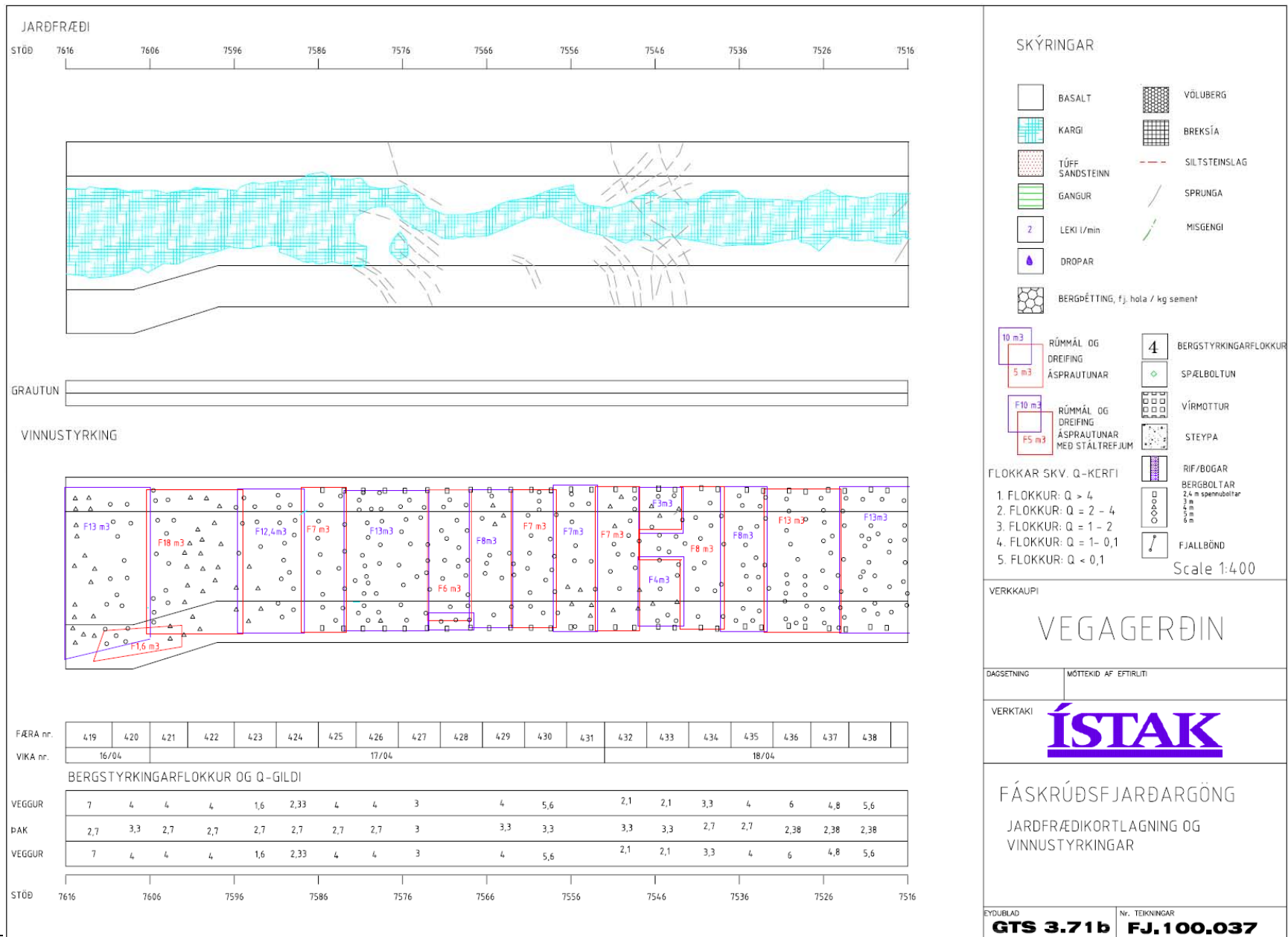
Athugasemdir:

Undirskrift:

Verktaki:

Verkkaupi:

Figure 5-7: Shotcrete report for station 6530 from Ístak.





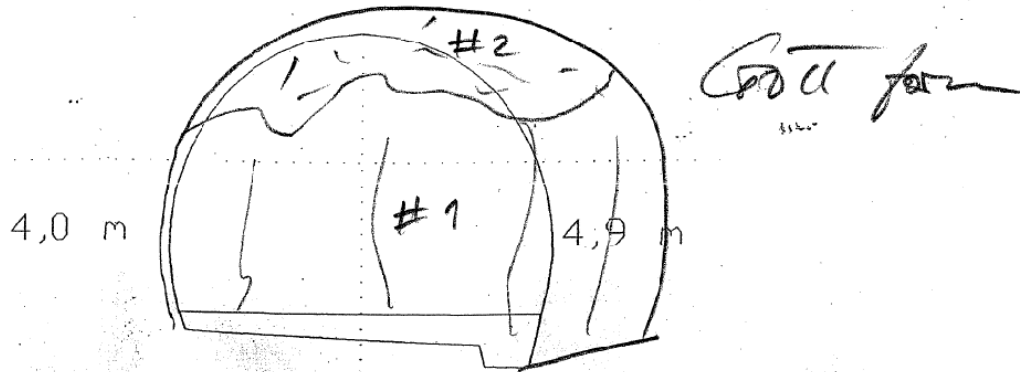
Fáskrúðstjarðargöng

GTS 3.71a

ÍSTAK

BERGFLOKKUN OG JARÐFRÆÐILEG KORTLAGNING

DAGS: 18/4 '04 UNDIRSKR: BG FÆRA: 419 STÖÐ FRÁ: STÖÐ TIL:



--	--	--	--

Stöð: 7610.5

Stöð: 7615.5

Lýsing á bergi:

Tegun bergs	# 1	# 2	#	#	#
Byggingarlag	Bas	Kalki			
Styrkleiki					
RQD	70	50			
Jn	10	9			
Jr	2.5	1.5			
Ja	2.5	3.0			
Jw	1	1			
SRF	1	1			
Q-index					
Vatn l/min					
Vatn °C					
Vatn pH					

Figure 5-8: Geological mapping for station 7615 from Ístak.

Fáskrúðsfjarðargöng

GTS 3.71d

**ÍSTAK**

SPRAUTUSTEYPUSKÝRSLA

Dags: 19-04-04.

Stafn: Suður.

Ásprautun hefst kl: 20<sup>35</sup>

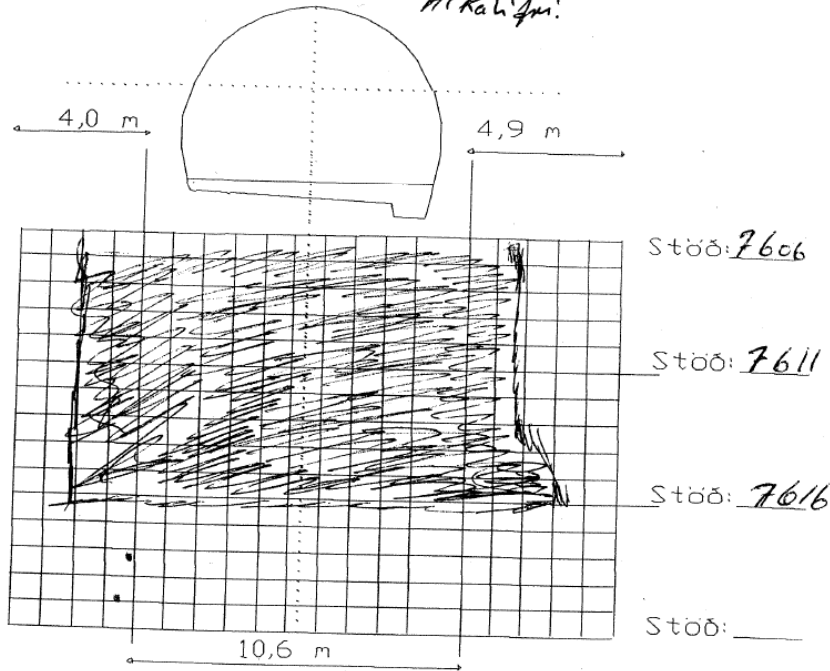
Ásprautun lýkur kl: 22<sup>50</sup>

Sprautari: Kjartan

	Stöð:		m <sup>3</sup> með stálfrefjum	m <sup>3</sup> án stálfrefja
	Frá:	Til:		
V. veggur	7616	7606	22 m <sup>3</sup>	
Hvelting	-11-	-11-	8,8 m <sup>3</sup>	
H. veggur	-11-	-11-	2,2	

Samtals:	13 m <sup>3</sup>	
Hraðari:	195 L	lítrar

11 Kalífun!



Athugasemdir:

Undirskrift:

Vérktaki: Kjartan

Verkkaupi: [Signature]

Figure 5-9: Shotcrete report for station 7615 from Ístak.

Fáskrúðsfjarðargöng

GTS 3.71d

**ÍSTAK**

SPRAUTUSTEYPUSKÝRSLA

Dags: 18.4.09

Stafn: 7610

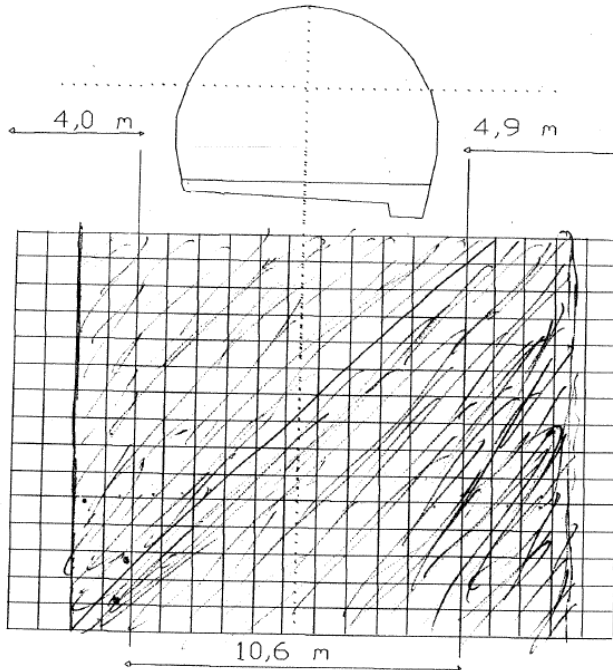
Ásprautun hefst kl: 12<sup>00</sup>

Ásprautun lýkur kl: 13<sup>30</sup>

Sprautari: Jón/Helga

	Stöð:		m <sup>3</sup> með stáltreffjum	m <sup>3</sup> án stáltreffa
	Frá:	Til:		
V. veggur	7616	7631	1.5	
Hvelfing	1	1	7.9	
H. veggur	1	1	2.6	

Samtals:	12	
Hraðari:	228	lítrar



*Yfirsprautad st. 7628-7631*

Athugasemdir:

~~Heita undirskrift Verktaka~~

Undirskrift:

Verktaki:

Verkkaupi:

Figure 5-10: Shotcrete report for station 7615 from Ístak.



## 6 Appendix

This appendix contains materials from the modelling phase of the thesis.

- ✓ Practical support model for station 6530.
- ✓ Supplementary support model 1 for station 6530.
- ✓ Supplementary support model 2 for station 6530.
- ✓ Practical support model for station 7615.
- ✓ Supplementary support model 1 for station 7615.
- ✓ Supplementary support model 2 for station 7615.

**Practical support model for station 6530.**

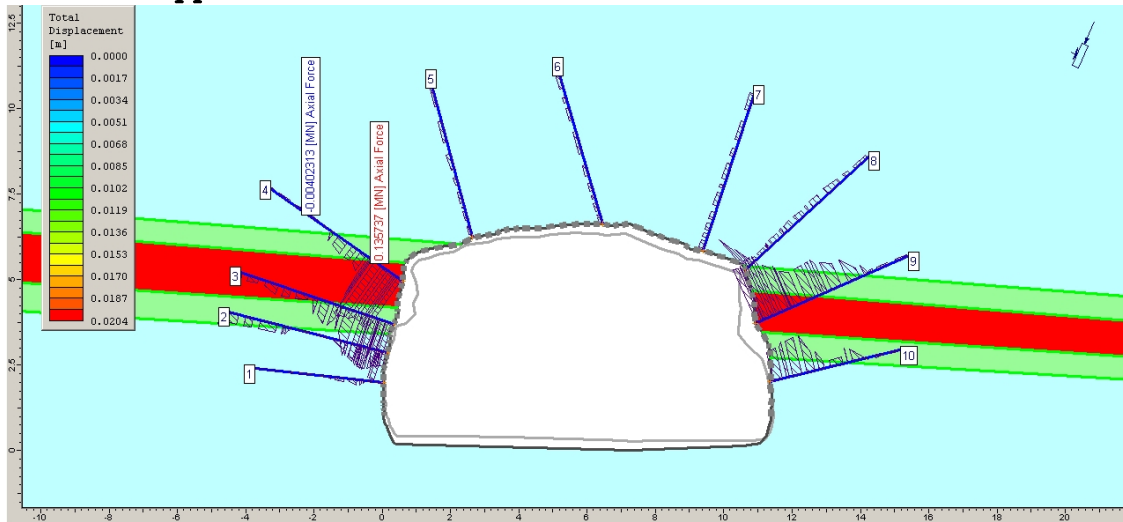


**Figure 6-1: Axial force in rock bolts in practical support model for station 6530.**

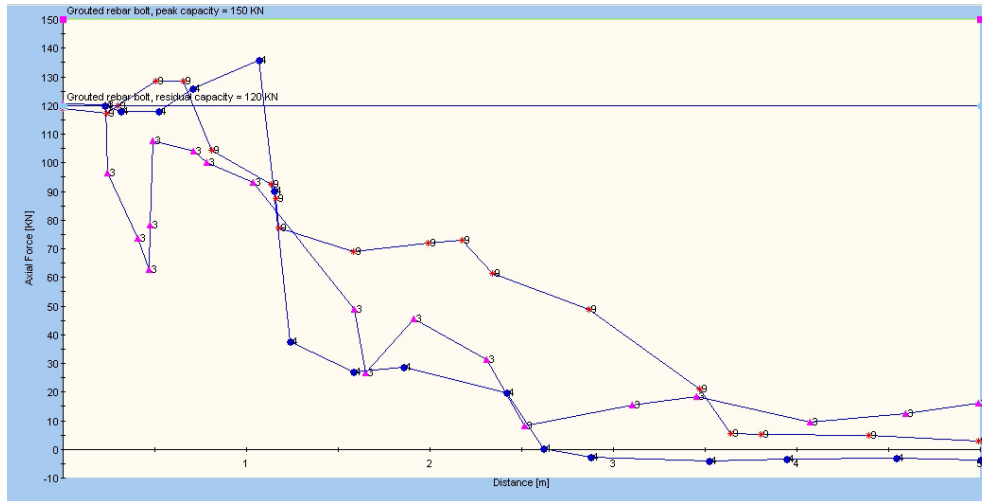


**Figure 6-2: Axial force in rock bolt in practical support model for station 6530, yielding presents in bolts nr. 3, 4 and 9.**

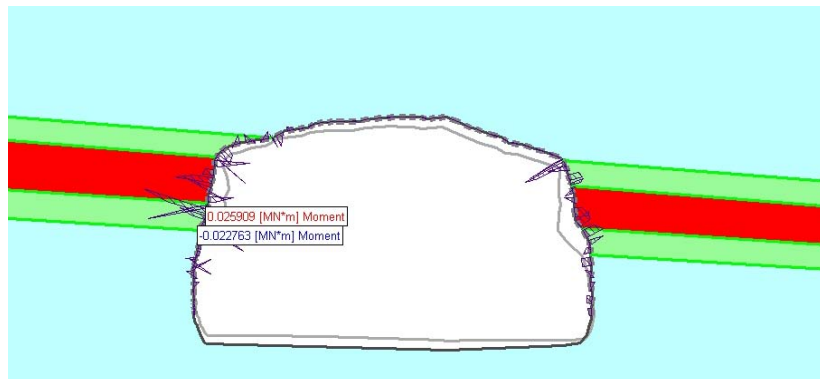


**Figure 6-3: Bending moment in the shotcrete in practical support model for station 6530.**

**Supplementary support model 1 for station 6530.**

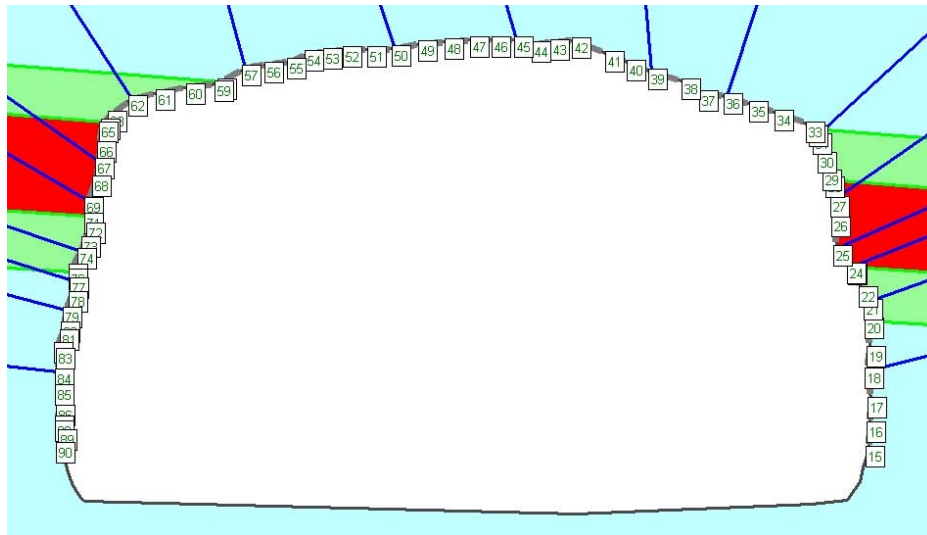


**Figure 6-4: Shotcrete elements in supplementary support model 1 for station 6530.**

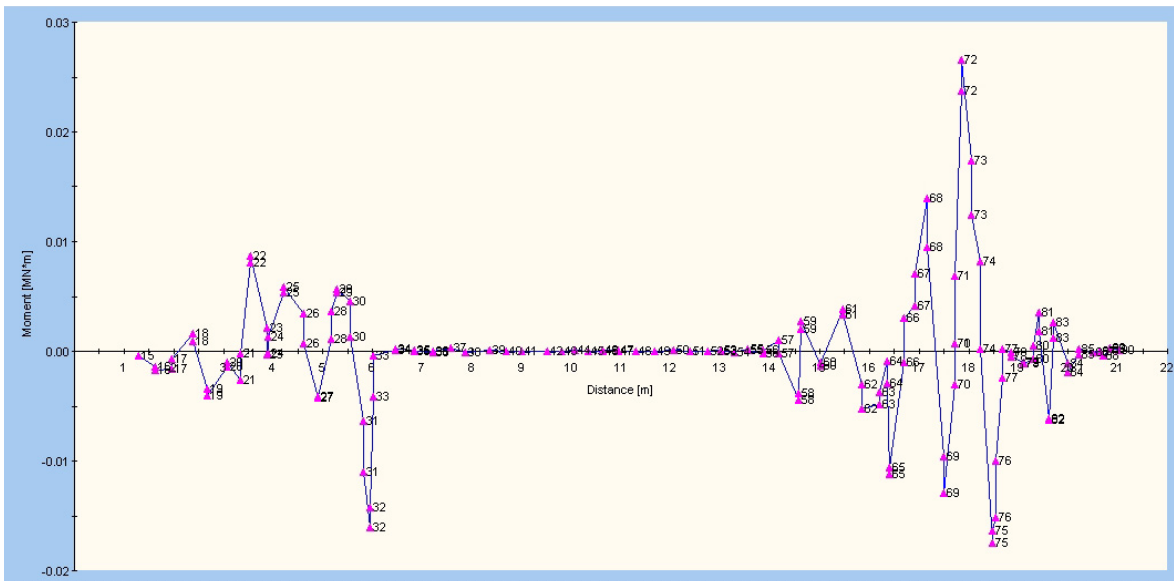


**Figure 6-5: Bending moment in shotcrete for supplementary support model 1 for station 6530.**

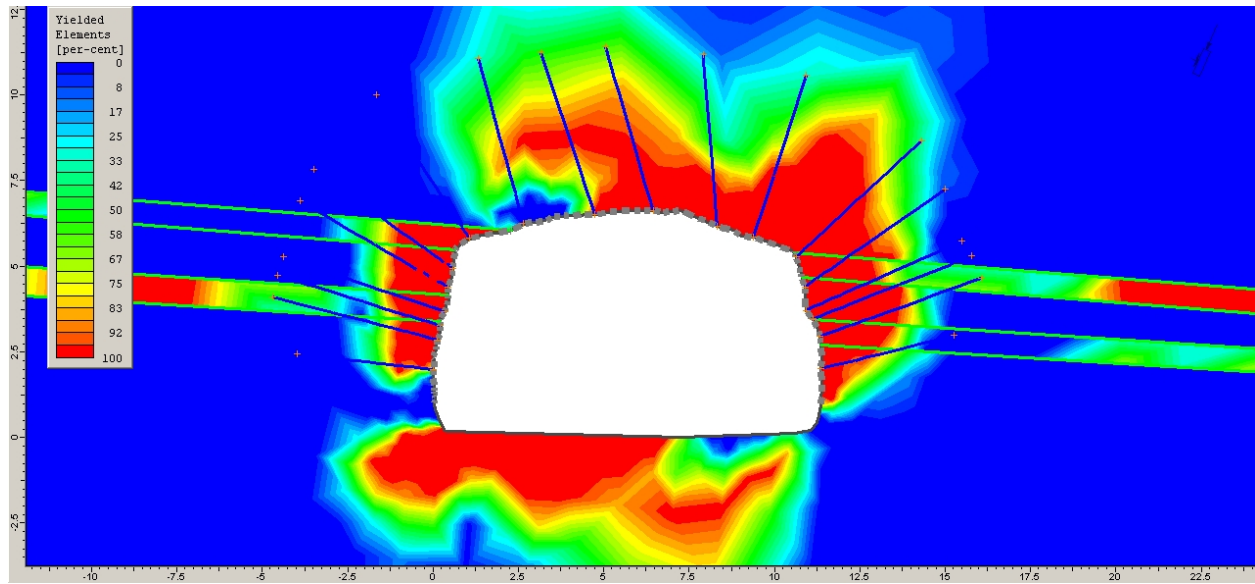
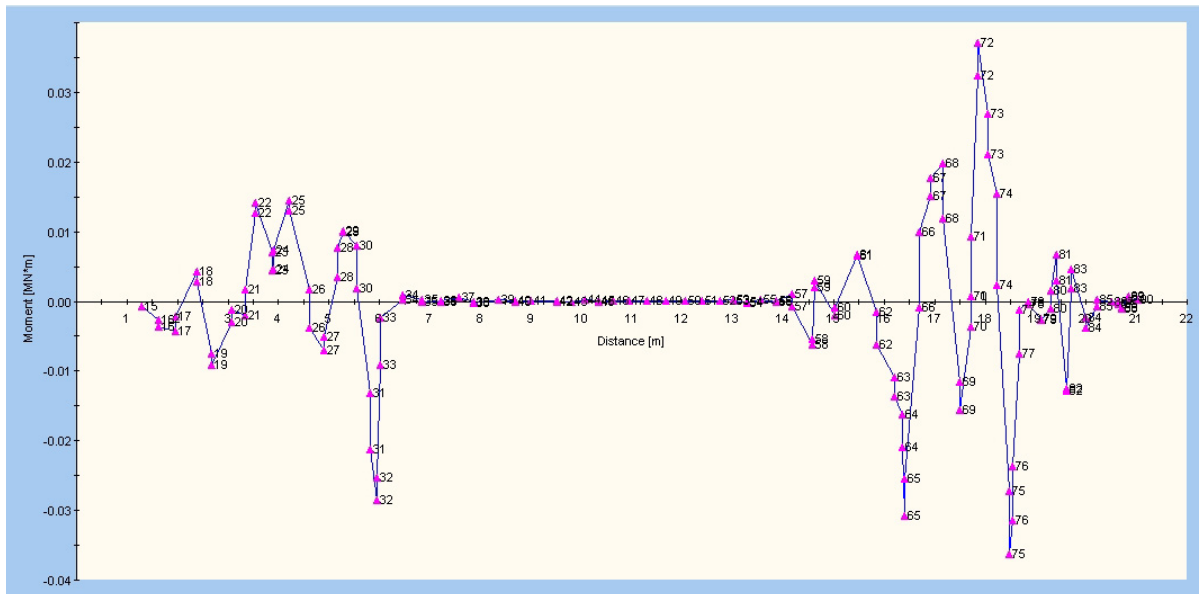


Figure 6-6: Yielded elements for supplementary support model 1 for station 6530.



**Supplementary support model 2 for station 6530.**



**Figure 6-7: Bending moment in shotcrete for supplementary support model 2 for station 6530.**

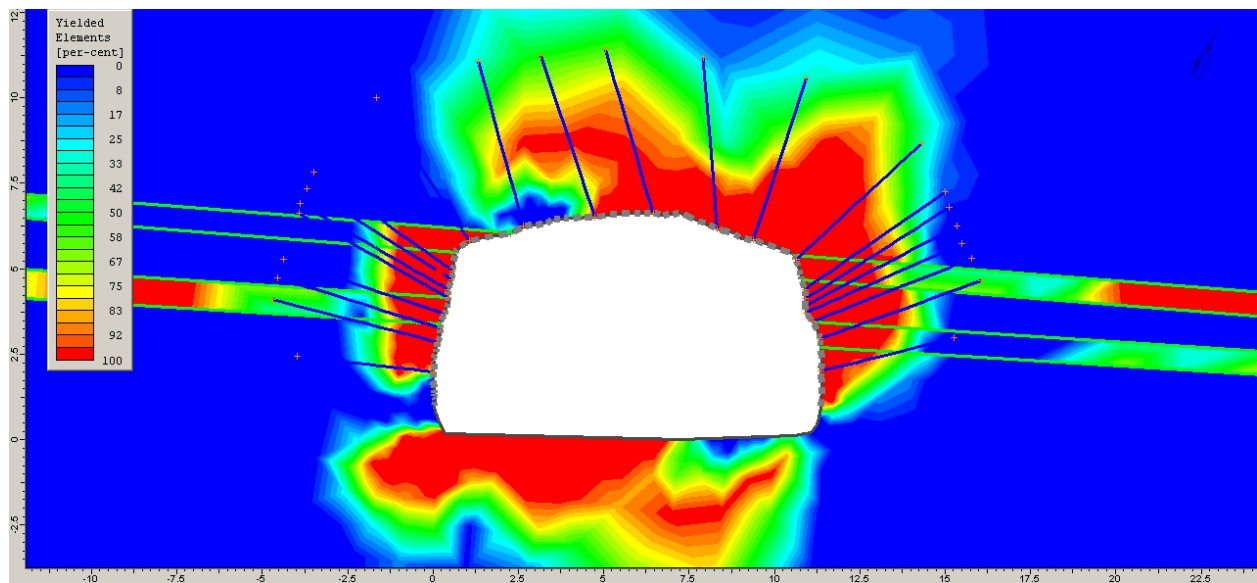


**Figure 6-8: Yielded elements for supplementary support model 2 for station 6530.**

**Practical support model for station 7615**

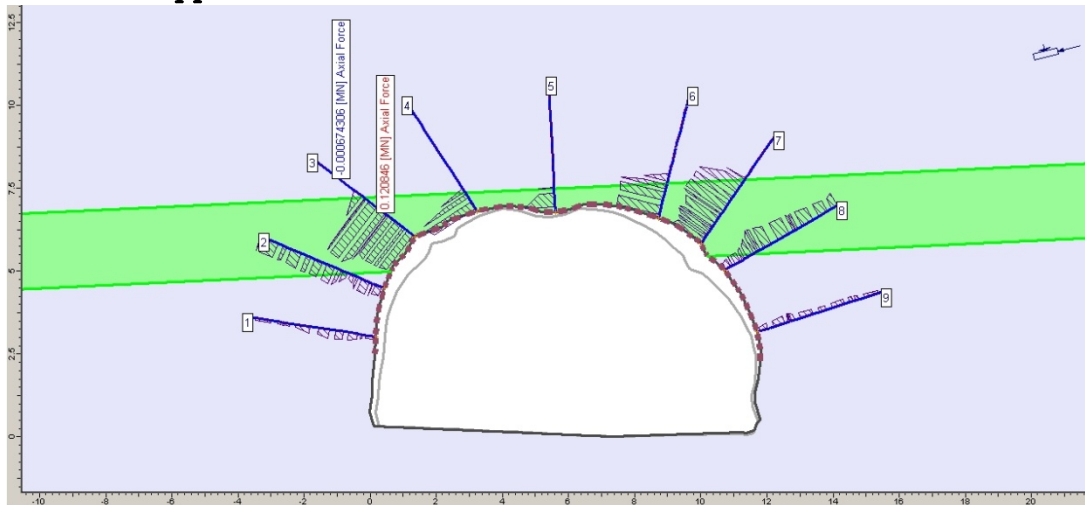


**Figure 6-9: Axial force in rock bolts in practical support model for station 7615.**

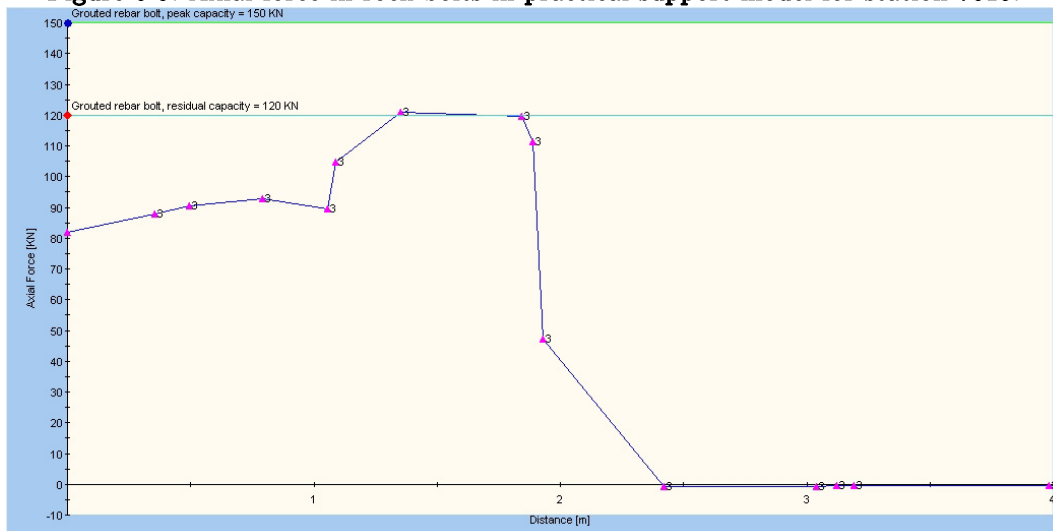


**Figure 6-10: Axial force in bolt nr. 3 in practical support model for station 7615, only bolt nr. 3 displayed yielding.**

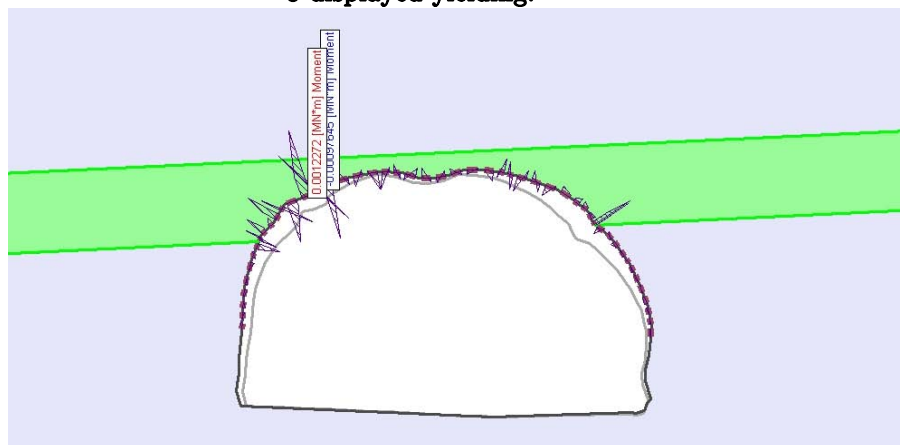


**Figure 6-11: Bending moment in the shotcrete in practical support model for station 7615.**

**Supplementary support model 1 for station 7615.**

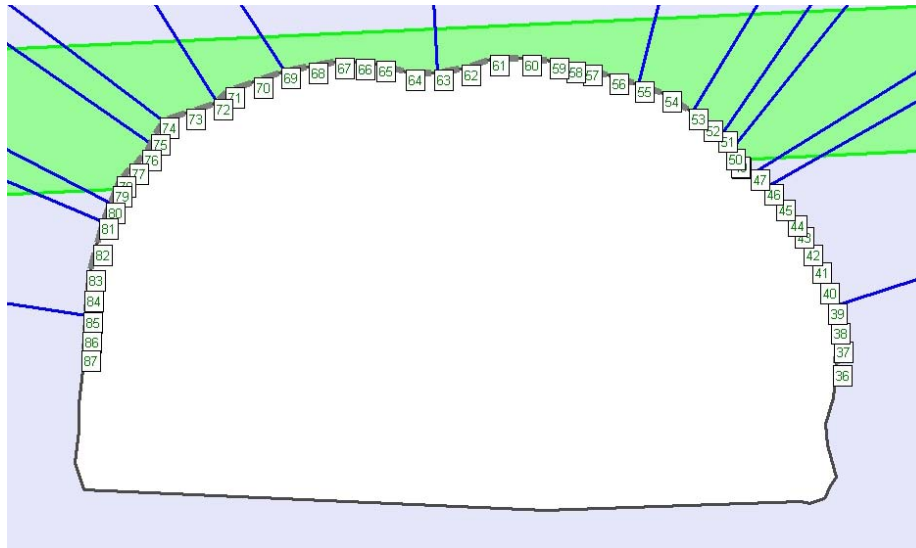


**Figure 6-12: Shotcrete elements in supplementary support model 1 for station 7615.**

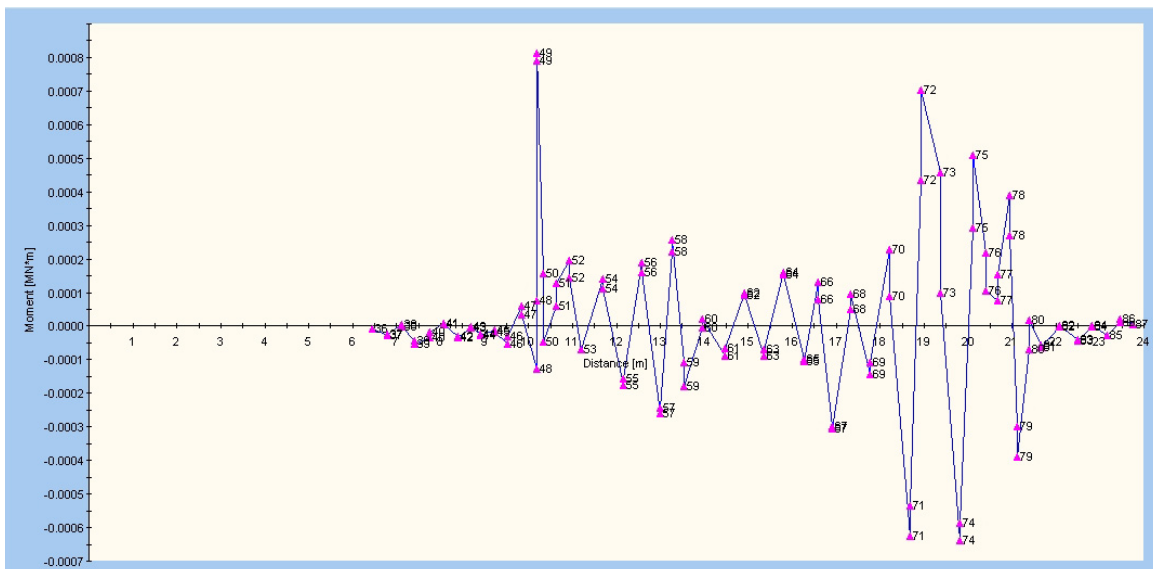


**Figure 6-13: Bending moment in shotcrete for supplementary support model 1 for station 7615.**

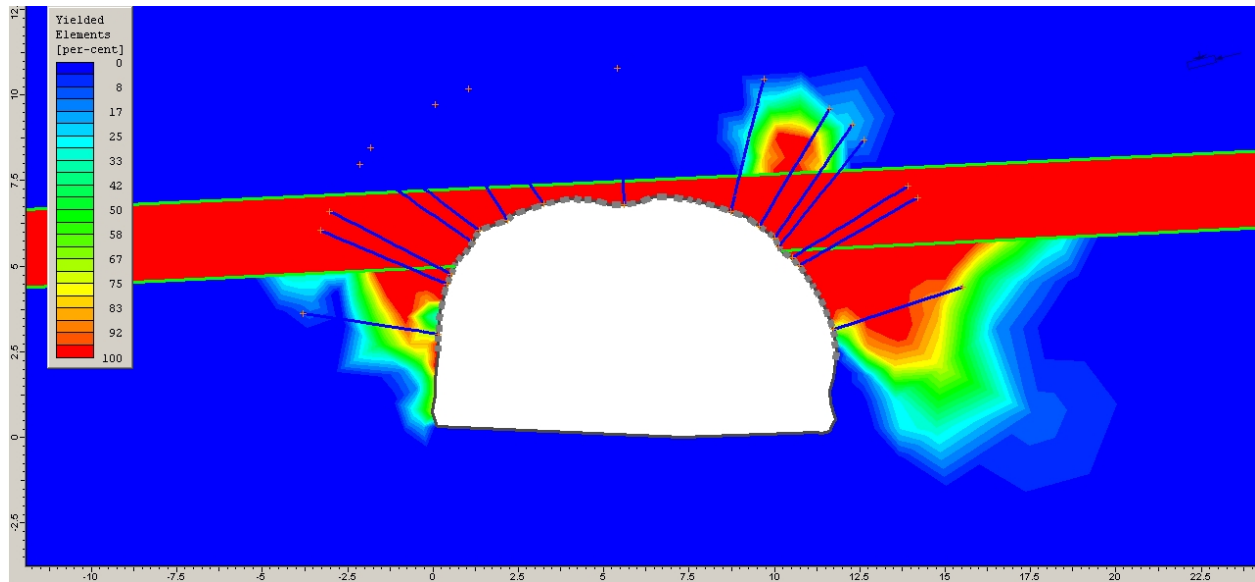
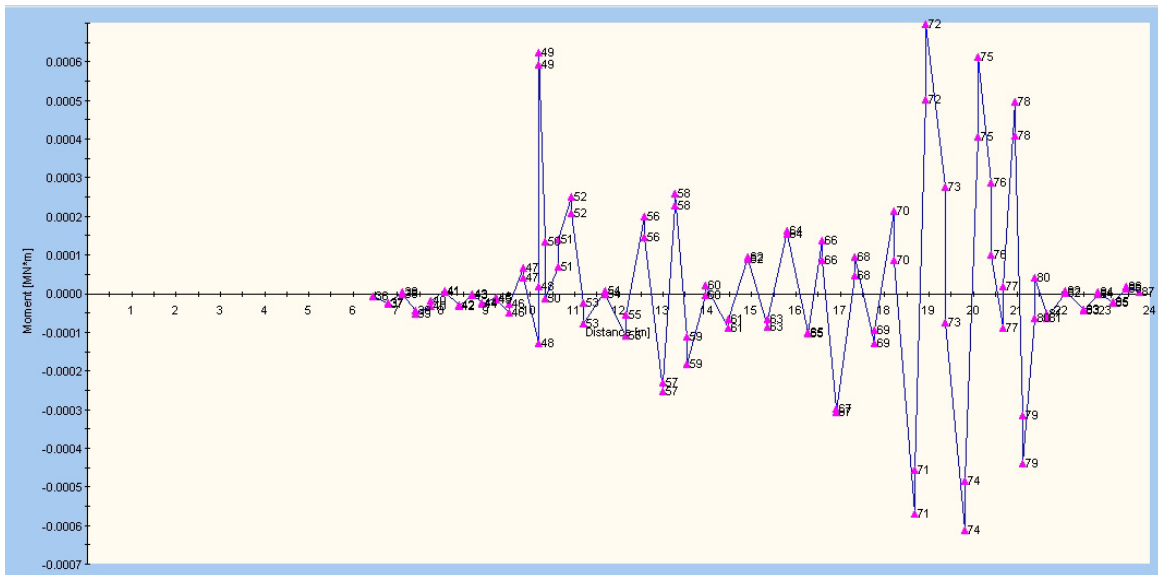
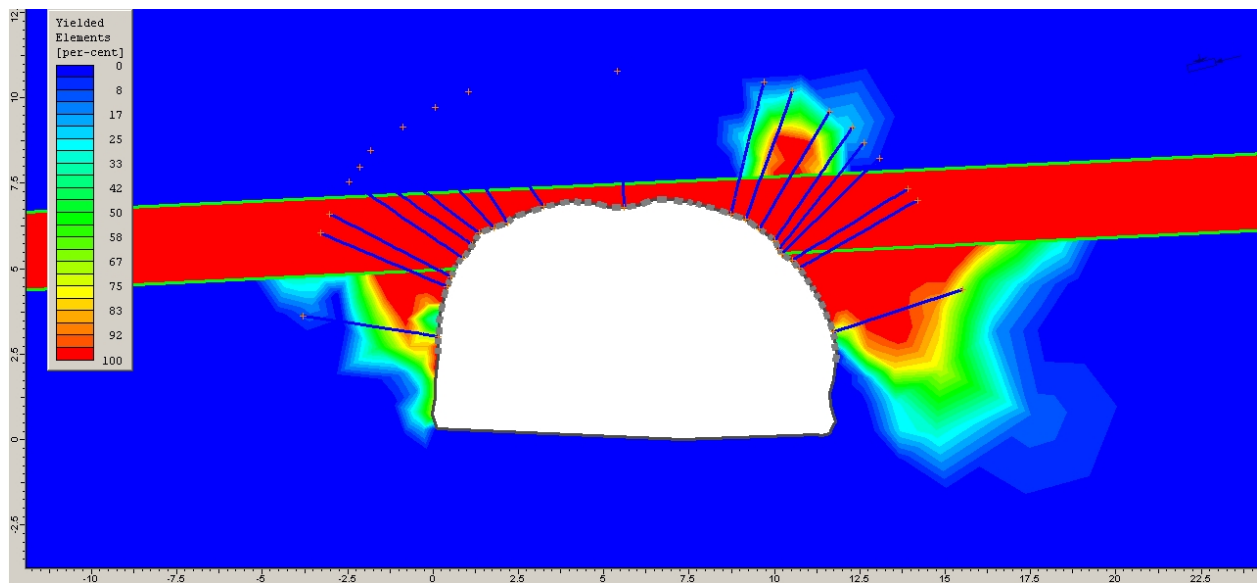


Figure 6-14: Yielded elements for supplementary support model 1 for station 7615.

**Supplementary support model 2 for station 7615.**



**Figure 6-15: Bending moment in shotcrete for supplementary support model 2 for station 7615.**



**Figure 6-16: Yielded elements for supplementary support model 2 for station 7615.**

